TECHNISCHE UNIVERSITÄT MÜNCHEN
TUM School of Engineering and Design

Cost and Benefit of Structural Health Monitoring in Commercial Aviation

Dominik Maximilian Steinweg

Vollständiger Abdruck der von der TUM School of Engineering and Design der Technischen Universität München zur Erlangung des akademischen Grades eines

Doktors der Ingenieurwissenschaften (Dr.-Ing.)

genehmigten Dissertation.

Vorsitz:	Prof. Dr.-Ing. Klaus Drechsler
Prüfer der Dissertation:	1. Prof. Dr.-Ing. Mirko Hornung
	2. Prof. Dr.-Ing. Christian Boller

Die Dissertation wurde am 03.03.2022 bei der Technischen Universität München eingereicht und durch die TUM School of Engineering and Design am 13.12.2022 angenommen.

Acknowledgments

During my time as a research assistant at Bauhaus Luftfahrt e.V. from 2018 to 2022, I wrote this dissertation with the support and contribution of many individuals to whom I express my gratitude. Without them, this work would not have been possible. I extend my deepest appreciation to my thesis supervisor, Prof. Dr.-Ing. Mirko Hornung, and second examiner, Prof. Dr.-Ing. Christian Boller, for their invaluable guidance and unwavering support. I am also grateful to Prof. Dr.-Ing. Klaus Drechsler for chairing the examination board.

I am particularly thankful to Dr. Kai-Daniel Büchter and Dr. Lily Koops for their academic expertise and constructive discussions, which significantly contributed to the success of this dissertation. My thanks also go to Dr. Kay Plötner, Dr. Anna Straubinger, Dr. Antoine Habersetzer, and Dr. Annika Paul for providing an excellent working environment, their empathetic support, abundant words of wisdom and valuable insights. I would also like to acknowledge the support of my former students, Carlos Sebastia Saez, Fabian Stephan, and Jenny Pham, who assisted me during my work. My sincerest thanks go to Dr. Patrick Vratny and Kimberly Sweetland for their critical feedback on the final draft of this dissertation, which greatly improved its readability and comprehensibility. I consider myself very fortunate to have been part of such a wonderful institution and to have had the freedom to pursue my research interests. During my time at Bauhaus Luftfahrt e.V., I not only gained valuable colleagues, but also made wonderful friends.

Finally, I would like to express my gratitude to my parents for their support not only during this endavour but also throughout my entire life. Additionally, I want to thank Sabine for her constant encouragement, especially during challenging times, and for consistently brightening my mood with her infectious smile.

Dominik Steinweg

Hamburg, April 2023

Abstract

During its operation, the structural integrity of commercial aircraft is essentially based on extensive, manual and thus cost-intensive structural inspections. In order to reduce the effort of these inspections without adversely affecting the safety of the airframe simultaneously, the use of built-in monitoring equipment has previously been discussed under the term Structural Health Monitoring (SHM). Although the underlying technologies used for this purpose are commercially available, their use is currently limited to individual pilot projects, as their financial benefits for aircraft operators are still unclear.

To quantify the economic impact of SHM, this thesis presents an integrated cost benefit analysis framework and applies it to a reference aircraft based on the Airbus A320. The entire aircraft life cycle from structural design, operation to retirement is considered. Results indicate that comprehensive and higher quality structural health information provided by SHM is more profitable for aircraft operators when used to extend the certified structural service limit than for weight-reduced structural design. Furthermore, based on the current use of the Airbus A320 fleet, it is shown that load monitoring of the structure can be used to significantly extend the airframe lifetime without affecting its safety. However, it depends on the performance parameters of the SHM system and share of instrumented airframe surface whether the total operating cost of the aircraft is affected positively or negatively. For an aircraft usage representative for the Airbus A320 fleet, the net present value (NPV) of a perfect weightless and costless damage monitoring (DM) system can be estimated at USD 1.39M. Furthermore, for SHM systems with false alarms, an NPV of more than USD 1M and a theoretical break even time of less than 5 years can be possible, even when considering system mass and installation costs. Hereby, only a portion of the airframe is instrumented with SHM. Furthermore, important levers in the development of SHM systems are identified, which drive the profitability of such a system.

Despite the simplification of this work and the fact that exact component geometries as well as failure mode and effects analysis for the airframe were not taken into account, the potential cost savings indicate that SHM should be considered in the design process for future aircraft generations to monitor selected hotspots and critical areas of the airframe.

Contents

List of Figures

List of Tables

Nomenclature

List of Latin Symbols

a	m	Crack length
a_0	m	Initial crack length
$\hat{a}_0$	-	Non-dimensionalized initial crack length
a_c	m	Critical crack length
$\hat{a}_c$	-	Non-dimensionalized critical crack length
$\hat{a}$	-	Non-dimensionalized crack length
A_{HMM}	-	State transition probability distribution
$a_{i,j}$	-	Transition probability from state i to state j
ap_n	-	Airport n
A_{part}	m^2	Surface area of monitored part
A_{PWAS}	m^2	Detection footprint per sensor
a_t	USD	Cash outflow in period t
A_{wsk}	m^2	Wing skin cross section area
AP	-	Set of airports served by airline
ap_n	-	Airports in routing sequence
b	m	Half width of structural specimen
b_F	g/(kN s)	Specific fuel consumption
$\hat{b}$	-	Backward variable
B_{HMM}	-	Observation symbol probability distribution
b_j	-	Observation symbol probability
B_t	-	Aircraft book value
C	$1/(\text{MPa}\sqrt{m})^3$	Material dependent parameter
C_1	MPa	Stress cycle curve parameter
C_2	MPa	Stress cycle curve parameter
C_3	-	Stress cycle curve parameter
C_4	-	Stress cycle curve parameter
c_{ap_n}	-	Expected flight cancellations at airport ap_n
C_{crew}	USD	Cost for crew
c_{fiber}	-	Fiber laying factor

C_{FO}	USD	Cost for flying operations
C_{fuel}	USD	Cost for fuel
C_{ins}	USD	Cost hull insurance
$C_{misc.}$	USD	Cost for miscellaneous flying operations
c_{patch}	-	Sensor patch factor
C_{PM}	-	Set of covered failures
C_t	USD	Net cash flow in period t
$C\hat{G}F$	-	Non-dimensionalized crack growth factor
d	m	Inner fuselage diameter
d_{ap_n}	h	Total delay time at aiport ap_n
$d_{ap_{n-1}}$	h	Reactionary delay at ap_{n-1}
d_{PWAS}	m	Side length of PWAS footprint
D_t	-	Periodic depreciation
E	-	Lift-to-drag ratio
e_t	USD	Cash inflow in period t
F	-	Set of possible failures
$\hat{f}$	-	Forward variable
$\vec{f}_{ap_n}$	-	Aircraft failures at ap_n
fl_{i,ap_n}	-	Inbound flights at airport ap_n
fl_{o,ap_n}	-	Outbound flights at airport ap_n
fl_{SA}	-	Avoided flight cancellations by spare aircraft
F_{wsk}	N	Force perpendicular to wing skin cross section
g_{jk}	-	Number of geodesics linking airports a_j and a_k
h	Cycles	Predictive horizon
I_0	USD	Initial cost of investment
I_i	-	Inspection interval
I_y	m^4	Second moment of area
K	MPa $m^{\frac{1}{2}}$	Stress intensity factor
K_{I_c}	MPa $m^{\frac{1}{2}}$	Fracture toughness
k_P	-	Shaft power factor
K_V	MPa $m^{\frac{1}{2}}$	Equivalent stress intensity factor
$l_{component}$	m	Length of the component
L_{FOSI}	m	Length of fiber in FOSI system
l_{min}	h	Minimum aircraft turnaround time
l_{ap_n}	h	Duration of layover at ap_n
L_{wire}	m	Length of wire
m	-	Material dependent parameter
m_0	kg	Total aircraft mass at take-off
$\dot{m}$	kg/s	Fuel mass flow rate of the aircraft
$\dot{m}_{F,P}$	kg/s	Electric generator fuel flow change
m_{FC}	kg	Mass of fiber connector
m_{FOSI}	kg	Mass of FOSI system

m_{PZT}	kg	Mass of PWAS sensing element
m_{SHM}	kg	SHM system mass
M_σ	-	Material constant
m_t	kg	Total fuel mass at take-off
m_{USI}	kg	Ultrasonic interrogator equipment mass
m_{wire}	kg	Mass of wire
M_y	N m	Wing bending moment
m_{ZFW}	kg	Aircraft mass without fuel
N	-	Load cycles
N_Δ	-	Differences of flight cycle or flight hours
$N_{EOL,LoV}$	-	Last cycle of the aircraft
$N_{FC,LoV}$	-	Flight cycles defined in limit of validity (LoV)
$N_{FH,LoV}$	-	Flight hours defined in LoV
n_{FOSI}	-	Number of fibers in FOSI system
N_{HMM}	-	Number of hidden states
$N_{M,A}$	-	Flight cycle or flight hour of maintenance event
$N_{next,T}$	-	Flight cycle or flight hour of upcoming task
n_{SA,ap_n}	-	Number of spare aircraft at airport ap_n
n_{USI}	-	Number of ultrasonic interrogators
n_{wire}	-	Number of signal and ground wires
$\mathcal{NP}$	-	Non-deterministic polynomial
o_t	-	Output observation
$P_{\hat{a}_c,max,OLM}$	-	Permissible structural damage probability
$p_{\Delta ff,\text{inf}}$	Pa	Difference fuselage and ambient pressure
P_{diss}	W	Dissipation loss
$p_{failure}(FC)$	-	Probability of failure during a given FC
P_t	USD	Proceeds of disinvestment at period t
P_{wire}	W	Power demand
$P(X \geq fl_{o,ap_n})_{ap_n}$	-	Probability of failure during cycle N
PM	-	Predictive maintenance performance set
R	-	Stress ratio
$\vec{r}_{ap_n}$	h	Aircraft repairs at ap_n
R_{flight}	m	Range of flight
R_r	-	Set of aircraft repairs
S_{ap}	-	Set of airport services
s	m	Structural thickness
S_a	MPa	Stress amplitude
S_{axial}	Pa	Axial stresses in the fuselage
S_{HMM}	-	Individual states in Hidden Markov Model
S_m	MPa	Mean stress
s_n		Service level at airport ap_n
S_{tan}	Pa	Tangential stresses in the fuselage

SFC	g h/kW	Specific fuel consumption
t	-	Period
t_{EOL}	-	Final period
t_{film}	m	Thickness of film
T_i	-	Inspection threshold
T_I	-	Total number of investment periods
t_{patch}	m	Thickness of patch
T_{taxi}	h	Aircraft taxi time
T_{wsk}	N/m	Wing skin shear flow
V	m/s	Aircraft velocity
w	-	Structural weight
w_{film}	m	Width of film
$W_{fuel,max}$	kg	Maximum weight of fuel
$W_{M.Acc}$	h	Access times of tasks
$W_{M,Acc,A}$	h	Total access time of aircraft inspection event
$\overrightarrow{W_{M,Acc,P}}$	h	Access time summarized by aircraft position
$W_{M,i}$	h	Inspection time without access time
$W_{M,T}$	h	Total inspection time including access time
W_{MTOW}	kg	Maximum take-off weight of aircraft
W_{OEW}	kg	Operating empty weight
w_{patch}	m	Width of patch
$W_{PL,max}$	kg	Maximum weight of payload
WACC	%	Weighted Average Cost of Capital
X	-	Bernoulli variable
x	-	False positive rate
y	-	True positive rate
Y	-	Geometry factor

List of Greek Symbols

α_1	-	Material scaling parameter
α_t	-	Normalizing constant
$\ddot{\alpha}_t$	-	Normalizing constant
$\dot{\alpha}_t$	-	Normalizing constant
ΔK_0	%	Minimum stress intensity for crack growth
δ_{patch}	kg/m^3	Density of patch
Δs	%	Decrease in sheet metal thickness
η	-	Allowed voltage drop per unit length
λ	-	Hidden Markov Model
λ_{AC}	-	Expected aircraft dispatch probability
λ_{AL}	-	Expected airline dispatch probability

λ_{fiber}	kg/m	Linear density of fiber
λ_{FOC}	kg/m	Linear density of fiber-optic cable
λ_{jacket}	kg/m	Linear density of jacket
λ_{wire}	kg/m	Linear density of wire
$\hat{\mu}$	-	Mean of initial crack size distribution
ν	-	Efficency chain shaft power to electrical power
π	-	Initial state distribution
ρ_{Cu}	kg/m^3	Density of copper
ρ_{film}	kg/m^2	Area density of film
ρ_{PWAS}	kg/m^2	Area density of PWAS
σ	Pa	Axial stress
$\hat{\sigma}_{a_0}$	-	Initial crack size standard deviation
σ_{Cu}	S/m	Electric conductivity of Copper
τ	Pa	Shear stress
τ_l	Pa	Shear stress orthogonal to crack and plane
Θ	-	Lehmann parameter
ξ	-	Technological progress factor

List of Subscripts and Superscripts

ff	Fuselage
fs	Fuselage skin
I	Type I crack growth
II	Type II crack growth
III	Type III crack growth
A	Aircraft
M	Maintenance event
T	Task
ls	Longitudinal stringer
MTOW	Maximum take-off weight
P	Position defined in the MPD
wr	Wing rip
ws	Wing spar
wsk	Wing skin
ZFW	Zero fuel weight

List of Acronyms

AD	Airworthiness directive
ADOC	Additional operating cost

ADS-B	Automatic Dependent Surveillance - Broadcast
AE	Accoustic emission
AMC	Acceptable means of compliance
ARP	Aerospace recommended practice
ATFM	Air traffic flow management
AU	Acousto ultrasonic
BVID	Barely visible impact damage
CAPEX	Capital expenditure
CBM	Condition based maintenance
CFRP	Carbon Fiber Reinforced Polymer
COC	Cash operating cost
COO	Cost of ownership
COVID-19	Coronavirus Disease 2019
CS	Certification specifications
CVM	Comparative vacuum monitoring
CW	Crack wire
DI	Detailed inspection
DM	Damage monitoring
DOC	Direct operating cost
DSG	Design service goal
EDMS	Environmental degradation monitoring sensor
ESG	Extended service goal
ETFS	Eddy current testing foil sensor
FAR	Federal Aviation Regulations
FBG	Fiber Bragg-grating
FC	Flight cycle
FDI	Fatigue damage index
FH	Flight hour
FMEA	Failure mode and effects analysis
FN	False negative
FOD	Foreign object damage
FOS	Fiber-optic sensor
FOSI	Fiber-optic interrogation
FP	False positive
FTA	Fault tree analysis
GM	Guidance material
GVI	General visual inspection
HMM	Hidden Markov model
IOC	Indirect operating cost
IU	Imaging ultrasonic
LoV	Limit of validity
MAD	Median absolute deviation
MP	Maintenance program

MPD	Maintenance planning document
MRB	Maintenance Review Board
MRBR	Maintenance Review Board report
MRO	Maintenance, repair and overhaul
MTBF	Mean time between failure
MTBRF	Mean time between reported failure
MTBUL	Mean time between unscheduled landing
MZFW	Maximum zero fuel weight
NAA	National aviation authority
NDT	Non-destructive testing
NPV	Net present value
OLM	Operational load monitoring
OLMOS	Onboard life monitoring system
PoD	Probability of detection
PUL	Previous unscheduled landing
PWAS	Piezoelectric wafer active sensor
ROC	Receiver operating characteristic
RPK	Revenue passenger-kilometers
SB	Service bulletin
SDI	Special detailed inspection
SHM	Structural health monitoring
TN	True negative
TOW	Take off weight
TP	True positive
TWIST	Transport Wing Standard
WFD	Widespread fatigue damage

List of Organizations

ASRS	Aviation Safety Reporting System
ASTM	American Society for Testing and Materials
ATA	Air Transport Association
DOT	Department of Transportation
EASA	European Union Aviation Safety Agency
FAA	Federal Aviation Administration
FR24	Flightradar24
IABG	Industrieanlagen-Betriebsgesellschaft
ICAO	International Civil Aviation Organization
ISC	Industry Steering Committee
MSG	Maintenance Steering Group
NASA	National Aeronautics and Space Administration
OAG	Official Aviation Guide of the Airways

SAE	Society of Automotive Engineers

Chapter 1

Introduction

Before the number of worldwide commercial flights dropped to 25% in April of 2020 compared to the previous year, because of the Coronavirus Disease 2019 (COVID-19) pandemic, a combined fleet of 25,900 aircraft generated a total revenue of USD 838 billion for commercial airlines worldwide in 2019 [3, p. 3, 4, 5, p. 8]. Their safe operation is the priority for airlines and the foundation of a profitable aviation business environment [6, p. 2–8]. To achieve this goal, regulations, staff training, and technological solutions are used to prevent latent, accident-causing errors due to flawed management decisions, inadequate organizational processes, poor working conditions, and other violations [6, p. 54–58]. On aircraft level, safety is driven, among other factors, by excess takeoff and landing lift, stopping distance, control system capability over a large speed range, and structural integrity [6, p. 270]. As the central system of the aircraft, the structural integrity of the airframe is paramount throughout its operational lifetime [6, p. 275–277]. To the aviation system's credit, airframe failure–related casualties have been steadily declining since the 1970s, approaching almost zero in recent years, as shown in Figure 1.1. The high level of structural safety is achieved by damage-tolerant structural designs and regular work-intensive inspections, which make up 18% of all aircraft maintenance costs or 3–4% of aircraft operating cost [6, p. 275–277, 7, 8, p. 46]. Despite the cost of labor, airframe inspections together with the inspection of engines and all other on-board systems require the aircraft to be temporarily removed from service, which inhibits its revenue-generating capability [9]. In comparison, excessive structural robustness decreases the number and frequency of inspections while increasing

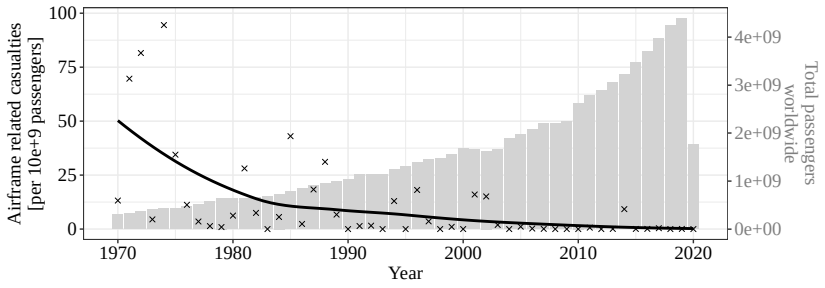

Figure 1.1: Airframe related casualties in commercial aviation, adapted from [1, 2].

structural weight and thus aircraft fuel consumption [10, p. 538–580]. In this context, an automated built-in inspection system, known as Structural Health Monitoring (SHM), is discussed as a solution to decrease manual labor requirements during airframe inspections without adversely impacting structural safety [11–19].

Patents covering SHM in aviation have been granted since the 1950s, and numerous proofs of concept have demonstrated their technological feasibility [14–19]. However, the widespread commercial adoption of SHM has failed to materialize, owing to an unclear business case [20, p. 38, 21, p. 1]. On the one hand, substantially reduced inspection efforts, along with extended aircraft lifetimes, structural design improvements, and better maintenance scheduling, were proposed [22–30]. Conversely, SHM equipment built into the aircraft could decrease airline productivity by reducing payloads and increasing fuel burn, rendering the commercial use of SHM highly unfavorable [31–33].

Even though the impact of SHM on airlines is highly diverse, current cost-benefit studies only focus on individual isolated aspects [34]. By considering the monitoring technology, aircraft design, or the operation of the aircraft separately, current cost-benefit studies yielded partially contradicting results [34]. To assist aircraft manufacturers and airlines in their investment decision for SHM, the sources of conflicting estimates on the profitability of SHM in previous studies are explored, and a novel approach is proposed to assess the economic impact of SHM holistically over the life of the aircraft. The introduced methodological framework is divided into three parts covering the effect of SHM: (1) operational aircraft performance metrics, (2) airline reliability metrics, and (3) a cost model unifying the diverse impact of SHM on aircraft and airlines in a single financial figure.

1.1 Research Objectives and Outline

To help understand the business case of SHM, the work at hand presents an integrated assessment of its cost and benefit in commercial aviation by extending current research twofold:

1. The techno-economic interaction between SHM and aircraft and airline performance is studied, considering specifically SHM performance, sensor technology, airframe design, aircraft inspection requirements, and the operational environment of airlines with a holistic approach.
2. Proposed benefits of SHM, including deferred aircraft decommissioning, improved inspection and maintenance, improved airline planning, and weight-saving potentials in airframe design, are compared and evaluated.

Fundamental performance considerations of monitoring systems can generally be described independently of the utilized technology [35, 36]. To determine the presence of a predefined condition, classifiers compare a measured variable against a given threshold associated with the predefined condition [36]. The ratio of the number of successfully recognized predefined conditions (true positive (TP)) to that of unrecognized predefined conditions (false negative

(FN)) is connected by the classification threshold [36]. The ratio of the number of successfully recognized predefined conditions (TP) to that of mistakenly reported predefined conditions (false positive (FP)) is given by the performance of the monitoring system [36]. While TP, FP, and FN rates are interconnected, aircraft safety and airline operating performance constitute opposing calibration requirements. To avoid unnecessary labor for inspections, the FP rate has to be minimized. In contrast, the TP rate has to be high enough to achieve a structural failure probability per flight hour below 10^{-3} to 10^{-9}, depending on the severity of a failure [37, p. 2-F-49]. To achieve both simultaneously, an almost perfect classifier is required, depending on the targeted failure probability [36]. However, the structural integrity of the airframe cannot only be inferred by means of a damage monitoring system but also using fundamental physical and empirical structural models [12]. The fatigue of metallic structures is a well-understood phenomenon, allowing the computation of the remaining useful lifetimes of structural components under cyclic loading [10, p. 538–580]. Although the occurrence of impact damage may not be predicted individually, their effect on the structural integrity of the airframe can be analyzed using well-established methods [10, 38].

While monitoring system performance, structural fatigue, and airframe integrity can be described by quantitative physical models, design requirements, as well as the cost and benefits connected to their usage, are socially constructed [39]. Thus, the benefit of an SHM system for an airline results from the economic environment in which it operates. The rate at which SHM is adopted may also depend on greater organizational and societal factors.

Both the physical phenomena involved in SHM and the economic operating environment of commercial aircraft are considered in this work as follows. A connection between SHM and airframe design is established, considering different technological monitoring approaches and operating modes. As the performance of the SHM system depends on the structure geometry, material, sensor technology, and measuring principle, different approaches are discussed to optimize its output. Performance assumptions of a single SHM technology based on strain gauges are validated using a demonstrator test conducted by Industrieanlagen-Betriebsgesellschaft (IABG), an Ottobrunn-based analysis and test-engineering company with competencies in full-scale fatigue testing of airframes. The established coherence between SHM and airframe design are transformed to a reference aircraft based on the Airbus A320, using a series of assumptions. While the proposed methodology is also applicable for other aircraft, the Airbus A320 is selected because of its widespread usage and more available data on its design, usage, and maintenance requirements compared to other commercial aircraft. The airframe model is based on simplified geometry consisting only of metal sheets. Structural fatigue is simulated using the Paris-Erdogan crack growth law. Hereby, local structural geometry, design drivers, and sizing load cases are neglected. Additionally, the failure behaviors of all other aircraft systems are simulated by binomial sampling. For the operation of the reference aircraft, a reference airline and representative flight plan are defined. The effects of aircraft dispatch reliability on the overall network reliability regarding its topology are studied by comparing two distinct airlines operating a hub and point-to-point network. Both the network and the aircraft flight plan are defined to be representative of the majority of the worldwide commercial air transport system. The resulting operational aircraft and airline

performance is translated to financial factors using a simplified empirical cost model relying on data for airlines published by the United States department of transportation (DOT).

Beneficial applications for the different SHM monitoring approaches are identified and discussed. Assuming the adaption of current regulatory guidelines governing the occurrence of widespread fatigue damages (WFDs), SHM can enable aircraft-specific operating limits compared to fleet-wide operating limits used today, achieving longer aircraft lives without compromising safety. Further, at a low instrumentation cost of less than USD 500 per m^2 and low false alarm rates, SHM can be suitable and financially beneficial to replace manual inspections. At this price point, the instrumentation cost covers the expenditures for purchasing, installing, maintaining, and evaluating the sensor measurements. However, the associated benefit depends heavily on labor cost and fuel prices, where high labor cost and low fuel prices increase the net present value (NPV) of an investment in SHM.

1.2 Thesis Layout

To answer the prevailing research questions, this thesis at hand is organized as follows.

In *Chapter 2*, fundamentals influencing the introduction of SHM in commercial aviation are summarized. A condensed overview of technological, regulatory, and financial aspects of airframe structural integrity is provided. The investigated prospects of on-board SHM systems are introduced, followed by a summary of technological approaches available to realize SHM. Finally, current cost-benefit analyses of SHM are discussed.

Chapter 3 introduces required methods to conduct the techno-economic cost-benefit analysis of SHM. The utilized analysis framework is structured in three parts. First, the aircraft simulation covers the structural fatigue and airframe design aspects and includes the SHM model. Further, a simplified equipment failure model is presented, along with maintenance-scheduling and aircraft-decommissioning models. The airline simulation addresses the implication of aircraft reliability on airline reliability as well as the use of spare aircraft. Finally, a cost model is introduced to transform all operative impacts of SHM to a unified financial factor.

Chapter 4 discusses the conceptual integration of SHM within commercial aircraft. Included is the design optimization problem of SHM from an airline perspective, followed by the definitions of reference airline and reference aircraft. The simulation results are validated for airlines not using SHM. Without operational data, the model cannot be validated for aircraft with SHM. Finally, the investigated SHM concepts are summarized.

Chapter 5 presents the results of the work, including the impact of SHM on the operational and financial performance of the selected commercial reference aircraft. These results define the design space for the investigated SHM systems. Finally, the chapter discusses their benefits as investment opportunities for airlines.

Chapter 6 discusses the overall results in more detail and compares them to existing research. Shortcomings stemming from the availability of data and the applied research methodology are explained.

Chapter 7 concludes the study of costs and benefits of SHM in commercial aviation and provides an outlook on future research questions. Airline field tests are suggested as means to improve and validate the results. Additionally, SHM as a retrofit system is compared to its implementation in the aircraft design stage, identifying the limitations.

Chapter 2

Structural Health Monitoring in Commercial Aviation

The introduction of SHM systems into the aircraft provides operators and maintenance personnel with a new information source about the state of the airframe, following the line of traditional non-destructive testing (NDT) methods. A variety of SHM technologies are available based on different monitoring principles, which were examined for a multitude of applications [12]. Serving as a basis of this work, the technological and operational environments in which SHM is deployed in commercial aviation are described in this chapter.

In *Section 2.1*, general methods currently used to ensure the structural integrity of airframes over their lifetime are reviewed. This includes selected aspects of aircraft structure design, a summary of current inspection methods, a review of the regulatory framework governing the operation of transport category aircraft, and SHM. Additionally, an excursion into the representation of continuing airworthiness in financial accounting provides a basis for the cost-benefit analysis presented in this work. *Section 2.2* summarizes the benefits of SHM discussed in the literature, focusing on the deferred decommissioning of aircraft, accelerated inspections, improved maintenance scheduling, and advantages of lightweight airframe design. Complementary, the general technological approaches to realize SHM, investigated as part of this thesis, are introduced in *Section 2.3*. Finally, *Section 2.4* presents previous cost-benefit studies on SHM in commercial aviation.

The definition of SHM used throughout this work is based on the aerospace recommended practice (ARP) 6461 by Society of Automotive Engineers (SAE) [40]. The classification of SHM within the overall aircraft health monitoring system and the categorization of different SHM applications are illustrated in Figure 2.1. In addition to the engine and systems health management, structural health management is a part of the overall aircraft health management [40]. Hereby, structural health management relies on different information sources, including crew observations, maintenance records, fleet-wide data analysis, and the potential use of SHM [40]. The SHM system can be classified by technology type and operation mode [40]. With damage monitoring (DM)–based SHM, a damage-dependent physical phenomenon is directly monitored. In contrast, operational load monitoring (OLM) records the operation of single structural components of the entire airframe and infers the health of the structure

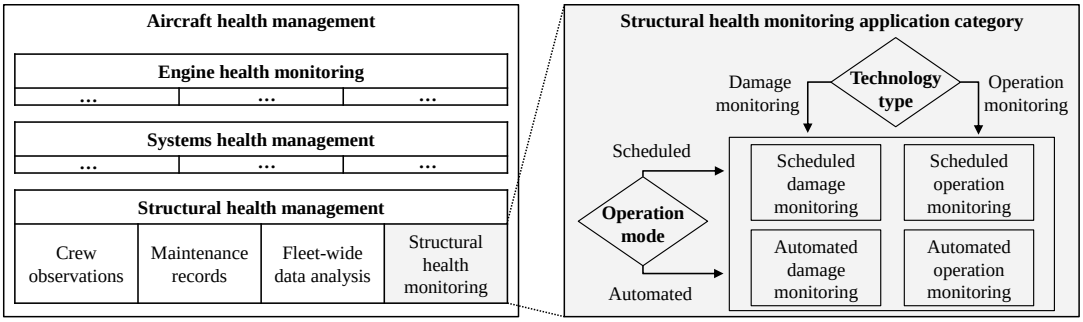

Figure 2.1: Classification of SHM within aircraft health management and categorization of SHM applications, adapted from [40, p. 20–25].

through comparisons with damage models [40]. Additionally, SHM systems are distinguished by their mode of operation into scheduled systems, which are used during scheduled maintenance, and automated systems, which do not have a predetermined interval for maintenance actions but inform maintenance personnel of required actions [40, p. 24].

2.1 Managing Structural Integrity of Airframes

The following section introduces current approaches to manage the structural integrity of airframes. A summary of the *design of aircraft structures* describes the technical environment of SHM. Furthermore, an overview of processes aiding *structural integrity during operation* is given, followed by a summary of the *current regulatory framework* governing structural integrity of airframes and the introduction of SHM. Finally, an excursus on *representing continuing airworthiness in financial accounting* summarizes how airframe maintenance is considered in accounting methods used by airlines.

2.1.1 Design of Aircraft Structures

Aircraft design is an iterative process including four primary activities: requirement definition, design concept proposition, design analysis, and sizing and trade studies [41, p. 3]. By iterating these activities, not necessarily in the same order, the aircraft design matures through three phases. The first phase is a conceptual design, where concept viability is the main concern [41, p. 13]. At this point, structures have no significant impact except on weight estimation [41, p. 491]. In the second phase of the preliminary design, the aircraft configuration is frozen, and actual structural components are drafted in the detailed design (third phase). Afterward, the aircraft goes into production [41, p. 13]. Weight savings compared to current aircraft are typically achieved during the design and stress analysis when drafting detailed designs [10, p. 5]. Throughout the design process, reliability analysis techniques, such as fault tree analysis (FTA) and failure mode and effects analysis (FMEA), are applied to substantiate the reliability of the structure [42]. Required data is gathered from basic load

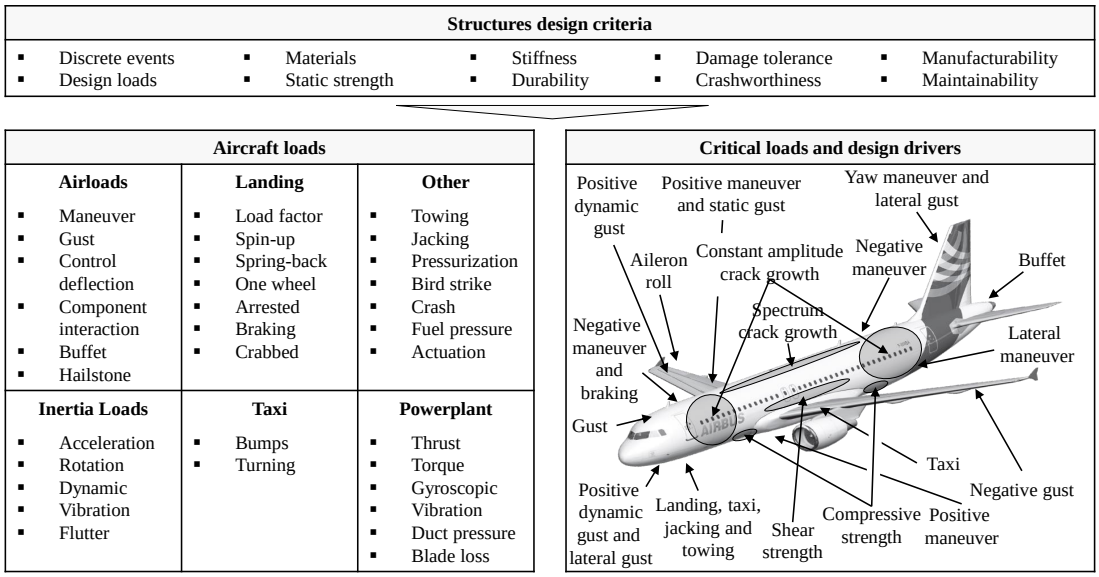

Figure 2.2: Airframe design requirements, loads and critical loads, adapted from [41, p. 493–494, 43, p. 814, 44, p. 6, 45, p. 3].

assumptions, laboratory experiments, and flight tests before the aircraft enters a certification test program that is successfully completed with an approved type certificate [10, p. 4].

For the design of structures, numerous design criteria and loads are considered, with each aircraft component having individual design drivers, as schematically illustrated in Figure 2.2. The challenge is to "provide maximum inherent safety, ... achieve superior structural performance in terms of weight and durability, and ... deliver an airframe with minimum costs of production and long-term ownership by the operator" [43, p. 814]. Therefore, the material and geometry of a structural component depend on its location within the airframe.

Consequently, different philosophies to design and certify airframes have evolved. Historically, the evaluation of the ultimate strengths of a few critical parts concluded the structural analysis [10, p. 3]. In the 1930s, this was expanded to evaluating the static ultimate strength of the entire airframe [10, p. 3]. In the 1940s and early 1950s, the importance of fatigue was realized in addition to considering static strength [10, p. 3]. To govern the occurrence of fatigue, the *safe-life*, *fail-safe*, and *damage-tolerance* design philosophies were developed, with only safe-life and damage-tolerance applied as stand-alone methodologies in airframe design today:

- With the *safe-life* approach, introduced in the 1940s, it is *"ensured that no fatigue cracks are developed in the component or structure during service"* [44]. *"The structure shall be designed, insofar as practicable, to avoid points of stress concentration where variable stresses above the fatigue limit are likely to occur in normal service ..."* [46, § 03.312]. Based on the implied service period or mandatory retirement, this approach is designated as "safety by retirement" [47].

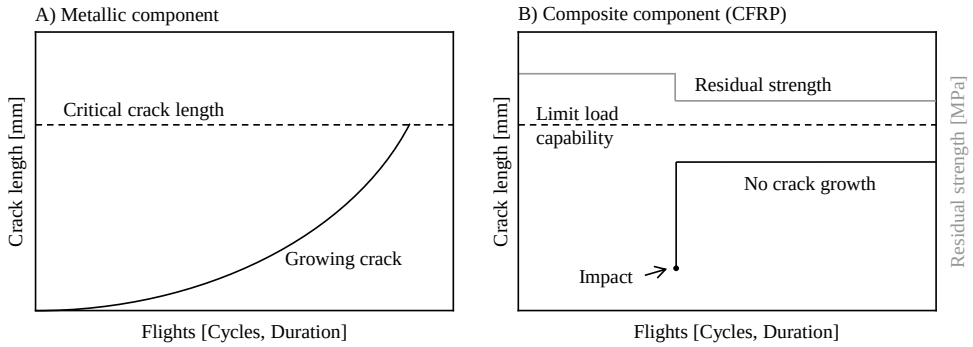

Figure 2.3: Model fatigue behavior of A) aluminum skin and B) CFRP sheet under cyclic loading after crack initiation assuming only limited strain. No crack growth occurs when the stress intensity factor is below the threshold value [52, p. 38].

- The *fail-safe* approach, introduced in 1956, requires *"by analysis and/or tests that catastrophic failure or excessive structural deformation, ... are not probable after fatigue failure or obvious partial failure of a single principal structural element"* [48, § 25.571]. In other words, fatigue damage is detected during normal maintenance, also termed "safety by design" [47 44, p. 11].

- The implementation of the *damage tolerance* approach in 1978 requires the following: *"should serious fatigue, corrosion, or accidental damage occur ..., the remaining structure can withstand reasonable loads without failure [...] until the damage is detected. ... [S]ufficient guidance information to assist operators in establishing the frequency, extent, and methods of inspection [must be provided]"* [49]. This approach is associated with "safety by inspection" [44, p. 11].

The regular inspections of damage-tolerant structures at predefined intervals aim to discover fatigue driven by a single crack before failure. However, the simultaneous emergence of cracks at multiple locations, referred to as WFD, can accelerate the deterioration of structural integrity [44, p. 43]. To address WFD, the maximum number of cycles or hours an aircraft with a damage-tolerant airframe can operate is limited [37, 50, § 25.571]. This limit is derived from the limit of validity (LoV) of the engineering data produced during full-scale fatigue tests of the airframe [37, 50, § 25.571]. The LoV and thus the validity of the fatigue prevention program can only be increased through additional fatigue testing [51, p. 1015–1016].

Although airframe design philosophies have continuously evolved, proper selection depends on the intended use of a structure and its material [41, p. 513]. Based on the combination of matrices and fibers, composite airframes, having a significantly higher static strength, do not suffer from corrosion and cracking compared to aluminum and most other metal alloys [53, p. 369,449]. However, composites can have a "limited ability to redistribute loads at structural features" because of their stiff and brittle fibers, unlike aluminum alloys that can redistribute stresses to some extent by local yielding [53, p. 449–450]. The fatigue behavior of metallic and composite materials is illustrated in Figure 2.3. Resulting from the complex damage growth mechanisms, composite material designs generally follow a safe-life approach

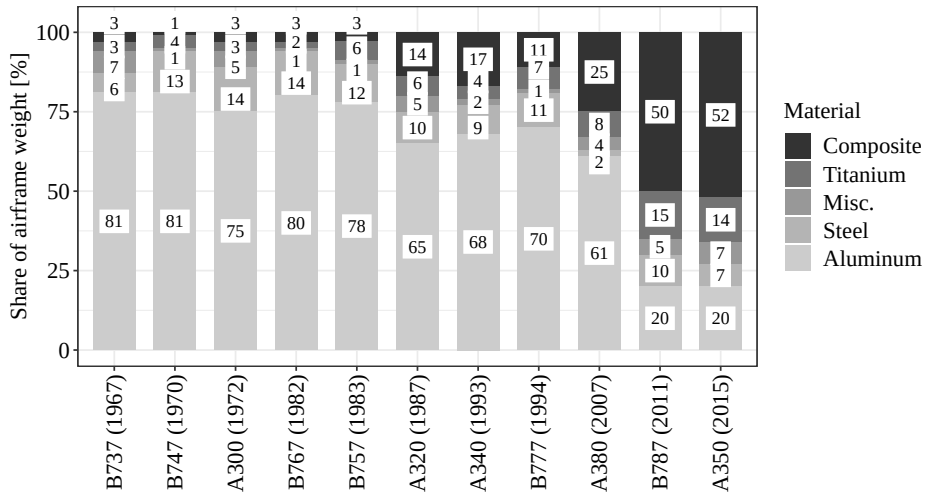

Figure 2.4: Airframe weight by materials for selected commercial aircraft sorted by year of entry into service, adapted from [54–57].

assuming the existence of barely visible impact damage (BVID), where damage growth under cyclic loading is not allowed [53, p. 458]. In the absence of fatigue considerations, the design of composites is driven by impact damage, specifically damage detectability and impact energy [52, p. 41].

Besides fatigue considerations, the choice of materials is influenced by *"yield and ultimate strength, stiffness, density, fracture toughness, creep, corrosion resistance, temperature limits, producibility, repairability, cost, and availability"* [41, p. 513]. Due to its excellent strength-to-weight ratio, moderate cost, and resistance to chemical corrosion, aluminum remains an appropriate material, even though the number of alternatives is increasing [41, p. 518, 44, p. 29]. Relying only on a "single material for the complete fuselage would result in a non-optimized structure" [44, p. 5]. Further, steel, titanium, magnesium, and high-temperature nickel alloys have widespread application [41, p. 519–525]. Next to metal alloys, the share of composite materials in commercial aviation has increased significantly in the last two decades, as illustrated in Figure 2.4. Further differences between metal alloys and composite materials are discussed extensively in [10, 38, 52, 53].

With all commercial aircraft being subject to similar design processes, the airframe architectures of different aircraft models are also alike. Figure 2.5 illustrates the Airbus A320 airframe as a representative commercial transport category aircraft, consisting of a fuselage, wing, stabilizers, nacelle, and undercarriage. The wing is generally made up of spars, ribs, stringers and external skin [10, p. 247]. The fuselage is a semi-monocoque design made of "longitudinal elements (longerons and stringers), traverse elements (frames and bulkheads) and ... external skin" [10, p. 376]. For safe operation of the airframe, inspection and maintenance procedures are in place, as summarized in the following section.

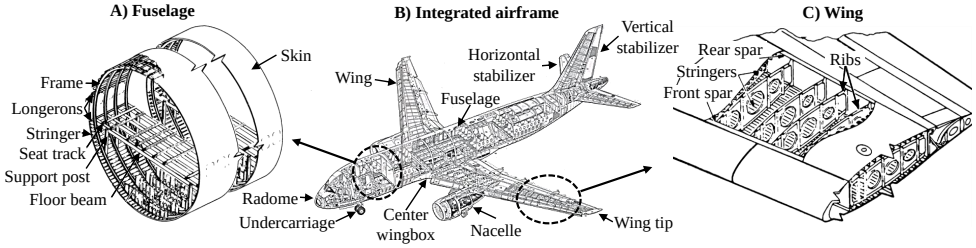

Figure 2.5: Typical architecture of airframes, adapted from [58, 10, p. 247&376].

2.1.2 Structural Integrity During Operation

During operation, an aircraft is subject to environmental deterioration, accidental damage, and fatigue [59, pp. 23-24]. As a result, regular maintenance, consisting of inspections and repairs, is conducted such that the aircraft continuously "*performs its intended function at its designed-in level of reliability and safety*" [59, p. 35].

The organization of maintenance in aviation has changed over time. In the beginning, experienced mechanics carried out maintenance at their discretion, and then structured maintenance programs set up by engineers emerged in the 1950s [60, p. 115]. Today, maintenance in commercial aviation follows a preventive and task-oriented approach to avoid in-service failures [59, p. 15]. The standardized process to derive individual maintenance tasks, including the involved stakeholders, documents, and content, is illustrated in Figure 2.6.

The scope, type, and frequency of maintenance measures are suggested by maintenance groups, which are supervised in parallel by the industry steering committee (ISC) and maintenance review board (MRB) [60, p. 114]. The ISC represents the aircraft manufacturer, suppliers, airlines, and maintenance experts. The MRB is composed of national aviation authorities (NAAs), which, in turn, are responsible for approving the maintenance review board report (MRBR) [60, p. 114]. To define the individual maintenance tasks, *"the aircraft is divided into zones, structural components and systems"* [60, p. 115]. Subsequently, a maintenance steering group (MSG)-3 analysis[1] is performed on every considered component of the aircraft. The MSG-3 analysis is a procedure used to define inspection intensity, required testing, tools, and maintenance measures for every part of the aircraft, based on the FMEA performed during the design process [60, p. 115]. The resulting MRBR specifies the minimum requirements for maintenance and generally serves as a guideline for creating a maintenance program [60, p. 114]. As an extension of the MRBR, the maintenance planning document (MPD) also contains time requirements necessary to schedule inspections and includes a description of the scope of work [60, p. 117]. To further consider individual aspects of operators that may not be addressed in the MRBR or MPD, each operator derives a maintenance program (MP) unique to the operated aircraft [60, p. 119]. Based on the required inspection frequency specified in the MPD, individual maintenance events can be scheduled with the aim of minimizing cost. To provide guidance in procuring the necessary capabilities during

[1] Compare Section 2.1.2.

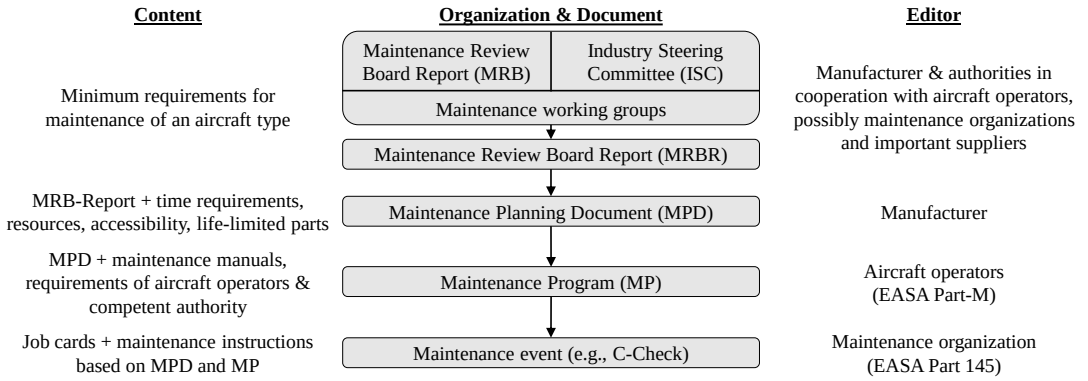

Figure 2.6: Organization, documentation, content, and editors involved in the definition of maintenance tasks, adapted from [60, p. 118].

maintenance, the MPD categorizes inspections of the airframe by skill and task codes. A summary of all defined skill and task codes is provided in Appendix A.1.

Airframe inspections are conducted with either non-standardized, using the unaided eye of an inspector, or standardized NDT procedures, depending on the component material and location within the aircraft [61]. The detectability of impact damage, fatigue cracks, and corrosion varies by inspection method [62, p. 226]. Even though visual inspections are inexpensive and comparatively fast, the detection of minor damage may require the use of NDT methods. The most widely used inspection methods are summarized in Appendix A.2.

With the high degree of regulation and standardization within the aviation industry, the maintenance organizations responsible for implementing the previously outlined maintenance processes are structured similarly in practice [60, p. 198]. As illustrated in Figure 2.7, they generally fulfill five core functions: production planning and engineering, aircraft maintenance, component maintenance, logistics, and quality management [60, p. 197]. As part of planning and engineering, aircraft-specific MPs are managed, task preparation and scheduling are conducted, and airworthiness directives (ADs) and service bulletins (SBs) are implemented [60, p. 198]. Aircraft maintenance can be divided into line maintenance, which *"neither requires extensive disassembly, nor complex functional testing"* and base maintenance, which covers events that require a *"high degree of detail or extensive disassembling"* [60, p. 201,208]. While significant maintenance is conducted directly on the aircraft, component maintenance is performed outside of the aircraft on removable parts, such as engines, landing gear, hydraulic pumps, navigational instruments, galleys, seats, and on-board toilets [60, p. 213]. Further, logistics is responsible for providing sufficient equipment and spare parts. Finally, quality management, as partially required by the NAAs, assures that all maintenance activities are performed as intended under controlled conditions [60, p. 191]. Comprehensive summaries of aircraft maintenance with a perspective on both the Federal Aviation Administration (FAA) and the European Union Aviation Safety Agency (EASA), as well as an overview on NDT methods, are given in [59, 60, 62, 63].

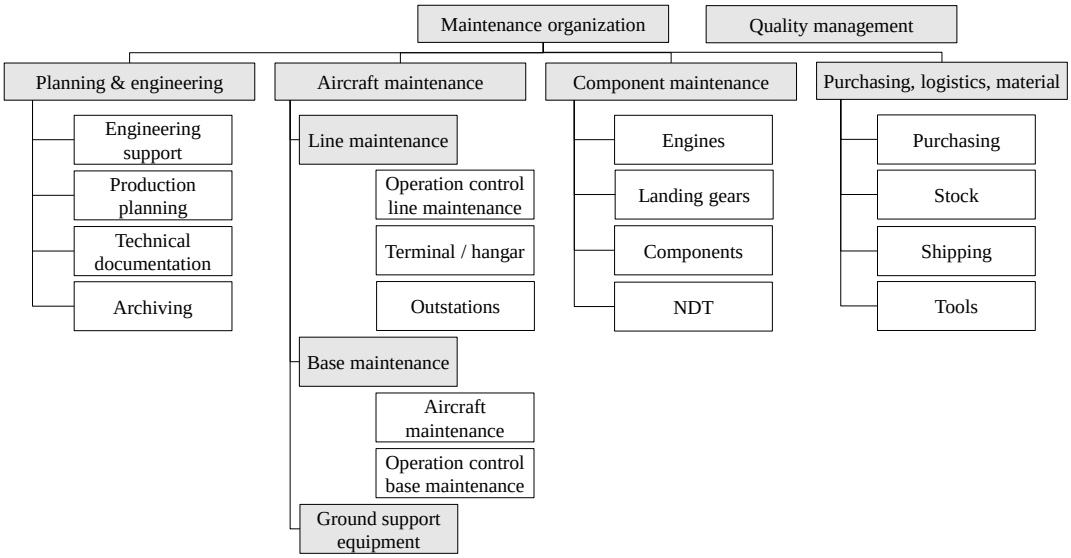

Figure 2.7: Generalized structure of an aircraft maintenance organization [60, p. 197].

2.1.3 Current Regulatory Framework

A summary of the current regulatory framework governing the operation of aircraft and SHM is provided in this section to describe the legal environment in which the presented techno-economic analysis is conducted.

As a specialized agency of the United Nations, the International Civil Aviation Organization (ICAO) is responsible for safe and efficient civil air traffic by means of standardization and regulation [60, p. 9]. ICAO standards and recommendations are translated into detailed aviation legislation on a national level by the NAAs [60, p. 9]. In the European Union, this responsibility is fulfilled by the EASA, and in the United States of America by the FAA[2]. They are responsible for attesting the airworthiness of aircraft, which is defined by the FAA as *"conform[ing] to its type design, and [being] in a condition for safe flight"* [64, 65, p. 1]. Airworthiness can be divided into initial airworthiness, where the product meets a safe and acceptable standard, and continued airworthiness, which covers procedures and rules for safe flight throughout operation [65, p. 1–2]. In this work, only commercial transport category airplanes subject to FAA federal aviation regulations (FAR) part 25 or EASA certification specifications (CS) 25, commonly referred to as part 25 aircraft, are considered [65, p. 6].

The legislation contained in part 25 and CS 25 generally covers the operational performance of the aircraft, airframe, control design, emergency provisions, propulsion systems, equipment for the use of flight crew members, limitations ensuring the safe operation, and electrical wiring [37, 50]. Further, the appendix of part 25 comprises additional instructions for continued airworthiness [37, 50]. Regarding the design and operation of SHM systems, the following excerpts from part 25 and CS 25 are noteworthy:

[2]In this work, only EASA and FAA guidelines are considered.

- *"Strength requirements are specified in terms of limit loads (the maximum loads to be expected in service) and ultimate loads (limit loads multiplied by prescribed factors of safety)..."* [37, 50, §25.301].
- *"Unless otherwise specified, a factor of safety of 1.5 must be applied to the prescribed limit load which are considered external loads on the structure..."* [37, 50, §25.303].
- *"The structure must be able to support limit loads without detrimental permanent deformation..."* [37, 50, §25.305].
- *"Compliance with the strength and deformation requirements ... must be shown for each critical loading condition ..."* [37, 50, §25.307].
- *"An evaluation of the strength, detail design, and fabrication must show that catastrophic failure due to fatigue, corrosion, manufacturing defects, or accidental damage, will be avoided ... [I]nspections or other procedures must be established, ... to prevent catastrophic failure ... Inspection thresholds for the ... structure must be established based on crack growth analyses and/or tests .... [Further, the damage-tolerance] evaluation must include a determination of the probable locations and modes of damage due to fatigue, corrosion, or accidental damage. [A] limit of validity, [stated as a number of total accumulated flight cycles, flight hours, or both,] must be established ..., during which it is demonstrated that widespread fatigue damage will not occur in the airplane structure. ... [Additionally, the] airplane must be capable of successfully completing a flight during which likely structural damage occurs as a result of, (1) Impact with a 4-pound bird ..., (2) Uncontained fan blade impact; (3) Uncontained engine failure; or (4) Uncontained high energy rotating machinery failure."* [37, 50, §25.571].
- *"Means must be provided to allow inspection, [...] for continued airworthiness. ... Nondestructive inspection aids may be used to inspect structural elements where it is impracticable to provide means for direct visual inspection ..."* [37, 50, §25.611].
- *"The Instructions for Continued Airworthiness must contain [i.a.] [s]cheduling information for each part of the airplane and its engines,... [a]n inspection program that includes the frequency and extent of the inspections necessary [must be provided] ..."* [37, 50, Appendix H25].

These regulations are supplemented by non-binding guidance material (GM) and acceptable means of compliance (AMC), which provide recommendations and assure compliance within the regulatory framework if followed [60, p. 15].

Supplementary to the general regulatory framework, NAAs can issue ADs for specific aircraft types, when an *"unsafe condition exists in the product; and ... [t]he condition is likely to exist or develop in other products of the same type design"* [66, 39.5]. An overview of previously issued ADs for the Airbus A320 is provided in Figure 2.8, distinguished by the required type of work and the affected aircraft system. ADs containing instructions not assignable to a type of work are labeled *unclassified*. ADs not applicable to specific aircraft systems

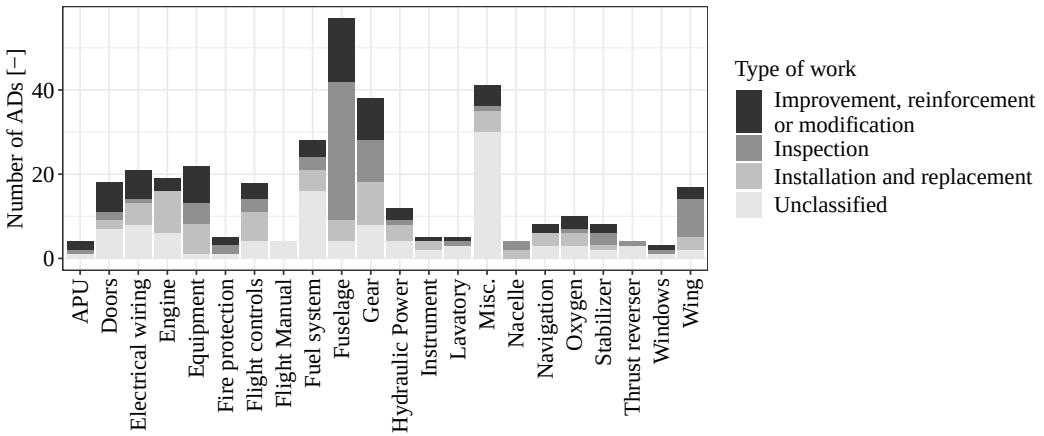

Figure 2.8: Type of required work categorized by covered aircraft systems in ADs issued between 03-22-1989 and 10-14-2020 for Airbus A320 aircraft.

are categorized as *miscellaneous*. A total of 42 ADs[3] have been issued for the wing or fuselage, specifically requiring only an inspection, beyond the requirements already defined in the MPD. While further ADs have been issued for the wing and fuselage, they require the improvement, reinforcement, modification replacement, or installation of a part.

Next to the existing general regulatory framework, guidelines have been developed specifically to address the integration of SHM into commercial aviation. For fixed-wing aircraft, the ISC on "structural health" (compare Figure 2.6) released “Guidelines for Implementation of Structural Health Monitoring on Fixed Wing Aircraft“ under the standard ARP6461 in 2013, which provides a structured overview on essential aspects of SHM, including operational considerations, system design challenges, validation approaches, test procedures, and certification requirements [40]. The guidelines also cover the qualitative effects of SHM on airframe design and maintenance procedures [40]. Since August 2021, an updated version of ARP6461 has been published with minor modifications under ARP6461A [67]. Notably, processes for the regulatory integration of SHM capabilities into the MSG-3 process and requirements for their technological qualification are refined. Additionally, the integration of SHM in the MRBR and MPD is included as an alternative inspection method, which has been regulated since Revision 2009.1 of the MSG-3 logic [40, 68]. Finally, the release of *Guidance for assessing the Damage Detection Capability of Structural Health Monitoring Systems* has been planned since September 2018 but has yet to be published [69].

2.1.4 Representing Continuing Airworthiness in Financial Accounting

The continuous airworthiness requirements not only impact the design and operation of aircraft but also affect airline finances. Selected aspects of financial accounting are summarized in this section to provide a basis for the cost-benefit study of SHM presented in this work.

[3]Superseded ADs are not included.

This includes brief remarks on *accounting systems*, the *classification of airline cost*, the *representation of continuing airworthiness efforts in airline cost*, and the *dependency between maintenance and delay count*.

Accounting systems are in place to measure the success of a business and its driving factors by tracking the in- and outflow of value beyond the organization over time [70, pp. 1–12]. In order to communicate the success of a business with respective stakeholders, various financial statements are produced [70, p. 1–12]. However, significant differences between these statements are prevalent, resulting from variations in accounting rules and reporting objectives [71]. Legislation on the recognition and measurement of assets, losses, provisions, and taxes can vary internationally, rendering the reconstruction of company profit mechanisms and cost drivers from publicly released statements difficult [71, p. 12]. Furthermore, the structure of the reported cost breakdown into individual cost objects changes with the reporting objectives [72, p. 100]. For airlines, a cost breakdown can serve as a general management and accounting tool to show temporal trends, cost efficiency, and operating profits or losses [72, p. 100]. Additionally, cost breakdowns are also used to evaluate investments in new aircraft, routes, and services and the "development of pricing policies and pricing decisions" [72, p. 100]. However, no single categorization or breakdown of cost can satisfy all purposes, leading to the need for different reports and cost breakdowns, which are not necessarily mutually translatable [72, p. 100]. Therefore, selected standard practices for the aviation industry are promoted by the ICAO and adopted by most airlines [72, p. 101].

In general, a *classification of airline cost* can be made based on operating and non-operating costs, which can be broken down into direct and indirect costs [72]. Operating costs are incurred during the provision of air transport services [72]. Non-operating costs result from activities not directly connected to airline operations, such as gains and losses from equipment sales, interest on loans for equipment, and government subsidies [72, p. 101]. Direct cost can be specifically and exclusively traced to a particular cost object, whereas indirect cost occur as overhead [73, p. 45]. In the absence of direct tracing, cost allocations can be used to attribute indirect cost to individual cost objects [73, p. 45]. Different cost allocation methods exist [73, p. 45]. The allocation can be conducted based on the knowledge of cause and effect, or the allocation is entirely arbitrary when cause and effect are unknown or complex [73, p. 45]. Arbitrary allocations bear the risk of a marginal change in production not yielding the expected change in the cost object [73, p. 45]. The different cost allocation methods are illustrated in Figure 2.9.

In aviation, the direct operating cost (DOC)s, which make up the largest share of operating costs, include expenses for flight operations, maintenance, overhead, depreciation, and amortization [72, p. 104]. Indirect operating costs (IOCs), on the other hand, include expenses for station and ground handling, passenger service, ticketing, sales, promotion, general administration, and other operating costs [72, p. 104]. Both DOC and IOC can be further divided into fixed costs, resulting from long-term commitments, and variable costs, which are directly escapable in the short run [72, p. 114]. When analyzing the performance of individual airline functions, the different types of cost can be allocated to individual cost objects or activities to identify cost drivers and the organizational units of origin [73].

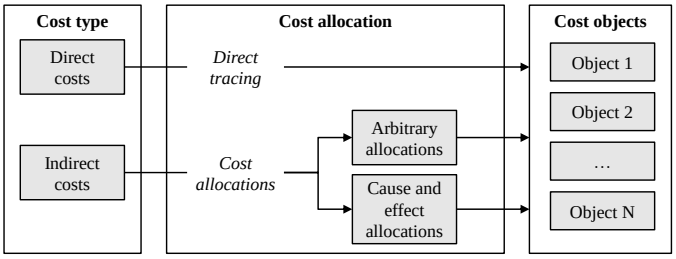

Figure 2.9: Cost allocation methods adapted from [74, p. 24, 73, p. 45].

Regarding the *representation of cost for continuing airworthiness*, the correct allocation of cost to individual cost objects presents a unique challenge. In practice, many joint costs occur simultaneously in separate areas of the maintenance process [72, pp. 105–106]. The way aircraft maintenance costs are broken down at most airlines generally follows the structure of maintenance organizations illustrated in Figure 2.7. Aircraft and component maintenance typically make up the direct maintenance costs, while the indirect costs consist of the expenses for planning, engineering, purchasing, logistics, material, and quality management.

Additionally, *maintenance strategies* can influence the magnitude and location, to which organizational unit of the airline maintenance cost are allocated. As aircraft components wear out, airlines must decide between corrective maintenance and preventive maintenance as a general strategy. Corrective maintenance includes the restoration or replacement of failed components. While this approach guarantees the usage of the entire component lifetime, component failures during operation cause delays, resulting in opportunity cost and additional expenses (e.g., for passenger compensation). Furthermore, the unexpected failures of components impact the safety of the aircraft. On the other hand, preventive maintenance aims for component upkeep before a failure occurs. While this approach avoids opportunity costs due to unscheduled repairs and improves safety, the component lifetime is usually not consumed, thus causing additional expenses over the aircraft's lifetime. Additionally, airlines can minimize unexpected breakdown costs by insuring themselves through the provision of spare aircraft or the scheduling of additional turnaround times. Therefore, airlines can influence where maintenance-associated costs appear within the organization. However, the overall goal is to minimize the total breakdown costs as well as the cost for minimizing breakdown costs [74, p. 24, 75]. This trade-off and the different maintenance approaches for the airline are illustrated in Figure 2.10.

2.2 Prospects of On-board Structural Health Monitoring Systems

SHM systems have been suggested for a variety of applications on commercial aircraft to facilitate regulatory compliance and decrease operational cost. The following sub-sections provide a compendium of direct and indirect benefits theoretically resulting from the implementation of SHM. This includes the possibility of deferred aircraft decommissions, improved inspec-

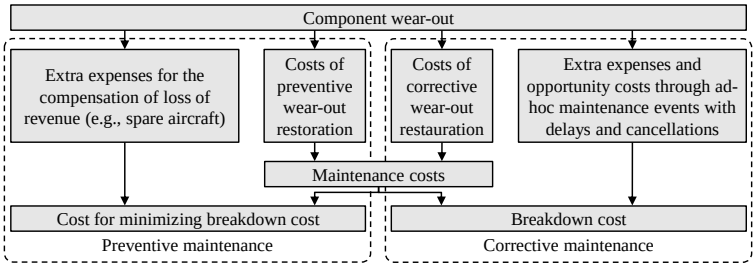

Figure 2.10: Cost of selected airline maintenance strategies and followup cost, adapted from [74, p. 24, 75].

tion and maintenance, improved flight scheduling, and weight savings in airframe design. Section 2.2 is solely dedicated to describing the upside potential of SHM, considerations about the technical feasibility and previous cost-benefit analyses are covered in Section 2.3 and Section 2.4.

2.2.1 Deferred Decommissioning

The lifetime of a damage-tolerant airframe is limited by the LoV, "*stated as a number of total accumulated flight cycles or flight hours or both,*" which limits the operation of the airframe in a way "*that widespread fatigue damage will not occur in the airplane structure*" [§25.571 37, 50]. The suitability of the defined LoV must be defined "*by full-scale fatigue test evidence*" [37, 50, §25.571]. Additional full-scale fatigue tests can be used to extend the LoV if WFD does not occur [51, pp. 1015–1016, 76]. An example of such an extension is the increased service goal of the Airbus A320, raised from 48,000 flight cycles (FCs) and 60,000 flight hours (FHs) to 60,000 FCs and 120,000 FHs [76, 77]. The increased service life is offered to customers for an additional cost and includes upgrades of selected components and structural parts [77].

"[It] is foreseen that SHM system[s] for operational monitoring may also play a role in defining and extending the LoV," which limits the useful life of airframes [69, p.16]. The definition of the LoV for an individual aircraft can thus be redefined as the level of fatigue rather than by the aircraft usage expressed in FC and FH, which drives fatigue. Therefore, the service limits arise from the usage history of the individual aircraft instead of the assumed fleet usage. A schematic illustration of this approach is provided in Figure 2.11.

Ultimately, increases in service lifetimes through SHM can be used in two ways, depending on the economic environment. (1) Ex ante, the increased service lifetime can enable additional revenue by operating the aircraft for a longer period. However, the aircraft's economic end of life should outlast its structural end of life. The economic end of life is defined by an alternative aircraft on the market whose sum of ownership costs and direct operating costs is lower than that of the current aircraft. The operating costs of new aircraft on the market, in turn, are driven by technological advancements, which may render the operation of aging aircraft uneconomical after a certain time. (2) If the aircraft's economic end of life is reached before its structural retirement, an increased structural lifetime is economically futile. However, ex

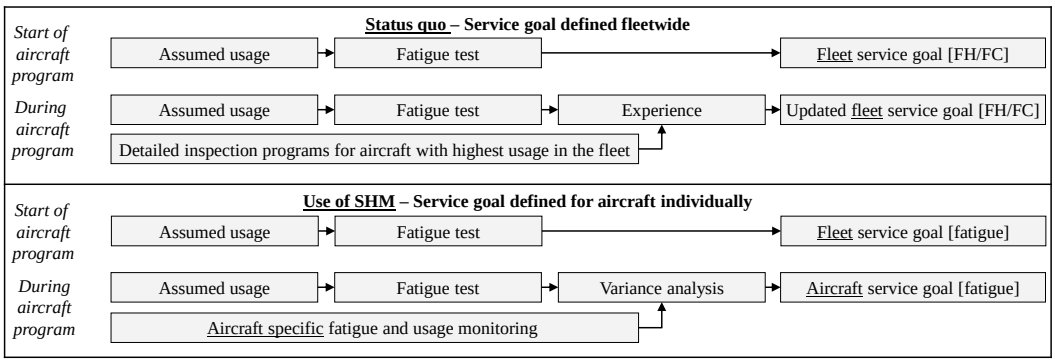

Figure 2.11: SHM can expand the current process used to define fleet service goals to individual aircraft level, thus enabling service goals defined for individual aircraft.

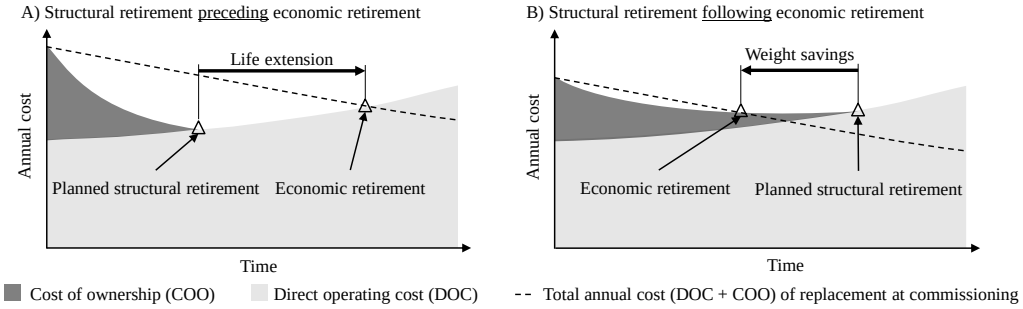

Figure 2.12: An increase in the certified structural lifetime can be used in two ways, depending on the time of economic and structural retirement of the aircraft. The economic retirement is defined as the point in time where the ownership and operating costs of the current aircraft exceed the cost of a new alternative aircraft on the market, which becomes more efficient over time. Adapted from [34].

post the gained excess in the structural lifetime can be decreased to match the economic lifetime by designing fatigue-prone parts less conservatively, i.e., lighter, and consequently save fuel over the operating lifetime. Both approaches are illustrated in Figure 2.12.

2.2.2 Improved Inspection and Maintenance

For damage-tolerant structures, *"[an] SHM technology capable of reliably detecting flaws of a specific nature and size over a specific line, area, or volume is a candidate alternative to conventional non-destructive evaluation such as visual, eddy current, ultrasonics, and X-rays inspections methods"* [40, p. 14]. As a consequence, aircraft servicing requires less time for the preparation and execution of manual inspections, *"yielding a lighter maintenance program for operators"* [40, p. 15]. More inspection process automation possibly reduces the variance in quality and thus results in better planning and scheduling of maintenance events at an airline level. Therefore, SHM can be an alternative inspection method in the MSG-3 process, which is used to derive the overall aircraft maintenance program [40, p. 22–24]. Depending on the utilized technological principles and mode of operation, SHM can influence the organization

and implementation of aircraft maintenance in numerous ways. The framework governing continued airworthiness is applicable to all operators equally.

However, inspections and maintenance in practice may differ, as described in Section 2.1.2. On the lowest organizational level, SHM can replace or modify existing inspection tasks. Depending on the degree of system autonomy, manual labor can either be supported or replaced [78]. Deficiencies of manual inspections due to poor eyesight, fatigue, differing damage interpretations, and work habits can be mitigated [78, 79]. Therefore, the documented damage description and classification can be standardized [78, 79]. Further, depending on the SHM system performance, the detectability of damages can improve [78]. Additionally, compliance with ADs requiring regular inspections may be fulfilled using SHM.

After replacing an inspection task with SHM, the provision of tooling, as well as required disassembly and subsequent assembly work, can be avoided. With less working time required for an inspection task, the critical path of the entire inspection may change. With a shorter duration of the overall critical path, the aircraft can resume service sooner, thus providing additional revenue opportunities. This decrease in total inspection time may also justify smaller maintenance facilities as fewer aircraft are simultaneously serviced, yielding additional cost savings. Finally, the procurement and stocking of spare parts may be optimized by investigating the structural state of the aircraft ahead of maintenance using the SHM system. Figure 2.13 illustrates the influence of SHM on the selected aspects of inspection and maintenance. Knowing the state of the aircraft ahead of the maintenance event also allows for a better clustering of tasks to be performed. Proactivity regarding a soon–to-fail part prevents redundant disassembly procedures at neighboring defects. Additionally, scheduling improves when the scope of necessary repairs is known ahead of an event.

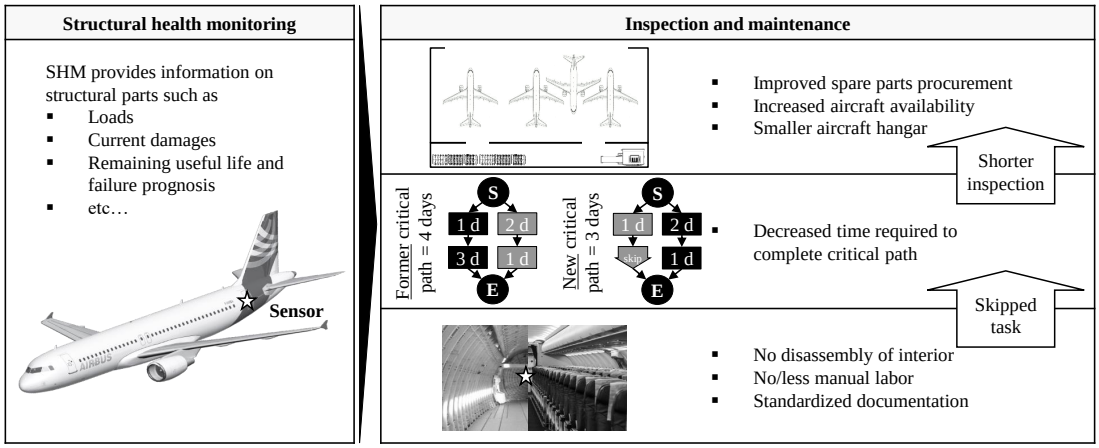

Figure 2.13: Benefit of SHM in aircraft inspection and maintenance.

2.2.3 Improved Airline Planning

This section outlines the airline planning process of medium to large airlines and highlights possible influences on SHM. Since the deregulation of aviation, most airlines are free to select

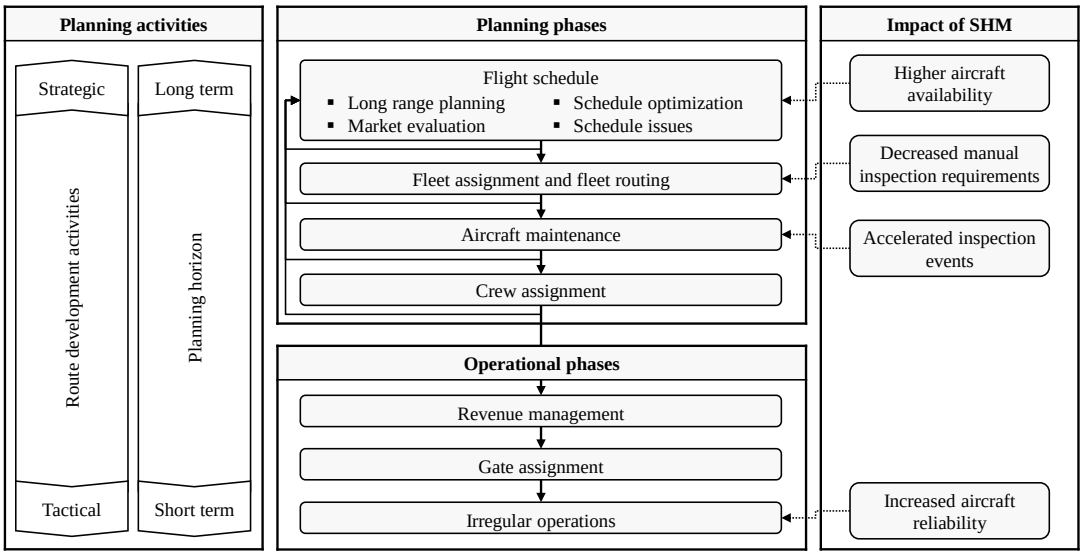

Figure 2.14: Planning phases in airline scheduling and possible impact of SHM, adapted from [80, p. 35].

networks, aircraft, prices, and schedules, operating in a market environment with a high level of competition [80, p. 1, 81, pp. 374–375]. To remain profitable, airlines rely on operations research throughout the airline planning process [80, pp. 1–2].

The first step in this process is the creation of a flight schedule, which depends on *"market demand forecasts, available aircraft operating characteristics, available manpower, regulations, and the behavior of competing airlines"* [80, p. 31]. The flight schedule design is an iterative process that may require extensive modifications to be operationally feasible and economically viable [80, 82, p. 31]. Airlines choose between a hub-and-spoke or point-to-point network structure, both being competitive in large markets [83]. Next, individual aircraft are assigned to the schedule such that the number of aircraft required to service the network is minimized [80]. Aircraft routing takes inspection and maintenance requirements into account [80]. In the final step of the planning phase, crews are assigned to individual aircraft [80].

During the operational phase, airline revenue management controls the price of available seats to maximize the revenue [80, p. 114]. Finally, airlines must deal with irregular operations resulting from *"mechanical problems, severe weather, crew sickness, airport curfews, and security"* on short notice [80, p. 151]. Some steps of the optimization problems are often combined, covering multiple optimization goals, e.g., minimum cost and maximum revenue [84, p. 17]. However, addressing all problems in a single optimization framework is challenging because of the computational complexity; hence, the investigated scenarios are limited [84, p. 17–19]. The airlines planning process is summarized in Figure 2.14 and sorted by planning time horizon.

SHM influences fleet assignment, aircraft maintenance, and the root causes for irregular operations if aircraft inspection requirements are changed. During the planning phase, reduced inspection requirements can result in fewer and shorter maintenance stops, allowing

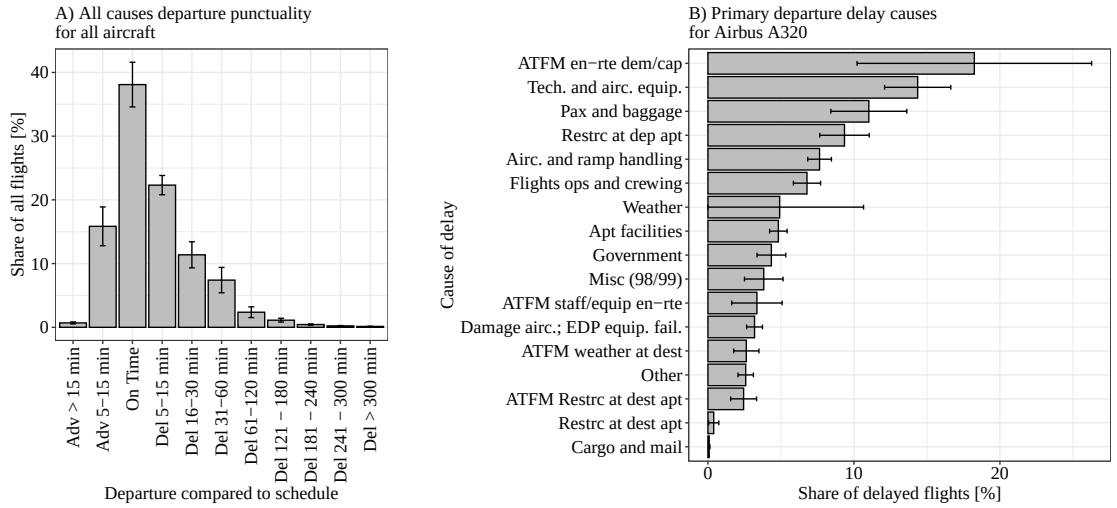

Figure 2.15: A) Departure punctuality of flights controlled by Eurocontrol in 2019 and B) primary departure delay causes for Airbus A320 controlled by Eurocontrol.

additional revenue-generating flights to be scheduled. In the operational phase, delays and cancellations due to unexpected structural damages can be mitigated through SHM. To this end, Figure 2.15 provides an overview of the most common causes for delays, in which most are connected to air traffic flow management (ATFM). Additional inspections at no cost allow for preventive checks at convenient times, e.g., a walkaround during an overnight stop, and decrease the chance of unexpected findings or sudden damage.

2.2.4 Weight Savings Potential in Airframe Design

Although the average fuel consumption per passenger-kilometer steadily has declined 1–3% annually since the 1960s, the cost of fuel still makes up 20–30% of all airline expenditures [85, p. 7]. Since fuel consumption and aircraft weight correlate, the airframe weight directly impacts airline operating costs. Depending on the aircraft, an incremental variation in aircraft operating weight by 1 kg changes the fuel burn of $4.5{\cdot}10^{-3}$ to $4.7{\cdot}10^{-2}$ kg/h for the average mission profile of airlines [86, pp. 7–8]. Hereby, a retrofit of a legacy aircraft is assumed without considering an aircraft resizing, which is required for constant payload-range performance. Both the share of total airline expenditure from fuel cost and the sensitivity of aircraft fuel consumption to incremental weight change are illustrated in Figure 2.16. Assuming a fuel price of USD 0.6 per kg, 1 kg of weight results in fuel cost of USD 840 to 970 over the lifetime of 60,000 FHs of an Airbus A320. According to [40, p. 14], *"[t]he use of SHM technology for inspection of inaccessible areas may yield a range of structural benefits including part count reduction [and] the potential for weight savings"* of designs currently optimized for accessibility. To integrate lighter airframes, SHM can be used in three different scopes:

On *(1) the component level*, SHM can be used to detect crack lengths in metallic structures that lead to fatigue [11, pp. 1342–1345]. The uncertainty in initial crack size, as well as

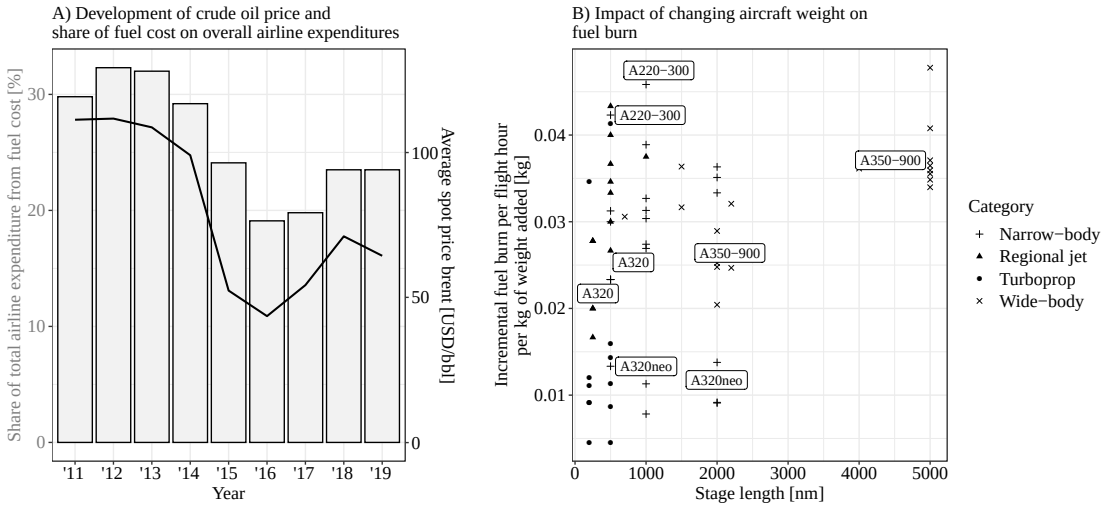

Figure 2.16: A) Share of airline expenditure from fuel cost (bars) and annual average Brent price (line), based on data from [92]. B) Influence of additional weight on increased fuel consumption for selected ranges and aircraft types, based on data from [86, pp. 7–8].

spectrum loading, requires conservative assumptions such that a single crack does not become critical during the specified inspection interval. The inspection intervals can be lengthened using NDT technologies capable of detecting microscopic cracks. On the other hand, the continuous surveillance of structures with SHM effectively increases the inspection frequency, thus allowing accelerated crack growth or reduced crack length uncertainty and, therefore, lighter structures. In addition, design requirements of parts prone to fatigue can be altered to assume less severe scenarios, resulting in lighter structures [87, p. 2]. Depending on the specific part and its location in the aircraft, this weight savings potential is limited based on other design requirements, such as for impact damages or limit loads.

On *(2) the assembly level*, the NAAs require aircraft manufacturers to design for inspectability [25.611 37, 50]. Without SHM, a design should be optimized for inspectability on a variety of parts, e.g., stringers [10, p. 142] and structural joints [10, p. 520], next to the integration of inspection cutouts (with doublers) [10, p. 162] and inspection doors [10, p. 259]. The convenience and necessity during inspection come at the price of increased structural complexity, leading to heavier parts. SHM provides the means to satisfy inspection requirements without requiring manual accessibility to all parts of the airframe. The airframe design can thus be optimized for weight without considering accessibility for structural inspections.

On *(3) the aircraft level*, onboard structural stress and strain analyses provide additional information to enhance aircraft control laws, moderating unwanted loading conditions [88, 89]. SHM provides the means to moderate the introduction of loads and observe experienced damages. The decrease in load spectra through active load alleviation for the operation of the aircraft allows for proportionally relaxed loading requirements during the design phase, thus enabling further weight savings [90, 91, p. 46].

2.3 Technological Approaches to Structural Health Monitoring

This section provides a summary of technological approaches for SHM in commercial aviation, defining the scope and scenarios of the cost-benefit analysis presented in Chapter 5 and Chapter 7. Additionally, selected applications of SHM in military aviation are discussed to demonstrate available and previously deployed technologies. A more comprehensive overview of SHM technologies is provided in [12] and the proceedings of the bi-annual *International Workshop on Structural Health Monitoring* [93–97]. Regardless of the technology used, the SHM process builds on four entities, namely the information source, diagnostics, prognostics, and system health management, as illustrated in Figure 2.17.

The process begins with the monitoring of the structure or *information source*, where structural actuation, structural response or both are recorded [98, p. 2]. Depending on the location within the aircraft, the prevailing damage types and thus applicable SHM technologies differ [40, p. 15]. SHM can be based on either the observation of a damage-dependent physical phenomenon, referred to as DM, or the analysis of structural loads to reconstruct the emergence of damages, referred to as OLM [40, p. 24–25]. Using this classification, four approaches to SHM are considered in this work—self-contained DM and self-contained OLM, which both require dedicated hardware, a combination of DM and OLM, and the adoption of existing information from available systems not installed for SHM.

Independent of the information-gathering tool used, the measurement data are subsequently processed during the *diagnostics* phase to identify the current structural state. During this step, data are compiled or aggregated using additional information sources. A comprehensive overview of approaches to information fusion on the data, feature, and decision levels is presented in [99]. Since the available SHM data depend on the monitored structure and the damage type, the implementation of these analytical approaches is beyond the scope of this thesis.

After the data analysis, SHM systems provide damage *prognostics*, using assumptions about future loads acting on the structure. This requires damage-behavior models based on physical laws or empiric observations.

Damage predictions provided by SHM and other health monitoring systems can be utilized within the overall *system health management* to improve the operational performance of the aircraft. Information about future structural failures can be used to improve repair and replacement decisions and thus the maintenance scheduling of the aircraft.

2.3.1 Damage Detection with Dedicated Sensor System

DM keeps track of the degradation of mechanic properties as a result of fatigue, corrosion, overload, or accidental damage from ground equipment impact or bird strike [40, pp. 21–22]. A sensor is installed at or near the monitored areas [40, pp. 21–22]. The DM systems use active or passive sensing [40]. Unlike passive approaches, which rely on ambient excitation of the

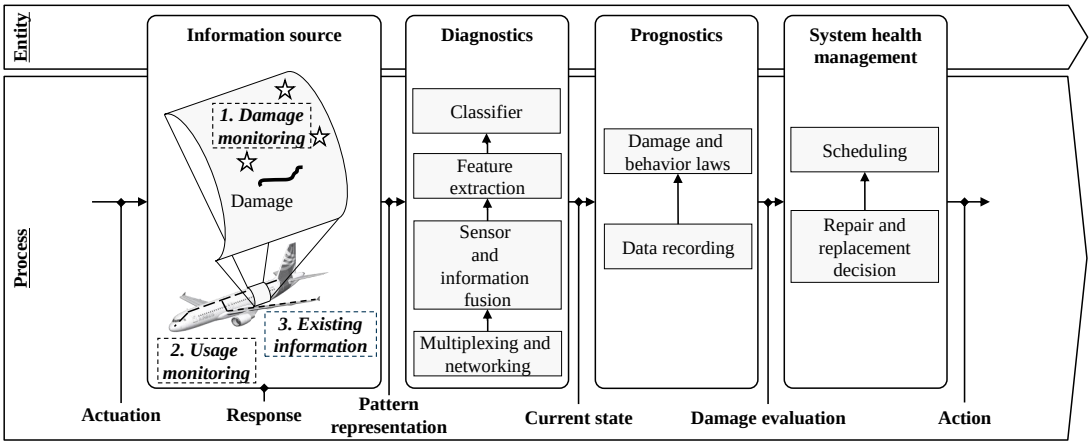

Figure 2.17: Process and organization of SHM, adapted from [98, p. 2, 100, p. 6, 40, p. 27].

structure, active sensing intentionally imparts energy to the structure to cause excitation and allow for measurements [101, 102]. The monitored physical phenomenon and data evaluation approach vary among technologies, as does their damage detection performance.

Several DM technologies are extensively discussed in the literature with varying degrees of technological readiness, including comparative vacuum monitoring (CVM), where open cracks are detected through a pressure drop between a series of steady-state vacuum volumes bounded to the structure [103, p. 3, 104, p. 4]. CVM sensors are certified by the FAA for particular NDT applications on Boeing aircraft, following a two-year test program with a small number of commercial airlines that started in 2005 [104, p. 4]. Eddy current testing foil sensors (ETFSs) monitor cracks and corrosion by tracking the interaction of defects with eddy current fields [105, p. 17]. ETFSs were tested for the use in the root joint area of the Airbus A380 in a full-scale fatigue test [106, p. 5–6, 107, p. 6]. Accoustic emission (AE) sensors record acoustic waves that are generated by structural events resulting from impacts, crack initiations, or crack growths [103, p. 3]. AE sensors were also used around the rear passenger doors and lower fuselage during the full-scale fatigue test of the Airbus A380 [106, pp. 5–6]. However, during commercial operation, signals from damage growth have to be distinguished from *"other high-frequency noise sources such as crack face rubbing, electromagnetic interference [...] and airframe structural noise due to inflight loads"* [104, p. 2].

Furthermore, acousto ultrasonics (AUs) and imaging ultrasonics (IUs) rely on sending and receiving ultrasonic pulses, where damage-dependent changes in reflected signals can be analyzed; both were tested during the full-scale fatigue test of the Airbus A380 [103, p. 3-6, 106, p. 5]. Crack wires (CWs), typically used during full-scale fatigue tests, rupture in the presence of cracks, as evaluated for the applicability of SHM during full-scale fatigue test of the Airbus A380 [106, pp. 5–6]. Additionally, CWs are currently used as a tail-strike indication system on the Airbus A340 and Airbus A380 [108].

Several fiber-optic sensors (FOSs) systems exist, with varying coverage areas and utilized physical principles [109, pp. 21–23]. FOSs used in aviation generally measure strain to infer

possible damage [109, p. 23]. One FOS system with extensive use in pilot studies and practical applications for SHM are Fiber Bragg-gratings (FBGs), which allow *"the measurement of strain at different places along a fiber using a single cable [...]. Typically, 10–50 gratings can be measured on a single fibre line"* [109, p. 23-26]. FBGs were used as part of an SHM system on the Airbus A340 in the rear pressure bulkhead [110, p. 4, 104, p. 6, 111]. Environmental degradation monitoring sensors (EDMSs) are *"multifunctional sensors capable of monitoring parameters such as temperature, humidity, time of wetness and pH. In conjunction with a corrosion model, corrosion prediction and detection [are] possible"* [103, p. 3]. An overview of sensor technologies is provided in Table 2.1. Depending on the expected damage, type of installation (factory-installed or retrofit during maintenance), position in the aircraft, and available onboard energy and data transmission infrastructure, the specific system weight and investment cost can vary [40].

Table 2.1: Applicability of selected technologies for damage monitoring and selected applications, expanded upon [112].

	CVM	**ETFS**	**AE**	**IU**	**CW**	**AU**	**FOS**	**EDMS**	**Source**
Detectable damages									
Cracks	■	□		□		□	□		
Ruptures	□			□	□	□			
Impacts			■				■		
Delamination			□	□		■	■		
Bond quality							■		
Bonded repair							■		
Debonding			□			□	■		
Corrosion	□							□	
Commercial applications									
Airbus A340							△		[104, p. 6]
Airbus A380	△	△	△	△	△	△			[107, p. 6, 106, pp. 5–6, 113, p. 10]
Boeing B767	△						△	△	[104, p. 2, 114, p. 16]
Boeing B757	△								[114, p. 16]
Douglas DC-9	△								[114, p. 16]
Military applications									
Lockheed F35							▲	▲	[115, pp. 5–6]
Lockheed C130			▲						[104, p. 1]
Northrop F5			▲						[104, p. 1]
Panavia Tornado			▲						[110, p. 5, 104, p. 1]

Legend: ■ good usage, □ limited usage, ▲ operational, △ field/full-scale fatigue tests

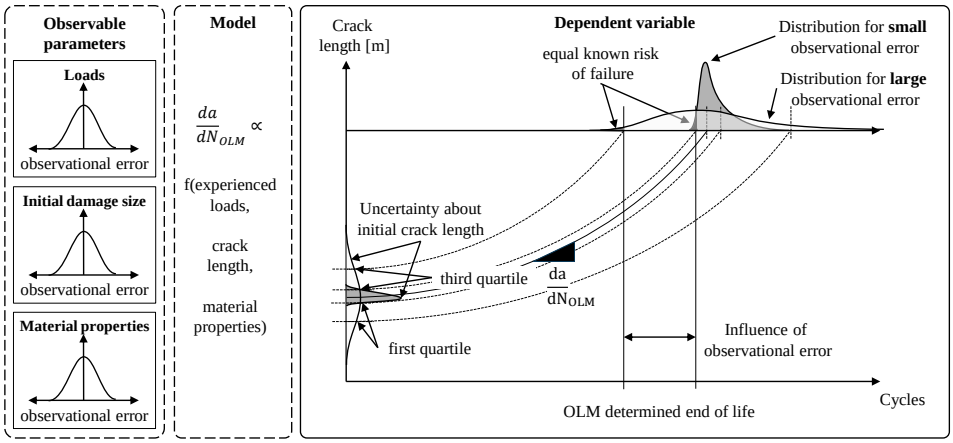

Figure 2.18: The derivation of both structural failure risk and thus structural end of life by means of OLM is highly dependent on the known distribution of fatigue model parameters.

2.3.2 Operational Load Monitoring

SHM systems based on OLM use *"sensors which do not directly check the structure for damage, but instead correlate various measurements (e.g., environmental conditions, [maneuver and gust] loads) to make an inference to the probability or likelihood of damage"* [40, p. 24]. The correlation between operational usage and damage is based on previous experiences, physical models, and full-scale fatigue tests [116]. The extent of the correlation depends on the observational error of the estimated damage-dependent parameter and the quality of the damage model [116]. Figure 2.18 illustrates this characteristic of OLM, using the example of crack growth in metallic structure. An assumption is that the structure has attained initial cracks through the manufacturing process before the aircraft enters into service [117, 118]. In metallic structures, the crack growth for a given load can subsequently be calculated, e.g. by using the Paris-Erdogan law, given the initial crack size, geometric properties of the part, and its material characteristics [117, 118]. A smaller distribution of measured input parameters yields better damage prediction and longer service for a structural part [117, 118].

Structural fatigue can be predicted with OLM by monitoring flight parameters or loads using accelerometers or strain gauges [119, pp. 5–6]. Flight parameters can be used to calculate loads, which in turn *"can be converted to stresses and strains at fatigue- critical locations using transfer functions either derived analytically or by numeric approaches such as finite element modeling"* [119, p. 5]. In addition, strain gauges installed in representative fatigue-critical areas can monitor loads [119, p. 5]. For DM, strain gauges are placed directly at hotspots to monitor damage-dependent strains (see Section 2.3.1). However, if a hotspot arises, the relation between loads, strains, and damages may change, impairing the simultaneous monitoring of loads and damage [119, p. 5].

In practice, OLM originated in the 1950s, when the United Kingdom Royal Air Force integrated accelerometers at the centers of gravity of fighter airplanes, counting the instances when loads exceeded a predefined threshold in order to calculate a flight or fatigue index

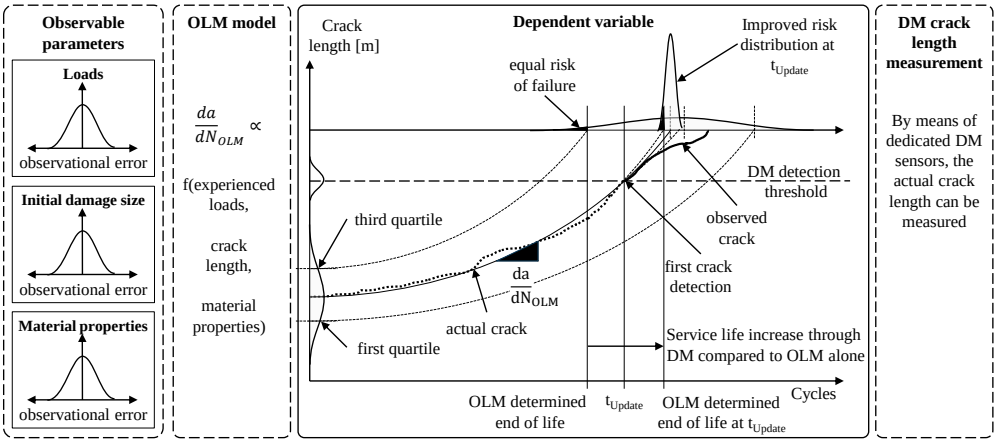

Figure 2.19: In hybrid SHM systems, OLM provides information about structural health for ensemble and DM can enhance this information for the individual aircraft or component in order to improve damage estimates.

[13, p. 4]. Later, the *"Panavia Tornado fighter airplane was possibly one of the first [aircraft] getting an operational loads monitoring system called onboard life monitoring system (OLMOS)"* [13, p. 6]. In addition to recording flight parameters, OLMOS also includes strain gauges to measure stresses or loads in fatigue-critical areas [120, p. 3, 110, p. 5–6]. *"To minimize the number of additional sensors to be implemented, OLMOS was mainly based on monitoring flight parameters only [...] with a few strain gauges [...] for verification"* [13, p. 7]. Furthermore, the CF-18 multi-role fighter introduced in the Canadian Forces in 1982 was equipped with strain gauges to monitor aircraft usage and accumulated fatigue damage [13, p. 7, 121, p. 1]. The gathered data indicated that the aircraft operated differently than assumed during design [121, p. 1]. Thus, they partially exceeded the certified load spectrum, leading to additional efforts in fatigue management and testing [121, p. 1]. Additionally, the Eurofighter Typhoon includes an SHM system that monitors aircraft usage information, significant structural events, and fatigue-life consumption based on flight parameters and strain gauge measurements [13, p. 7, 122, p. 1]. Finally, the F-35 Joint Strike Fighter has an advanced SHM system that records overloads, aircraft flight parameters, door usage, landing data, and environmental data for corrosion sensing [123, p. 8]. OLM in the F-35 uses parametric models that are continuously validated using strain sensors distributed in selected locations across the airframe [123, p. 9].

2.3.3 Hybrid Systems

Hybrid SHM systems are combinations of DM and OLM [119, p. 6]. DM can calibrate and validate fatigue damage analyses based on OLM [119, p. 15]. Various methods are used to combine information about structural health from DM and OLM, including sensor fusion, model-based reasoning, systems specific logic or rules, and feature extraction [123, p. 6]. As illustrated in Figure 2.19, DM can continuously improve the observational error of OLM transfer functions to calculate damages. The ensemble-based knowledge gained with OLM

about the structural state of a specific component can improve using information from DM. Vice versa, OLM can be used for plausibility checks of DM systems to identify possible false alarms.

Both the Eurofighter Typhoon and the F-35 Joint Strike Fighter use hybrid means of SHM [119, p. 15, 123, p. 6]. With data fusion approaches, information from DM and OLM systems can be combined in a single SHM system to improve monitoring performance [124]. For an unmanned aerial vehicle's main wing beam made of CFRP, damage detection capabilities were improved by combining data from in-flight autopilot telemetry and strain data from 20 FBGs using raw sensor data and feature-level data fusion techniques [124, p. 453]. Inversely, a single SHM system can be used to perform DM and OLM, as shown in [125], where an FBG is *"used simultaneously for both a strain-sensing-based load-monitoring system and a Lamb-wave-based damage-detection system"* [125, p. 453]. *"FBG sensors were used to record the load history of the test [...]. Piezoceramic transducers and the same FBG sensors that already monitored the load history were applied to record the Lamb-wave signals"* [125, p. 453]. With only one sensor and one sensor interrogation system, installation weight, size, and cost can be reduced [125, p. 460]. Generally, hybrid systems improve the monitoring performance of SHM systems while mitigating associated costs from false alarms, system weight or both.

2.3.4 Co-opt Existing Information

In addition to the use of dedicated SHM hardware, readily available information sources can be co-opted to gain insights into the state of the structure. Furthermore, hardware and software modifications to legacy aircraft systems enable dual use by extending their original functionality with SHM capabilities.

In practice, OLM systems of military aircraft make use of flight computer data for load estimation [115, p. 4, 110, pp. 3–5]. The Lockheed F35 uses the *"control surface deflections, [...] masses per station, individual fuel tank states, engine parameters, [...] weight-on-wheels, door positions [...]"* and more for SHM [115, p. 4]. Further suggested data sources for OLM include cameras currently intended as taxiing aids to measure the in-flight deformation of the wing, slats, and flaps [126, p. 545, 127]. Additionally, fuel sensors can expand load monitoring capabilities by considering the dynamic response of oscillating fuel in the tank [128, p. 63, 129, 130, 131].

Hardware can be adapted to unlock additional SHM potential. Coaxial or multimode graded-index fibers were suggested to bundle the role of FOSs and cabin illumination in one system [128, pp. 105–106]. While fibers had to be routed along a monitored structural area, the combination of functionalities might provide a weight benefit compared to separate systems. The dual usage approach is also suggested for fire protection sensors, which can be replaced with sensors detecting both heat and strain [128, pp. 107–108]. Furthermore, the onboard data and communication system can be modified to use fibers that transmit data and monitor pressure [132, p. 1]. The modified data cables can be rerouted to bypass damage-prone structural areas.

Table 2.2 provides an overview of locations on an Airbus A320 where co-opting of information may be used for SHM. However, the bundling of functionalities increases complexity and may influence system reliability, thus requiring an updated FMEA. Still, SHM systems relying on co-opted information may be lighter than dedicated monitoring equipment, thus improving overall aircraft weight and, hence, fuel cost.

2.4 Current Cost-benefit Analyses of Structural Health Monitoring

While a variety of SHM technologies are currently used in military aircraft, few airlines are pursuing the implementation of onboard SHM as part of pilot studies [134]. The absence of a widespread and rapid commercial adoption of SHM can be attributed to an unclear business case [20, p. 38, 21, p. 1]. Therefore, numerous studies investigating the profitability of SHM in commercial aviation have been presented. This section provides an overview of these studies, including results and employed methodologies. The considered studies are based on an analysis of 1836 peer-reviewed publications listed in the Scopus® database containing "structural health monitoring" and "aircraft" or "aviation" in the title, abstract, or keywords[4]. Together with articles reviewed in a previous literature study on the cost and benefit of SHM, 1865 unique articles were considered [34]. For a manual review of the identified literature, only articles that included either "economic," "cost," "benefit," or "competitive" in their keywords were considered, yielding 143 articles. An extensive in-depth study of the selected articles revealed that only 30 cover the financial cost and benefits of SHM. The remaining 113 articles do not consider cost or cover applications outside the aviation domain. Figure 2.20

[4]The search was conducted on November 24, 2020. The subjects medicine, biochemistry, sociology, arts, agriculture, and neurology were excluded from the results.

Table 2.2: Selected aircraft systems providing co-optable information for SHM.

Aircraft system	**Required modification**	**Provided data**	**Purpose**	**Ref.**
Flight mngmt. system	non to minor	Flight performance	OLM	[115, p. 7, 110, pp. 3–5]
Tail camera	non to minor	Images of wing	OLM	[126]
Proximity sensor	non to minor	Frequency patterns	DM	[128, p. 44, 133]
Fuel sensor	non to minor	Fuel oscillations	OLM	[129, 131, 130]
Cabin illumination	Modified fibers and installation	Strain data	DM	[128, pp. 105–107]
Data network	Modified fibers and installation	Strain and vibration	DM	[132]
Fire detection	Modified fibers and installation	Strain data	DM	[128, pp. 107–108]

illustrates the annual number of profitability-oriented SHM studies as a share of the entire surveyed literature.

The profitability-oriented studies relied on qualitative approaches in 16 publications and quantitative methods in only 14 publications. A qualitative statement about the profitability of SHM using a series of assumptions and arguments can be found in the following studies:

A description of how efforts in continuing airworthiness benefit from SHM and an overview of connected challenges for the aircraft manufacturer were provided in [135, 136]. While focusing on the qualification process of SHM, time and cost reductions during inspections were proposed by [137]. The same proposition as made by [138], studying sensor placement and design. In addition, improved inspections in areas difficult to access and extensions of aircraft lifetimes were proposed in a study covering new sensor technologies by [139]. [30] emphasized the benefits of SHM during maintenance and inspection through better logistics.

A novel solution for fatigue life estimation on general aviation aircraft was proposed and validated in [29], suggesting a decrease in inspection and maintenance cost. Decreasing inspection efforts were also proposed in [140]. [141] recommended implementation approaches and discussed the benefits of increased knowledge about structures on the cost-effectiveness of inspections, considering Bragg grating sensors for aircraft health monitoring. Additionally, the combination of SHM and augmented reality in aircraft inspections, including the connected efficiency gains, were outlined in [142]. The potential of OLM for improved cost-effectiveness of aircraft inspections using neural networks was shown in [143]. [144] discussed specifically tailored SHM systems provided by the manufacturer. Furthermore, decreased inspection requirements through SHM were demonstrated in [145] using a demonstrator. The use of SHM based on Lamb-waves for corrosion detection in aluminum alloys to decrease inspection requirements was covered in [146]. Finally, a general reduction of structural repair and inspection expenses was mentioned in [147], when using SHM in the overall aircraft health management.

However, quantitative studies considered in this section present diverging results regarding the profitability of SHM. Airframe weight and associated fuel cost vary between a 3% increase and a 15% decrease. The deviation in the influence of SHM on inspection cost is even greater,

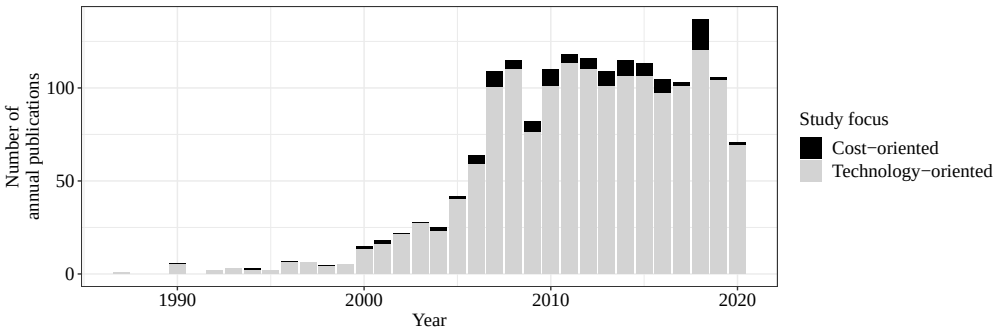

Figure 2.20: Peer-reviewed publications covering SHM in commercial aviation and share of studies considering financial profitability.

averaging from a 70% increase to an 83% decrease. The disparity of results can be attributed to the different scopes and considered SHM performances. Based on a simulation of the aircraft maintenance process in the software environment ARENA, the influence of SHM on the critical path of an aircraft inspection was studied in [148] (Figure 2.21,Bol 07). An automated airframe inspection using SHM was shown to not impact the critical path of the inspections and thus not decrease the overall duration of aircraft maintenance events [148] (Figure 2.21,Bol 07).

On the other hand, SHM enables condition based maintenance (CBM), allowing improved repair thresholds, which decrease the cost attributed to airframe maintenance [149] (Figure 2.21,Che 14). However, the savings depends on the scope of CBM [149] (Figure 2.21,Che 14). The same author additionally considered the impact of SHM on aircraft risk of failure in a different study, resulting in significantly reduced cost benefits enabled by SHM [150] (Figure 2.21,Che 14). A laboratory simulation investigating CBM of aircraft structures based on SHM as substitute for a single inspection task of military aircraft in the United States of America concluded that up to 79% of costs linked to aircraft downtime could be saved compared to regular scheduled inspections [22] (Figure 2.21,Der 16). Cost savings in structural inspections for commercial aircraft were also found for a Boeing 737 [31, 32] (Figure 2.21,Don 18).

However, when considering the increased cost of fuel and lost payload from additional SHM equipment weight, significant cost increases occurred for manual inspection tasks replaced by SHM [31, 32] (Figure 2.21,Don 18). Hereby, the location of SHM equipment within the aircraft and partial airframe coverage with built-in test equipment was not considered [31, 32] (Figure 2.21,Don 18). SHM as an enabler for CBM, which aimed to skip unnecessary structural inspections, was compared to regularly scheduled inspections considering the probability of fatigue, yielding cost savings for structural inspections in [26] (Figure 2.21,Pat 12). The effects of SHM on inspection accuracy and thus airframe design requirements and weight are investigated using a probabilistic failure model, demonstrating possibilities for structural weight savings in [25] (Figure 2.21,Pat 11).

Using a Paris-Erdogan crack growth model, a Monte Carlo simulation showed that progressive structural inspections based on SHM were 50% more cost effective than scheduled inspections [24] (Figure 2.21,Pat 10)[5]. Using a risk assessment, SHM was shown to reduce the structural inspection and maintenance costs of airframes by 30% without considering weight [151] (Figure 2.21,Sun 18). While maintaining the airframe safety level, SHM enabled a cost-driven predictive maintenance policy to significantly reduce structural inspection cost [27] (Figure 2.21,Wan 17). Without considering the impact of SHM equipment on airframe weight, the inspection cost improvements were up to 67% on the fleet level [27] (Figure 2.21,Wan 17). A subsequently updated study by the same authors found cost savings of up to 83% [28] (Figure 2.21,Wan 18). The conclusions on the profitability of SHM from both quantitative and qualitative studies are summarized in Figure 2.21.

[5]The quantified cost benefit of SHM presented by the author decreased steadily with three consecutive publications from 50% to 5%.

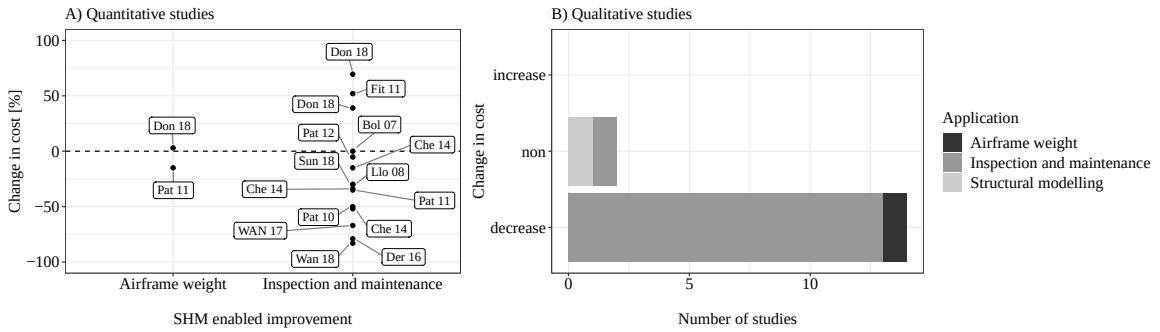

Figure 2.21: Proposed impact of SHM on aircraft life-cycle cost by application and type of study. A list of references is provided in Appendix A.3.

Depending on the consideration for airframe safety, weight, maintenance scheduling approaches, and study scope, ranging from a single part to the whole aircraft to entire fleets, the results of cost-benefit studies vary significantly. Hereby, current studies specifically failed to address the implications of other onboard systems besides the airframe, when addressing the overall maintenance scheduling of the aircraft. Furthermore, operational drawbacks resulting from SHM equipment weight, such as reduced payload and increased fuel burn, were only considered in studies instrumenting the entire airframe with SHM [31, 32]. Trade-offs enabled by only instrumenting parts of the airframe with high area-specific inspection requirements were not considered. Additionally, estimates of the cost of payload reductions resulting from SHM equipment weight did not account for the difference between certified payloads, actually flown payloads, and passenger seat loads during operation. Therefore, possible synergies between unused payload capacity and decreased inspection effort were neglected. Moreover, most studies considered SHM and the airframe separately from the rest of the aircraft. Thus, the interference between the airframe and overall aircraft with regard to monitoring technology information sources and maintenance scheduling requirements was ignored when analyzing the financial impact of introducing SHM. Finally, SHM was evaluated only based on its cash flow impact, neglecting the cost of capital required for a holistic evaluation when treating the technology as an investment opportunity for an airline. Therefore, the techno-economic assessment methodology presented in Chapter 3 closes the aforementioned research gaps in the literature by assessing previously isolated investigated aspects of SHM in an integrated framework to better estimate its financial impact on commercial aviation.

Chapter 3

Methods

The methods for investigating the cost and benefit of SHM in commercial aviation are introduced in this chapter. The *aircraft simulation* incorporates models of structural fatigue, impact damages, system failures, maintenance requirements, aircraft decommissioning, fuel consumption, and SHM. Of note, aircraft maintenance records were not accessible for this thesis. In addition, approaches to calibrate the models are described. *Airline simulation* is discussed to investigate how the aircraft reliability influenced by SHM affects the overall airline reliability, given its network topology. Finally, a *cost model* is introduced to unify all investigated aircraft and network metrics into a single financial metric representing the overall profitability of SHM.

3.1 Aircraft Simulation

This section discusses the methodologies applied to simulate the operational life of an aircraft from entry into service until decommissioning. Wear and tear is considered in the form of structural fatigue, impact damage, and system failure. Generic models representing the performance of SHM systems are described, and an approach to model aircraft maintenance, repair and overhaul (MRO) is introduced. In order to estimate the impact of changes in aircraft weight due to improved design and SHM equipment mass, a simplified fuel model is provided. The systematization provided in the MPD divides the aircraft into individual positions. Each position reflects one small part of the aircraft. For example, the Airbus A320 considers 1048 unique positions. For positions included in the structural and zonal program, fatigue failures are simulated using the structural fatigue and damage model provided in the subsequent subsection.

Simulations of failures occurring in aircraft systems are based on mean time between failure (MTBF) rates. To satisfy continuing airworthiness requirements, the aircraft is subject to regular inspections that are scheduled to fulfill the requirements of every position provided in the MPD with maximum time efficiency. For structural components, SHM systems can alternatively provide information about the states of positions listed in the structural or zonal program of the MPD. Figure 3.1 provides an overview of the aircraft simulation methodology, covering the required inputs, utilized models, and outputs.

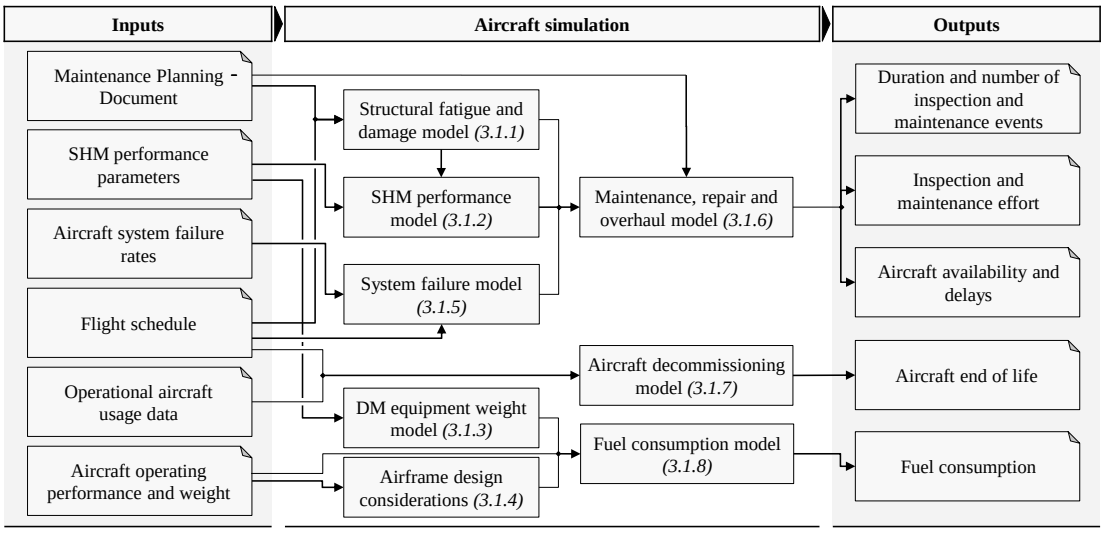

Figure 3.1: Structure of aircraft simulation framework including inputs, models, and outputs.

3.1.1 Structural Fatigue and Damage Model

The structural fatigue and damage model approximates the airframe fatigue for every position in the airframe using the inspection requirements provided in the MPD. The methodology is based on a previous conference publication in [34] and described in Subsection 3.1.1.1. Using the Paris-Erdogan law describing cracks in metallic structures, a single leading crack for every airframe position is calculated. Every structural component is assumed to have a crack initiated during manufacturing. Based on the inspection intervals provided in the MPD, the crack growth factors are calibrated individually for every position of the airframe, as described in Subsection 3.1.1.2. While this approach does not represent the exact fatigue behavior of every position of the aircraft, it provides a suitable coherence between inspection requirements, structural weight, and fatigue damage. The approach is validated by comparing calculated and actual structural fatigue damages over the aircraft lifetime derived from publicly available data on structural repair efforts and aircraft dispatch reliability in Section 4.4.

3.1.1.1 Crack Growth Model

The stress intensity factor indicates the intensity of the stress field in the apex of a structural crack and describes its severity [34, 152]. As described in [34] for metallic aircraft structures, the *"dependence of the stress intensity factor K on stress resulting from external loads, the crack length a as well as the dimensions of the loaded body can be put as follows*

$$K_I = \sigma\sqrt{\pi a} \cdot Y_I \tag{3.1}$$

$$K_{II} = \tau\sqrt{\pi a} \cdot Y_{II} \tag{3.2}$$

$$K_{III} = \tau_l \sqrt{\pi a} \cdot \sqrt{\frac{2b}{\pi a} tan \frac{\pi a}{2b}} \tag{3.3}$$

where σ is the axial stress, τ is the shear stress, τ_l is the stress orthogonal to the crack and the plane, 2b is the width of the specimen, Y_I and Y_{II} are parameters representing the geometry, type of loads and crack formation [...] [152]. The fracture mode I (opening) is of practical importance, since the resistance of the material against stress in mode I is generally lower compared to the resistance against stresses in mode II (in-plane shear) and mode III (out-of-plane shear) [153]. Numerical values for the [geometry factors] Y_I and Y_{II} can be derived using

$$Y_I = Y_{II} = \left(1 - 0.025 \cdot (\frac{a}{b})^2 + 0.06 \cdot (\frac{a}{b})^4\right) \cdot \sqrt{sec(\frac{\pi a}{2b})} \tag{3.4}$$

[154]. For mode I where the fracture toughness K_{I_c} depends on the material and its temperature as well as its loading frequency, the fracture criterion can be formulated as

$$K_I \leq K_{I_c} \tag{3.5}$$

[152]. K_{I_c} is generally determined by tests conducted in accordance with the norm American Society for Testing and Materials (ASTM) E399 [152]. For mixed mode loads, which rather correspond to real loading, the equivalent stress intensity factor K_V can be formulated for mode I and mode II crack growth as

$$K_V = \frac{K_I}{2} + \frac{1}{2}\sqrt{K_I^2 + 4 \cdot (\alpha_1 K_{II})^2} \leq K_{I_c} \tag{3.6}$$

where α_1 is a parameter to fit the criterion to the failure limit curve of different materials [152]. In practice α_1 can usually be assumed to equal 1.225 [152]. K_V can in turn be compared to the fracture toughness K_{I_c} for mode I [152]. Local mixed-mode-loading conditions at cracks can also occur as a combination of the three basic fracture modes where K_V can be formulated according to [155] as

$$K_V = \frac{K_I}{2} + \frac{1}{2}\sqrt{K_I^2 + 5.336 \cdot K_{II}^2 + 4 \cdot K_{III}^2}. \tag{3.7}$$

It is assumed that normal and shear stresses at a single critical location govern the fatigue life of a component [156]. [...] The stress intensity factors of the individual parts depend on the assumed leading crack growth mode, type of loading and resulting stresses. Table 3.1 outlines load sources and primary crack growth modes of considered standard aircraft parts [...].

The following stress intensity factors are based on [154]. Assuming flat metal sheets as aircraft parts, the stress intensity factors can be written as (3.1) to (3.3) as well as (3.6) and (3.7). For mixed mode I and mode II cracks the equivalent stress intensity factor can be written as

$$K_V = \frac{\sigma\sqrt{\pi a} \cdot Y_I}{2} + \frac{1}{2}\sqrt{(\sigma\sqrt{\pi a} \cdot Y_I)^2 + 6 \cdot (\tau\sqrt{\pi a} \cdot Y_{II})^2} \tag{3.8}$$

[...]. The stress in the frame is primarily a result of the varying cabin pressure and can be written as

$$\sigma_{ff} = \frac{p_{\Delta ff,\text{inf}} \cdot d_m}{2 \cdot s} \tag{3.9}$$

[157]. A seamless fuselage is assumed, where $p_{\Delta ff,\text{inf}}$ is the pressure differential between fuselage and environment, $d_m = d + s$ with d being the inner diameter and s being the thickness of the wall. For a longitudinal stringer, the stress can be formulated as

$$\sigma_{ls} = \frac{p_{\Delta ff,\text{inf}} \cdot d_m}{4 \cdot s} \tag{3.10}$$

and for the fuselage skin as

$$\sigma_{fs} = max \left\{ \begin{array}{c} \frac{p_{\Delta ff,\text{inf}} \cdot d_m}{2 \cdot s} \\ \frac{p_{\Delta ff,\text{inf}} \cdot d_m}{4 \cdot s} \end{array} \right\} \tag{3.11}$$

$$\tau_{fs} = \frac{|\sigma_1 - \sigma_2|}{2} \tag{3.12}$$

Table 3.1: Sources of loading and primary crack growth modes of principal structural components [34].

Part	**Assembly**	**Load sources**	**Crack growth modes**
Frame (ff)	Fuselage	Pressure difference and maneuvers	Mode I
Longitudinal stringer (ls)	Fuselage	Pressure difference and maneuvers	Mode I
Fuselage Skin (fs)	Fuselage	Pressure	Mode I + Mode II
Wing spar (ws)	Wing	Bending moments and aerodynamic loads	Mode I
Wing rib (wr)	Wing	Aerodynamic loads	Mode I
Wing skin (wsk)	Wing	Aerodynamic loads	Mode I + Mode II

where σ_1 is the maximum stress and σ_2 the minimum stress. The stresses in the wing spar and wing rib resulting from bending moments M_y can be formulated as

$$\sigma_{ws}(x,z) = \sigma_{wr}(x,z) = \frac{M_y(x)}{I_y(x)} \cdot z \tag{3.13}$$

with M_y being a result of the aircraft load carried by the wing, maneuver loads and gusts. I_y is the second moment of area. Normal and shear stress in the wing skin caused by aerodynamic forces can be formulated as

$$\sigma_{wsk} = \frac{F_{wsk}}{A_{wsk}} \tag{3.14}$$

$$\tau_{wsk} = \frac{T_{wsk}}{s} \tag{3.15}$$

[where] A_{wsk} represents the cross section of the wing skin, [F_{wsk} the force acting on the wing skin perpendicular to A_{wsk}], T_{wsk} the shear flow and s the material thickness [...]. Assuming a cycling loading condition, the time varying stress intensity factor for mode I cracks can be formulated as

$$K_I(t) = \sigma(t)\sqrt{\pi a} \cdot Y_I \tag{3.16}$$

and the maximum and minimum stress intensity factors $K_{I_{max}}$ and $K_{I_{min}}$ as

$$K_{I_{max}} = \sigma_{max}\sqrt{\pi a} \cdot Y_I \tag{3.17}$$

and

$$K_{I_{min}} = \sigma_{min}\sqrt{\pi a} \cdot Y_I. \tag{3.18}$$

For fatigue crack growth governed by cyclic stress, the stress intensity factors can be written as ΔK_I, ΔK_{II} and ΔK_{III}. For ΔK_I cyclic loading results in

$$\Delta K_I = K_{I_{max}} - K_{I_{min}} = \Delta\sigma\sqrt{\pi a} \cdot Y_I \tag{3.19}$$

and stress ratio R of

$$R = \frac{\sigma_{min}}{\sigma_{max}} = \frac{K_{I_{min}}}{K_{I_{max}}} \tag{3.20}$$

[152]. Fatigue loading with unstable crack growth occurs when the maximum stress intensity factor K_V reaches a critical value of K_C or K_{I_c} [152]. [...] [The stress intensity factor ΔK_I of all airframe components is assumed at $\Delta K_0 < \Delta K_I < \Delta K_c$ for the entire lifetime of the aircraft, where ΔK_0 describes the stress intensity threshold, below which no crack growth is

measurable. Therefore, the] crack growth per cycle can be described with reasonable accuracy by the Paris-Erdogan law

$$\frac{da}{dN} = C(\Delta K_I)^m \tag{3.21}$$

where m represents a material dependent parameter and C depends on the material and stress ratio R. [Assuming structural components are made out of Al 2024-T3, it can be approximated that m=3 [158].] For crack growth from the initial crack length a_0 to the critical crack length a_c, a specific number of load cycles N_C is required. [Using [153]], the remaining life can be calculated by using the Paris-Erdogan law

$$N_C = \int_{a_0}^{a_c} \frac{da}{C(\Delta K_I)^m} \tag{3.22}$$

which, assuming constant $\Delta\sigma$, Y_I and $m \neq 2$, results in

$$N_C = \frac{1}{(\frac{m}{2}-1)\cdot C\cdot(\Delta\sigma\sqrt{\pi}Y_I)^m}\cdot\left(\frac{1}{a_0^{\frac{m}{2}-1}} - \frac{1}{a_c^{\frac{m}{2}-1}}\right) \tag{3.23}$$

and for m=2 in

$$N_C = \frac{1}{C\cdot(\Delta\sigma\sqrt{\pi}Y_I)^2}\cdot ln\left(\frac{a_c}{a_0}\right)" \tag{3.24}$$

[34].

3.1.1.2 Crack Growth Factor Selection

To simulate the fatigue behavior of the airframe, the crack growth factors are calibrated using an approach presented in [34]: "*It is assumed that the MPD incorporates all information about the fatigue crack growth of the structure at [certified] design loads [...] and therefore assumes a crack growth curve at the maximum aircraft stresses [expected during an operation on the design mission. The calibrated crack length a is non-dimensionalized by scaling it with the critical crack length to $\hat{a}=\frac{a}{a_c}$, through dividing (3.23) by $a_c^{1-\frac{m}{2}}$. Then, material geometry and stress-dependent factors unknown for the structural parts within the aircraft can be summarized in a single crack growth factor $C\hat{G}F$ as following*

$$C\hat{G}F = \frac{C\cdot(\Delta\sigma\sqrt{\pi}Y_I)^m}{a_c^{1-\frac{m}{2}}}, \tag{3.25}$$

assuming C, $\Delta\sigma$ and Y to be constant. Using (3.23) the assumed material properties, cyclic stresses and geometry factor at 100% loading of a part can be determined by using

$$C\hat{G}F = \frac{1}{(\frac{m}{2}-1)N_C} \cdot \left(\frac{1}{\hat{a}_0^{\frac{m}{2}-1}} - \frac{1}{\hat{a}_c^{\frac{m}{2}-1}} \right) \tag{3.26}$$

where N_C is the number of cycles between $\hat{a}_0$ and $\hat{a}_c$, $\hat{a}_c = 100\%$ is the critical crack length and $\hat{a}_0$ the initial crack length, which is assumed to be 1% of the critical crack length. The initial crack length at entry into service $N = 0$ is given by

$$\hat{a}_0 = \left(\frac{1}{(N_c + T_i) \cdot (\frac{m}{2}-1) \cdot C\hat{G}F + 1} \right)^{\frac{1}{\frac{m}{2}-1}} \tag{3.27}$$

where T_i is the [inspection] threshold value provided in the MPD. Using (3.25) and substituting $\hat{a}_c$ with $\hat{a}_N$, the crack length $\hat{a}_N$ after N cycles can be written as follows

$$\hat{a}_N = \left(\frac{1}{\frac{1}{\hat{a}_0^{\frac{m}{2}-1}} - N \cdot (\frac{m}{2}-1) \cdot C\hat{G}F + 1} \right)^{\frac{1}{\frac{m}{2}-1}} \text{”} \tag{3.28}$$

[34]. Employing the formulated coherence for the individual aircraft parts, their crack growth curves depend on load deviations and changes in wall thickness as follows:

$$\left((\Delta\sigma\sqrt{\pi}Y_I)^m\right)_{adjusted} = \frac{\left((\Delta\sigma\sqrt{\pi}Y_I)^m\right)_{assumed}}{\left(\frac{loads_{100percent}}{loads_{occured}}\right)^m \cdot (1-\Delta s)^m} \tag{3.29}$$

where Δs is the percentage decrease in wall thickness . The influence on occurring stresses is independent of the crack growth mechanism in all investigated parts under the utilized assumptions. The percentage weight savings Δw in each part is assumed to be equal to the change in wall thickness:

$$\Delta w_{InvestigatedStructure} = w_{InvestigatedStructure} \cdot \Delta s. \tag{3.30}$$

This approach does not take sizing limits presented by other failure modes besides structural fatigue, such as buckling, into account. The cockpit section, as well as nuts, bolts, door frames, and non-primary structural components, is not investigated within this work [34].

3.1.1.3 Structural Fatigue Damage Probability

As described in Section 2.1, an airframe is subject to a non-deterministic load spectrum throughout its operational lifetime. As a result, cracks inherent to the structure grow and continuously reduce its strength. The crack length, remaining strength, and rupture load of a component depend, among other factors, on material properties, geometry, and temperature

[159, pp. 1159–1385]. Given the complexity of the structural fatigue problem, a damage definition relying on multiple nominal-actual comparisons is unpractical for the work at hand. Therefore, structural components degrade until they are considered critically damaged when their principal crack length is equal to or greater than the critical crack length a_c. Thus, the crack length $\hat{a}_c$ at which a failure occurs is defined as

$$\hat{a}_c = 100\%. \tag{3.31}$$

Based on the results from full-scale fatigue tests and analytical methods, the relation between initial crack length, crack growth, and loads are known. However, during the manufacturing process, initial flaws can be detected reliably only up to a certain size, leaving undetected micro cracks in the structure. While selected NDT approaches can measure even smaller cracks, only a distribution of initial crack lengths is known for individual structures of the airframe. In this work, a normal distribution of the initial crack length is assumed. The standard deviation of the initial crack length distribution $\hat{\sigma}_{a_0}$ is arbitrarily assumed as

$$\hat{\sigma}_{a_0} = \hat{\mu}^{\frac{1}{4}}, \tag{3.32}$$

where $\hat{\mu}= \hat{a_o}$ is the mean of the distribution. Assuming the probability density function of $\varphi(\hat{a_0})$ as normally distributed, it can be written as

$$\varphi(\hat{a}_0) = \frac{1}{\sigma_{a_0} \cdot \sqrt{2\pi}} \cdot e^{-\frac{1}{2}\left(\frac{\hat{a}-\hat{\mu}}{\sigma_{\hat{a}_0}}\right)^2}. \tag{3.33}$$

Substituting the initial crack size in 3.28 with $\varphi(\hat{a}_0)$, the probability of a damaged structure after N cycles is given by

$$P\left(\hat{a}_c(N)\right) = \int_1^{\infty} \left(\frac{1}{\frac{1}{\left(\frac{1}{\sigma_{a_0}\cdot\sqrt{2\pi}} \cdot e^{-\frac{1}{2}\left(\frac{\hat{a}-\hat{\mu}}{\sigma_{\hat{a}_0}}\right)^2}\right)^{\frac{m}{2}-1}} - N \cdot \left(\frac{m}{2}-1\right) \cdot C\hat{G}F + 1} \right)^{\frac{1}{\frac{m}{2}-1}} d\hat{a}. \tag{3.34}$$

3.1.1.4 Structural Fatigue and Damage Model Calibration

To calculate the fatigue of the investigated airframe components, the crack growth parameters are calibrated using the information about the inspection intervals for structural components provided in the MPD. Specifically, the MPD contains threshold limits, including the flight cycles, flight hours, or calendar time until the first inspection, and interval limits, including the flight cycles, flight hours, or calendar time between every subsequent inspection. It

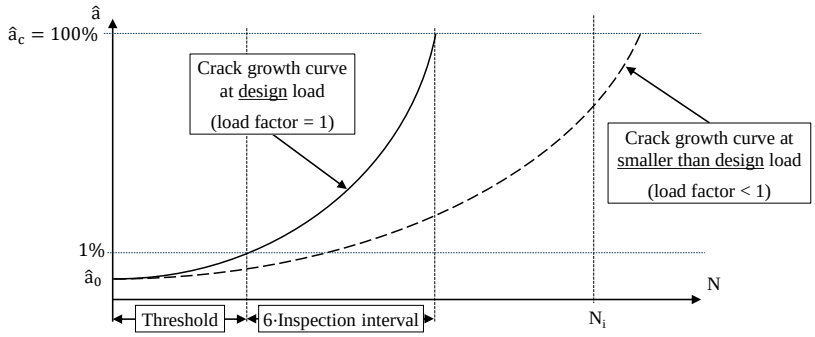

Figure 3.2: Schematic illustration of crack growth factor calibration at design loads.

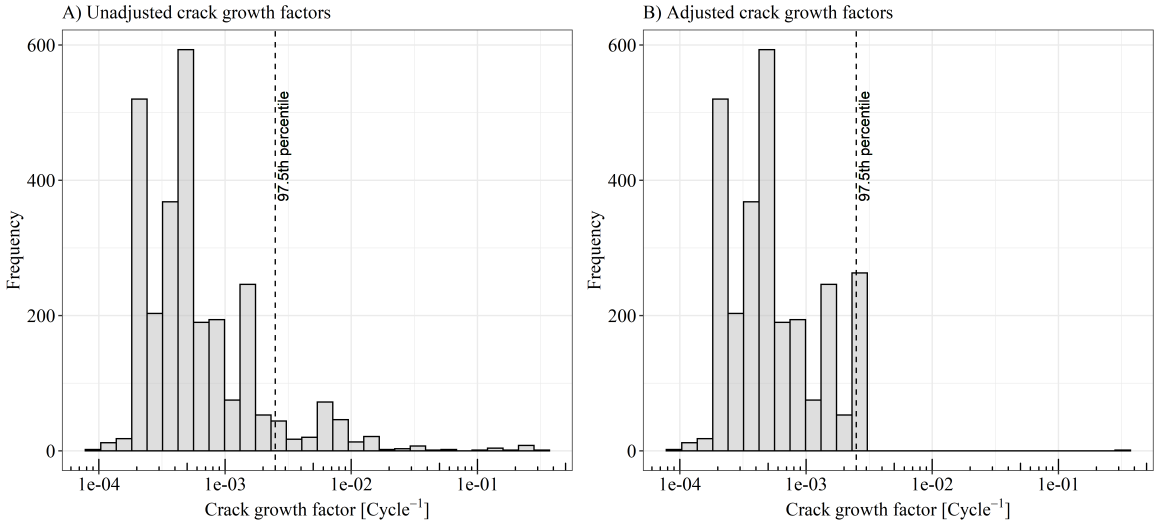

Figure 3.3: A) Distribution of crack growth factors $C\hat{G}F$ derived from MPD. B) Adjustment of assumed crack growth factors by limiting their size at the 97.5^{th} percentile, avoiding high fatigue in frequently inspected structures.

is assumed that under design load, a critical crack length $\hat{a_c} = 100\%$ is reached after a usage of six times the inspection interval I_i, starting from a crack length of $\hat{a} = 1\%$. This approach aims at providing a baseline failure behavior rather than modeling exact failure characteristics. Figure 3.2 illustrates the crack growth behavior of a representative component within the simulation.

A drawback of the calibration of the crack growth model with inspection intervals is that frequently inspected components have an unrealistically high crack growth factor, as illustrated in Figure 3.3. Notably, these are primarily structures within the landing gear. High inspection rates of the undercarriage can be attributed primarily to the severity of its failure rather than its expected fatigue or accessibility, as landing gear components are primarily designed for safe-life [160, p. 5]. Therefore, to mitigate unrealistically high failure rates within the simulation, the crack growth factor is arbitrarily limited to values smaller than the 95^{th} percentile.

3.1.2 Aircraft System Failure Model

The failure behavior of aircraft systems listed in the *Systems and Powerplant Program* of the MPD are simulated based on their MTBF. Given the MTBF rate, the probability of failure $p_{failure}(FC)$ during a given FC, can be calculated by

$$p_{Failure}(FC) = 1 - \left(1 - \frac{1}{MTBF}\right)^{\frac{FH}{FC}}, \tag{3.35}$$

given the flight time per flight cycle $\frac{FH}{FC}$. Based on the known probability of a failure occurring at a given flight, inverse transform sampling is used to simulate the failure of a part. The probability of experiencing a failure at a given FC $p_{failure}(FC)$ increases with every load cycle.

3.1.3 Structural Health Monitoring Performance Model

Three models are introduced in the following subsections to represent each DM, OLM, and hybrid SHM systems. In practice, the specifications of the fatigue damage and performance of a correspondingly assigned SHM system highly depend on geometry, loads, materials, and failure modes of the monitored structure. These practical constraints are considered by generic SHM performance parameters to decrease the computational complexity. For DM and hybrid SHM systems, the performance parameters used in this work are calibrated using data from a laboratory experiment conducted by IABG.

3.1.3.1 Damage Monitoring

In this thesis, DM systems are modeled as binary classifiers. They report the state of a structural component as "undamaged" or "damaged." However, as DM sensors provide a continuous measuring signal, a threshold is chosen defining the signal cutoff level between different states. The threshold-dependent monitoring performance of a DM system can therefore be represented as a receiver operating characteristic (ROC) curve, giving the relation between TP and FP [35, 36, 161–163]. To simplify the DM performance characteristic in this thesis, the relation between the TP rate $y \in [0, 1]$ and FP rate $x \in [0, 1]$ is assumed as a Lehmann model by

$$y = x^{\frac{1}{\Theta}}, \tag{3.36}$$

where $\Theta > 0$ is the Lehmann parameter, which can be interpreted as the diagnostic accuracy or performance of the DM system [163, p. 9, 162, 161]. Thus, for a random classifier, $\Theta = 1$ holds, and, for a perfect classifier, $\Theta \to 0$ is valid. In Figure 3.4, the relation between the measured signal, damage classification threshold, and ROC curve is illustrated. For a single monitoring system, the ROC curve is generated by determining the TP and FP rates for a series of different classification thresholds. Thus, ROC curves can be used to compare different

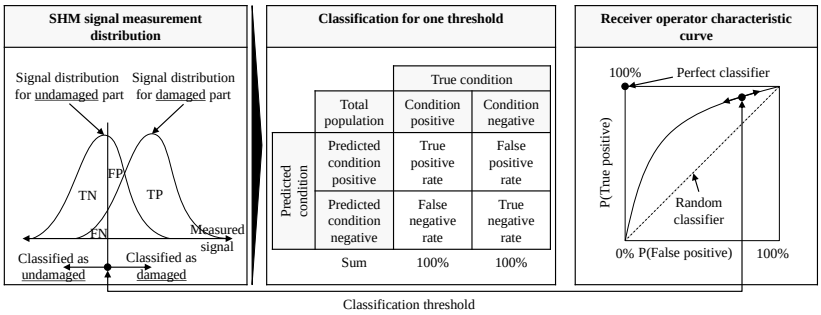

Figure 3.4: ROC curves are used to represent the adjustable performance settings of a DM system.

monitoring systems or evaluation algorithms. Depending on the choice of technology, DM systems have varying resolutions and can detect cracks of different lengths. The probability of detection (PoD) of a crack depends on the chosen DM technology and its system architecture [40, 67]. For the certification of SHM systems, the crack-length-dependent PoD demonstrates that structural integrity is maintained throughout operation [40, 67]. In this work, the PoD is assumed to be constant and is set for every structural position in the aircraft using the corresponding inspection task code (general visual inspection (GVI), detailed inspection (DI), special detailed inspection (SDI)) given in the MPD. This achieves comparability between the different investigated MRO scenarios including and excluding the use of SHM.

3.1.3.2 Load Monitoring

Unlike DM, SHM by means of OLM relies solely on the observation of fatigue driving loads acting on the structure. Therefore, to derive the state of fatigue, both the initial condition of the structure and the incremental fatigue per load fraction have to be known. The crack growth model introduced in Section 3.1.1 provides both the initial crack size $\hat{a}_0$ and incremental crack growth per load cycle $\frac{d\hat{a}}{dN}$. However, the initial crack length $\hat{a}_0$ is known in practice as a distribution rather than an exact length. Given that the initial crack length distribution is known, the probability of a damaged structure $P\left(\hat{a}_c(N)\right)$, defined as $\hat{a} = \hat{a}_c$, can be calculated. The end of life for an individual structural part can thus be defined by its maximum tolerable damage risk $P_{\hat{a}_c,max,OLM}$. The decommissioning criterion when using OLM is thus given by

$$P\left(\hat{a}_c(N)\right) > P_{\hat{a}_c,max,OLM}. \tag{3.37}$$

3.1.3.3 Combination of Load and Damage Monitoring

As described in Section 2.3.3, DM and OLM can be combined into a single SHM system, decreasing the uncertainty in structural state estimation. In general, the performance of a hybrid SHM system depends on the hierarchy level where data is shared, the performance of the individual system, and the classification performance of the individual applications. To

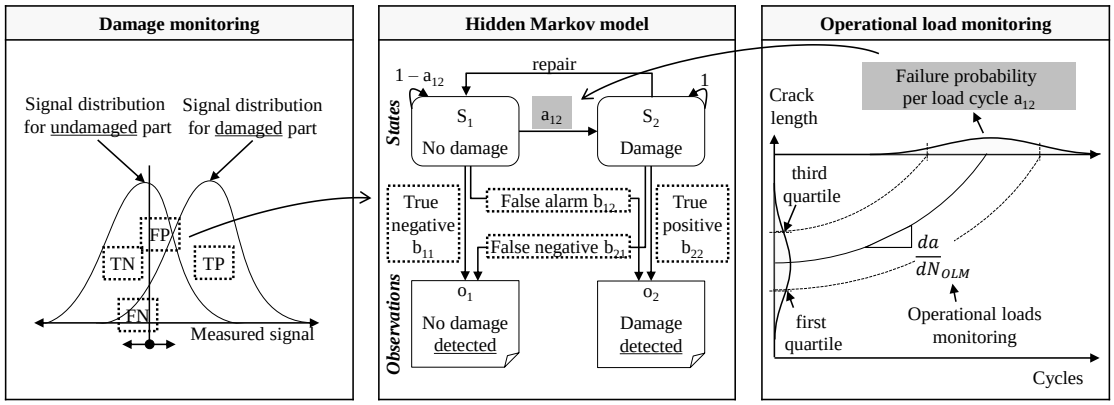

Figure 3.5: Hidden Markov model representing the interaction of OLM and DM in a hybrid SHM model.

assess the impact of a hybrid SHM system, the interaction of OLM and DM is assessed in a non-homogeneous (or time-variable) hidden Markov model (HMM), previously discussed by the author in [163]:

"*A complete specification of the HMM according to [164, 165] is given as follows:*

- Number of hidden states N_{HMM} in the model. Individual states are represented as $S_{HMM} = \{S_1, S_2, S_3, ..., S_N\}$; the state at time t is represented as q_t.
- State transition probability matrix: $A_{HMM} = \{a_{ij}\}$, to represent state transition from state i to state j, where $a_{i,j} = \mathbb{P}(q_{t+1} = S_j | q_t = S_i)$, $1 \leq i, j \leq N_{HMM}$ and $p_{i,j} \geq 0$.
- Observation symbol (i.e. "damage", "no damage") probability matrix: $B_{HMM} = \{b_j(k)\}$ for state j, where $b_j(k) = \mathbb{P}(x_t = o_k | q_t = S_j)$, $1 \leq j \leq N_{HMM}$ and $1 \leq k \leq M$.
- Initial state matrix: $\pi = \{\pi_i\}$, where $\pi_i = \mathbb{P}(q_1 = S_1)$, $1 \leq i \leq N$.

The HMM as described here, additionally relies on the assumption that the current state is only depending on the previous state and that an output observation o_t at time t is dependent only on the current state [165]. [Figure 3.5] provides a schematic illustration of the employed non-homogenous HMM including the defined states and their meaning. Here, a system is considered possessing $N_{HMM} = 2$ states where two observations $o \in O_{HMM}$, with $O_{HMM} = \{damage\ detected, damage\ not\ detected\}$ are possible.

The time-variable transition probability from an undamaged to a damaged state $a_{12}(t)$ can be derived from the crack growth model [or OLM system]. The probability to observe a specific emission depends on the considered health monitoring system. The probability of being in the state S_i when having x_t at a fixed time t can be calculated by employing the forward-backward algorithm as described in [166] for a given HMM $\lambda(S, O, A, B, \pi)$ [...]. For a given word $X = x_i, x_2, ..., x_t \in V$, $\mathbb{P}(X|\lambda)$ is the probability of having X in the model λ. In order to

calculate the probability of a given state $\mathbb{P}(S_i)$, the forward-backward algorithm can be used [165]. It can be calculated in matrix form according to [166] as follows:

$$\hat{f}_{1:t+1} = \alpha_t O_{t+1} A^T \hat{f}_{1:t}, \tag{3.38}$$

where $\hat{f}_{0:t}$ is the forward variable at time t and $\hat{f}_{0:0} = \pi$. A normalizing constant α_t is introduced to make the probabilities sum up to 1. The backward variable $\hat{b}$ can be calculated by

$$\hat{b}_{k+1:t} = \dot{\alpha}_t A O_{k+1} \hat{b}_{k+2:t}, \tag{3.39}$$

with $\hat{b}_{k+1:t} = (1 \;\; 1)^T$ for $k+1 = t$ as start for the backward equation and $\dot{\alpha}_t$ being a normalizing constant. The probability $\mathbb{P}(q_t = s_i|o, \lambda)$ of being in a state S_i at a given time t can be written as

$$\mathbb{P}(S_i|o, \lambda) = \ddot{\alpha}_t \hat{f}_{0:t} \hat{b}_{t:T} \tag{3.40}$$

with $\ddot{\alpha}_t$ being a normalizing constant" [163]. The HMM demonstrates one approach how different SHM systems that provide information about damages and operational loads can be combined. Depending on the utilized sensor system and type of damage, other sensor fusion approaches can be used as well.

3.1.3.4 Structural Health Monitoring Performance Calibration

Before the different SHM systems can be considered in the economic analysis, their performances are calibrated. In commercial operation, SHM systems are tailored specifically to the monitored damage type and size, structural geometry, operational loads, and prevailing environmental influences. Prior to operational use, the system's durability and PoD of damages are determined. Furthermore, a damage classification threshold is chosen to satisfy regulatory safety requirements governing structural integrity [167, 168]. However, the exact structural specifications of the airframe and design drivers of the SHM are not accessible as part of this work. Therefore, the performances of the investigated SHM systems—OLM, DM, and hybrid—are as follows:

As assumed for *OLM systems*, the structural failure probability of every individual flight cycle can be derived without uncertainty from the fatigue model. The OLM system cannot directly detect damage but can derive the risk of structural failure. The load cycle at which the OLM system requires the operator to replace a structural part is reached when the risk of structural failure $P(\hat{a}_c(N))$ is at least equal to the minimum tolerable structural failure probability $P_{\hat{a}_c,max,OLM} \in (0, 1)$. In contrast, *DM systems* are capable of directly detecting a damage in the structure. To evaluate the DM system in this study, the *ROC curve* and *maximum tolerable FN rate* are defined as follows.

The damage classification threshold and thus the *maximum tolerable FN rate* in this work are derived from design regulations for aircraft structures. For transport category aircraft, the required material strengths for structures where failures result in losses of structural integrity are defined for single members and redundant structures [§ 25.613 37, 50]. For single-member structures, material strength has to be assured with a 99% probability and 95% confidence [§ 25.613 37, 50]. For redundant structures, material strength has to be assured with a 90% probability and 95% confidence [§ 25.613 37, 50]. Assuming that a damaged part is identified at the same level of probability, the FN rate of a DM system can therefore be set to 1% for single-member structures and 10% for redundant structures. However, as discussed in Section 2.2.4, the information provided by SHM influences the overall reliability of the airframe. The required performance and thus the FN rate depend on structural design parameters, material properties, and operational environment. Therefore, the assumed minimum FN rate is arbitrary to decrease the complexity of the study and independent of the specified confidence level.

The assumed DM performance characteristic, or *ROC curve*, is calibrated using data from an SHM experiment conducted by IABG. Documentation and detailed results of this SHM test are provided in Appendix A.4. Since the demonstrator test was on a generic airframe specimen, the results serve as a generalized reference for the DM model rather than a source of operational performance data. The investigated damage classification performance is based on defining damage as a structural rupture, as shown in Appendix A.4. However, damage to a structural specimen does not automatically result in the loss of structural integrity of the entire airframe, which in turn does not inevitably lead to aircraft failure [37, 50, AMC §25.571]. In the IABG SHM test, four sensors were used to measure the lengths of the cracks occurring under cyclic loading. A performance comparison of the different sensors and utilized statistical methodologies is provided in the Appendix A.4.

Based on the performance of the IABG demonstrator, the Lehmann parameter Θ, which represents the ROC curve and thus the DM performance, is fitted using the method of least squares. When only the best performing statistical method found for every sensor is considered, the Lehmann parameter can be set to $\Theta_{best} = 3.7{\cdot}10^9$. Considering all investigated statistical models equally, the Lehmann parameter can be specified as $\Theta_{avg} = 73$. The great difference between Θ_{best} and Θ_{avg} stems from the Lehmann model, where Θ specifies the degree of the root used to express the TP rate as a function of the FP rate. For a perfect classifier it holds that $\Theta \rightarrow \infty$. Since the operational load spectrum and path of a crack are initially unknown, the DM model with Θ_{best} can be considered as the best-case scenario and Θ_{avg} as a more realistic scenario. The achieved performances of the IABG demonstrator and the derived DM model are illustrated in Figure 3.6.

Structural parts can be in either an operational or nonoperational state $S \in \{S_{damaged}, S_{\overline{damaged}}\}$ during the life of the aircraft. Therefore, four possible outcomes are created by the DM system, described as follows. A replacement of a damaged part is represented by

$$\mathrm{TP} = S_{damaged} \cdot p(\mathrm{TP}), \tag{3.41}$$

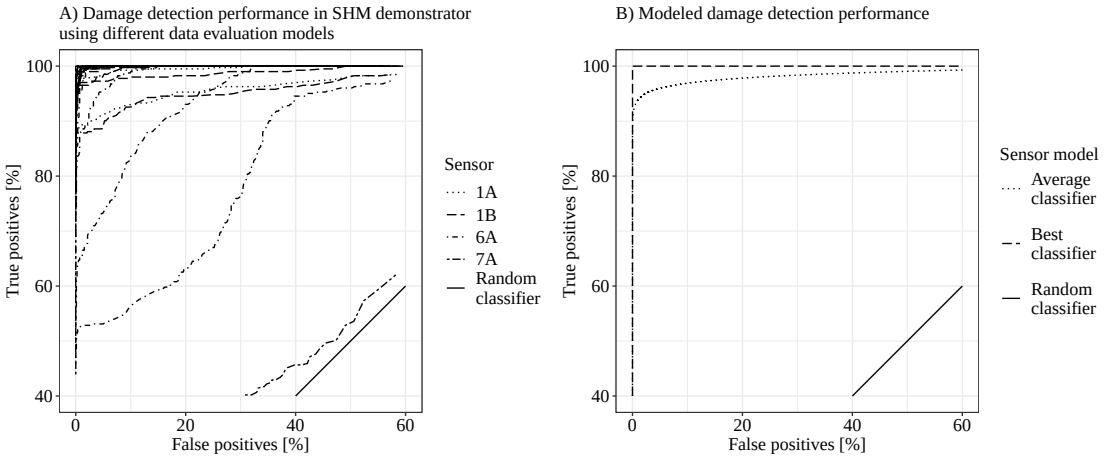

Figure 3.6: Investigated DM performance in IABG SHM experiment compared to assumed DM performance in cost-benefit analysis.

and a replacement of an undamaged part by

$$\mathrm{FP} = S_{\overline{damaged}} \cdot p(\,\mathrm{FP}). \tag{3.42}$$

Keeping an undamaged part is simulated by

$$\mathrm{TN} = S_{\overline{damaged}} \cdot (1 - p(\,\mathrm{FP})), \tag{3.43}$$

and failing to replace a damaged part is represented by

$$\mathrm{FN} = S_{damaged} \cdot (1 - p(\,\mathrm{TP})). \tag{3.44}$$

As discussed in Section 3.1.3.3, the combination of load and damage monitoring in a *hybrid SHM system* can improve the damage classification performance. Therefore, for the work at hand, the performance of a hybrid SHM system is assumed to be better compared to DM alone. Thus, three improved performance levels are considered for the representation of hybrid SHM systems. For the cost-benefit study, distinct operating points of all considered SHM systems are listed in Table 3.2.

3.1.4 Damage Monitoring Equipment Weight Model

The mass of the SHM system is derived using the methodology presented in [169], which is based on airframe geometry and size estimates for the considered Airbus A320 reference aircraft. This section summarizes key assumptions and aspects of this approach:

For the instrumentation of the airframe with SHM, "*[i]t is assumed that beam-type components are monitored with FOS, while plate- and features-type components are instrumented with US*

Table 3.2: Selected OLM, DM, and hybrid SHM operating points in the cost-benefit study.

Scenario	FP rate [-]	TP rate [-]	$P_{\hat{a}_c,max,OLM}$ [%]	SHM system
1	0	1	-	Ideal DM
2	$1{\cdot}10^{-5}$	0.99	-	Hybrid SHM system
3	$1{\cdot}10^{-3}$	0.99	-	Hybrid SHM system
4	$1{\cdot}10^{-1}$	0.99	-	Hybrid SHM system
5	$4.8{\cdot}10^{-1}$	0.99	-	DM with $\Theta = 73$ and non-redundant structure
6	$4.56{\cdot}10^{-4}$	0.9	-	DM with $\Theta = 73$ and redundant structure
7	-	-	$1{\cdot}10^{2}$	OLM
8	-	-	$1{\cdot}10$	OLM
9	-	-	1	OLM
10	-	-	$1{\cdot}10^{-1}$	OLM
11	-	-	$1{\cdot}10^{-2}$	OLM

sensors. For beam-type structures, only the length is considered to derive the sensor weight. [...] [A] factor c_{fiber} to account for fiber laying such that the effective fiber length is longer than the component length, [is considered]. [It is assumed] that the fiber-optic interrogation (FOSI) system covers a total fiber length of $n_{FOSI} \cdot L_{FOSI}$ and weighs m_{FOSI} [...]. Therefore, the sensor mass for a beam-type component is

$$m_{FOS} = c_{fiber} \left(\frac{m_{FOSI}}{n_{FOSI} \cdot L_{FOSI}} + \lambda_{FOC} \right) l_{component} + 2m_{FC} \tag{3.45}$$

with the linear density λ_{FOC} of the fiber-optic cable [and length of the structural component $l_{component}$]. For each fiber, two fiber connectors are considered, adding a respective mass of m_{FC}. The linear density [of the fiber-optic cable λ_{FOC}] is

$$\lambda_{FOC} = \lambda_{jacket} \left(1 - c_{patch}\right) + c_{patch} \delta_{patch} t_{patch} w_{patch} + \lambda_{fiber}. \tag{3.46}$$

With linear densities λ_{jacket} and λ_{fiber} of protective jacket and fiber, respectively. The factor c_{patch} accounts for the fractional length sensor patches, with thickness t_{patch}, width w_{patch} and density δ_{patch} [...].

In the case of a plate-type structural component, the number of sensors is obtained by dividing its area with the sensor-dependent detection footprint. [It is assumed] that a Piezoelectric Wafer Active Sensor (PWAS) that uses ultrasonic waves is needed approximately every 25.4 cm for crack detection in metal [170]. Assuming a rectangular arrangement, the detection footprint A_{PWAS} per sensor is given by

$$A_{PWAS} = d_{PWAS}^2, \tag{3.47}$$

where d_{PWAS} is the side length of the covered square. The total number of sensors for unit coverage of a component with area A_{part} is therefore

$$n_{PWAS} = \frac{A_{part}}{A_{PWAS}}. \tag{3.48}$$

[The area density of the PWAS ρ_{PWAS} is thus assumed by]

$$\rho_{PWAS} = \frac{4m_{PZT} + \left(4w_{film}t_{film}\rho_{film} + n_{wire}\lambda_{wire}\right) d_{PWAS}}{d_{PWAS}^2} \tag{3.49}$$

In addition to the mass of the sensing element m_{PZT}, a film of width w_{film}, thickness t_{film} and density ρ_{film} is considered. Wiring assumes a linear density of λ_{wire}, considering an averaged number of signal and ground wires n_{wire} within a section of film of length d_{PWAS}. Overall, area density of the ultrasonic system, including interrogation equipment of mass m_{USI} and supporting n_{USI} sensors, is

$$\rho_{US} = \frac{m_{USI}}{n_{USI} \cdot A_{PWAS}} + \rho_{PWAS}. \tag{3.50}$$

The overall figure is calculated assuming interrogation equipment of mass m_{USI}, supporting n_{USI} sensors. [...] As for a single sensor to monitor a certain component feature,

$$m_{PWAS} = \frac{m_{USI}}{n_{USI}} + m_{PZT} + d_{PWAS}w_{film}t_{film}\rho_{film} + 2d_{PWAS}\lambda_{wire} \tag{3.51}$$

[...]. [For the power distribution network, it is assumed that] a voltage of 28V is employed, and that a voltage drop of 1% per 100 ft. is tolerable [171]. The overall cable weight model considers two-wire copper cable, with 10–µm Aluminum shielding and 150–µm polyvinylidenfluorid-insulation. The mass of the wire m_{wire} itself was calculated from the electric power demand on the respective cable in the network using

$$m_{wire} = c_{wire}L_{wire}\frac{\rho_{Cu}}{\sigma_{Cu} \cdot V_0^2 \left(\eta - \eta^2 L_{wire}\right)}P_{wire}. \tag{3.52}$$

With length L_{wire}, density of Copper ρ_{Cu}, electric conductivity of Copper σ_{Cu}, allowed voltage drop per unit length η, and power demand P_{wire}. [...] [A] minimum acceptable wire diameter similar to AWG22 [is assumed]. The overall mass of the sensor network is

$$m_{SHM} \approx \sum_i m_{PWAS}^i n_i + \sum_j \rho_{US}^j A_j + \sum_k \lambda_{FOC}^k L_k + \sum_l m_{wire}^l \tag{3.53}$$

With component indices i, j and k for each of the defined sensor types, considering component feature counts n_i, and part areas and lengths A_j and L_k, respectively. Regarding the power

and data network, wire masses are summed with index l. [...] In case of ultrasonic sensors, the power per sensor is calculated simply as

$$P_{WAS} = \frac{P_{USI}}{n_{USI}} \tag{3.54}$$

and per unit area

$$p_{A,US} = \frac{P_{USI}}{n_{USI} A_{PWAS}} \tag{3.55}$$

respectively. In the case of FOS, per fiber length

$$p_{L,FOS} = \frac{P_{FOSI}}{n_{FOSI} L_{FOSI}} \tag{3.56}$$

Moreover, dissipation loss P_{diss} is considered in each cable in the power network, to calculate the overall dissipation loss. Dissipation loss is considered per cable as

$$P_{diss} \approx \eta \cdot c_{wire} L_{wire} \cdot P_{wire} \tag{3.57}$$

The overall power demand of the sensor network is

$$P_{SHMS} \approx \sum_i P^i_{PWAS} n^i + \sum_j p^j_{A,US} A^j + \sum_k p^k_{L,FOS} L^j + \sum_l P^l_{diss}. \tag{3.58}$$

With indices i, j and k summing components with each of the defined sensor types, considering feature counts n^i, and part areas and lengths A^j and L^j, respectively. Moreover, dissipation loss P^l_{diss} is considered in each cable in the power network, to calculate the overall dissipation loss. [...] The change in fuel flow $\dot{m}_{F,P}$ resulting from increased system power demands is calculated by

$$\dot{m}_{F,P} \approx \frac{k_P \cdot SFC \cdot P_{SHMS}}{\nu} \tag{3.59}$$

[172]. Here, k_P is the shaft power factor and SFC is the specific fuel consumption. The factors ν consider the efficiency chain of accessory gearbox, variable frequency generator efficiency, and electrical conversion" [169]. The assumed mass and power figures for the ultrasonic sensors, fiber-optic sensors, data network, and power network are summarized in Appendix A.5.

Military OLM systems currently in service, such as OLMOS in the Panavia Tornado, primarily use flight parameters to calculate structural loads and rely on a few strain gauges for verification only [12, pp. 6–7]. As the overall SHM sensor weight of the OLMOS system becomes negligible compared to the full instrumentation of the airframe, no weight penalty is assumed for OLM in this thesis.

Hybrid SHM systems are assumed to have the same weight penalty as DM systems.

3.1.5 Airframe Design Considerations

As noted in Section 2.1.1, SHM may render access doors obsolete, which can result in a lighter design of the airframe. Figure 3.7 illustrates selected types of cutouts in the airframe for different loading scenarios. Depending on the loading, cutouts can decrease or increase the structural weight of the airframe. For lightly loaded beams, incorporating flanged lightening holes instead of stiffeners may be advantageous in terms of weight considering minimum gauge requirements or other restrictions due to the part size, as shown in Figure 3.7 A) [10, p. 165]. In moderately or heavily loaded beams, on the other hand, access holes may require weight-increasing stiffeners to withstand required loads [10, p. 165]. Cutouts in the skin stringer panel used on the wing and empennage are challenging because of stress concentrations; therefore, increased sheet thickness and larger cross-sectional areas near the cutout add weight [10, p. 177]. The exact extent of weight-driving structural improvements depends on the load cases, hole size, material, position of the aircraft, and other concerns raised during a FMEA, as different damage cases have to be considered.

Since this information is not available for the considered aircraft, a simplified weight estimation method is used based on [10, pp. 162–206] and additional arbitrary assumptions. For trainer and fighter aircraft, the area density of unpressurized access panels on the fuselage is specified at 8.3 to 28.2 $\frac{kg}{m^2}$, based on the analysis of 16 service doors on the F4, F104, and F105 aircraft [173, 508 21-02]. For transport category aircraft, no statistics on access panel weight could be obtained as part of this work. However, an analysis of 14 passenger jet aircraft emergency doors in [173, 508 22-02] identified their weight to be between 5.8 and 25.3 kg, with a mean of approximately 10 kg. Even though the total weight penalty may increase with the area of the cutouts, this empirically based approach provides a first indication given the available data.

The MPD provides information on which access panels are used with every inspection task. In case a specific access panel only serves structural inspection tasks, its integration into the airframe may be avoided. Therefore, all inspection tasks using this access panel have to be conducted by SHM, assuming that direct structural access is no longer needed. In this case, no structural cutouts, including doublers, stiffeners, hinges, and locking mechanisms, are required. The cost-benefit study assumes that the avoidance of a single structural cutout during airframe design leads to a weight saving of 5.8 kg [173, 508 22-02].

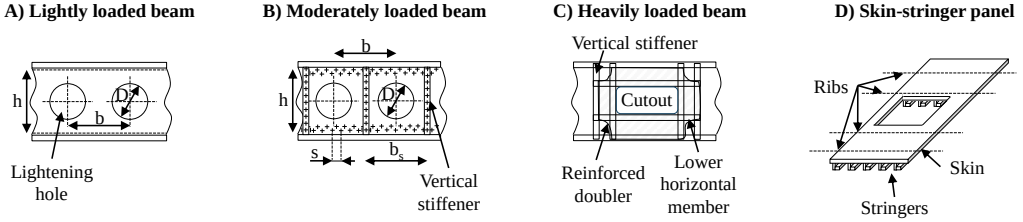

Figure 3.7: Selection of structural cutouts on aircraft adapted from [10, pp. 162–206].

3.1.6 Maintenance, Repair, and Overhaul Model

The operation and upkeep of the simulated aircraft are orchestrated in the service model, where maintenance schedule planning, scheduled inspection and repair, and operation are considered. This section outlines the individual steps of the simulation and introduces the utilized methodologies.

In the *maintenance schedule planning* step introduced in Section 3.1.6.1, an individual usage-dependent maintenance plan is constructed for the simulated aircraft using the inspection requirements provided in the MPD. This step is executed before the first flight cycle and after every scheduled inspection. Once a *scheduled inspection or repair* is due, as described in Section 3.1.6.2, the pending inspection tasks are clustered and packaged to minimize inspection and access times. Subsequently, the inspections are conducted either manually or by means of automated systems, and detected damages are repaired. When scheduling the next maintenance event, the future flight plan of the aircraft is considered so that maintenance is carried out at an airport with an available maintenance base. Hereby, the individual tasks are scheduled to maximize the time between inspections. During the simulation of aircraft *operation* introduced in Section 3.1.6.3, a preflight check is conducted before every flight. This check represents the pilot's obligatory walkaround and the optional usage of SHM or other automated system health checks. Depending on the assumed capabilities of these systems, prognostic health management can additionally be used to update the maintenance schedule. If a damage is detected during the preflight check, an unscheduled repair is initiated. In the scope of this work, all simulated aircraft parts are assumed to be contained in the minimum equipment list, and thus, work cannot be postponed to the next layover.

Finally, the aircraft is decommissioned when it reaches its regulatory end of life. The methodologies used to derive the corresponding criteria are introduced in Section 3.1.7. An overview of the aircraft service model is provided in Figure 3.8.

3.1.6.1 Maintenance Schedule Planning

Airlines conduct their planning and scheduling process in subsequent hierarchical steps, as outlined in Section 2.2.3. An optimization of flight schedules, fleet assignment, fleet routing, aircraft maintenance, and crew assignment can be conducted by a variety of approaches to maximize airline profit [80, pp. 205–207]. They generally address the optimization problem in a sequential manner without covering all optimization phases in one model [84, p. 1]. Additionally, flight schedules have to be robust against distributions and profitable with unreliable passenger demand [84, p. 2–3].

However, solutions to the optimization problems are not determined analytically but rather through algorithms, which present a computational challenge to the researcher and practitioner. In practice, the required number of steps to solve the problem with current algorithms and methodologies, e.g., linear programming, typically grows exponentially with the increase in problem size [80, p. 207]. For these non-deterministic polynomial ($\mathcal{NP}$) time algorithms, optimal solutions for the flight schedule, fleet assignment, and aircraft maintenance rout-

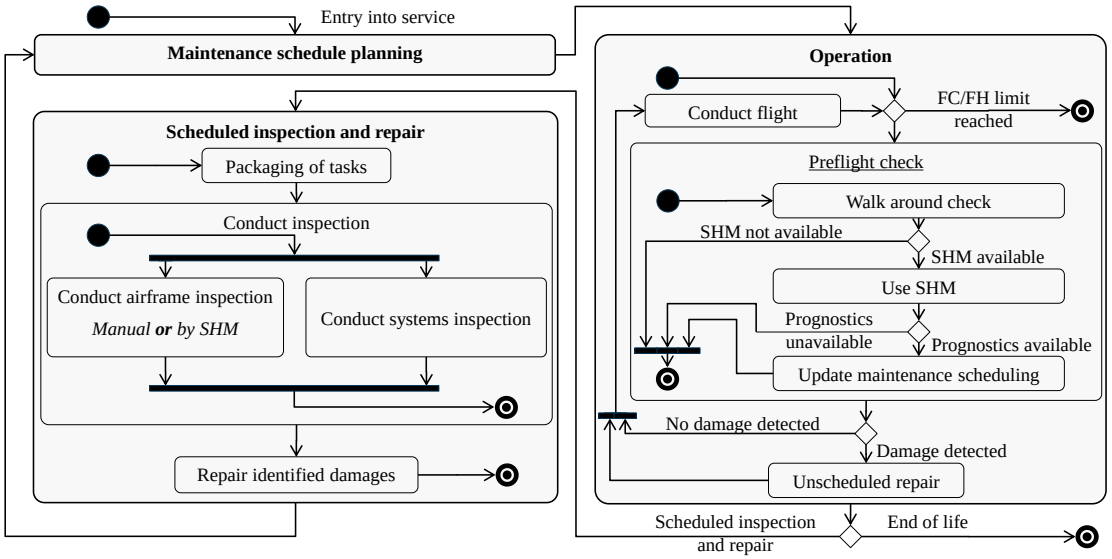

Figure 3.8: State machine diagram of the service model, which performs the maintenance schedule planning, operation and scheduled inspections, and repairs of the simulated aircraft.

ing for a typical airline are nearly impossible to obtain in a reasonable amount of time [80, p. 207]. The scheduling of inspection and repair events in this work is thus based on a simplified two-step approach, maximizing the inspection intervals for individual parts and the entire aircraft. The cycle N of the upcoming scheduled maintenance event M of the aircraft A, written as $N_{M,A}$, is determined by the cycle of the first upcoming inspection $N_{next,T}$ of task T out of all upcoming inspection tasks $\overrightarrow{N_{next,T}}$ as follows

$$N_{M,A} = min \begin{pmatrix} N_{next,1} \\ N_{next,2} \\ \vdots \\ N_{next,T} \end{pmatrix}. \tag{3.60}$$

At $N_{M,A}$, all pending inspection and maintenance tasks are completed such that the number of cycles between the current inspection $N_{M,A}$ and the next inspection $N_{M+1,A}$ is maximized, while the number of tasks due is minimized. Given the fixed inspection requirements in the MPD in terms of FCs or FHs, moving an inspection task earlier by a number of cycles N_{Δ}, automatically moves up all consecutive events of that task by N_{Δ}. The time between individually scheduled inspections is thus determined by the smallest inspection interval I_i of a task T, such that

$$N_{M+1,A} = N_{M,A} + min \begin{pmatrix} I_{i,1} \\ I_{i,2} \\ \vdots \\ I_{i,T} \end{pmatrix}. \tag{3.61}$$

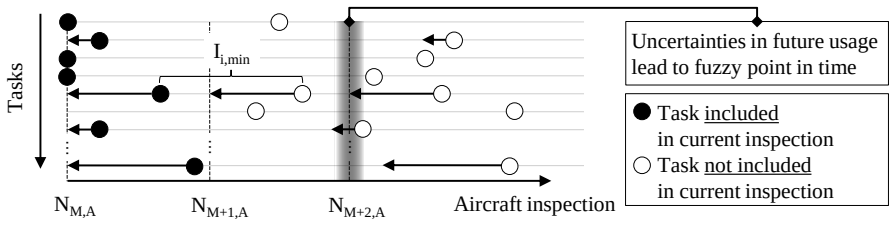

Figure 3.9: The shortest inspection interval of a task drives the inspection interval of the aircraft, with the remaining tasks being clustered in a way to decrease the overall inspection effort of the aircraft. Adapted from [174].

The utilized scheduling process is illustrated in Figure 3.9.

While this approach does not optimize maintenance scheduling for cost, it provides a computationally inexpensive method to construct an aircraft maintenance program that satisfies regulatory requirements, considering aircraft availability and inspection effort.

3.1.6.2 Scheduled Inspection and Repair

Within the *maintenance schedule planning*, the cycle $N_{M,A}$ of an upcoming scheduled aircraft inspection is selected. During the inspection and repair event, the required work is organized to minimize the required labor. The MPD provides an estimation of the length of every task divided into access and inspection times based on information from the manufacturer. Additionally, the MPD defines the zones to be accessed during the inspection. To minimize the set-up or access time during the inspection, the pending inspection tasks are combined in work packages to avoid multiple disassemblies of the same part. Since the maintenance facility, staffing, and tooling are not considered in the work at hand, the modeling of task packaging is straightforward. The total access time of a single aircraft inspection event $W_{M,Acc,A}$ is calculated by summarizing the access time per position, only considering the task with the largest access time duration per aircraft position. Thus, $W_{M,Acc,A}$ can be calculated by

$$W_{M,Acc,A} = \sum \begin{pmatrix} max(\overrightarrow{W_{M,Acc,1}}) \\ max(\overrightarrow{W_{M,Acc,2}}) \\ \vdots \\ max(\overrightarrow{W_{M,Acc,P}}) \end{pmatrix}, \tag{3.62}$$

where $\overrightarrow{W_{M,Acc,P}}$ is a vector of all access times associated with tasks due at inspection M by position P. During the inspection and maintenance event, all tasks due before the next aircraft inspection are performed. The inspection can be carried out manually, where the total work time $W_{M,T}$ is given by

$$W_{M,T} = W_{M,i} + W_{M,Acc}, \tag{3.63}$$

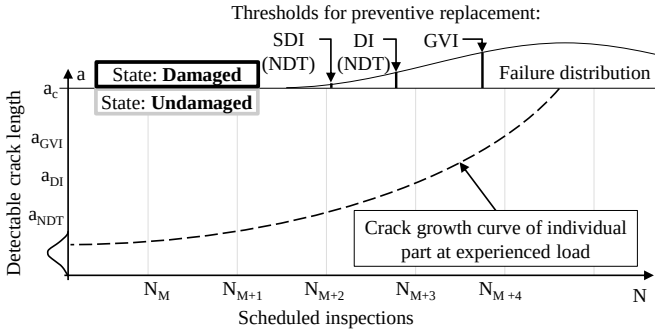

Inspection method	Threshold failure probability
GVI	2e–3
DI	2e–4
SDI	2e–5

Figure 3.10: Preventive replacement of structural components are simulated using the modeled failure probability and specified task code of the inspection.

where $W_{M.Acc}$ is the access time and $W_{M,i}$ is the inspection time of a task. When using SHM to carry out the respective inspection task, $W_{M,T} = 0$ is assumed. If a failure is found, the part is replaced, and the corresponding damage simulation is reset to reflect a new and undamaged part. Manual inspections are assumed to be perfect. The performance of using an SHM system is described in Section 3.1.3.

To moderate the effects of the damage definition used for aircraft structures, inspected parts can be replaced preventively. As introduced in Section 2.1.2, metallic fatigue is a continuous process. The replacement decision for an individual part relies on a binary definition for damage. As a result, structural parts that are defined as undamaged may be considered damaged only one FC or FH after the inspection. Therefore, preventive replacements are conducted during manual inspections based on their calculated failure rate, as illustrated in Figure 3.10.

3.1.6.3 Preflight Check

Before every flight, a manual preflight check is conducted. During this check, damages in positions with task codes given in Table 3.3 can be detected with a probability of 10%. Alternatively, SHM systems can be used for the preflight check. Depending on the outcome of the inspection, unscheduled repairs may be initiated at the current location of the aircraft, possibly leading to delays.

3.1.7 Aircraft Decommissioning Model

The decommissioning process of aircraft is driven by economic considerations and regulatory factors based on safety concerns. Assuming technological progress leads to a steady increase in aircraft cost-efficiency per seat, airlines can replace aircraft after a certain time to achieve economic benefits. However, they cannot postpone the replacement decision indefinitely since the maximum usage of the aircraft is regulated to govern the occurrence of structural fatigue in airframes. Therefore, the aircraft's lifetime is limited in both economic and regulatory terms. In this section, three independent aircraft decommissioning approaches are introduced. The

Table 3.3: Failures detectable during a walkaround of parts connected to tasks with the following task codes based on [175, p. 18].

Task code	Definition
CHK	Check for condition, circuit continuity, fluid reserve, fluid level, leakage, tension and charge pressure
FC	Functional check or test
GVI	General visual inspection
OP	Operational check or test
SV	Drain, servicing, replenishment (fluid change)
VC	Visual check

first is based on the optimal *economic retirement* driven by the performance improvement of new alternative aircraft. The second is based on the currently used *LoV* described in Sections 2.1.1 and 2.1.3, while the third is based on an OLM-enabled *fatigue damage index (FDI)*.

3.1.7.1 Economic Retirement

As a result of increasing aircraft efficiency and limited lifetimes, airlines can improve profitability by optimizing the timing of aircraft replacements. To provide guidance in this decision, different investment appraisal methodologies have been proposed to identify the cost and benefits associated with a replacement. An extensive overview of the most common techniques and the methodologies used in this section are provided in [176]. In this thesis, the NPV, which estimates the value a new aircraft adds to the airline over its lifetime, is used to evaluate an investment decision. As a dynamic investment appraisal methodology, the NPV considers the profitability of an investment over multiple periods (i.e. years) and takes into account the varying value of money over time by discounting cash flows [176, pp. 91–147]. The NPV can be calculated by

$$NPV = \sum_{t=1}^{T_I} \frac{C_t}{(1 + WACC)^t}, \tag{3.64}$$

where t is the individual investment period, T_I is the total number of investment periods, and C_t is the net cash flow in period t. For airlines, the Weighted Average Cost of Capital (WACC) can be assumed at 8% [177]. The net cash flow C_t of a period can be calculated by

$$C_t = \begin{cases} -I_0 & \text{for } t = min\{t, \ldots, T\} \\ e_t - a_t & \text{else} \\ e_t - a_t + P_t & \text{for } t = max\{t, \ldots, T\} \end{cases} \tag{3.65}$$

where I_0 is the initial investment in period $t = 0$, e_t is the cash inflow in period t, a_t is the cash outflow in period t, and P_t represents the proceeds of selling the investment after its

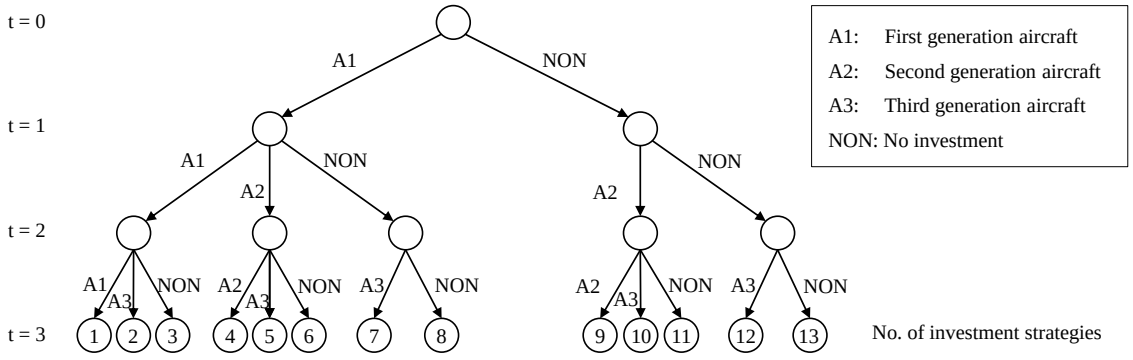

Figure 3.11: Investment decision tree covering multiple periods, resulting in an exponentially growing number of different investment strategies, adapted from [197, p. 209]. An investment into used aircraft is not considered.

use in period t. Assuming the disinvestment proceeds P_t to be equal to the book value of the disposed asset B_t, they can be calculated by depreciating the initial investment I_0. In practice, most airlines use a linear depreciation method [178]. However, to better represent the market value of aging aircraft and the initially high cost of customizing an aircraft, the sum-of-year-digits method is used in this work to depreciate the aircraft book value [70, p. 61]. A comparison of both depreciation methods is provided in Appendix A.7. The depreciation in every period D_t can be calculated with the sum-of-year-digits method by

$$D_t = I_0 \cdot \frac{t_{EOL} - t}{\sum_{n=1}^{t_{EOL}} t_n}, \tag{3.66}$$

where I_0 is the initial investment and the number of periods until the aircraft is written off at $t_{EOL} = t\,(B_t = 0)$. Subsequently, the residual value P_t can thus be calculated by

$$P_t = I_0 - \sum_{n=1}^{t} D_t. \tag{3.67}$$

As a result of the assumed technological progress, the net income generated by every new generation of aircraft improves. The net operating cost a_t of a generation decreases with the technological progress factor ξ. The rate of technological development is derived in Appendix A.6 and estimated as an improvement in fuel efficiency per seat of 0.7968% annually [179–196]. Furthermore, the investment cost I_0 for every new aircraft generation can be assumed constant over time when neglecting inflation. Different investment or replacement strategies can now be generated, as illustrated in the decision tree in Figure 3.11.

In the first period, the airline has the choice to invest in a first-generation aircraft or wait one period. In every subsequent period, the airline can decide between investing in the current generation aircraft (and selling their old one), keeping the old aircraft, or not investing. The corresponding cash flows of the investment decision and influences of the technological progress factors are provided in Table 3.4.

Table 3.4: Periodic cash flows C_t and disinvestment proceeds P_t of the available investments over time [197, p. 209].

t	**0**	**1**	**2**	**3**	**...**	**N**
Aircraft A: C_t	$-I_0$	$e_1 - a_1$	$e_2 - a_2$	$e_3 - a_3$	...	$e_N - a_N$
Aircraft A: P_t	I_0	P_1	P_2	P_3	...	P_N
Aircraft B: C_t		$-I_1$	$e_2 - a_2 \cdot \xi$	$e_3 - a_3 \cdot \xi$	...	$e_N - a_N \cdot \xi$
Aircraft B: P_t		I_1	P_2	P_3	...	P_N
Aircraft C: C_t			$-I_2$	$e_3 - a_3 \cdot \xi^2$	...	$e_N - a_N \cdot \xi^2$
Aircraft C: P_t			I_2	P_3	...	P_N

A solution to the replacement problem can now be identified from the possible investment strategies summarized in Table 3.4 by combining available investments to maximize the total NPV over a given time frame. However, an optimal investment strategy for repeated investments that are not equal is not possible to derive analytically [176, p. 220, 197, p. 209]. Still, a solution to this problem can be obtained by using branch-and-bound methods, dynamic programming, or full enumeration. In the work at hand, a full enumeration approach is used. Additionally, the airline is assumed to be always invested in only one type of aircraft.

3.1.7.2 Limit of Validity

From a regulatory standpoint, aircraft are decommissioned once their usage exceeds the LoV specified for their type. As described in Section 2.1.3, the LoV is derived from the maximum period of safe usage demonstrated during the full-scale fatigue test. Through additional tests, the manufacturer can extend the LoV. With the LoV being measured by the maximum number of flight cycles $N_{FC,LoV}$ and maximum number of flight hours $N_{FH,LoV}$, the last usable cycle of the aircraft $N_{EOL,LoV}$ is defined as

$$N_{EOL,LoV} = N : N_{FC} \leq N_{FC,LoV} \vee N_{FH} \leq N_{FH,LoV} \tag{3.68}$$

For the Airbus A320, the initially specified LoV or design service goal (DSG) has already been extended to the extended service goal (ESG) by means of additional full-scale fatigue testing. The corresponding aircraft usage limits are summarized in Table 3.5.

Table 3.5: Airbus A320 original and extended service limits based on [198, 199, 77].

Service goal	$N_{FC,LoV}$ [-]	$N_{FH,LoV}$ [-]
DSG	48,000	60,000
ESG I	60,000	120,000
ESG II	90,000	180,000

3.1.7.3 Fatigue Damage Index

The intention of limiting the usage of aircraft with the LoV is to prevent WFD. However, the LoV does not consider the magnitude of the experienced fatigue driving loads during operation. With the capabilities provided by SHM through DM and OLM, the occurrence of WFD and its driving forces can be monitored directly. Therefore, an aircraft retirement criterion that reflects the state of fatigue rather than the number of used cycles can be defined. Thus, this section introduces the FDI as aircraft retirement criterion. The methodology for calculating the FDI is based on a previous collaboration published in [200]. The non-dimensionalized fatigue models simulating structural failure, as introduced in Section 3.1.1, are not suitable for the calculation of the FDI since they rely on artificially calibrated crack growth to simulate local structural failures rather than connect aircraft mission profiles to crack growth. Therefore, additional standard fatigue life equations and assumptions are introduced in this section to compute the FDI. Simplified models are also described to estimate the proposed FDI for the current Airbus A320 fleet.

"*Since the load spectrum during a flight does not occur with a fixed stress ratio R, an approximation of the Haigh diagram [201] is used in order to map the load spectrum to an equivalent load spectrum with $R = -1$. The stress amplitude $S_{a,R=-1}$ for $R = -1$ is therefore dependent on the mean stress S_m, the amplitude stress S_a for a known $R \neq -1$, and the material constant M_σ.*

$$\begin{aligned} &\text{for } 1 < R\text{:} \\ &S_{a,R=-1} = S_a(1 - M_\sigma) \end{aligned} \tag{3.69}$$

$$\begin{aligned} &\text{for } 0.5 < R \leq 1\text{:} \\ &S_{a,R=-1} = S_a \tfrac{(1+M)^2}{3+M_\sigma} \end{aligned} \tag{3.70}$$

$$\begin{aligned} &\text{for } 0 < R \leq 0.5\text{:} \\ &S_{a,R=-1} = S_a \tfrac{(1+M_\sigma)(3+M_\sigma \frac{S_m}{S_a})}{3+M_\sigma} \end{aligned} \tag{3.71}$$

$$\begin{aligned} &\text{for } -\infty \leq R \leq 0\text{:} \\ &S_{a,R=-1} = S_a(1 + M_\sigma \tfrac{S_m}{S_a}) \end{aligned} \tag{3.72}$$

After computing the stress amplitude for $R = -1$, the FDI, which describes the remaining useful life by a factor between 0 and 1 (where $FDI = 1$ indicates no remaining useful life) can be evaluated by the corresponding S-N curve and Miner's rule (Eq. 3.73). Miner's rule [202] assumes that the fatigue damage of different stress amplitudes accumulates linearly, where the fatigue damage is the ratio of the number of cycles of the applied load n_i to the number of cycles N_i, which can be withstood by the structure according to the S-N curve.

$$\text{FDI} = \sum_i \frac{n_i}{N_i} \tag{3.73}$$

To consider the different fatigue drivers, the aircraft is divided into two main structural parts: the wing and the fuselage [...]. Taxi time, payload, maximum flight altitude, and flight time are considered causes for fatigue damages. For both the wing and fuselage the aluminum Al 2024-T3 with $M_\sigma = 0.4$ *[153] is assumed. Moreover, the corresponding S-N curve (Eq. 3.74) with a stress concentration factor of* $K_t = 2.5$*, which is usually found at holes, is used (S-N parameters:* $C_1 = 63\,MPa$*;* $C_2 = 470\,MPa$*;* $C_3 = 3.50$*;* $C_4 = 2.07$*) [203].*

$$N_i = 10^{C_3\left[ln\left(\frac{C_2-C_1}{S_{a,i}-C_1}\right)\right]^{1/C_4}} \tag{3.74}$$

In order to compute the FDI of the wing, the stress amplitudes and the mean stresses during flight have to be evaluated. The transport wing standard (TWIST) shown in Figure 3.12 depicts the frequency distribution of the bending moment at a wing root of civil and military transport aircraft for 40,000 flights [204]. The TWIST was generated using measurements and computations and is divided into three parts: loads during flight, loads on the ground (due to taxi), and ground-to-air loads.

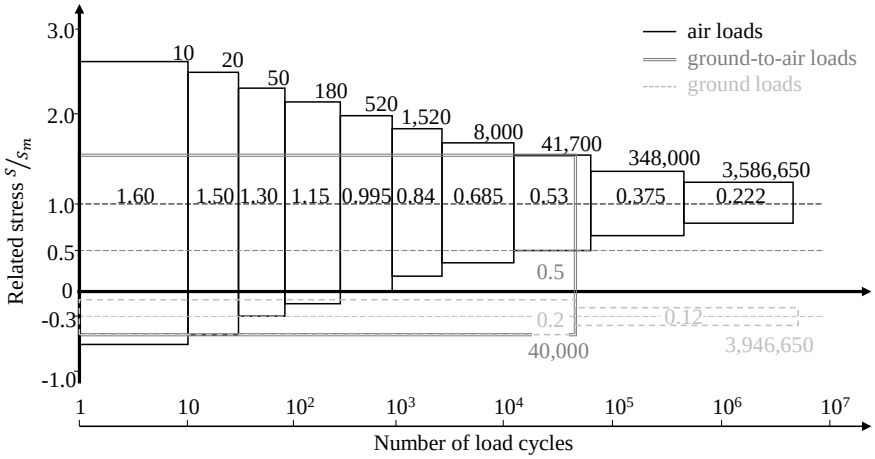

Figure 3.12: Transport Wing Standard for 40,000 flights based on [204].

First, the fatigue life based on the design loads can be computed with Eq. 3.69-3.74. The TWIST stresses are related to the mean stress, which is assumed to be $100\,MPa$ *for the design loads at a maximum take-off weight (MTOW) of* $W_{MTOW} = 73.5\,t$*, maximum payload* $W_{PL,max} = 16.6\,t$*, operating empty weight* $W_{OEW} = 42.2\,t$*, and maximum weight of fuel* $W_{fuel,max} = 20\,t$ *for an Airbus A320 type aircraft [205]. The corresponding number of cycles are shown in Figure 3.12. Furthermore, the design flight time is set to* $FH_{des} = 2\,h$ *[205], and the design taxi time to* $T_{taxi,total,des} = 25\,min$ *[206]. These times are assumed to lead to the numbers of cycles presented by the TWIST. Considering the taxi time rather than distance allows for a straightforward computation of fuel burn and weight changes during taxiing and further takes airport congestion into account [...].*

Second, since both the takeoff weight W_{TOW} *(herein estimated through the aircraft seat load factor and fuel weight) and the flight time are known, relative changes can be taken into*

account for the fatigue computation. [It is assumed that the] mean stress is linearly dependent on the aircraft weight, the number of cycles during flight is linearly dependent on the flight hours, and the number of cycles on the ground are reduced in proportion to the reduction of the taxi time. Now, the difference in the fatigue life represented by the change of the FDI due to monitoring can be evaluated.

The stresses in the fuselage result mostly from the difference between inner and outer pressure. Due to lift forces of the wing, the fuselage is also subjected to bending loads, [... which] is neglected. Therefore, the tangential stress S_{tan} and axial stress S_{axial} present in the fuselage can be modeled by Barlow's formula (see Eq. 3.75) with the differential pressure Δp, average of the fuselage diameter d_m, and sheet thickness t. Since the tangential stress is twice as great as the axial stress, only the tangential stress is considered in the following. The thickness is set to $t = 1.0\,mm$ and according to [205] the fuselage diameter is $d_m = 4.14\,m$.

$$S_{tan} = \frac{p\,d_m}{2\,t}, S_{axial} = \frac{p\,d_m}{4\,t} \tag{3.75}$$

The differential pressure is mostly affected by the highest altitude reached on an individual flight [...]. This altitude is assumed to be only dependent on the distance between origin and destination as illustrated in Figure A.6 in the Appendix. The dependency is modeled in Eq. 3.76, where $p_0 = 1013.25\,hPa$ is the pressure at sea level, $H_0 = 8,435\,m$, and H is the flight altitude.

$$p = p_0 \left(1 - e^{-\frac{H}{H_0}}\right) \tag{3.76}$$

According to [205], the maximum design flight altitude is set to $H_{max,des}(= 11,917.68\,m)$. Given that the pressure results in a pure swelling load with $R = 0$, the mean stress S_m and the amplitude stress S_a can be computed as

$$S_m = S_a = \frac{S_{tan}}{2} \tag{3.77}$$

The fuselage FDI corresponding to the design parameters can be computed with Eq. 3.69-3.74. Since the actual flight altitude is known, it can be taken into account and the change of the FDI due to monitoring can be computed. [The influences of operational usage parameters on the FDI of the wing and fuselage of the aircraft are illustrated in Figure 3.13, changing only one parameter, ceteris paribus.] The wing FDI shows a strong dependency on the seat load factor. Due to a larger mass, the mean stress intensifies, increasing the FDI. In contrast, the fuselage FDI is not affected by the seat load factor since it is completely driven by the flight altitude based on previously mentioned assumptions. The fuselage FDI is also [assumed to be] independent of the taxi time, whereas the wing FDI shows a minor dependency on it because the taxi load's mean stress is negative and the amplitude stress is rather small (see Figure 3.12). Furthermore, the wing FDI is assumed to be independent of the flight altitude, whereas the fuselage FDI shows a strong dependency on it" [200]. The FDI for a varying average flight

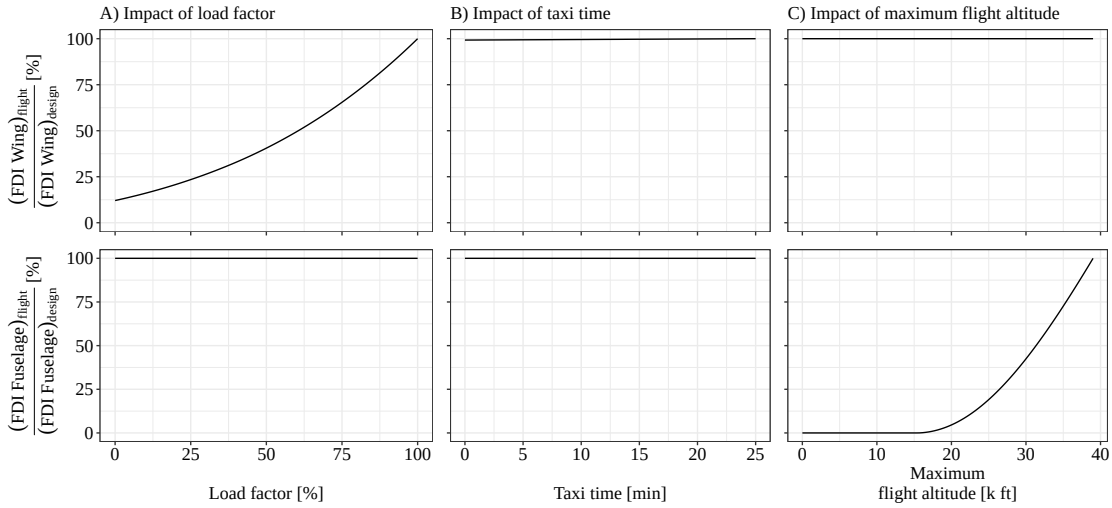

Figure 3.13: Impact of A) seat load factor, B) taxi time, and C) maximum flight altitude on FDI of a single flight compared to the FDI of the certified aircraft mission profile, adapted from [200].

distance over the entire aircraft lifetime is given in Appendix A.9. Aircraft usage parameters are derived as described in Appendix A.8.

3.1.8 Fuel Consumption Model

The fuel consumption model aims to estimate the relative change in aircraft lifetime fuel consumption resulting from increased aircraft dry weight driven by the introduced SHM equipment mass.

The aircraft fuel consumption is estimated using a Breguet approximation, which is only sufficiently valid for stationary cruise flight. However, the increase in fuel burn during a climb and decrease in fuel burn during an equivalent descent are assumed to be equal and, thus, cancel each other out. Furthermore, the SHM equipment is assumed to be retrofitted without resizing the aircraft[1]. With the Breguet equation, the range R_{flight} of an aircraft is given by

$$R_{flight} = E \cdot \frac{V}{b_F \cdot g} \cdot ln\left(\frac{m_0}{m_0 - m_t}\right) \tag{3.78}$$

where E is the lift-to-drag ratio of the aircraft, V is the aircraft velocity, b_F is the specific fuel consumption, g is the gravity constant, m_0 is the aircraft mass at take-off, and m_t is the fuel mass excluding reserves. After rearranging the Breguet equation to isolate m_t and

[1]The payload-range performance of the aircraft is, therefore, incrementally decreased with every incremental increase in SHM equipment mass.

including in the aircraft weight without fuel $m_{ZFW} = m_0 - m_t$, the fuel mass for a given flight distance R_{flight} can thus be calculated by

$$m_t = m_{ZFW} \cdot \left(e^{\frac{R_{flight} \cdot b_F \cdot g}{E \cdot V}} \right). \tag{3.79}$$

Assuming that the introduction of SHM does not impact the flight distances flown by the reference aircraft, the relative change in fuel burn through increased weight is given by

$$m_{t,SHM} = \frac{m_{ZFW} + m_{SHM}}{m_{ZFW}} \cdot m_t + \dot{m}_{F,P} \cdot \frac{R}{V} \tag{3.80}$$

where $m_{t,SHM}$ is the fuel mass required for aircraft with SHM system, m_{SHM} is the SHM system mass, and $\dot{m}_{F,P}$ is the increased fuel flow due to the increased onboard electrical power demand driven by the SHM system. This approach is only valid if the distances flown in practice are below the design range, considering an unchanged MTOW.

3.2 Airline Simulation

The implementation of SHM impacts the reliability and maintenance requirements of aircraft and thus influences the execution of airline operations. Specifically, researchers suggest that a reduction in airframe inspection effort increases aircraft availability and thus allows airlines to schedule additional flights. Additionally, the replacement of manual inspections with SHM systems allows for improved aircraft routing by decreasing the number of mandatory stops at designated maintenance airports. Relaxing boundary conditions for aircraft routing may enable more flights with a constant number of aircraft within a given time frame. With tactical planning at airlines, SHM systems with predictive capabilities can lead to fewer technical delays resulting from airframe failures and damages, currently affecting 0.01 to 0.5% of all departures [207–210]. Improved aircraft reliability can also reduce the number of spare aircraft in cases of sudden failures. A detailed overview of benefits for airline operations connected to SHM is given in Sections 2.2.2 and 2.2.3.

To estimate the magnitude of the proposed benefits, the following subsections derive and describe methodologies to connect aircraft maintenance requirements and reliability to the performance of airlines. The required scope of the introduced methodologies is defined in Subsection 3.2.1. Assumptions based on initial studies and results of previously conducted research on this topic are used to simplify the investigated problem. Subsequently, Subsection 3.2.2 introduces a method to derive the influence of predictive maintenance on airline networks. Finally, an approach to link aircraft reliability and available spare aircraft to airline performance is described in Subsection 3.2.3.

3.2.1 Definition of Airline Model Scope

Airlines are faced with complex and often $\mathcal{NP}$-hard problems which cannot be solved using analytical approaches, as mentioned in [80, pp. 205–208]. This circumstance is also reflected

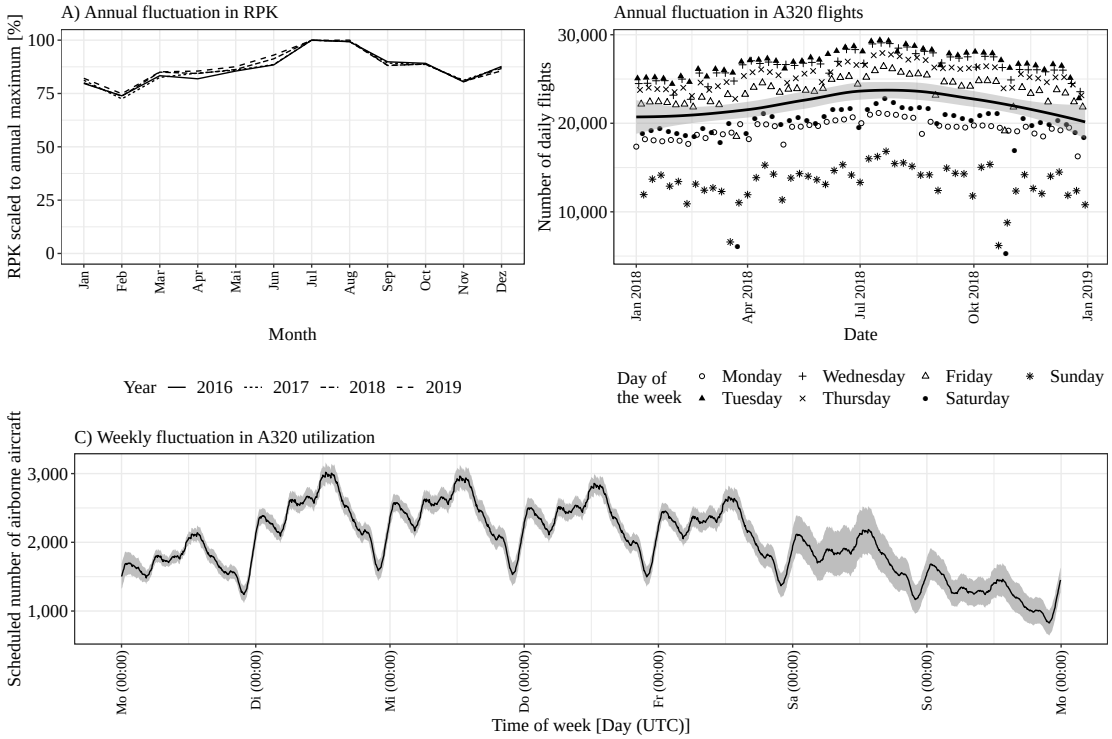

Figure 3.14: A) Annual fluctuation of global RPK based on [211, p. 1]. B) Daily Airbus A320 departures and local regression for 2018 based on data provided by OAG. C) Local regression of weekly fluctuation in scheduled airborne A320 aircraft in 2018 based on data provided by OAG. Gray area represents the 95% confidence interval of a local regression. All Airbus A320 family variants and all airlines are included.

in the organization of airlines, where the overall optimization problem of maximizing airline profitability is divided into numerous smaller problem sets, each addressed individually to reduce complexity [80, p. 208–212]. Different aspects of airline operations are possibly impacted by SHM. Therefore, *flight scheduling*, *aircraft routing*, *maintenance*, and *daily tactics or disruption management* are considered separately in this work. Available data, model requirements, and the representation of levers influenced by SHM are summarized in this subsection to define the scope of the utilized airline model.

The first step in operating an airline is the creation of a *flight schedule*, which is generally optimized for maximum airline profits, considering the expected passenger demand and available aircraft. Figure 3.14 A) illustrates the annual fluctuation in RPK, which oscillates within 12.5% of the mean. The seasonality in demand is matched by a varying supply of scheduled flights, as shown in Figure 3.14 B). The annual peak and minimum numbers of scheduled Airbus A320 flights deviate by approximately 10% from the mean. However, the daily variation is comparatively higher, floating between 30 and 100% of the weekly peak, as illustrated in Figure 3.14 C). Given the fluctuating aircraft usage throughout the week, a window of several hours exists daily, in which less than two-thirds of the required aircraft are scheduled for flight. SHM possibly reduces the overall maintenance burden and thus allows airlines to plan more flights for a single aircraft.

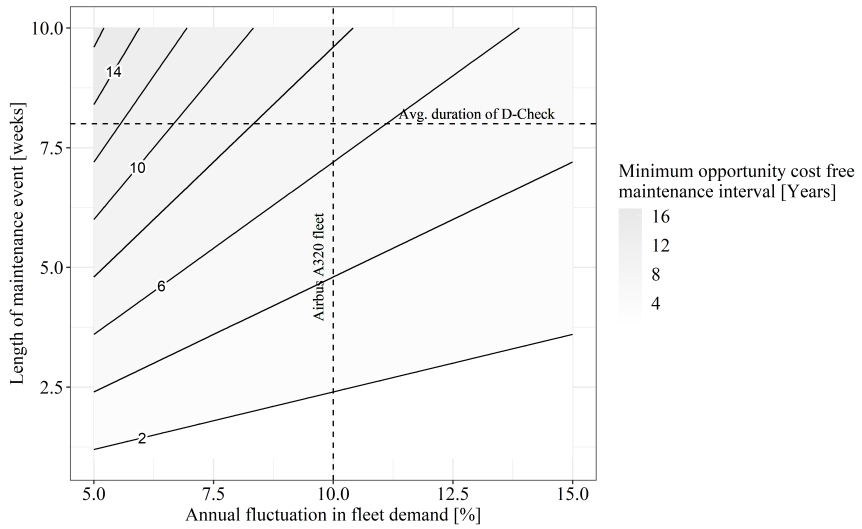

Figure 3.15: Annual fluctuation in fleet demand allows opportunity-cost-free inspection and maintenance events. The resulting interval between consecutive revenue neutral inspections depends on the annual fluctuation in fleet usage and duration of the inspection event.

However, the seasonality in demand provides airlines with the opportunity to conduct work-intensive maintenance events during times with less demand. In a letter-check maintenance approach for the Airbus A320, the work-intensive C-check and D-check are typically scheduled every 18^{th} and 72^{nd} to 144^{th} month, depending on the aircraft usage, and they require several weeks of work [212, pp. 12–13]. Assuming the fleet size is scaled according to the peak usage during July and August, the timeframe to conduct maintenance for the entire fleet without losing revenue-generating flights can be calculated based on annual fluctuation in fleet usage and the length of a maintenance event, as illustrated in Figure 3.15. Given the annual fluctuation in passenger demand, airlines can conduct extended aircraft maintenance events over several weeks without suffering opportunity costs in the form of lost revenue. Additionally, a detailed investigation of the base maintenance process by [148] demonstrated that the use of automated SHM technologies does not influence the critical path of the aircraft inspection, leaving the overall duration of the maintenance event constant. Therefore, the work at hand does not further investigate the impact of SHM on airline fleet schedules.

The next step for airlines, the optimization of the individual *aircraft routing*, is complicated by regulatory and technological constraints in practice. The lack of required freedoms of air may prevent an efficient routing [213, Ch. 4.1]. Inspection requirements call for airlines to route aircraft to selected maintenance stations after a specified interval, even if another more profitable routing may be feasible. Substituting regular manual structural inspections with SHM allows aircraft to operate away from maintenance locations, thus enabling improved routing. However, the driving inspection tasks behind frequent overnight or line maintenance checks are not structural components but rather parts of the aircraft's system and power plant. Aircraft inspections quoted in the MPD can be categorized by ATA-chapters. Regular inspection events are driven by work not concerned with the structural state of the aircraft,

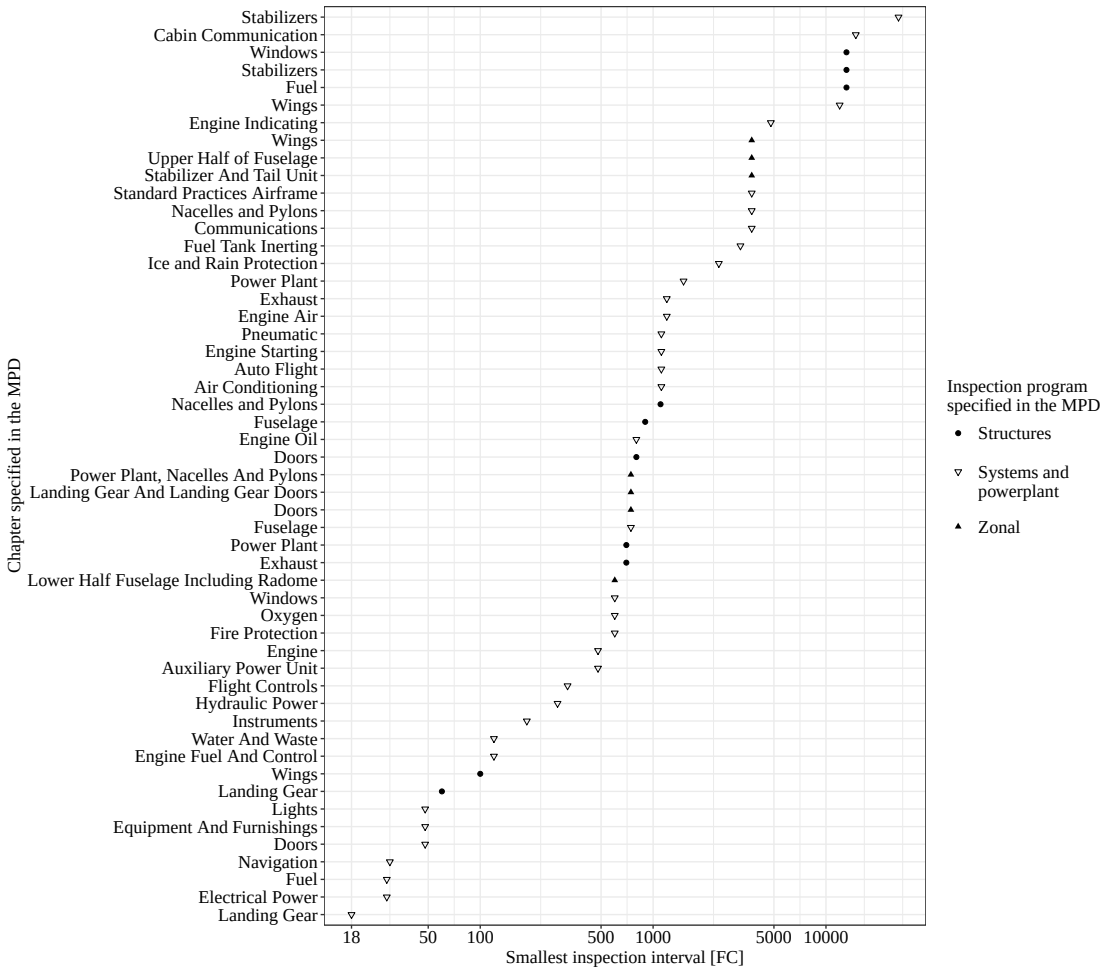

Figure 3.16: Shortest inspection intervals specified in the Airbus A320 MPD categorized by program and chapter, based on data from [175]. An average usage of 1.25 FH per FC and 6 FCs per day are considered.

as illustrated in Figure 3.16. An impact of SHM on the schedule of regular inspections only comes into effect if other schedule driving inspections are automated as well. The shortest inspection interval driven by structural components is greater than 50 flight cycles. For an aircraft operating in a hub structure, multiple opportunities for maintenance are provided before the first structural inspection is due. For large point-to-point networks, an increase in the time between inspections possibly yields improved aircraft routing. An investigation of local arrival times and layover lengths for the Airbus A320 fleet based on automatic dependent surveillance - broadcast (ADS-B) data reveals daily opportunities to conduct frequent inspections, as illustrated in Figure 3.17. Approximately one-tenth of all flights operate from airports with night curfews, providing a brief maintenance opportunity. Additionally, a significant increase in the duration of layovers has occurred at airports without curfews, either due to curfews at the next destinations, maintenance activities, or decreased demand. Still, the average ground times at night are significantly higher at airports with curfews. As opportunity cost free maintenance stops are available within the network and the

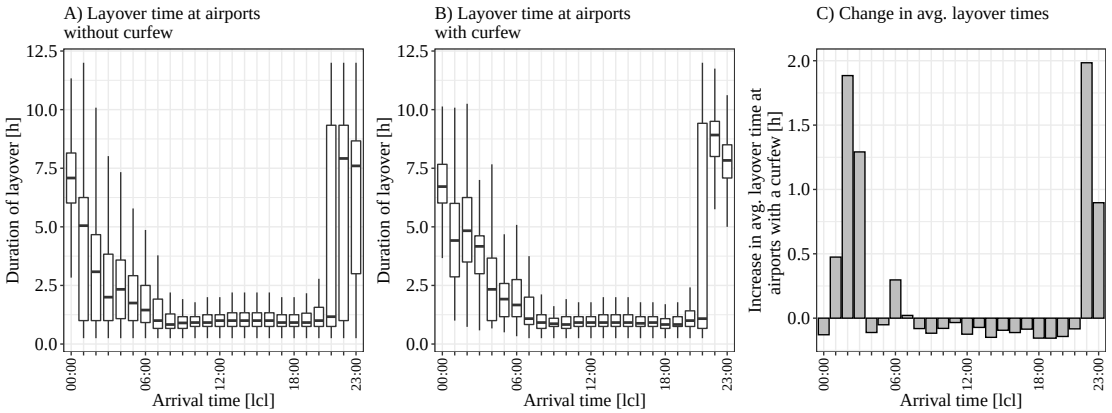

Figure 3.17: Layover on airports A) without nightly curfews, B) with nightly curfews, and C) impact of curfews on layover times. A total of 12,653,221 flights without curfews and 1,458,881 flights with curfews are considered between 2017-09-24 07:10:00 and 2019-11-29 14:15:00 for 6443 unique Airbus A320 aircraft.

frequency of planned aircraft maintenance events is not determined by structural inspections, the impact of SHM on the aircraft routing problem is not further evaluated as part of this work.

Furthermore, SHM can be used to mitigate unexpected failures causing *irregular operations* at airlines. As shown in Figure 2.15 on page 23, technical problems are the second largest cause for delay. Predictive maintenance can be used to preventively conduct repairs to mitigate unexpected breakdowns. Alternatively, airlines can prevent delays from unexpected breakdowns by resorting to unused spare aircraft that are not scheduled for regular operation. The number of required spare aircraft depends on the reliability of the aircraft. The proposed influences of SHM on different steps in the airline planning process are summarized in Table 3.6. Based on the initial investigation presented in this section, only the use of SHM in airline disruption management is further considered.

To this end, the following subsections provide a model to estimate airline reliability based on aircraft reliability, while considering the number of available spare aircraft. Hereby, approaches to investigate the effects of failures and false alarms during operation, as well as predictive maintenance requirements, are introduced. A method to derive the influence of predictive maintenance is also described in the following subsection.

3.2.2 Predictive Maintenance in Airline Networks

The unexpected failure of aircraft can lead to delays and disrupt airline operations. Depending on the magnitude of a previous delay, subsequent flights possibly have reactionary delays. To address this problem, airlines are presented with a variety of strategies. In the flight schedules, layover times can be increased to provide a buffer against unexpected delays, resulting in a decrease in airline revenue, however. Alternatively, predictive maintenance on the aircraft level allows airlines to enhance their scheduled inspection and maintenance activ-

Table 3.6: Scope of airline model utilized in this thesis.

Airline hierarchy	Suggested SHM benefit	Initial investigation	Considered in airline simulation
Flight scheduling	Decreased maintenance requirements to allow more flights	Flight schedule is seasonal. Fluctuation in demand allows opportunity cost free maintenance	No
Aircraft routing	Decreased inspection frequency allows better routing	Inspection frequency is driven by aircraft systems and powerplant	No
Maintenance scheduling	Decreased inspection requirements, shorter inspection, thus more flights	Ground time at night provides opportunity cost free maintenance	No
Disruption management	Avoid unscheduled inspections and repairs	Unexpected airframe, system and powerplant failures can equally lead to delays	Yes

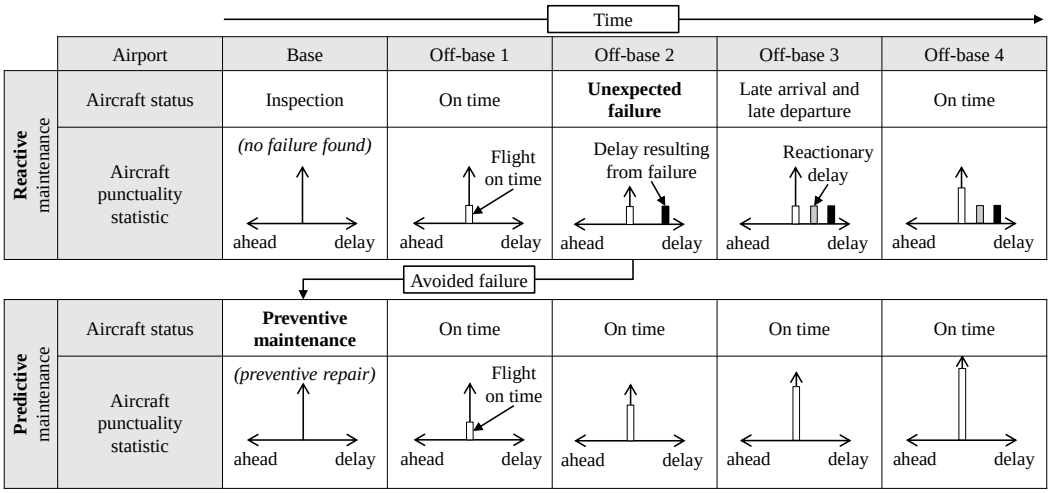

Figure 3.18: Influence of reactive and predictive maintenance on airline punctuality.

ities. Therefore, unexpected latent failures can be addressed at a more convenient time before they materialize. A comparison of the effects of an unexpected failure on aircraft delays is illustrated in Figure 3.18. The benefits of predictive maintenance depend on the aircraft's reliability, predictive maintenance performance, forecast horizon and share of aircraft coverage, the airline network, locations of maintenance stations, and routing of the individual aircraft.

For every aircraft routing, a series of consecutively visited airports $(ap_n)_{n=1}^{k}$ with $ap \in AP$ is defined, where AP are all airports served by the airline. For every airport ap_n in the routing of an aircraft, the corresponding failures $\vec{f}_{ap_n} = \begin{bmatrix} f_1 & f_2 & \dots & f_n \end{bmatrix}^T \in F$ shall be known, with

F being a set of all possible failures of the aircraft. Using the methodologies introduced in Section 3.1, the failures $\vec{f}_{ap_n}$ can be derived. The performance of predictive maintenance shall be given by $PM(x, y, h, C_{PM})$, with the FP rate x, TP rate y, predictive horizon in load cycles h, and the covered failures C_{PM}, which specifies the failures $\vec{f}_{ap_n}$ that can be predicted. For every ap_n, the corresponding layover duration $(l_{ap_n})_{n=1}^{k}$ is given. The minimum turnaround time l_{min} for the Airbus A320 is assumed to be 30 min [205, Ch. 5.2-5.3]. Unexpected failures lead to unscheduled maintenance $\vec{r}_{ap_n} = \begin{bmatrix} r_1 & r_2 & \dots & r_n \end{bmatrix}^T \in R_r$, where R_r represents the length of the repair in the presence of a failure F. R_r is calculated by arbitrarily multiplying the inspection and access time for a position provided in the MPD by ten. The total delay time d_{ap_n} at an airport is thus given by

$$d_{ap_n} = \underbrace{\sum_{n=1}^{k} \vec{r}_{ap_n}}_{\text{technical delay}} + \underbrace{d_{ap_{n-1}}}_{\text{reactionary delay}} - \underbrace{(l_{ap_n} - l_{min})}_{\text{make up for a delay}} . \tag{3.81}$$

The total delay d_{ap_n} is the sum of the technical delay occurring at that airport and the reactionary delay $d_{ap_{n-1}}$ from late departures at the previous airports less the excess planned layover time exceeding the minimum layover time. Using predictive maintenance, potential failures can be forecasted and avoided. For every ap_n, the service level $(s_n)_{n=1}^{k} \in S_{ap}$ is known, with $S_{ap} = \{M, \overline{M}\}$, where M denotes airports with maintenance facilities and $\overline{M}$ without. For every airline, the location of maintenance facilities is assumed to be known. Maintenance can be conducted without a penalty in terms of delayed flights when the aircraft is at a maintenance base and has a layover of more than five hours.

3.2.3 Airline Reliability and Provision of Spare Aircraft

A simplified model is introduced to capture the effect of changing aircraft reliability influenced by SHM on the number of required spare aircraft and canceled flights for a given airline network.

Within the model, airline networks are represented by airports and number of daily flights, as illustrated in Figure 3.19. The number of scheduled inbound flights $fl_{i,ap_n} \in \mathbb{N}_0$ and scheduled outbound flights $fl_{o,ap_n} \in \mathbb{N}_0$ for every airport $ap_n \in AP$ shall be known, where AP is the set of airports within the airline network. Furthermore, the expected technical

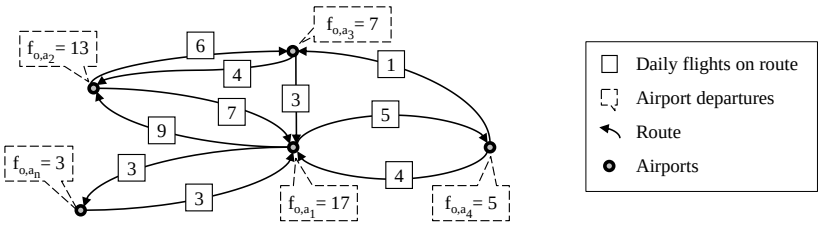

Figure 3.19: Simplified airline network consisting of airports and sums of scheduled flights used to derive the impact of spare aircraft on cancellations and airline reliability.

dispatch reliability per flight $\lambda_{AC} \in [0,1]$ shall be known and is assumed independent of the number of flights and operated aircraft. The expected number of canceled flights c_{ap_n} at airport ap_n is thus given by

$$c_{ap_n} = \mathit{fl}_{o,ap_n} (1 - \lambda_{AC}) . \tag{3.82}$$

The dispatch reliability of the entire airline λ_{AL} is thus given by

$$\lambda_{AL} = 1 - \frac{\sum_{n=1}^{|AP|} c_{ap_n}}{\sum_{n=1}^{|AP|} \mathit{fl}_{o,ap_n}}. \tag{3.83}$$

Assuming the existence of $n_{SA,ap_n} \in \mathbb{N}$ spare aircraft at airport ap_n, of which each can replace $\mathit{fl}_{SA} \in \mathbb{N}$ canceled flights per days, the expected number of canceled flights becomes

$$c_{ap_n} = max\{\mathit{fl}_{o,ap_n} \cdot \lambda_{AC} - n_{SA,ap_n} \cdot \mathit{fl}_{SA} \cdot (1 - \lambda_{AC}) , 0\}. \tag{3.84}$$

In practice, n_{SA,ap_n} and fl_{SA} are time-dependent since their availability coincides with the failure of an aircraft. However, this requires the routing of aircraft to be known, which is not considered in the model. Another assumption is that spare aircraft can only be used at a single airport. The probability of conducting all flights from a given airport without cancellations $P(X \geq \mathit{fl}_{o,ap_n})_{ap_n}$, assuming a Bernoulli process, is given by

$$P(X \geq \mathit{fl}_{o,ap_n})_{ap_n} = \sum_{i=k}^{n} \binom{\mathit{fl}_{o,ap_n} + n_{sa,ap_n} \cdot \mathit{fl}_{SA}}{i} \lambda_{AC}^{i} \cdot (1 - \lambda_{AC})^{(\mathit{fl}_{o,ap_n} + n_{sa,ap_n} \cdot \mathit{fl}_{SA}) - i} \tag{3.85}$$

where fl_{o,ap_n} is the number of scheduled flights, $n_{sa,ap_n} \cdot \mathit{fl}_{SA}$ is the sum of available spare aircraft flights , and X is the Bernoulli variable [214, p. 330]. The probability of fulfilling all flights of an airline without cancellations $P\left(c_{ap_n} = 0\right)_{AL,total}$ is given by

$$P\left(c_{ap_n} = 0\right)_{AL,total} = \prod_{n=1}^{|AP|} P(X \geq \mathit{fl}_{o,ap_n})_{ap_n}. \tag{3.86}$$

The departure-weighted probability of having no cancellations at airports in the network $P\left(c_{ap_n} = 0\right)_{AL,weighted}$ is given by

$$P\left(c_{ap_n} = 0\right)_{AL,weighted} = \frac{1}{|AP|} \sum_{n=1}^{|AP|} P(X \geq \mathit{fl}_{o,ap_n})_{ap_n} \cdot \mathit{fl}_{o,ap_n}. \tag{3.87}$$

For the model, airlines are assumed to strategically position spare aircraft at airports where the probability of operating all scheduled flights is lowest. The influence of ferry flights and

last-minute flight schedule adjustments on the positioning of spare aircraft is neglected. The location of the next spare aircraft $ap_{SA,n_{SA}+1}$ is given by

$$ap_{SA,n_{SA}+1} = \{ap_n | max\left(P(X \geq fl_{o,ap_n})_{ap_n}\right)\}. \tag{3.88}$$

Depending on the network topology, spare aircraft affect the overall airline reliability differently. To distinguish the topology of an airline network in this work, the Freeman network centrality index based on betweenness centrality is used, which *"is a measure of similarity to a perfect star"*, providing an intuitive understanding of an airline network layout [215, p. 15]. Appendix A.12 illustrates different network layouts and the corresponding Freeman network centrality index. However, an accurate description allowing the reproduction of an airline network requires additional metrics not considered in this work. Based on [216, 217], the Freeman network centrality index based on betweenness is calculated as follows. *"If g_{jk} is the number of geodesics linking [airports] ap_j and ap_k in a network, and $g_{jk}(ap_n)$ is the number of such paths that contain [airport] ap_n then:*

$$b_{jk}(ap_n) = \frac{g_{jk}(ap_n)}{g_{jk}} \tag{3.89}$$

is the proportion of geodesics linking ap_j and ap_k that contain ap_n. To determine the centrality of [airport] ap_n, [...] all these values for all unordered pairs of [airports] where $j < k$ and $j \neq k \neq i$ [are summed up]:

$$C_B(ap_n) = \sum_{j<k}^{n} \sum_{j<k}^{n} b_{jk}(ap_n) \tag{3.90}$$

[...] The betweenness $C_B(ap_n)$ of a [airport] ap_n [...] provides a measure of the overall centrality of [airport] ap_n in the network. [...] Let ap^* be the node with highest centrality, and then the Freeman centrality index of the network is as follows:

$$C_B = \frac{\sum_i^n [C_B(ap^*) - C_B(ap_n)]}{n^3 - 4n^2 + 5n - 2} \tag{3.91}$$

The Freeman network centrality index expresses the degree of inequality or variance in our network as a percentage of a perfect star network of the same size. This measure takes 1 for a star [or pure hub and spoke configuration] and 0 for a complete graph [pure point to point configuration]" [216, pp. 112–113]. An overview of the centrality of Airbus A320 operated networks is provided in Figure 3.20 itemized by airline. Additionally, the introduced spare aircraft model is applied to two selected airlines, illustrating the impact of aircraft reliability on airline reliability.

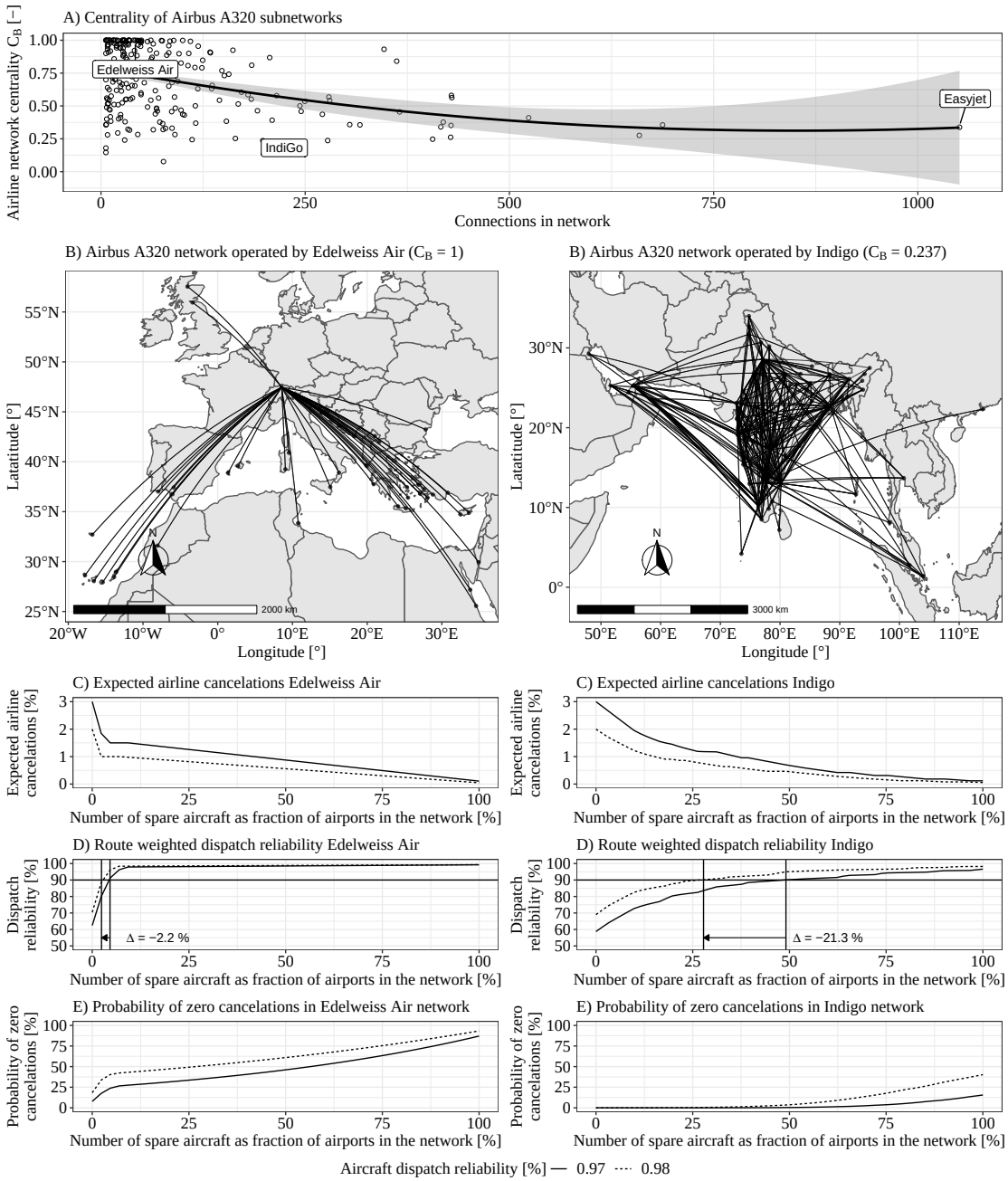

Figure 3.20: The airline network layout determines the impact of spare aircraft on expected airline cancellations, dispatch reliability, and probability of zero cancellations in the entire network: A) Similarity of Airbus A320 networks to a hub layout for every airline using the network centrality index C_B based on OAG data from the year of 2018, including local regression (black line) and 95% confidence interval (gray area). B) Routes of selected airlines, representing two extreme network configurations with $C_B = 1$ and $C_B = 0.237$. Subsequent placement of spare aircraft occurs by maximizing the weighted airport dispatch reliability of every airline. C) Average delay as a function of available spare aircraft. D) Dispatch reliability of airline based on dispatch reliability at every airport weighted by the number of routes served by this airport. The impact of spare aircraft is higher in hub structure; however, the impact of aircraft reliability is higher in the point-to-point structure. E) Probability that zero routes are canceled in a given day, assuming each route is served once every day.

3.3 Cost Model

The impact of SHM on the design, operation, and decommissioning of aircraft is analyzed in different dimensions. To compare the investigated effects of SHM on airline profitability and determine its economic value, a simplified model translates them into cost factors. Two types of costs are considered in the study. First, the *DOC*, which covers expenditures on the aircraft level, are typically broken down into *cash operating cost (COC)*, *cost of ownership (COO)*, and *additional operating cost (ADOC)*. Second, *capital expenditures (CAPEXs)*, which includes the costs associated with the financing of aircraft and investment into SHM equipment, are covered. IOC, which includes expenses for passenger services, ticketing, sales, promotion, ground services, and administration, is not considered since it is independent of SHM. The methods utilized to translate the performance of aircraft into cost are introduced in this section. All cost factors considered in the model are summarized in Table 3.7.

Table 3.7: Structure of cost model organized by type, category and factor of cost including the considered impact of SHM.

Type	**Cat.**	**Factor**	**Component**	**SHM Impact**
DOC	COC	Flying operations	Crew	
			Fuel	System weight
			Hull insurance	
			Misc. flying operations	
		Direct maintenance	Airframe repairs	Repair threshold
			Airframe materials	Repair threshold
			Airframes inspections	Automation
			Aircraft engines	
			Deferrals and provisions	
		Applied maintenance	Applied maint. burden	
		Net obsolescence and deterioration[a]	Net obsolescence and deterioration[a]	
	COO	Depreciation	Airframes	Service goal
			Engines	
			Other flight equipment	
			SHM system	Investment
	ADOC	Delay cost	Crew	Unsched. repair
			Passenger compensation	Unsched. repair
CAPEX	-	Interest	Aircraft	
			Fractional spare aircraft	Aircraft reliability
			SHM system	Debt-service costs

[a] "*Provision for losses in value of expendable parts inventory*" [DOT definition].

The individual cost components are quantified using *form 41* operating cost data reported by major airlines to the United States DOT. The DOT provides data for every quarter from 1990 to 2020 by aircraft type and airline. Only expenses attributed to the aircraft are considered. Based on the *form 41* operating cost data, the average expenditure per FH C_x can be calculated including the corresponding standard deviation. A comprehensive overview of the data and its application to the utilized cost model is provided in Appendix A.10. The introduction of SHM is assumed to impact only selected cost factors, as follows. Furthermore, airport fees, which vary significantly with the operated network structure and destinations, are not considered. Additionally, possible impacts on the applied maintenance cost in the form of optimized logistics, spare part budgeting, and improved engineering are not considered because of the lack of operational data, even though improved situation awareness enabled by SHM may influence these costs.

3.3.1 Cash Operating Cost

The COCs comprise expenses directly originating from flying the aircraft, including the cost factors for *flying operations*, *direct maintenance*, *applied maintenance*, and *obsolescence and deterioration*, which can be further broken down into individual components, as shown in Table 3.7.

The cost for *flying operations* C_{FO} includes the expenditures for crew C_{crew}, fuel C_{fuel}, hull insurance C_{ins}, and miscellaneous flying operations $C_{misc.}$. Since aircraft are assumed to be owned by the airline, leasing is not considered in the cost for flying operations. Therefore, the total expenditures for flying operation are given by

$$C_{FO} = C_{crew} + C_{fuel} + C_{ins} + C_{misc.}. \tag{3.92}$$

However, the fuel cost per flight hour C_{fuel} of the considered aircraft increases with the weight added by the SHM system and additional power requirements. The fuel cost for aircraft with SHM $C_{fuel,SHM}$ is calculated by

$$C_{fuel,SHM} = \underbrace{\frac{m_{t,SHM}}{m_t} \cdot C_{fuel}}_{\text{weight}} + \underbrace{\frac{\dot{m}_{F,P}}{\dot{m}} \cdot C_{fuel}}_{\text{power requirements}} \tag{3.93}$$

where m_t is the mass of fuel without SHM, $m_{t,SHM}$ is the mass of fuel with SHM, $\dot{m}$ is the fuel mass flow rate without SHM, and $\dot{m}_{F,P}$ is the fuel consumption increase from SHM power requirements. Thus, the total expenditures for flying operations with SHM become

$$C_{FO,SHM} = C_{crew} + C_{fuel,SHM} + C_{ins} + C_{misc.}. \tag{3.94}$$

The cost for *direct maintenance* C_{DM} includes expenditures for airframe repairs $C_{af\ rep}$, airframe materials $C_{af\ mat}$, airframe inspections $C_{af\ inspect}$, aircraft engines C_{eng}, and deferrals

and provisions $C_{def\&prov}$. The total expenditures for direct maintenance are therefore given by

$$C_{DM} = C_{af\ rep} + C_{af\ mat} + C_{af\ inspect} + C_{eng} + C_{def\&prov}. \tag{3.95}$$

The cost of airframe repairs with SHM $C_{af\ rep,SHM}$ are derived by comparing the total labor required to conduct airframe repairs without SHM $L_{af\ rep}$ to that with SHM $L_{af\ rep,SHM}$. Both $L_{af\ rep}$ and $L_{af\ rep,SHM}$ are derived from the aircraft simulation, which was introduced in Section 3.1. While SHM does not influence the process of repairing the structure, it can impact the frequency of repairs and thus influences the total time spent on repairing the airframe. Hence, $C_{af\ rep,SHM}$ is calculated by

$$C_{af\ rep,SHM} = \frac{L_{af\ rep,SHM}}{L_{af\ rep}} \cdot C_{af\ rep}. \tag{3.96}$$

The ratio of airframe repair cost $C_{af\ rep}$ to airframe material cost $C_{af\ mat}$ is assumed to be constant with and without SHM, such that

$$C_{af\ mat,SHM} = \frac{L_{af\ rep,SHM}}{L_{af\ rep}} \cdot C_{af\ mat}. \tag{3.97}$$

Furthermore, the inspection cost of the airframe $C_{af\ inspect}$ is based on the simulated aircraft inspection effort $L_{af\ inspect}$. The airframe inspection cost with SHM $C_{af\ inspect,SHM}$ is thus given by

$$C_{af\ inspect,SHM} = \frac{L_{af\ inspect,SHM}}{L_{af\ inspect}} \cdot C_{af\ inspect}. \tag{3.98}$$

Assuming the maintenance cost of engines C_{eng} and the cost of deferrals and provisions $C_{def\&prov}$ are unaffected by SHM, the expenditures for direct maintenance when using SHM is thus given by

$$C_{DM,SHM} = C_{af\ rep,SHM} + C_{af\ mat,SHM} + C_{af\ inspect,SHM} + C_{eng} + C_{def\&prov}. \tag{3.99}$$

Both the cost for *applied maintenance* C_{AM}, which includes overhead from maintenance activities, and the cost for *obsolescence and deterioration* $C_{obs\&det}$, which covers the regularly replacement of components, are assumed to be independent of SHM. Table 3.8 summarizes the assumptions for every cost factor based on DOT *form 41* data [7]. The standard deviation of a cost factor when considering SHM is defined by

$$\frac{SD_{cf,SHM}}{SD_{cf}} = \frac{C_{cf,SHM}}{C_{cf}}. \tag{3.100}$$

3.3.2 Cost of Ownership

As discussed in Section 2.2.1, an aircraft has a definite end of life after which it must be replaced. Therefore, every flight hour depreciates its value. The COO reflects this consumption of capital invested into the aircraft as a function of its usage. In accounting, the depreciation is not always determined by usage, but a variety of other depreciation methods are used, depending on the airline and prevailing jurisdiction [178]. *"Depreciation methods and residual value estimates are disclosed in financial statements. Generally aircraft assets are depreciated over 15 to 25 years with residual values of between 0 to 20%. The straight-line method of depreciation is the most commonly used. [However, small] changes in useful economic life and residual value estimates can have a significant impact on the profit or loss in a period"* [178, p. 12]. In this work, aircraft are not depreciated over calendar time but FHs. The utilized *form 41* data provides the cost for airframe depreciation $C_{depr\ af}$, flight equipment depreciation $C_{depr\ fe}$, and engine depreciation $C_{depr\ eng}$.

However, airlines report depreciation costs only for aircraft they own. For leased aircraft, the leasing costs C_{leas} are reported as part of their expenses for flying operations, or COC.

Table 3.8: Airbus A320 COC per FH based on DOT *form 41* data.

Cost Factor	Cost component	Median [USD]	MAD [USD]	Mean [USD]	SD [USD]	N[a] [-]
Flying Operations	Crew [C_{Crew}]	694.6	313.0	812.3	369.8	957
	Fuel [C_{Fuel}]	1889.0	682.4	1992.8	714.3	957
	Hull insurance [C_{ins}]	6.4	5.8	16.5	26.5	913
	Misc. flying operations [$C_{misc.}$]	79.2	42.7	87.9	64.5	913
Direct maintenance	Airframe repairs [$C_{af\ rep}$]	134.0	98.1	158.8	106.6	957
	Airframe materials [$C_{af\ mat}$]	53.0	35.4	73.6	57.3	901
	Airframe inspections [$C_{af\ inspect}$]	95.0	56.1	115.5	70.7	957
	Aircraft engines [C_{eng}]	181.9	201.3	223.7	174.5	949
	Deferrals and provision [$C_{def\&prov.}$]	188.5	20.2	172.6	60.9	39
Applied maintenance	Applied maintenance Burden [C_{AM}]	176.4	77.8	188.5	85.8	729
Net obsolescence	Net obsolescence [$C_{obs\&det}$]	7.1	7.1	10.1	9.3	470
Total	-	3505.2	-	3852.5	180.4	-

[a] Available data points (unique quarterly report and airline) for respective cost factor.

However, the data provided by the DOT include both leasing and depreciation expenditures for airlines if they rely on both ownership models within a reported quarter. Since this work assumes aircraft are owned entirely by the airline, the leasing costs C_{leas} specified in the *form 41* data are added to the depreciation cost as follows:

$$C_{depr\ af} = C_{depr\ af,DOT} + \frac{C_{depr\ af,DOT}}{C_{depr\ af,DOT} + C_{depr\ fe,DOT} + C_{depr\ eng,DOT}} \cdot C_{leas}, \tag{3.101}$$

$$C_{depr\ fe} = C_{depr\ fe,DOT} + \frac{C_{depr\ fe,DOT}}{C_{depr\ af,DOT} + C_{depr\ fe,DOT} + C_{depr\ eng,DOT}} \cdot C_{leas}, \tag{3.102}$$

$$C_{depr\ eng} = C_{depr\ eng,DOT} + \frac{C_{depr\ eng,DOT}}{C_{depr\ af,DOT} + C_{depr\ fe,DOT} + C_{depr\ eng,DOT}} \cdot C_{leas}, \tag{3.103}$$

where $C_{depr\ af}$, $C_{depr\ fe}$, and $C_{depr\ eng}$ are the adjusted depreciation costs after distributing the leasing cost C_{leas}, and $C_{depr\ af,DOT}$, $C_{depr\ fe,DOT}$, and $C_{depr\ eng,DOT}$ are the depreciation costs provided in DOT *form 41*. The allocation of leasing costs does not change the distribution of the different depreciation costs. Furthermore, a change in aircraft lifetime following the introduction of SHM is assumed to affect the airframe depreciation cost only since aircraft engines are regularly moved between aircraft and flight equipment is typically replaced multiple times over the lifetime of the aircraft. Therefore, both $C_{depr\ fe}$ and $C_{depr\ eng}$ are independent of SHM.

Since no SHM system is used on a large scale in commercial aviation as of the writing of this thesis, the estimates for the investment costs are based on general assumptions. The *total investment cost for an SHM system* $C_{SHM\ inv\ total}$ includes the purchase price of the system and required work for its installation.

The total investment cost for the system is specified by

$$C_{SHM\ inv\ total} = A_{part} \cdot C_{inv\ area\ specific}, \tag{3.104}$$

where $C_{inv\ area\ specific}$ are the area-specific installation and purchase costs. The depreciation per FH $C_{SHM\ inv}$, assuming a linear depreciation, can be calculated by

$$C_{SHM\ inv} = \frac{C_{SHM\ purchase} + C_{SHM\ install\ total}}{60,000FH}. \tag{3.105}$$

For OLM and hybrid systems, the purchase price is assumed equal to the cost of DM systems. These assumptions are merely educated guesses, owing to the lack of existing programs. No reference values have been published for existing military systems, and development costs are not declared separately. However, the acquisition costs for SHM are quoted separately in this work and may be adjusted with improved knowledge in the future.

Additionally, amortization costs of flight equipment $C_{amort\ fe}$ are considered. Unlike depreciation costs for tangible assets, amortization costs cover intangible assets that have no resale value, such as the cost of branding the aircraft. The expenditures for every component of the COO are quantified in Table 3.9. Summarizing the total COO per FH over 60,000 FHs, the aircraft usage originally specified in the DSG and neglecting the cost of SHM, results in a mean lifetime COO of USD 40,728,000 and median lifetime COO of USD 49,866,000. Given the assumed COO and average list price for the Airbus A320 of USD 101M, a reduction on the list price of 49% to 59% is implied, which is in line with typical discounts for airlines [218, p. 1].

3.3.3 Additional Operating Cost

Additional operating costs C_{ADOC} capture expenses resulting from delays caused by technical failures. The costs from delayed flights include hard delay costs, comprised of additional crew cost expenses and passenger compensation, which are based on [219]. Of note, the study presented by [219] specifically covered European airlines, and the results are published in Euro, requiring conversion to USD. A loss in market share of the airline due to unpunctuality, reactionary delays in the aircraft routing, and additional fuel cost and maintenance expenditures are not considered. Delays due to technical failures are calculated in the aircraft simulation. The additional crew cost resulting from a delay is therefore assumed to be

$$C_{delay,crew} = 7.8 \cdot t_{delay} \cdot \frac{USD}{EUR}, \tag{3.106}$$

Table 3.9: Airbus A320 COO per FH based on DOT *form 41* data. Depreciation of SHM is calculated as part of this work.

Cost factor	Cost component	Median [USD]	MAD [USD]	Mean [USD]	SD [USD]	N [-]
Depreciation cost	Depreciation airframes [$C_{depr\ af}$]	450.4	-	505.3	227.2	884
	Depreciation flight equipment [$C_{depr\ fe}$]	70.3	-	106.3	117.1	417
	Depreciation engines [$C_{depr\ eng}$]	131.8	-	174.1	115.9	906
	Depreciation SHM [$C_{depr\ SHM}$]	NA	NA	NA	NA	NA
Amortization	Flight equipment [$C_{amort\ fe}$]	26.3	24.4	45.4	41.2	471
Total	-	678.8	-	831.1	139.7	-

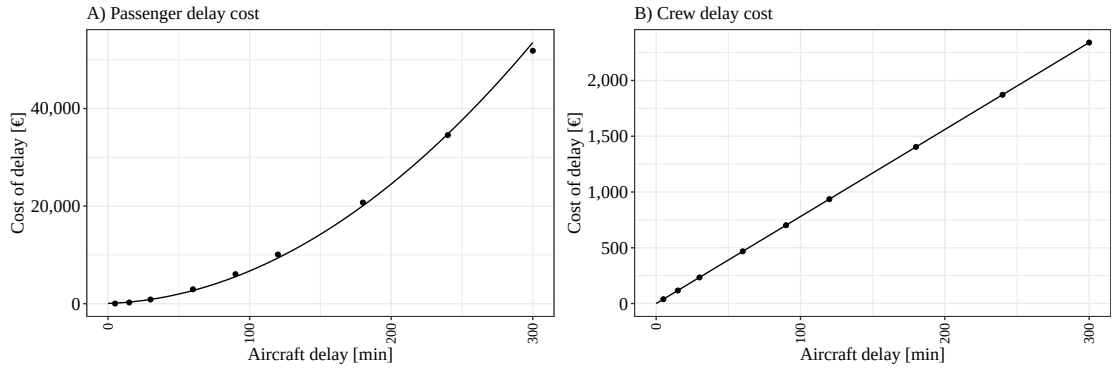

Figure 3.21: Regression of passenger delay cost driven by compensations in A) and crew delay cost B). The utilized data is based on [219, p. 34, 37] and marked by a dot.

where EUR 1 = USD 1.2 [219]. The cost of a delay due to passenger compensation is assumed at

$$C_{delay,passenger} = \left((7.1207 + 0.7474 \cdot t_{delay})^2 - 50.7\right) \cdot \frac{USD}{EUR} \tag{3.107}$$

[219]. Thus, the total delay cost $C_{delay,total}$ can be estimated as

$$C_{delay,total} = \begin{cases} C_{delay,crew} + C_{delay,passenger} & \text{for } t_{delay} \leq 300 \\ 67,030 & \text{for } t_{delay} > 300 \end{cases} . \tag{3.108}$$

Once reaching a delay of 300 min, the flight is canceled and the total delay cost of USD 67,030 is assumed. A comparison of the delay cost presented by [219] and the derived delay cost regression in Eq. 3.106 and Eq. 3.107 are provided in Figure 3.21.

Additional cost associated with the use of SHM can arise from reduced payload capacities. As described in [174], "*if SHM is considered as retrofit system in an existing aircraft, the SHM weight reduces the payload capacity and thus the opportunity to generate revenue. However, the magnitude of this effect depends on the payload and range distribution serviced by the airline. In cantilever wing aircraft, the maximum payload is effectively limited by the maximum zero fuel weight (MZFW) and MTOW. [A reduced maximum payload decreases the revenue generation only if an airline uses the entire load capacity of the aircraft.] Second, the location within the aircraft where the SHM system is installed determines if the equipment weight is considered as part of the aircraft zero fuel weight (ZFW) or not. Weight added to the wing is not considered part of the ZFW, but only take off weight (TOW). However, the MTOW limits the payload for missions beyond a certain range. Therefore, the impact of retrofit SHM equipment weight on the revenue-generating capability of aircraft depends on the distribution of typical payloads and ranges, as illustrated in Figure 3.22. The loss in revenue Δ_{Rev} from SHM equipment installed on the wing is based on [220] and calculated by*

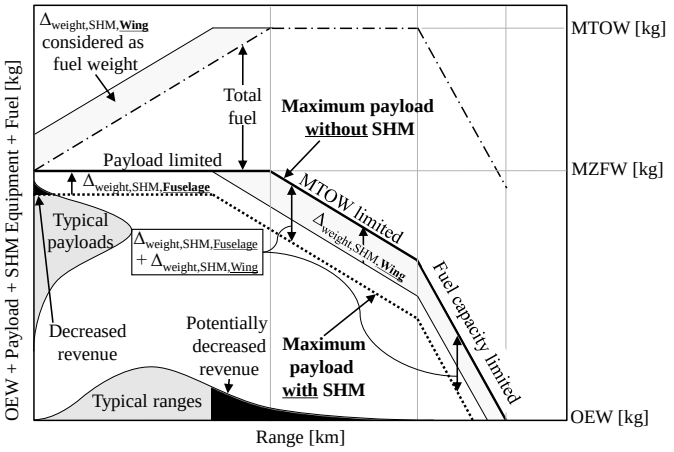

Figure 3.22: Weight added to the fuselage increases $\Delta_{WeightFuselage}$ and Δ_{Weight} equally, while weight added to the wing is considered only through Δ_{Weight}. Thus, SHM equipment weight impacts payload capacity differently depending on location. Potential airframe weight savings connected to the use of SHM are neglected in this figure. The payload-range diagram is adapted from [221, p. 7, 174, p. 10].

$$\Delta_R = \begin{cases} 0, & \text{for } 0 \leq \Delta_{MTOW} \leq 2\% \\ 4.8333 \cdot \Delta_{MTOW}^2 - 0.105 \cdot \Delta_{MTOW} + 0.0002, & \text{for } 2\% < \Delta_{MTOW} \leq 10\% \\ \text{undefined}, & \text{for } \Delta_{MTOW} > 10\% \end{cases} \quad (3.109)$$

where $\Delta_{MTOW} = \frac{m_{SHM}}{m_{MTOW}}$ *and MTOW is assumed to be 73,500 kg. The revenue Rev of the aircraft is assumed to be USD 5,900 per flight hour for the reference aircraft. At a median load factor of 81% and maximum average load factor of 95 %, it is assumed that 8 of the 160 seats mostly remain empty. Assuming a passenger weight of 100 kg, the first 800 kg of equipment mass added to the fuselage does not impact the revenue-generating capabilities of the aircraft. For every additional 100 kg, the revenue decreases by* $\frac{5900\ USD}{152} = 38.82$ *USD per FH*" [174].

3.3.4 Capital Expenditure

CAPEXs result from borrowing capital to invest into the ownership of assets. In this work, they comprise the *interest for owning the aircraft* $C_{debt\ AC}$, the *interest for owning spare aircraft* $C_{debt\ spare}$, and the *interest for owning an SHM system* $C_{debt\ SHM}$. The annuities payable by the airline to the capital provider are assumed to be constant. They include the redemptions that are considered in the COO and the interest payments represented in the CAPEX. While the annuities stay constant over time, the ratio between interest and redemption, which make up the annuities, changes. In order to provide a constant cost breakdown per FH over time, both redemptions and interest are considered as lifetime averages and are distributed equally to every FH. The redemption of the loan is represented by the COO. Since they are typically paid over time rather than usage, the assumption is

made that the airline pays back the loan over $t_l = 20$ yr and 60,000 FCs, corresponding to an average daily usage of 8.2 FHs. As introduced in Section 3.1.7.1, the WACC in aviation can be assumed to be 8% annually from the outstanding loan.

The total interest $C_{debt\ AC\ total}$ payable by the airline over t_l is computed by

$$C_{debt\ AC\ total} = \underbrace{C_{AC}}_{\text{credit volume}} \cdot \underbrace{\left(t_l \cdot \frac{WACC}{(WACC+1)^{t_l}-1} \cdot (WACC+1)^{t_l} - 1 \right)}_{\text{debt-cost factor}}, \tag{3.110}$$

where C_{AC} is the purchase price of the aircraft, assuming an annuity loan or level-payment mortgage [222, p. 46]. The effects of WACC and credit period t_l on the debt-service cost factor are illustrated in Figure 3.23. The interest cost for the aircraft per FH $C_{debt\ AC}$ is thus given by

$$C_{debt\ AC} = \frac{C_{total\ debt\ AC}}{60,000FH}. \tag{3.111}$$

Airlines can provide spare aircraft to address the issue of inherent unreliability. Assuming that spare aircraft are not used until they are replaced, they do not depreciate. At a replacement after t_l, the aircraft has the entire 60,000 FHs to fly. However, their market value has depreciated with the efficiency improvements of alternative aircraft, as described in Section 3.1.7.1. Since the usage of spare aircraft results from the unreliability of the aircraft, these costs are distributed via the CAPEX in the form of additional capital requirements. The residual value of unused spare aircraft $C_{res\ spare\ AC}$ after the time $t_l = 20$ yr is given by

$$C_{res\ spare\ AC} = C_{spare\ AC} \cdot \frac{1}{(\xi+1)^{t_l}}. \tag{3.112}$$

The total cost to finance a spare aircraft is thus given by

$$C_{total\ spare\ AC} = \underbrace{C_{spare\ AC} - C_{res\ spare\ AC}}_{\text{lost value}} + \underbrace{C_{debt\ spare\ AC\ total}}_{\text{interest}}, \tag{3.113}$$

where $C_{spare\ AC}$ is the purchase price of the spare aircraft and $C_{debt\ spare\ AC\ total}$ is the total interest cost for the spare aircraft, which are computed by Eq. 3.110. The cost for a spare aircraft can now be distributed to the operating costs of every aircraft, given the total number of aircraft N_A in the fleet and total number of spare aircraft N_{SA}:

$$C_{spare\ AC} = \frac{C_{total\ spare\ AC}}{60,000FH} \cdot \frac{N_{SA}}{N_A}. \tag{3.114}$$

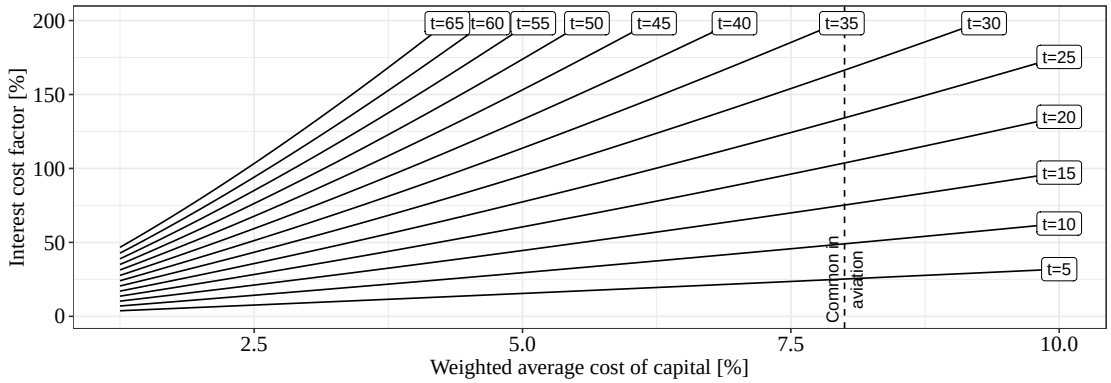

Figure 3.23: Influence of WACC and credit period t on debt-service cost factor.

The interest payable due to an investment into SHM is given analogous to Eq. 3.110 by

$$C_{debt\ SHM\ total} = C_{SHM} \cdot \left(t_{l,SHM} \cdot \frac{WACC}{(WACC+1)^{t_{l,SHM}} - 1} \cdot (WACC+1)^{t_{l,SHM}} - 1 \right), \tag{3.115}$$

where $t_{l,SHM}$ is the investment period in the SHM system and C_{SHM} is the investment cost into an SHM system. For retrofit SHM systems, $1 \leq t_{l,SHM} \leq t_l$ holds.

Chapter 4

Conceptual Integration of Structural Health Monitoring in Commercial Aircraft

This chapter describes the conceptual implementation of SHM into commercial aircraft. The optimization problem faced by manufacturers, operators, and other respective stakeholders when implementing SHM is discussed in Section 4.1. As a result, simplifications are presented, on which the conducted cost-benefit analysis of SHM is based. Subsequently, a reference airline is defined in Section 4.2 to describe the operative environment in which SHM is used. Additionally, a reference aircraft is defined in Section 4.3. The definitions of both reference airline and reference aircraft are based on actual Airbus A320 flight movements. Finally, the investigated SHM scenarios are described in Section 4.5.

4.1 Considerations on Multi-Objective Optimization

The design and implementation of SHM systems in commercial aviation can be a multi-objective optimization problem, characterized by multiple conflicting objective functions [223, p. 1]. Generally, a solution to this problem *"is represented by a curve [or surface,] constituted by a set of points that are all equally important, differently from single-objective optimization problems, where the solution is given by a single point"* [223, p. 1]. However, with increasing system complexity, the number of possible combinations of boundary conditions increases. In the context of SHM, different optimization objectives across the airline system hierarchy exist, as illustrated in Figure 4.1. Because of the complex impact of SHM on the operation of aircraft and airlines, researchers and practitioners need to define suitable problem boundaries. As described extensively in Section 2.4 (see page 31), the setup of cost-benefit studies covering SHM in commercial aviation significantly impacts the analysis results. Once the scope is defined, the multi-objective optimization problem can be solved using various methods.

In *a priori methods*, information about the preference among different objectives has to be available, e.g., as expressed by a specific goal for every objective or by a transfer func-

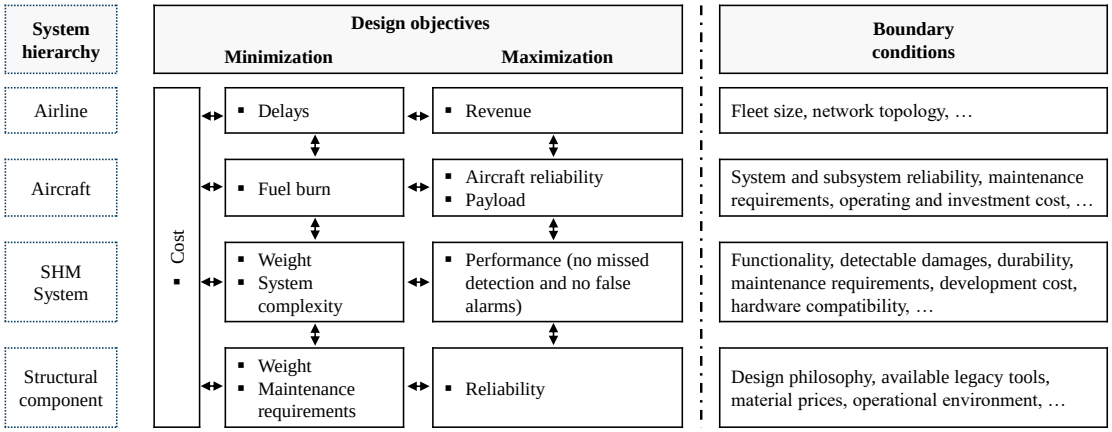

Figure 4.1: System design objectives are contradictory across the entire air transport system hierarchy, from the design of aircraft structures, the SHM system itself, and the overall aircraft design up to the organization of the airline. Given environmental boundary conditions, optimum airline and aircraft system designs can be found.

tion, mapping all objectives to the same dimension [223, p. 22]. When transforming the multi-objective optimization problem to a single-objective function problem, a point solution becomes achievable [223, p. 25]. If SHM implementation is considered a strict business problem, each affected dimension may be transformed to airline profit. However, the operational environment of airlines is highly heterogeneous, and the availability of detailed financial data is poor, rendering this solution infeasible for this work.

With *a posteriori methods*, all non-dominant Pareto-optimal solutions to the multi-objective optimization problem are identified and presented as a curve or surface. This can theoretically be achieved by a full enumeration of the problem set or by a variety of other approaches, as presented in [223]. With the numerous input parameters and significant time consumption of a single simulation, this approach is considered impractical for this thesis because of the required computational resources.

Further, *interactive methods* are neglected in the scope of this work, as they rely on a user to incrementally reveal a preference [223, p. 22]. Also, *non-preference methods* are not considered since they neglect weights between different objectives.

Therefore, instead of treating the introduction of SHM as a multi-objective optimization problem across multiple airline hierarchies, a reference airline (Section 4.2) and reference aircraft (Section 4.3) are defined to reduce the problem complexity. Their definitions reflect the operational reality of a wide range of airlines or aircraft. SHM is evaluated by the cases described in Section 4.5.

4.2 Reference Airline Composition

The reference airline used to investigate the effect of SHM on network-level airline metrics is derived in this section. Based on selected airline characteristics that influence the im-

pact of SHM, as discussed in Section 3.2, the reference airline is defined with respect to its *network centrality index*, *average flight time*, *number of airports in the network*, and *availability of maintenance stations*. To quantify the selected metrics, ADS-B data gathered by Flightradar24 (FR24) for 7,952 aircraft over 797 days between September 23$^{\text{rd}}$, 2017 and November 29$^{\text{th}}$, 2019, amounting to 16,625,103 flights, and the OAG flight-schedule database for 2018 are used. To avoid an over-representation of small airlines, the reference airline metrics are quantified using aircraft-weighted median values.

The topology of the airline network, which accounts for the effect aircraft reliability has on the provision of spare aircraft, is approximated by the *network centrality index*. As shown in Figure 3.20 on page 74, improved aircraft reliability has a greater impact on the required number of spare aircraft in a point-to-point network.

The *average flight time* per FC drives the scope of the aircraft maintenance plan and, therefore, determines the maintenance effort required for individual aircraft systems.

The *flights between consecutive overnights at a station* reflect the frequency with which opportunity-cost-free maintenance stops are possible for the aircraft. In the scope of this work, the aircraft station, or home base, is identified using FR24 data. The airport with the most overnight stops, characterized by the last flight of a day before a longer ground time, is assumed to be the home base of the aircraft. Subsequently, the number of flights between two consecutive overnight stops at an aircraft's home base can be computed. Any maintenance activity can presumably be conducted at the home base. Every other airport is considered to be off-base. The number of flights between consecutive overnight stops at a station is therefore driving the influence of the prognostic horizon of remaining useful life methods.

Respectively, the *duration of overnights at a station* provides an indication about the time frame available for opportunity-cost-free maintenance.

The considered metrics are illustrated for every airline operating Airbus A320 aircraft in Figure 4.2. The reference airline is selected to best resemble the median operating environment of the Airbus A320 aircraft. Each airline operating the Airbus A320 is compared to the overall fleet-wide, aircraft-weighted median values for network centrality, aircraft flight time, consecutive flights between overnight at a station, duration of overnight stops at a home base, and the number of aircraft in the fleet. The resulting short list of suitable reference airlines is summarized in Table 4.1. Based on the considered metrics, Juneyao Airlines is selected as the reference airline, as it best resembles the operating environment of the median aircraft. Of note, the cost model introduced in Section 3.3, which uses data for airlines based in the United States of America, is applied to the reference airline without considering the local operating cost structure, that is e.g., driven by labor and fuel cost.

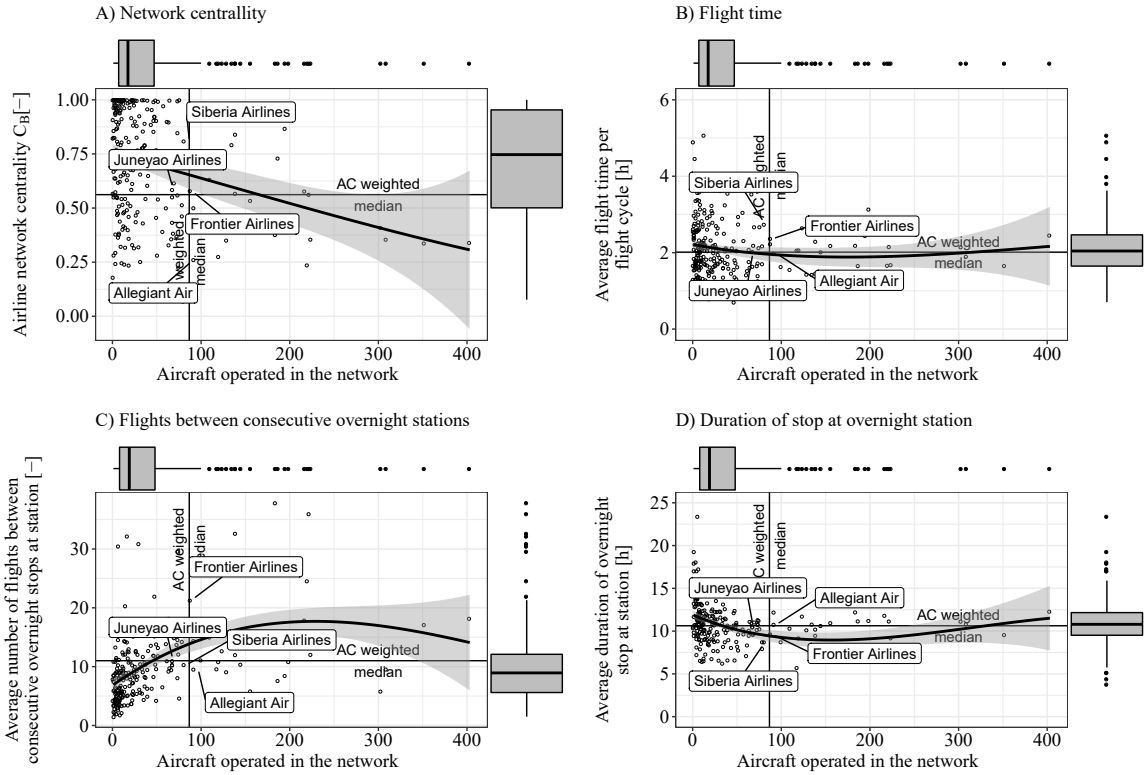

Figure 4.2: Comparison of A) network centrality index, B) flight time, C) number of flights between consecutive overnight stops, and D) duration of overnight stops with regard to airline size, based on data from FR24 and OAG for the Airbus A320. The gray area represents a 95% confidence interval of local regression.

Table 4.1: Comparison of reference airline candidates with median Airbus A320 operating environment using fleet level metrics.

Metrics	**Aircraft weighted median**[a]	**Siberia airlines**	**Frontier airlines**	**Allegiant air**	**Juneyao airlines (reference)**
Network centrality index [-]	0.56	0.81	0.58	0.26	0.59
Aircraft flight time [h]	2.01	2.74	2.37	1.97	2.03
Consecutive flights between overnight at station [-]	11.01	10.35	21.30	9.57	11.01
Duration of overnight stop at home base [h]	10.62	8.74	9.55	10.79	10.50
Airbus A320 in fleet [-]	86.65	81.00	88.00	92.00	68.00

[a] for all Airbus A320 airline fleets.

4.3 Reference Aircraft

This section discusses the reference aircraft to be used in the cost-benefit study. Based on the Airbus A320, the *aircraft performance parameters*, *typical usage*, *failure behavior*, *structural properties*, and *maintenance requirements* are defined using publicly available information and assumptions. However, reliability and maintenance performance metrics tracked by airlines on the aircraft component level are typically not shared with the manufacturer and the public, limiting the quality and quantity of available resources.

4.3.1 Aircraft Performance Parameters

The aircraft performance parameters assumed for the reference aircraft are summarized in Table 4.2. Together with the assumed airline network and aircraft flight plan, the performance parameters are used to reconstruct operational loads and calculate aircraft fatigue to investigate the effect of different decommissioning criteria on available aircraft lifetime. Specifically, a new decommissioning criterion based on monitoring fatigue is compared to the numbers of fatigue-driving FCs and FHs, similar to the current LoV approach.

Table 4.2: Selected reference aircraft performance characteristics based on the Airbus A320, adapted from [200, p. 2] including primary sources.

Performance characteristics	**Size**	**Source**
Additional fuel reserve $W_{Fuel,res}$[a]	2,500 kg	Assumption
Cruise speed at FL 390 M_c	0.79	[224]
Fuel consumption during taxi F_{Taxi}	0.1 kg/s	Assumption
Fuel reserve factor $F_{Fuel,res}$[b]	1.05	Assumption
Lift-to-drag ratio $\frac{L}{D}$	15	Assumption
Maximum payload $W_{PL,max}$[c]	16,600 kg	Assumption
Maximum takeoff weight (MTOW) W_{MTOW}	73,500 kg	[218, pp. 26–27]
Maximum weight of fuel $W_{Fuel,max}$	20,000 kg	[218, p. 29]
Minimum payload (Crew, e.g.) W_{misc}	600 kg	Assumption
Minimum weight of fuel $[W_{Fuel,prop,min}]$[d]	5,000 kg	Assumption
Number of seats N_{Seats}	160	[218, pp. 53–54]
Operating empty weight W_{OEW}	42,200 kg	[225]
Specific fuel consumption SFC_{cruise}	16.88 g/(kN·s)	[226]
Weight per passenger W_{PAX}	100 kg	Assumption

[a] Assumed fuel reserve additional to required fuel for specific flight distance.
[b] Flight distance–dependent fuel reserve.
[c] Defined as minimum payload plus the number of seats times the weight per passenger.
[d] A flight with less fuel is considered to be prohibited by airline policies.

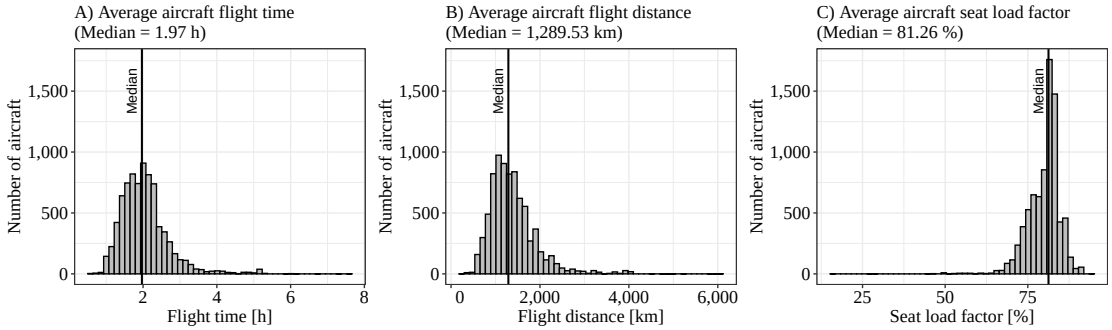

Figure 4.3: Average usage of Airbus A320 aircraft with regard to A) flight time, B) flight distance, both based on FR24 data, and C) seat load factor based on Sabre® data.

4.3.2 Operational Usage

The operational usage of the aircraft describes the assumed average flight time, flight distance, and seat load factor of the reference aircraft. Flight time and distance of the Airbus A320 aircraft are derived from FR24 data. The average seat load factor of the considered aircraft and airlines is based on Sabre® data for 2017. The operational usage of all Airbus A320 aircraft is illustrated in Figure 4.3. For the reference aircraft, a seat load factor of 81%, a flight distance of 1290 km, and a flight time of 2 h are assumed, representing the average flight of the median aircraft in the Airbus A320 fleet.

4.3.3 Aircraft Reliability

As previously noted, the public availability of aircraft reliability data is limited, specifically on the component level. However, unexpected failures drive unscheduled maintenance, which affects the overall cost of the airline. Within this study, airframe failures are simulated using the methodologies presented in Section 3.1.1. The simulations of other failures are based on the generic reliability assumptions presented in this section. The share between system and structural failures and thus the leverage of SHM on aircraft dispatch reliability are influenced by the presented reliability assumptions, which are based on the National Aeronautics and Space Administration (NASA)-administered *aviation safety reporting system (ASRS)*, the EUROCONTROL *central office for delay analysis*, and *scientific literature*, specifically [209, 210].

The *ASRS* includes reports from *"[p]ilots, [...] mechanics, ground personnel, [about incidences or situations ...], in which aviation safety may have been compromised"*, such as incidences where aircraft equipment failed during operation [227]. *"All submissions are voluntary"* to improve safety and data quality [227]. The reported incidences also cover the failure of aircraft equipment during operation. Using the number of recorded airborne hours for a specific aircraft model reported by the DOT, the mean time between reported failure (MTBRF) for commercial aircraft operating under US jurisdiction can be calculated based on the number of observed and reported failures in the ASRS database. For an Airbus A320 operating in the United States of America, the MTBRF can be broken down by ATA-chapter, as illustrated

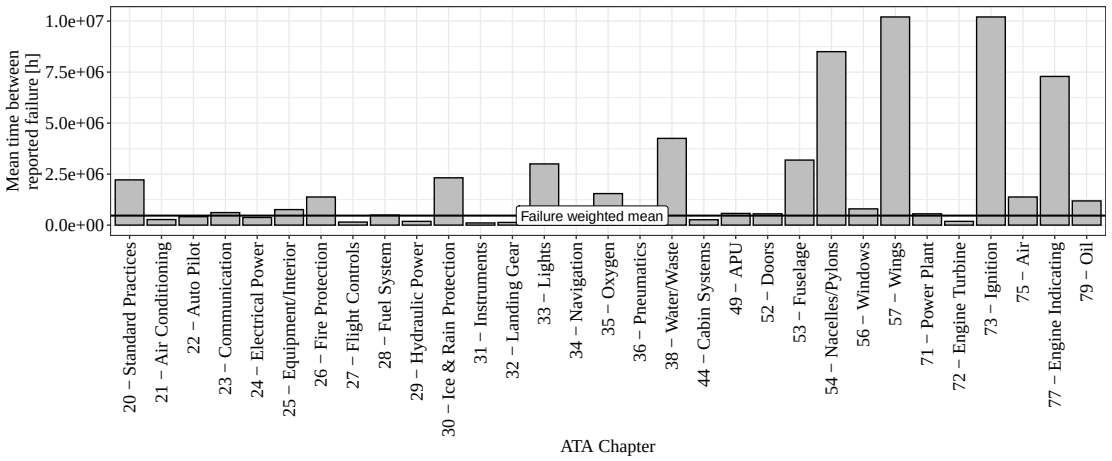

Figure 4.4: MTBRF rate for Airbus A320 operating in the United States of America, broken down by ATA-chapter. The MTBRF rate is based on voluntary confidential safety information submitted to ASRS between 2003 and 2020. Of the 51,012,370 FHs assessed by the DOT, 3,401 problems were reported, leading to a failure-weighted mean MTBRF of 466,072 FHs per ATA-chapter. Of the 2,945 incidences, a component malfunctioned or failed, or it was improperly designed; in the remaining 456 cases, improper operation was the reason for a report.

in Figure 4.4. Based on the ASRS, the failure-weighted average MTBRF is 466,072 FHs on the ATA-chapter level and 15,034 FHs on the aircraft level. However, the MTBRF only covers failures detectable during regular operation, which typically includes primary flight equipment with human-machine interfaces, e.g., autopilot, navigation, communication, and lighting. Failure or fatigue in single structural components, except for obvious impact damage, does not attract attention during operation. Furthermore, with the nature of the ASRS reporting system, not all failures are reported, likely resulting in an MTBRF higher than the actual MTBF. The highest MTBRF rate is calculated for the instruments in ATA-Chapter 31,107,394 FHs. The estimated MTBF for all components of the reference aircraft excluding the structure is thus set to 90,000 FHs.

The EUROCONTROL *central office for delay analysis* regularly publishes all-causes delay analyses, as illustrated in Figure 2.15 for Airbus A320 aircraft operating in 2019. Based on this data, 4.27% of all Airbus A320 flights were delayed by more than 60 min, while 14.36% of all delays could be attributed to technical failures of the aircraft. Thus, assuming a uniform distribution of delay causes, 0.61% of Airbus A320 flights experienced a technical failure leading to a delay over 60 min, which corresponds to a technical dispatch reliability of 99.39%. Assuming 2 FHs per FC implies an MTBF of 325.5 FHs on the aircraft level.

Additionally, MTBF rates for the Airbus A320 have been published in *scientific literature*. The technical dispatch reliability for the A320 world fleet in September 2005 was specified at 99.26%, corresponding to an MTBF of 270.3 FHs on the aircraft level, assuming 2 FHs per FC [210, p. 2]. For a fleet of eight Airbus A320 operated by Croatia Airlines, the technical dispatch reliability between June 2005 and May 2006 was between 98.57% and 99.59%, corresponding to an MTBF rate of 139.9 FHs and 487.8 FHs on the aircraft level,

Table 4.3: Summary of selected MTBF, MTBRF and MTBUL rates for Airbus A320 and Boeing 757-200.

Aircraft	**Reliability** [Value]	[Unit]	**Considered period**	**Source or database**
A320	15,034.0	MTBRF	2003 – 2020	NASA ASRS
A320 by ATA-Chapter	466,072.0	MTBRF	2003 – 2020	NASA ASRS
A320 in Europe[a]	325.5	MTBF	2019	Eurocontrol CODA
A320 worldwide[a]	270.3	MTBF	2005	[210, p. 2]
A320, Croatia Airlines[a,b]	139.9	MTBF	06/2005 – 05/2006	[210, p. 2]
A320, Croatia Airlines[a,c]	487.8	MTBF	06/2005–05/2006	[210, p. 2]
B757-200, 0 PUL	2,186.3	MTBUL	1992 – 2002	[209, p. 9]
B757-200, 1 PUL	1,135.1	MTBUL	1992 – 2002	[209, p. 9]
B757-200, 2 PUL	582.7	MTBUL	1992 – 2002	[209, p. 9]
B757-200, 3 PUL	101.0	MTBUL	1992 – 2002	[209, p. 9]
B757-200, 4 PUL	96.0	MTBUL	1992 – 2002	[209, p. 9]

[a] To convert dispatch reliability to MTBF, it is assumed that 1 FC = 2 FHs.
[b] Minimum value specified for Croatia Airlines.
[c] Maximum value specified for Croatia Airlines.

respectively, assuming 2 FHs per FC [210, p. 2]. For a cohort of 20 Boeing B757-200 aircraft operated by a single operator between 1992 and 2002, a time-varying mean time between unscheduled landing (MTBUL) of 2186.3 FHs to 96 FHs was observed [209, p. 9]. With every previous unscheduled landing (PUL) of the aircraft, the MTBUL decreases [209, p. 9]. A summary of the different failure rates is given in Table 4.3.

4.3.4 Structural Properties

Using the additional information characterizing inspection tasks provided in the MPD, the airframe is divided into fuselage, nacelles/pylons, and wings according to the ATA-systematic. Each assembly consists of multiple positions, for which all inspection requirements are provided in the MPD. Using publicly available resources, every structural position of the Airbus A320 is manually modeled to estimate its surface area. The resulting simplified aircraft model enables weight estimates of the SHM system, as well as the airframe. The resulting surface and weight distribution of the Airbus A320 reference aircraft is summarized in Table 4.4. All aircraft positions are assumed to be assembled from sheet-like components, neglecting nuts and bolts. The assumed properties for composite structures are 4.5 mm wall thickness and a density of 1500 kg/m^2. For metallic structures, a thickness of 3.5 mm and density of 2800 kg/m^2 are assumed.

Table 4.4: Breakdown of reference aircraft airframe surfaces by ATA chapter.

ATA chapter	Material	Sheet area [m^2]	Weight [kg]	Share [%]
53 - Fuselage	Composite	325.6	2197.9	12.4
53 - Fuselage	Aluminium	800.5	7844.7	44.2
54 - Nacelles/Pylons	Composite	22.0	148.8	0.8
54 - Nacelles/Pylons	Aluminium	189.0	1852.2	10.4
55 - Stabilizers	Composite	124.8	842.1	4.7
55 - Stabilizers	Aluminium	93.0	911.5	5.1
57 - Wings	Composite	21.5	144.9	0.8
57 - Wings	Aluminium	389.9	3821.5	21.5
Subtotal	Composite	493.9	3333.6	18.8[a]
Subtotal	Metal	1472.4	14429.9	81.2[b]
Total	-	1,966.3	17763.4[c]	100.0

[a] The estimated share of composite materials 1.3% lower as in [57, p. 28].
[b] The estimated share of metallic materials is 0.3% higher, as in [57, p. 28].
[c] The estimated total airframe weight is 1.9% lower than the total 18,103 kg given in [228, 508 52-01, 228, 501 52-01].

4.3.5 Maintenance Requirements

The *maintenance requirements* assumed for the reference aircraft are based on the Airbus A320 MPD. A total of 3,663 individual maintenance tasks are considered in this thesis. A summary of all tasks by ATA-chapter, including the number of positions, inspection intervals, and labor requirements, is provided in Appendix A.13. Every task contains a single inspection activity for a specified position of the aircraft.

The *skill code* specifies the required skill of the worker. Seven skill codes are distinguished in the Airbus A320 MPD as follows. *Airframe (AF)* covers work on "hydro-mechanical, environmental, fuel, oxygen and cargo systems, [...] requiring a certain qualification such as: flaps/slats, landing gear, trimmable horizontal stabilizer actuator or structure visual inspection" [175, p. 17]. *Instruments (AV)* comprises labor on the "autopilot, instruments, digital equipment or fire protection" [175, p. 17]. *Cabin (CA)* involves "furnishing and galleys" [175, p. 17]. *Electrical (EL)* specifies work on "electrical generation, distribution and associated services and components" [175, p. 17]. *Power plant (EN)* includes "engines and auxiliary power unit accessories or associated services" [175, p. 17]. *NDT* covers "all non-destructive test inspection and borescope inspection" [175, p. 17]. *Radio (RA)* encompasses work on radio and "radio navigation, audio interphone, cockpit voice recorder and passenger address" [175, p. 18]. Finally, *Utility (UT)* covers labor on "toilets water, wastewater" [175, p. 17–18].

As part of the simulation, the skill codes further refine the problem boundary conditions. Only inspection tasks requiring the skill codes *AF* and *NDT* are considered for the automation with SHM if included in the structural or zonal program of the MPD. An overview of all inspection tasks broken down by skill code is provided in Appendix A.1.

Table 4.5: Threshold probability triggering preventive structural repair during inspection.

Task code	**Threshold structural fatigue probability for preventive repair**
GVI	$2{\cdot}10^{-3}$
DI	$2{\cdot}10^{-4}$
SDI	$2{\cdot}10^{-5}$

Table 4.6: Damages to parts with task codes *CHK, FC, GVI, OP, SV* or *VC* can be detected during a walkaround check. Parts from "Structural Program" are excluded. Parts from "Zonal Program" are included.

ATA chapter	**Detectable**		**Not detectable**	
	[N]	**[%]**	**[N]**	**[%]**
Aircraft systems	563	15.3	409	11.1
Power plant	56	1.5	124	3.4
Structure	321	8.7	2198	59.9
Total	940	25.6	2731	74.4

Analogous to the skill code, inspection tasks are further categorized using *task codes*, which specify the kind of work to be conducted [175, p. 18]. A summary of task codes for the Airbus A320 is given in Table A.4. The task codes are utilized twofold in the present study.

First, task codes are used within the simulation to decide if *preventive structural replacements* during a scheduled structural inspection are possible, which reflects NDT procedures in place today. Preventive replacements are based on the simulated failure probability, which triggers a structural replacement during scheduled maintenance, depending on three thresholds associated with task codes of inspections, as summarized in Table 4.5.

Second, the casual discoveries of failures on the aircraft during a *walkaround check* are also based on the task codes. Not all failures are necessarily visible during this check, confining the discoverable failures to positions associated with inspections having the following task codes: *CHK, FC, GVI, OP, SV,* or *VC*. The resulting overall share of positions with detectable and undetectable damages are summarized in Table 4.6.

Furthermore, the *inspection time* specified in the MPD is doubled for every task considered in the cost-benefit study since a series of activities connected to aircraft inspections is not recognized. The person-hours originally quoted in the MPD can be considered optimistic estimates. For the values quoted in the MPD, an aircraft is assumed to be in a general maintenance condition before the inspection [175, p. 22]. Additionally, the following activities are not included in the quoted inspection time: off-aircraft inspections performed in the workshop[1], troubleshooting, aircraft cleaning, one-time actions, embodied modifications, and non-productive periods, such as shift changes, tool set-ups, and procedure planning [175,

[1]For long-range aircraft in 1997, the labor cost between on- and off-aircraft was 1 to 1.5 [229, p. 2].

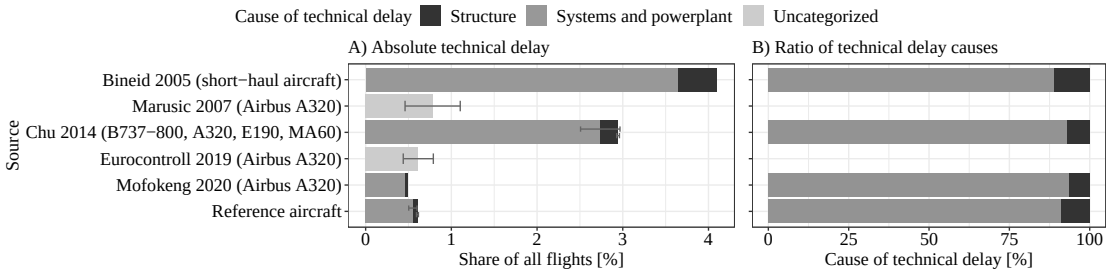

Figure 4.5: Simulated technical dispatch reliability of reference aircraft ($\varepsilon_E = 2.0\%$) in A) absolute values and B) relative ratio, compared to selected sources [207, 208, 210, 231], considering only delays above 60 min. For [208] and [231], the technical dispatch reliability is derived from all delays.

p. 22]. A large share of off-aircraft maintenance involves aircraft engines; therefore it can be noted that doubling the inspection time contained in the MPD may lead to an overestimation of structural inspection requirements.

4.4 Simulation Validation

To describe the service performance of the aircraft and measure the impact of SHM, previously defined operational and cost metrics are used. These metrics are quantified for a reference aircraft without SHM and compared to reference values from existing literature in the following two subsections. The results are obtained using Monte Carlo sampling. Because of the complexity of the proposed methodology and required simulation time, the number of Monte Carlo runs is set to 20. The resulting fractional accuracy, i.e., standard error around a calculated mean ε_E of the obtained estimates, is given by

$$\varepsilon_E = \frac{s}{\sqrt{n} \cdot |E|}, \tag{4.1}$$

where s is the standard deviation, $n = 20$ is the number of Monte Carlo runs, and $|E|$ is the expectation of a respective metric [230, p. 425].

4.4.1 Operational Performance

The simulated *dispatch reliability* of the reference aircraft without SHM is illustrated in Figure 4.5, together with selected reference values from literature. Hereby, every unscheduled maintenance before a flight leads to an assumed delay greater than 60 min. The figure shows the simulated technical dispatch reliability is in line with references for the Airbus A320, which has high reliability compared to other aircraft. Furthermore, the ratios of the technical delay causes of the structures to those of the systems and power plant are approximately equal for the reference aircraft and the considered references.

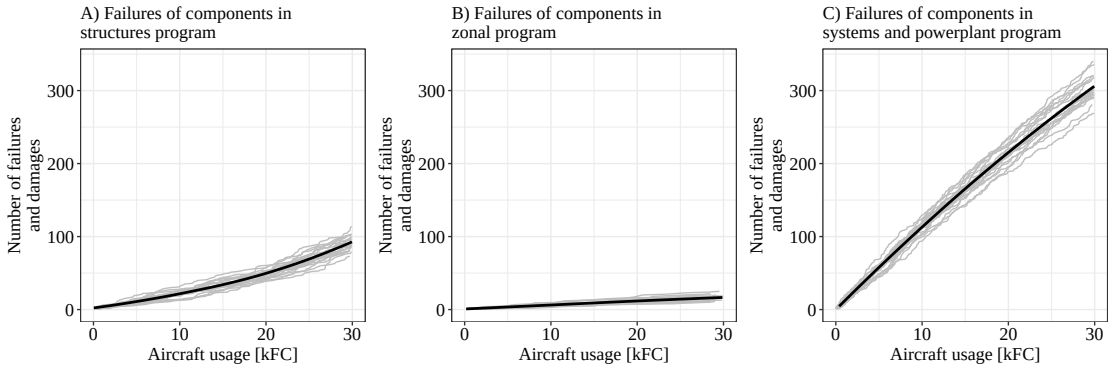

Figure 4.6: Simulated failures over aircraft lifetime for components contained in the A) structures program ($\varepsilon_E = 0.5\%$), B) zonal program ($\varepsilon_E = 1.1\%$), and C) systems and powerplant program ($\varepsilon_E = 0.3\%$) of the MPD.

The *numbers of failures* over the aircraft lifetime are illustrated in Figure 4.6. While the quantity of component failures in the structures program increases over time from fatigue, the number of simulated failures in the zonal program remains almost constant, as they reflect random failures caused by ground operations and foreign object damage (FOD). Similarly, the simulated failure rates of components in the systems and power plant program are distributed almost equally over the aircraft lifetime, with a slightly decreasing tendency at the end of the lifetime.

A more detailed breakdown of *structural failures*, as shown in Figure 4.7, reveals the nature of these failures and repairs. The majority of repairs are conducted during scheduled inspections, which include the repair of failures, which rapidly increase in the second half of the aircraft lifetime, and preventive structural replacements, which are conducted by means of NDT. An absolute or relative reference value could not be obtained as part of this thesis. Unscheduled structural repairs are triggered by failures discovered during a walkaround check. The average of 16.5 structural failures leading to unscheduled structural repairs is 16.3% higher than the combined 7.8 FOD and 6.0 ground-handling damages per 30,000 FCs stated in [232, p. 2, 233, p. 28]. Furthermore, the number of undiscovered structural damages on the aircraft increases during the first half of the aircraft's lifetime. Subsequently, the number of unrepaired structural failures decreases as a result of the extensive scheduled structural inspections mandated in the MPD. With the damage-tolerant design of the airframe, it is assumed that a failed structural component does not lead to a disintegration or crash of the entire aircraft.

A breakdown of total lifetime *inspection and repair efforts* by inspection program is provided in Figure 4.8. The required inspection times for the components in the structures or zonal program of the MPD make up 35.6% of the total inspection time. No reference could be obtained to verify the presented breakdown of the inspection effort.

The *aircraft inspection and repair effort over time* is illustrated in Figure 4.9 and compared to reference values in issues of the trade journal "Aircraft Commerce" from 1999 and 2006, based on [8, 234]. To break the total maintenance effort quoted in "Aircraft Commerce" down into

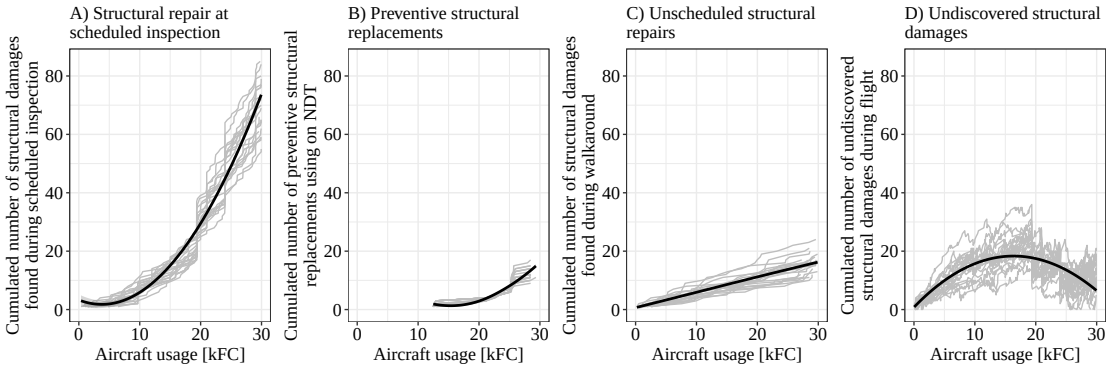

Figure 4.7: Detailed overview of simulated structural repairs of reference aircraft. A) Cumulated number of repairs at a scheduled inspection ($\varepsilon_E = 0.6\%$), B) preventive replacements during structural inspections ($\varepsilon_E = 0.8\%$), C) unscheduled structural repairs triggered during walkaround checks ($\varepsilon_E = 1.1\%$) [232, p. 2, 233, p. 28], and D) number of failed structural components within the aircraft at any time during the operation ($\varepsilon_E = 1.0\%$). The increasing number of scheduled inspections after 10,000 to 20,000 FCs improves the discovery of structural failures, which reduces the number of undiscovered latent damages. The inspection quality depends on the requirements defined in the MPD and remains unchanged throughout the lifetime of the aircraft.

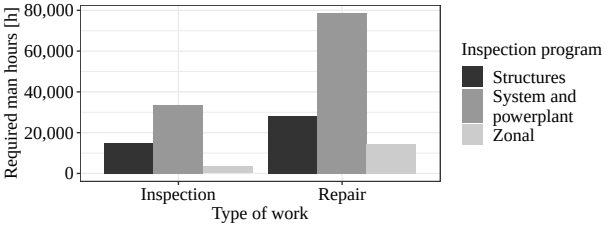

Figure 4.8: Overview of simulated inspection, preparation, access, and repair times for reference aircraft by MPD inspection program. A table including values is provided in Appendix Table A.14.

inspection and repair times, a ratio of inspection to repair times of 1:2.5 is assumed. For the reference aircraft, the repair time of a position is estimated to be 125 times the corresponding inspection time stated in the MPD.

A more detailed view of the *location and time of maintenance* conducted on the reference aircraft is provided in Figure 4.10. The classifications of inspection and repair efforts in "base" and "off-base" are derived from the aircraft flight plan and available maintenance stations of the airline. Work conducted after the last flight of the day is considered to be "overnight," for which scheduled inspections are planned. All other inspections between two consecutive flights during the day are classified as "turnaround." A similar categorization for line and base maintenance is typically used, where line maintenance is characterized as work conducted during regular operation to achieve airworthiness of the next flight, or in "line" [236, p. 2]. When assuming that transit, ramp, service, pre-flight, daily, weekly, and supplemental checks specified in literature are conducted half at overnight and half at

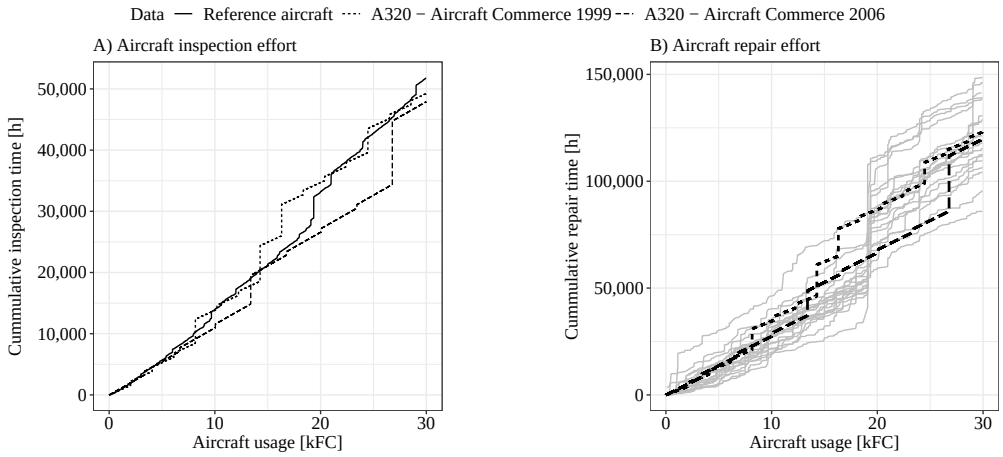

Figure 4.9: Comparison of simulated A) deterministic inspection effort and B) Monte Carlo–sampled repair effort (task-based maintenance using MPD) with values (letter-check-based maintenance) published in [8, p. 46, 235]. For the comparison, the simulated inspection time is doubled since the MPD neglects maintenance set-up times away from the aircraft, such as crew preparation and tool gathering. Under the given assumptions, the reference aircraft causes 5% more inspection effort compared to literature. The mean total inspection time is 51,826 h with $\varepsilon_E = 0.0\%$. The mean total repair time is 121,220 h with $\varepsilon_E = 0.7\%$.

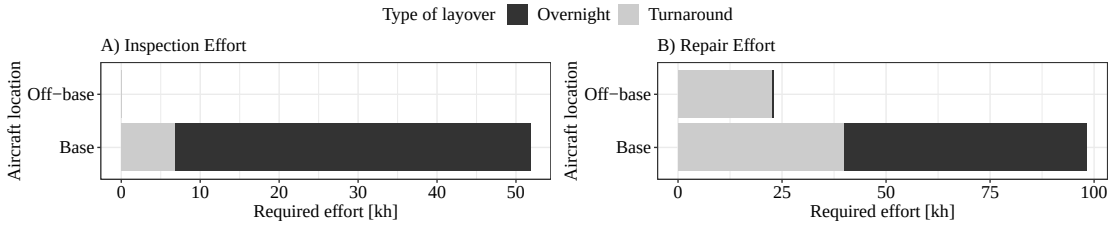

Figure 4.10: Reference aircraft maintenance effort depending on the time of day and location for A) inspection $\varepsilon_E = 0.0\%$ and B) repairs $\varepsilon_E < 6.8\%$ (neglecting off-base overnight repair effort).

turnaround, in addition to the base maintenance work conducted at overnight checks, the total share of overnight maintenance work (inspection and repair) is 72.5 to 84.5%[8, 234]. In comparison, the simulated share of inspections conducted during an overnight stop is 86.8%, and the simulated share of repairs conducted during an overnight stop is 59.3% for the reference aircraft.

The number of required *spare aircraft* to realize a predefined reliability of the reference airline is illustrated in Figure 4.11. The most reliable airlines achieved 90% punctuality in 2019, and the technical dispatch reliability of aircraft regularly exceeds 95%. The question can be raised of whether airlines even rely on idle spare aircraft placed throughout the network. However, the leverage of spare aircraft on dispatch reliability tends to increase with rising network centrality.

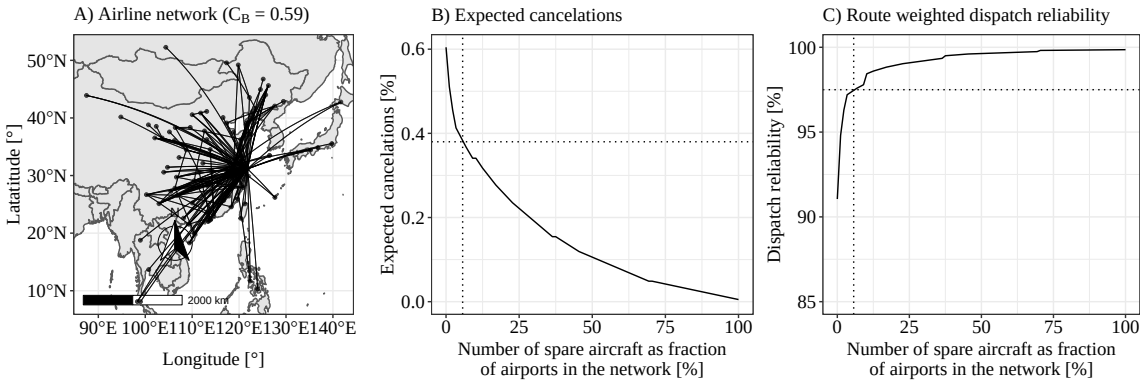

Figure 4.11: A) Layout of the Juneyao network with 88 destinations, B) expected cancellations per departure, and C) airline dispatch reliability with an assumed target of 97.5%. The technical dispatch reliability of the reference aircraft is 99.4%. To achieve the targeted route weighted airline dispatch reliability in the presented Juneyao network, it is estimated that five spare aircraft are required, representing 5.7% of the number of airports. Given the 68 aircraft in the network, the required number of spare aircraft equals 7.4% of the total operating aircraft count.

4.4.2 Cost Performance

The model used to translate the operational performance of the aircraft into cost is based on *form 41* data provided by the DOT for a single reference aircraft operated by a single reference airline. The resulting costs per FH of the reference aircraft are summarized in Table 4.7. Since the model is based on data provided by airlines based in the United States of America, the extent and distribution of the costs are unique to this region, and the cost structures of airlines operating in other regions or operating other aircraft may differ.

Delay costs are based on the time required to repair unexpected component failures. Based on the data provided in the MPD, the required repair time for a failure is estimated to be 125 times its inspection time. The CAPEXs are calculated for an aircraft operating over 20 years for 60,000 FH and 30,000 FC. The timing of an investment in a substitute aircraft depends on the efficiency of available aircraft entering the market at a respective time in the future. To consider this, a technology progress factor for aircraft of 0.8% per year is assumed. For the reference airline, the target dispatch reliability is achieved when five spare aircraft are distributed among the destinations in the network. Therefore, the spare aircraft count is equal to 5.7% of the number of airports in the network and 7.4% of the number of operating aircraft.

Table 4.7: Total operating cost for reference aircraft based on US DOT form 41 data and the literature.

Cat.	Cost component	Cost [USD/FH] Simulation	Literature	Δ [%]	Source
COC	Crew	694.6			
	Fuel	1,889.0			
	Hull insurance	6.4			
	Misc. fly ops	79.2			
	Total flying operations	2,669.2			
	Airframe materials	53.0	84.3	−37.1	[8, p. 46]
	Airframe repairs	134.0	[ab]135.7	−1.3	[237, 238]
	Aircraft engines	181.9			
	Deferrals and provisions	188.5			
	Airframe inspections	95.0	[ac]58.0	63.8	[237, 238]
	Subtotal direct maintenance	652.4	716.3	−8.9	[239, p. 12]
	Applied maintenance burden	176.4			
	Net obsolescence	7.1			
	Subtotal indirect maintenance	183.5			
	Total maintenance	899.8	834.7 to 1089.0	7.8 to −17.4	[9, 240]
COO	Depreciation airframes	450.4			
	Depreciation flight equipment	96.6			
	Depreciation engines	131.8			
	Total depreciation	678.8	841.7	−19.4	[218]
ADOC	Technical delay cost	150.3	[d]88.3 to 135.0	70.2 to 11.3	[241, 242]
CAPEX	CAPEX Aircraft	703.9			
	CAPEX Spare AC	59.1			
	Total CAPEX	763.0			

[a] Compensation of USD 67.19/h for maintenance workers.
[b] Reference aircraft requires 2.02 person-hours of repair per FH.
[c] Reference aircraft requires 0.86 person-hours of inspection per FH.
[d] Assuming that 14% of delays are of technical nature.
[e] Assuming 180 passengers per flight, USD 300 compensation cost per passenger and delay, and 99.5% technical dispatch reliability.

4.5 Investigated Structural Health Monitoring Concepts

In the work at hand, the financial and operational impacts of SHM on the reference aircraft and airline are quantified. SHM based only on DM and OLM is investigated using four representative concepts. Therefore, the assumed performance metrics and the investigated benefits of scheduled DM, automated DM, scheduled OLM, and automated OLM are summarized in this section. Hereby, the distinction of the SHM operation mode as *scheduled* or *automated* describes if the information provided by such a system is only used during a scheduled maintenance event or throughout the operation of the aircraft.

In this line, *scheduled DM* is used to directly substitute manual scheduled inspections of the airframe specified in the MPD. However, the built-in scheduled DM does not trigger ad-hoc inspections during aircraft operation. Therefore, the impact of scheduled SHM on maintenance scheduling and aircraft dispatch reliability is not considered. Additionally, the DM system is assumed to have varying predictive capabilities, allowing the prognosis of damages, enabling their restoration before they materialize. Finally, aircraft lifetime increases are considered, enabled by changed decommissioning criteria. Analogously, *automated DM* is used to directly substitute manual scheduled inspections of the airframe. Unlike *scheduled DM*, *automated DM* is assumed to warn the aircraft operator about an existing structural damage outside of scheduled inspection events. Therefore, *automated DM* can lead to unscheduled maintenance activities, resulting in delays. The assumed operating procedures of scheduled and automated DM, including possible monitoring system outputs and corresponding actions, are described in Figure 4.12.

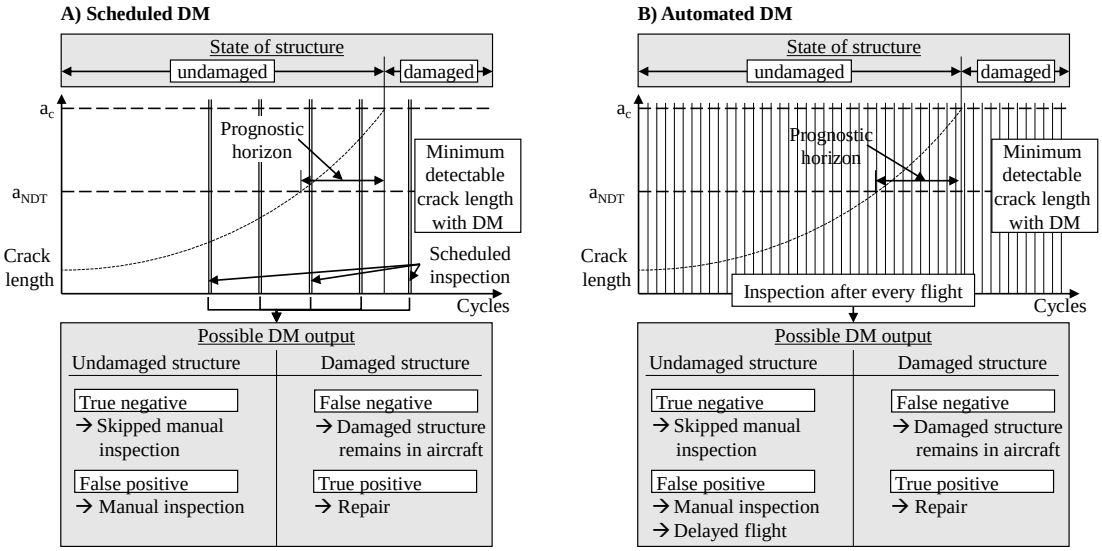

Figure 4.12: Assumed operating procedure of DM and its influence on aircraft maintenance. A) Scheduled DM occurs during scheduled structural inspections to replace manual labor. B) Automated DM occurs after every FC of the aircraft and requires ad-hoc manual inspections and repairs in case of a DM system alarm.

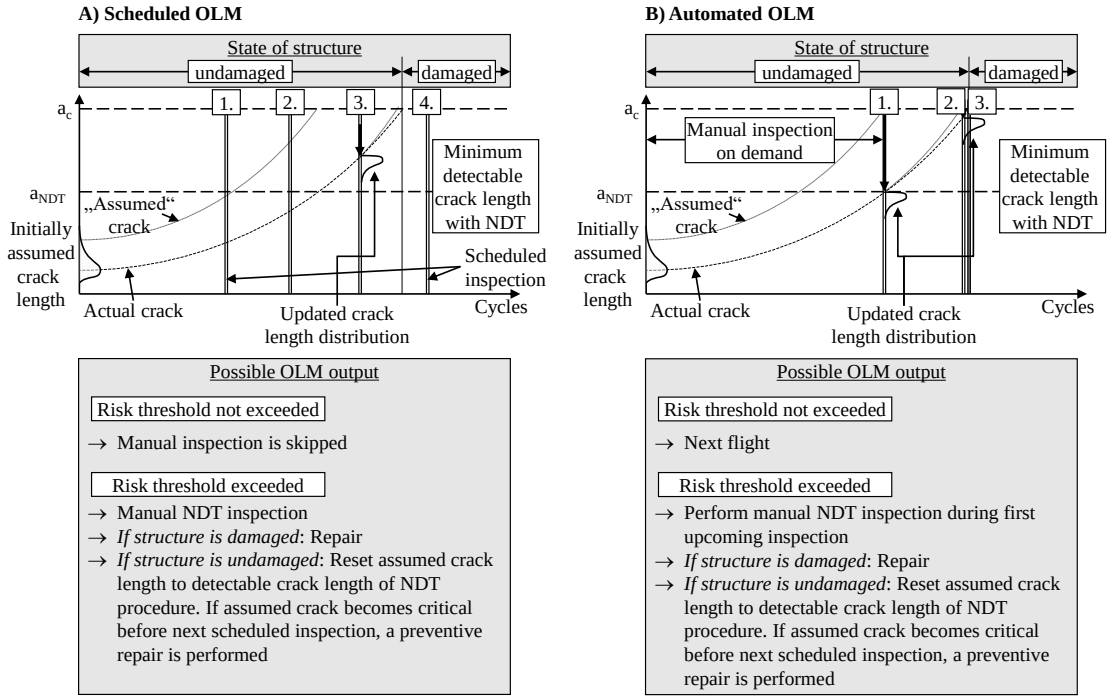

Figure 4.13: Influence of OLM on aircraft operation and maintenance. A) Scheduled OLM occurs during scheduled inspections. B) Automated OLM provides information to the operator about the structural state of the aircraft after every FC.

Scheduled OLM allows to skip manual inspections during scheduled maintenance events. Since OLM does not directly monitor a damage-dependent phenomenon, assumed design loads and initial crack lengths are used to derive the probability of present damage. If the probability of a present fatigue damage is not expected to exceed a specified threshold, a scheduled manual structural inspection may be skipped. This work assumes OLM does not require dedicated built-in equipment within the aircraft but relies on acceleration, attitude, position and velocity measurements provided by the inertial reference system. *Automated OLM* schedules ad-hoc inspections of the structure once a predefined-risk threshold on the presence of structural fatigue is exceeded. OLM does not monitor a damage-dependent phenomenon but is based on monitored loads and crack growth statistics. Therefore, exceeding a threshold does not necessarily require an immediate repair or manual inspection of the structure resulting in aircraft delays, and the next scheduled inspection event is sufficient, which is assumed to occur every 18 FCs, as illustrated in Figure 3.9 (on page 56). The operating procedure of OLM and its impact on the operation of the aircraft are illustrated in Figure 4.13. The assumed SHM performance of the investigated DM and OLM systems are summarized in Table 4.8.

Finally, this work investigates how *hybrid SHM systems based on DM and OLM* perform compared to independent DM or OLM systems.

Table 4.8: Summary of investigated SHM system benefits and performance assumptions.

	Scheduled DM	**Automated DM**	**Scheduled OLM**	**Automated OLM**
		Performance assumptions		
False positive rate [%]	0–48	0–48	-	-
True positive rate [%]	90–100	90–100	-	-
Risk threshold [%]	-	-	0.1–100	0.1–100
Prognostic horizon [FC]	0–10,000	0–100	-	-
		Investigated benefits		
Inspection time	☑	☑	☑	☑
Airframe weight	☑	☑	☐	☐
Dispatch reliability	☐	☑	☐	☐
Airframe damages	☑	☑	☑	☑
Lifetime increases	☑	☑	☑	☑

Chapter 5

Results

Based on the introduced methodology and assumptions, this chapter presents the impact of SHM on the reference aircraft and airline. In the first section, the operational impacts of SHM in terms of aircraft inspection and repair efforts, structural integrity, dispatch reliability, spare aircraft use, airframe lifetime, and weight impact are covered. Subsequently, Section 5.2 presents economic considerations connected to SHM. This includes a profitability-based aircraft decommissioning strategy, which indicates if SHM should be used for airframe lifetime extension or weight savings through improved lightweight design but decreased structural fatigue life. Additionally, the impact of SHM on individual aircraft COC, CAPEX, additional operating costs, maintenance costs, and spare aircraft costs are summarized. SHM is evaluated as a possible investment project for airlines in Section 5.3. Section 5.4 presents implications of the presented results on the design space of SHM.

5.1 Operational Impact of Investigated Structural Health Monitoring Concepts

SHM influences the operation of the aircraft by providing information on the state of the airframe. The respective effects on the reference aircraft are shown on the basis of *structural maintenance effort*, *structural integrity*, *dispatch reliability*, *spare aircraft provision*, *increased airframe lifetime*, and *change in airframe weight*.

5.1.1 Structural Maintenance Effort

The total labor time required for airframe maintenance is divided into *inspection* and *repair effort*. Each is presented for aircraft using scheduled DM, automated DM, scheduled OLM, or automated OLM. SHM systems operating in a scheduled mode are assumed to be used only during regularly planned maintenance checks. In contrast, automated SHM is used after every FC. For DM systems operating in an automated mode, an alarm triggers an ad-hoc manual inspection. If the structure is determined to be damaged, repairs immediately follow.

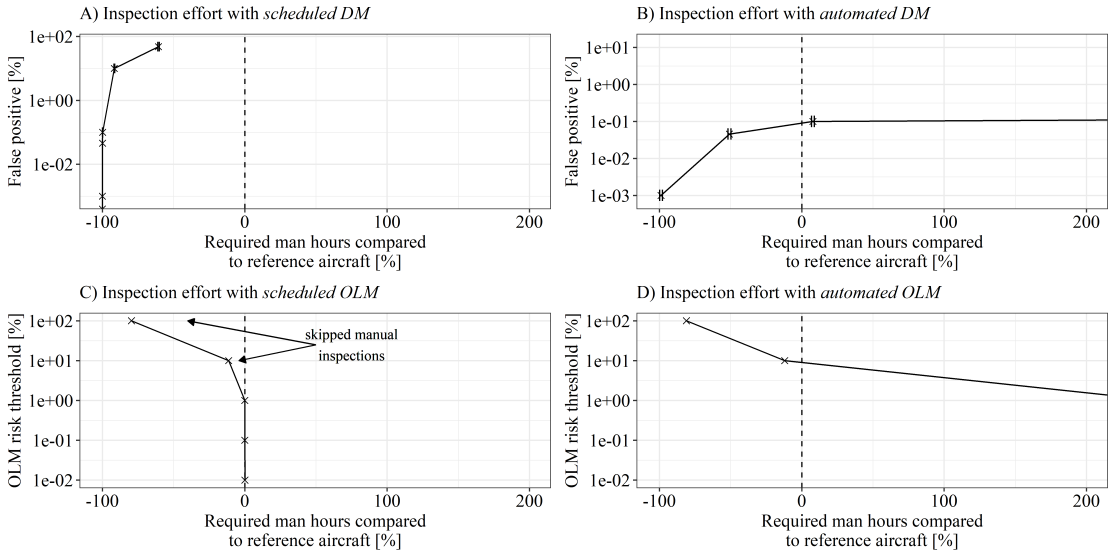

Figure 5.1: Structural inspection effort of aircraft using SHM compared to reference aircraft when using A) scheduled DM, B) automated DM, C) scheduled OLM and D) automated OLM.

Otherwise, the DM system has produced a false alarm. The incurred time penalty of a false alarm equals the inspection time specified in the MPD.

The resulting airframe *inspection effort* with SHM compared to the reference aircraft without SHM is illustrated in Figure 5.1. The simulation results indicate that the inspection effort for structural components can be reduced by up to 100% when using DM. For DM systems, the figure indicates that the required inspection time is dependent on the false-alarm rate of the DM system, as every alarm triggers a manual inspection before a possible replacement. For scheduled DM, all considered operating performances lead to a decrease in inspection time during planned maintenance. Since automated DM is used after every FC, high false-alarm rates lead to an inspection effort significantly higher than the inspection requirements of the reference aircraft. However, the presented inspection requirements are an artefact of the rate with which the automated DM system is used, which is further addressed in Section 5.4. With scheduled OLM, a significant number of planned manual inspections can be skipped if the allowed risk threshold of present structural fatigue remains above 1 %, given the assumptions. For a lower risk of structural fatigue, manual inspections cannot be avoided, yielding no inspection time savings compared to the reference aircraft. For automated OLM, the manual inspections are not scheduled using the MPD but are triggered ad-hoc using the risk threshold. Therefore, a low risk threshold leads to more manual inspections than for the reference aircraft.

The simulated *repair effort* for aircraft using SHM compared to the reference aircraft is provided in Figure 5.2. The operational loads on aircraft with SHM are equal to the reference aircraft, leading to equivalent structural fatigue. For the reference aircraft, most structural damages are repaired, and only a few remain undetected over the aircraft's lifetime. Given the simulated manual inspection capabilities with NDT techniques, some structural parts

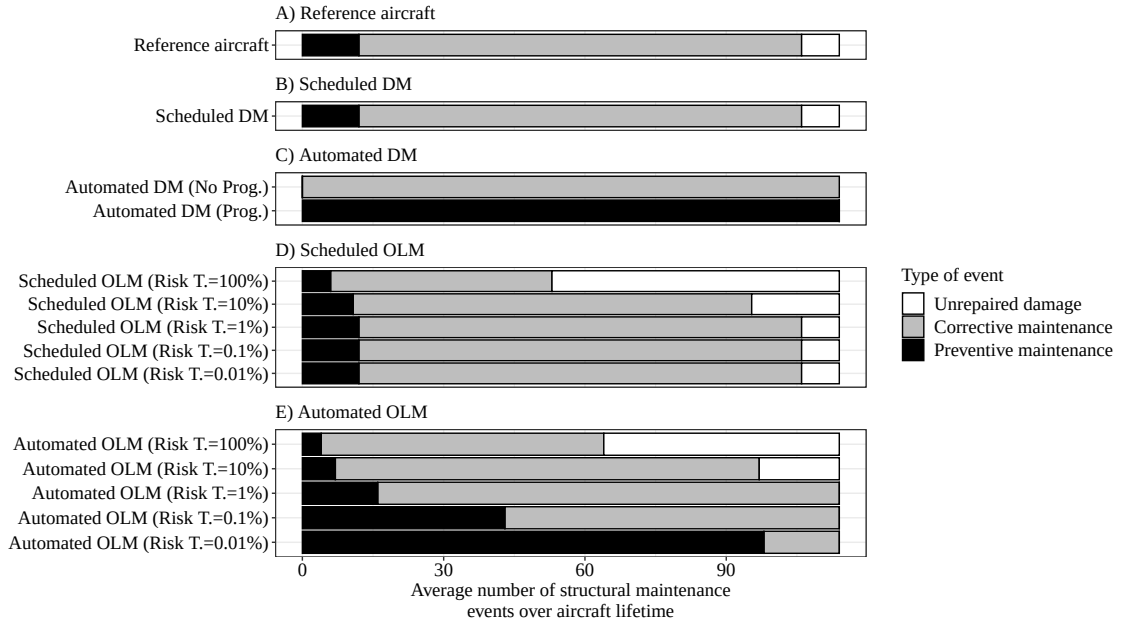

Figure 5.2: Average number of structural repairs and missed damages over lifetime of aircraft with and without SHM.

are also replaced preventively before a failure. For scheduled DM, the simulated work required for corrective and preventive replacements is similar to that for the reference aircraft. Since automated DM is used after every FC for all monitored structural parts, the number of corrective repairs approaches zero with only a few FCs of the predictive horizon. In this case, structural fatigue damage exceeding the tolerable limit is avoided, and all corrective maintenance events on structural parts with intolerable damages are transformed into preventive maintenance actions, where structural parts are repaird just before tolerable damages become intolerable. For scheduled OLM, the number of detected damages decreases with a higher failure risk. Conversely, a lower tolerated failure risk results in the distribution of structural repairs comparable to that of the reference aircraft. For automated OLM, more manual inspections allow the discovery of more unrepaired damages over the aircraft's lifetime compared to the reference aircraft without SHM. Additionally, the share of preventive maintenance increases with automated OLM, as the effective increase in inspection frequency for individual parts increases the chance to prevent failures.

5.1.2 Structural Damage Detection

SHM impacts the detectability of structural damage and influences the structural integrity of the aircraft during operation. Since the exact airframe geometry and experienced structural loads are unknown, the simulated number of FCs between the occurrence and its repair is used to infer the impact of SHM on structural integrity. The average time required to repair a damage within each of the investigated SHM concepts is illustrated in Figure 5.3. The median number of FCs to repair structural fatigue damages occurring on the reference

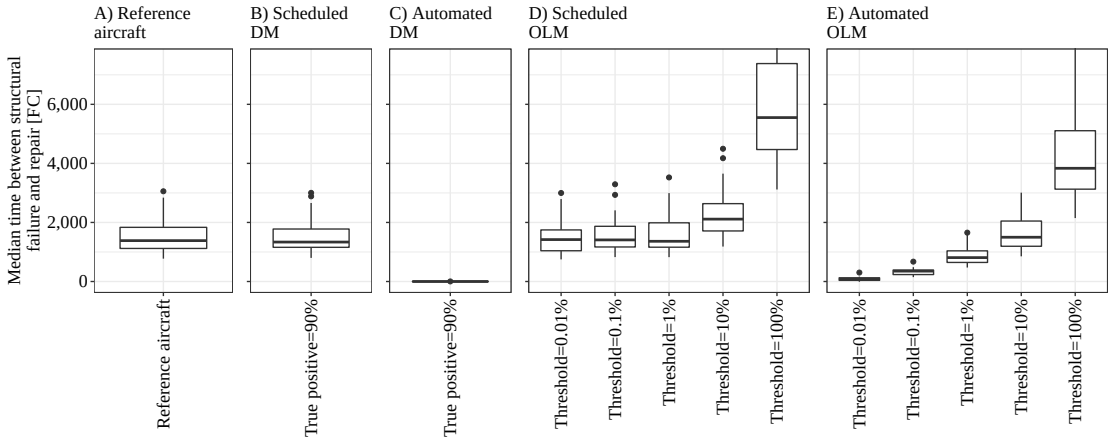

Figure 5.3: Time between structural fatigue damage and repair given in FC for the A) reference aircraft and aircraft using SHM based on B) scheduled DM, C) automated DM, D) scheduled OLM, and E) automated OLM.

aircraft is 1400, with 25% remaining damaged for more than 1850 FCs and 25% damaged for less than 1100 FCs. When substituting planned manual inspections with scheduled DM, the average time between structural failures and repair does not significantly deviate from that of the reference aircraft. However, for automated DM, which is used after every FC, structural fatigue damages are discovered almost immediately, as every structural component of the aircraft is checked after every flight. With scheduled OLM, the manual inspections during scheduled maintenance can possibly be skipped. As shown in Figure 5.1 C), a risk threshold of 1% of present fatigue damage does not allow the skipping of any manual inspections. Therefore, no significant changes in the average number of FCs to repair a structural damage can be seen. However, a higher tolerable risk of a present fatigue damage allows more manual inspections to be skipped. As OLM does not directly monitor a damage-dependent phenomenon, a higher risk tolerance increases the time until a structural failure is detected and repaired. For automated OLM, which is used either after every FC or overnight stop for all covered structural parts, the number of FCs until repair decreases with a smaller threshold. However, improved structural integrity is achieved with an increase in manual inspections, as shown in Figure 5.1 D).

5.1.3 Dispatch Reliability

SHM systems can negatively impact aircraft dispatch reliability if structural damages are uncovered during a regular aircraft turnaround instead of a scheduled maintenance event. As scheduled SHM is only used during planned maintenance events, neither scheduled OLM or scheduled DM are assumed to impact the dispatch reliability of the aircraft. For automated DM, exceeding a risk threshold does not necessarily lead to an immediate manual inspection event but rather requires an inspection during the next planned maintenance event. However, automated SHM can lead to poorer dispatch reliability within the simulation depending on the prediction performance and false alarm rate. According to the definition of automated

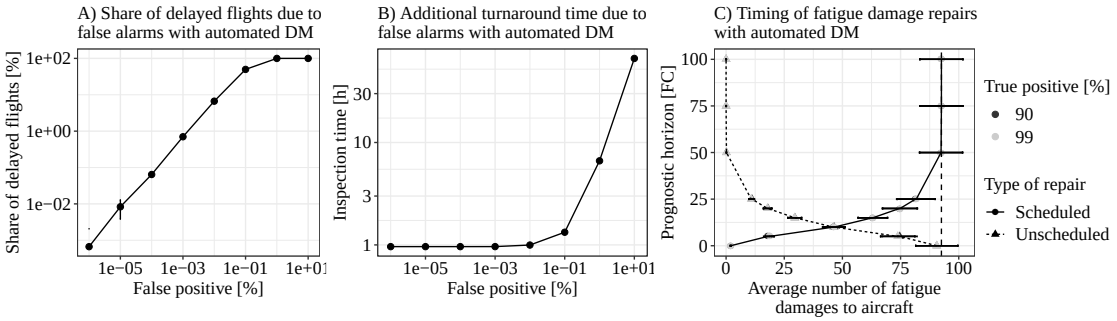

Figure 5.4: Impact of automated DM on dispatch reliability. A) Share of delayed flights, B) additional turnaround time in case of a false alarm, and C) timing of repairs, where scheduled repairs are conducted during a planned overhaul and unscheduled repairs during an aircraft turnaround.

DM used in the [67, p. 27], any alarm from such a system will result in an immediate maintenance event. The predictive capability of the DM system is represented by a forecast horizon, which indicates how far in advance an upcoming alarm is known. Figure 5.4 shows that the number of flights impacted by delays through false alarms increases with the false positive rate. Until a false alarm rate of 0.01% is reached, the produced delay caused by a structural inspection is on average just under one hour. However, the predictive horizon can reduce the number of unscheduled damages, as the inspection can be planned as part of a scheduled maintenance event.

Figure 5.5 illustrates the impacts of false alarms and predictive horizon on the overall dispatch reliability of the simulated aircraft. The figure indicates that the false alarm rate of automated DM systems affects the share of flights that experience technical delays. Under the given assumptions, a false alarm rate of over $1{\cdot}10^{-6}$ per FC per structural component leads to a severe increase in aircraft delay compared to the reference aircraft. In this line, technical delays can be reduced if the DM system can signal an alarm in advance of a structural failure. Given the assumed flight plan of the aircraft, a prognostic horizon of over 50 FCs reduces the number of technical delays caused by the airframe to a level similar to the reference aircraft since failures can be repaired preventively during a scheduled maintenance event.

5.1.4 Provision of Spare Aircraft

By impacting the aircraft dispatch reliability, automated DM also influences the overall airline reliability. Airlines can counteract this by making use of spare aircraft held in reserve. The effect of an automated DM system's false alarms and prognostic horizon on route-weighted airline reliability and expected cancellations are illustrated in Figure 5.6 based on the number of available spare aircraft. Assuming the airline targets a predefined overall reliability, an excessive false alarm rate and short predictive horizon require additional spare aircraft.

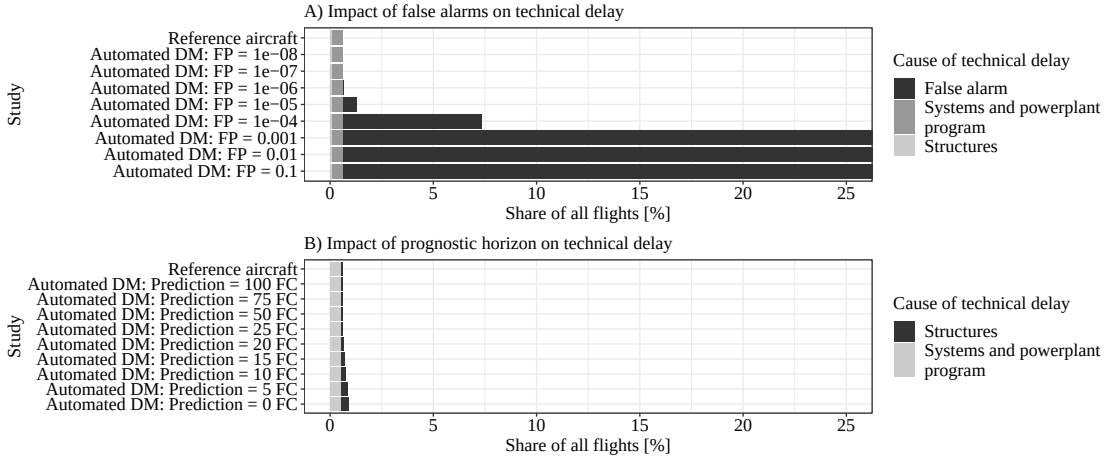

Figure 5.5: Simulated share of delayed flights for aircraft with automated DM for A) varying false alarm rate, assuming no prognostics, and B) different prognostic horizons, assuming a false alarm rate of $1.5{\cdot}10^{-6}$ per FC.

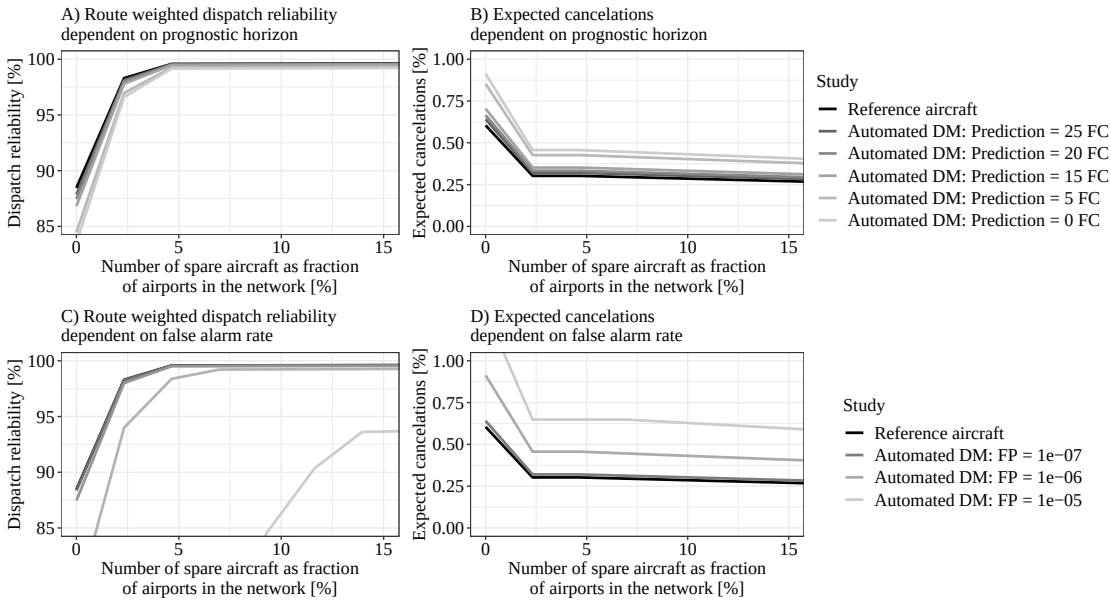

Figure 5.6: Simulated impact of automated DM on required spare aircraft, A) and C) displayed in terms of route-weighted airline dispatch reliability and B) and D) expected number of cancellations, depending on fatigue prediction horizon and FP rate. A decrease in technical dispatch reliability resulting from unscheduled repairs, which are initiated by the automated DM system, can be addressed by either using additional spare aircraft, increasing damage forecast horizons, or decreasing FP rates.

5.1.5 Airframe Service Limit

To prevent widespread structural fatigue, airframes have a predefined end of life expressed in FCs and FHs, which are established with full-scale fatigue testing. Extending this limit currently requires additional extensive fatigue tests by the aircraft manufacturer. Instead of defining a single service limit for the entire fleet, SHM helps define service limits for individual aircraft by monitoring the consumed structural life during every FC. Relying on this service limit definition provides additional FCs and FHs to aircraft that did not experience their certified design loads. To investigate the benefit of such a decommissioning approach, the aircraft's end of life is defined by an FDI, which equals 100% once the structural life of the airframe is consumed. The proposed FDI relies on a comparison of certified airframe fatigue levels with those of an actual individual aircraft. Hereby, the health state of the airframe can be determined by tracking loads acting on the structure with OLM or observing fatigue damages directly with DM systems.

To demonstrate the potential lifetime increases, external factors driving loads on the aircraft are investigated as part of this thesis. This includes the experienced payload, top of descent, and taxi time on flights by individual aircraft within the Airbus A320 fleet. The estimated lifetime increases for aircraft of the Airbus A320 fleet are illustrated in Figure 5.7, assuming the Airbus A320 DSG is the original service limit. Despite the additional FCs and FHs of the aircraft, levels of tolerable structural fatigue are not exceeded, as an FDI of 100% reflects a fatigue level of an aircraft operating on the certified design mission. For the considered reference aircraft, an individual service limit based on the proposed FDI yields a lifetime extension of 60%.

5.1.6 Weight Impact

SHM equipment *increases the airframe weight* but enables airframe design changes with lighter structural components. A *decrease in airframe weight* can be achieved by both the removal of access panels and doors used only for structural inspections and relaxation of fatigue damage tolerance requirements for structural components.

The analysis presented in [169] estimated the *increase in airframe weight* resulting from the introduction of DM equipment. The assumed DM system is based on fiber-optic sensors for beam-like components and ultrasonic sensors for plate-like components. Under the assumptions presented in Section 3.1.4, the overall weight of the DM system is heavily dependent on the number of ultrasonic sensors, as shown in Figure 5.8 A). Additionally, Figure 5.8 B) presents the corresponding magnitude of potential inspection time savings subject to the instrumented area, where the marginal benefit decreases with an increasing share of instrumented structural components.

SHM also provides the opportunity for airframe design changes that *decrease the weight of the airframe*. The substitution of manual inspections by SHM systems may render the use of access panels for inspections currently required by CS25 useless. Based on data indicating the access required for each individual inspection task listed in the MPD, access panels and doors

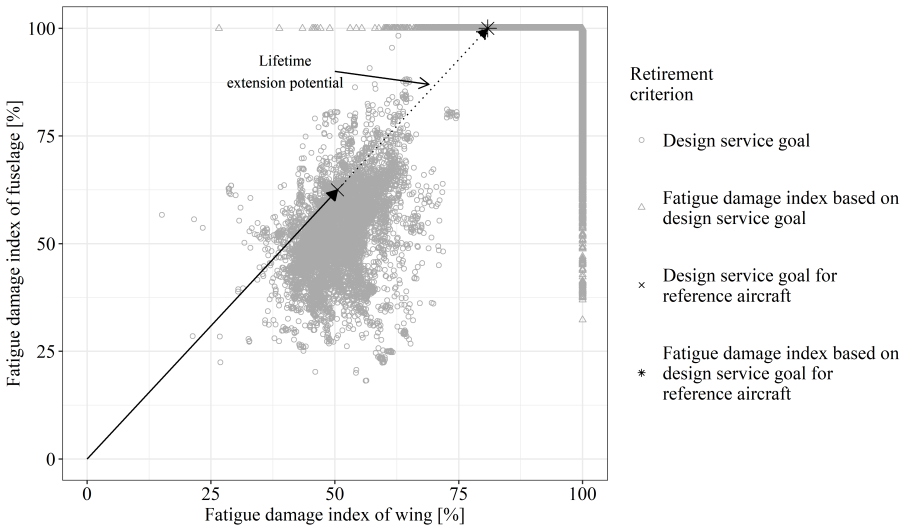

Figure 5.7: Aircraft operating until the DSG, defined in FCs and FHs, reach 25–75% of their certified fatigue level. Allowing an aircraft to be decommission using its actual fatigue unlocks additional FCs and FHs without exceeding the certified fatigue levels. For the considered reference aircraft (arrow), the use of a fatigue damage based decommissioning criterion in the form of the proposed FDI allows a lifetime extension of 60% (dotted arrow). Adopted from [200].

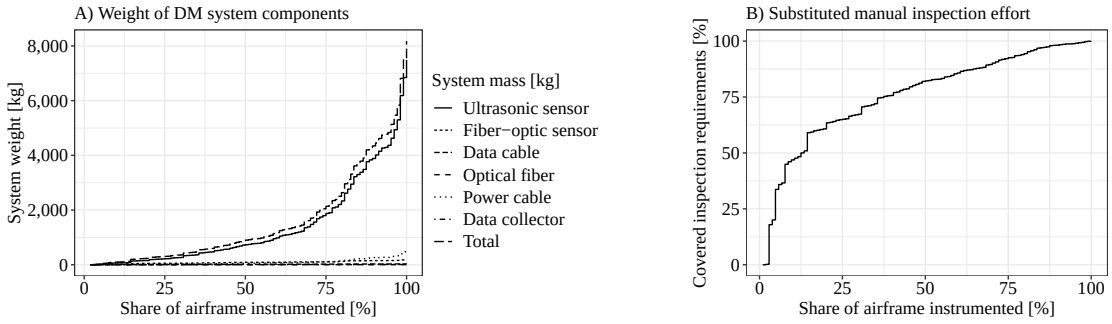

Figure 5.8: Impact of introducing a DM-based SHM system in terms of A) added equipment weight and B) decreased manual inspection effort. The depicted instrumentation order is cost-optimized rather than by inspection time savings per area. Adapted from [169].

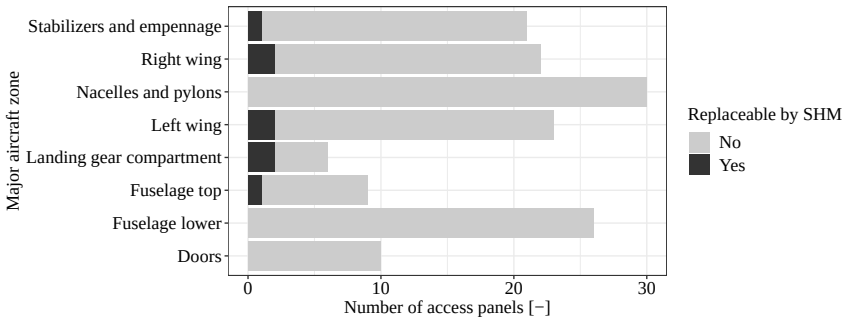

Figure 5.9: Access panels exclusively used for structural inspections, possibly expendable after the introduction of SHM.

exclusively used for structural inspections are identified. In this line, Figure 5.9 summarizes expendable access panels for major zones of the Airbus A320, which become obsolete when using SHM. Only eight access panels on the aircraft are used extensively for structural inspections, with the remainder of 139 openings serving other purposes. As neither the exact geometry and material of the aircraft's access panels and openings are known as part of this work, a precise computation of possible weight savings by foregoing the installation of structural cutouts on the airframe is infeasible.

However, an estimate of the weight impact without the consideration of loads, FMEA, and other effects can be given based on the experience with other aircraft. Based on empirical evidence, the weight of access panels on the pressurized fuselage can be assumed to be approximately 10 kg [173, 508 21-02]. For all other access points located on unpressurized parts of the airframe, the weight of each access panel can be specified at 0.83 to 2.82 kg when assuming a panel area of 0.1 m^2. If only one access panel located on the top of the fuselage is connected to the pressurized cabin, the total weight savings by removing access panels enabled by SHM are estimated between 15.81 and 29.74 kg (compare to Section 3.1.5). Of note, the described design changes may negatively impact repair procedures in the case of damage, as time consuming disassembly procedures may be required when direct access is needed.

5.2 Financial Impact of Selected Structural Health Monitoring Concepts

This section summarizes the effects of SHM on aircraft and airline finances. First, an improved tracking of structural fatigue is deemed more profitable when utilized for delayed airframe retirement instead of lighter fatigue-prone structures, when optimizing the *aircraft decommissioning* economically. Given the increased aircraft lifetime, the simulated impact of SHM on *cash operating cost and capital expenditures*, *aircraft procurement cost*, *additional operating cost*, *fuel cost*, *maintenance cost*, and *spare aircraft cost* is presented.

5.2.1 Economic Aircraft Decommissioning

The retirement of aircraft is driven by not only technical lifetime limits set by the LoV but also financial factors. SHM can improve either airframe design or technical lifetime limits, depending on the optimum economic date of retirement, as proposed in Section 2.2.1. If structural fatigue limits require the decommissioning of the airframe before the aircraft reaches its optimum economic end of life, SHM can be used for structural lifetime extension. Vice versa, if the economic retirement is required before the structural decommissioning limit is reached, the design of fatigue-prone airframe components has been too conservative, and thus, they are unnecessarily heavy. In this case, SHM can achieve lighter designs of fatigue-prone structures by enabling more frequent or continuous inspections and relaxing fatigue requirements.

The time of optimal economic aircraft retirement is determined by maximizing the NPV of a finite asset replacement chain, based on the following assumptions. The reference airline has a WACC of 8% per annum. The replacement aircraft requires an investment of USD 50M. The annual revenue per aircraft is USD 23.8M, and operating costs are USD 20.23M, of which 40% comprise fuel cost. Aircraft depreciate with the sum-of-years' digits method, which is explained in more detail in Appendix A.7. As it is assumed that airlines generally intend to continue their business, an investment horizon of 200 years is selected. At the given WACC, the considered investment horizon is rather academic, as the investment decisions are mainly driven by developments within the first two decades. Additionally, the market value of used aircraft is assumed at book value. Under these assumptions, the airline optimizes the investment into new aircraft by timing the introduction of a replacement aircraft. When specifying the economic time of replacement as a fraction of technological lifetime, the impact of increased lifetime limits and improved fuel burn on airline replacement decisions and the NPV of the investment can be investigated.

The model results are presented in Figure 5.10. As a reference, the average historical age of Airbus A320 aircraft at the time of decommissioning is illustrated in Figure 5.10 A); Figure 5.10 B) shows the modeled driver behind aircraft retirements; and Figure 5.10 C) presents the associated NPV of the aircraft investment chain. The optimum economic retirement of the aircraft is determined as a fraction of the technical lifetime and is based on the technical lifetime and annual improvement in fuel burn of an alternative aircraft. Proceeding from the historical averages of retirement age and annual fuel burn improvements, the effect of the estimated 60% increase in technical lifetime for the reference aircraft on the airline NPV can be investigated.

First, SHM can increase the NPV of the aircraft investment chain and thus extend the technical airframe lifetime. Second, the hypothetical increase in the fatigue life of a new aircraft can allow for weight reductions in fatigue-prone structures. Based on equation 3.29, a 60% potential increase in structural fatigue life allows a 14.5% weight decrease of aluminum sheets if the lifetime increase is forfeited. At an average seat load factor of 80%, the take-off weight reduction is 3.7%[1]. An equal amount in fuel burn reduction over the aircraft lifetime

[1] This is the theoretical maximum, as only a fraction of the airframe is designed for fatigue [243].

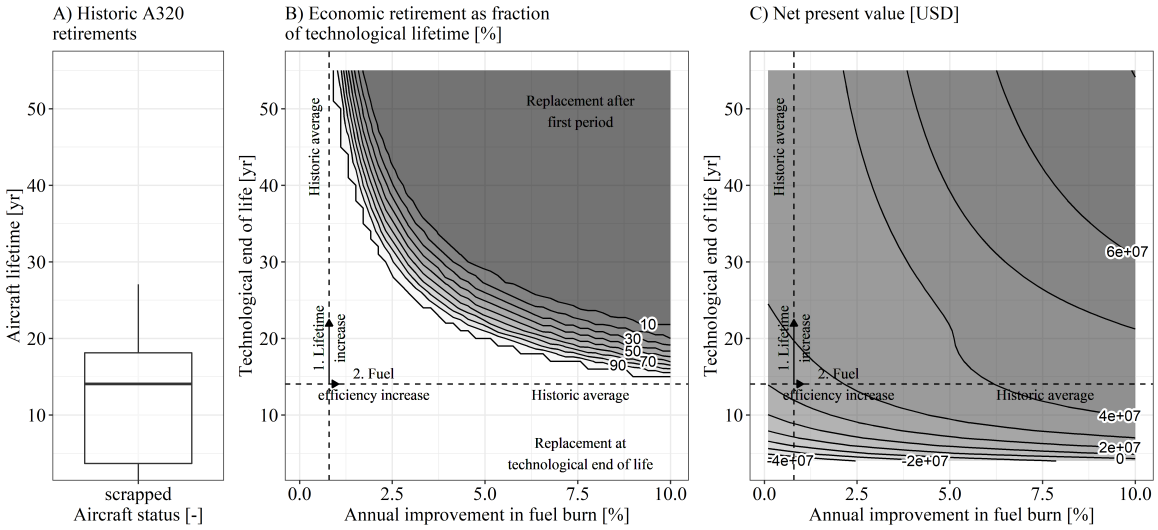

Figure 5.10: Historical average until decommissioning, optimal economic retirement and NPV of a finite investment chain covering 200 years, where airlines continuously replace their assets.

translates into an additional 0.26% fuel burn reduction annually over 14 years—the historical average Airbus A320 lifetime. As shown in Figure 5.10 C), the NPV that is achievable when operating the aircraft longer is significantly greater than when reducing fuel burn. Therefore, under the presented assumptions, lifetime increases enabled by SHM should be fully materialized and not used for structural weight optimizations during the design phase.

5.2.2 Cash Operating Cost and Capital Expenditure

A lifetime increase enabled by SHM can reduce the average aircraft depreciation cost and CAPEX per FH. Assuming that the credit period remains unchanged and the overall interest costs are constant, the 60% lifetime increase of the reference aircraft leads to a 37.5% reduction in airframe depreciation cost and CAPEX per FH. As a result, the overall aircraft depreciation costs decrease by 24.9%. The impact on the COO and CAPEX of the aircraft are summarized in Table 5.1.

5.2.3 Additional Operating Costs

Additional operating costs include expenses incurred from the integration of SHM due to either *lost revenue* from reduced payload capabilities or possible increases in *technical delay cost*.

Without resizing the aircraft, SHM equipment weight impacts both the TOW and ZFW and decreases the aircraft's capability to generate revenue. Each increment of retrofit SHM equipment weight added to the aircraft reduces the payload and fuel that can be added before the MTOW or MZFW is reached. As outlined in Section 3.3.3, the location of the

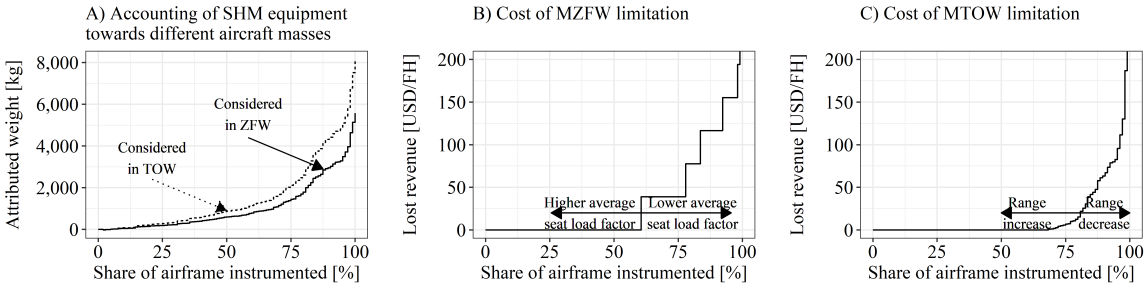

Figure 5.11: SHM mass counts towards different aircraft weights depending on its position within the airframe. A) Impact of DM equipment weight on aircraft ZFW and TOW. B) Cost of MZFW limitation assuming an average seat load factor for the reference aircraft of 80%. C) Cost of MTOW limitation assuming an average flight time of 2 h per FC.

SHM system within the airframe determines if added weight counts towards both TOW and ZFW or only TOW. While additional weight on the wings is only added to TOW, weight added to the fuselage or stabilizers impacts TOW and ZFW. Using the estimated mass of the DM system, the changes in ZFW and TOW, along with their impact on revenue generation, are illustrated in Figure 5.11. The MZFW limitation requires the airline to leave revenue-generating seats empty once the share of airframe instrumented with DM equipment exceeds 60%, given the presented assumptions of this study. Furthermore, limitations in the MTOW inhibit the airline from operating routes exceeding a certain range, thus incurring additional lost revenue.

Next to its impact on the revenue generated by the aircraft, automated SHM can disrupt the turnaround process by producing alarms followed by a fatigue-damage inspection or repair, which leads to *technical delay costs*.

Since automated OLM quantifies a risk rather than detecting actual structural fatigue damage, exceeding the risk threshold does not typically require an immediate repair of the airframe during turnaround but rather at the following overnight maintenance stop. Therefore, no ad-

Table 5.1: Change in COO and CAPEX through increased aircraft lifetime.

Cat.	**Cost component**	**Cost [USD/FH]**		Δ [%]
		Reference	**SHM**	
COO	Depreciation airframes	450.4	281.5	−37.5
	Depreciation flight equipment	96.6	96.6	0
	Depreciation engines	131.8	131.8	0
	Subtotal depreciation	678.8	509,9	−24.9
CAPEX	CAPEX aircraft	703.9	439.9	−37.5
	CAPEX spare AC	59.1	36.9	-37.5
	Total CAPEX	763.0	476,8	−37.5

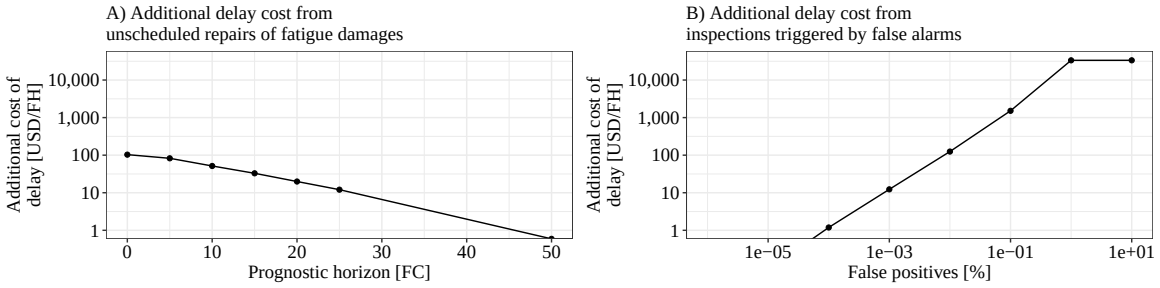

Figure 5.12: The unscheduled repair of structural fatigue damages increases turnaround time and leads to additional delay cost. Predicting such damages can improve the timing of their repair, which reduces associated delay cost, as shown in A). If automated DM produces alarms when the structure is intact, departures are delayed by additional inspections, which increases delay cost as shown in B). Flight cancellations are assumed to occur when delays exceed 300 minutes, with a fixed associated cost. Beyond this threshold, additional false alarms do not result in further delay costs.

ditional operating costs in terms of passenger compensations are considered for automated OLM as part of this work, as the system is assumed to not influence the turnaround process.

The automated DM system, on the other hand, triggers an alarm that requires an immediate manual inspection and possibly a repair since it monitors a damage-dependent physical phenomenon directly. Therefore, no overdraft tolerance is assumed for automated DM, requiring the operator to consider the aircraft not airworthy once an alarm is produced. Depending on the length of a technical delay, the airline incurs additional crew expenditures and passenger compensation costs, as summarized in Figure 5.12, depending on the prognostic horizon and false positive rate of the automated DM system. With an increasing prognostic horizon, imminent structural damages can be addressed earlier on a scheduled maintenance stop to avoid interruptions during a turnaround. On the other hand, an increasing false alarm rate directly increases the overall number of alarms and thus the amount of aircraft turnaround time during which airframe inspections are required.

5.2.4 Fuel Cost

The addition of a DM system influences the fuel burn of the aircraft by increasing equipment weight and onboard power consumption. If the change in airframe weight stems from a retrofitted SHM system and the weight increase is marginal compared to the overall aircraft weight, the fuel cost is estimated to be USD 0.016 per added kilogram of equipment weight and FH [86, pp. 7–8]. The resulting changes in fuel costs are illustrated in Figure 5.13 for a variable DM coverage ratio. However, the fuel cost depends on jet fuel prices, assumed at USD 0.6/kg, and the average flight time of the aircraft, given at 2 h per flight.

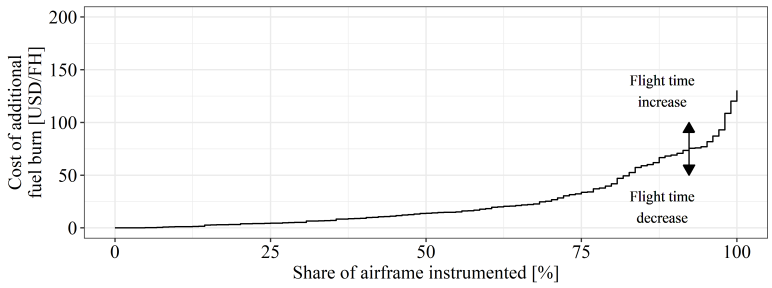

Figure 5.13: Impact of added DM equipment weight and power consumption on aircraft fuel cost per FH, assuming an average flight time of 2 h per FC.

5.2.5 Maintenance Cost

SHM influences the *inspection cost* and *repair cost* of the simulated aircraft, when substituted for manual inspections, as summarized below.

SHM systems are intended to decrease *inspection costs* but can produce false alarms, which trigger unnecessary manual inspection events, as illustrated in Figure 5.14. For scheduled DM, all considered scenarios lead to significant inspection cost savings. While a DM system that is not producing any false alarms leads to inspection cost savings of up to USD 95 per FH, the false positive rate has a stronger adverse effect on financial performance when the DM system is automated. As alarms require a manual inspection before a repair is deemed necessary, a high false alarm rate in automated DM systems can lead to structural inspections outside planned intervals, even increasing the airframe inspection costs. The same occurs with OLM, where scheduled OLM during planned maintenance events at best allows manual inspections to be skipped and at worst does not impact the total inspection effort. As OLM requires manual inspections once the defined risk threshold is exceeded, only 80% of structural inspection costs can be avoided when using such a system. Since the required area-specific inspection effort is not constant for the entire airframe, a leverage effect can be used when instrumenting the aircraft.

Further, SHM also influences *repair costs*, as illustrated in Figure 5.15. While failing to detect structural damages decreases the repair cost, the structural integrity of the airframe is affected adversely, as previously shown in Section 5.1.2. However, automated SHM can improve the detectability of structural fatigue damages, resulting in more repairs and thus slightly increased structural repair cost of USD 14 at most, compared to the reference aircraft. For automated DM, an increasing true positive rate improves damage detectability and thus cost. For OLM, the damage detectability and thus repair costs are reduced with a decreasing risk threshold. With automated OLM, the number of structural damages that are repaired during the aircraft's lifetime can increase moderately if a small risk threshold is selected. At the same time, automated OLM systems with a small risk threshold heavily increase the cost of structural inspection.

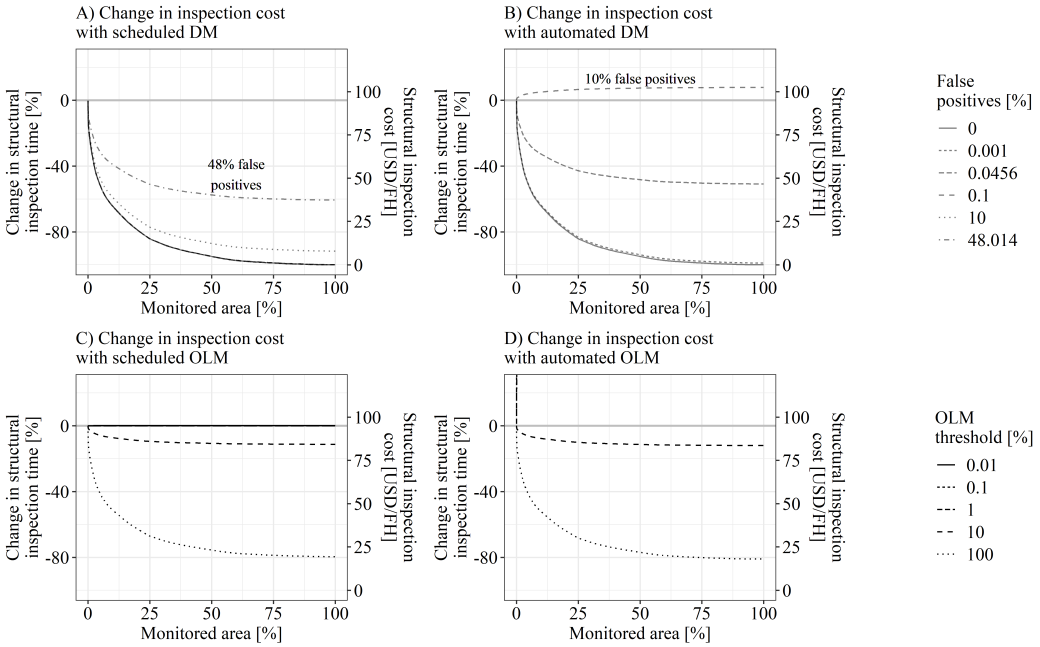

Figure 5.14: Structural inspection cost when using A) scheduled DM, B) automated DM, C) scheduled OLM, and D) automated OLM.

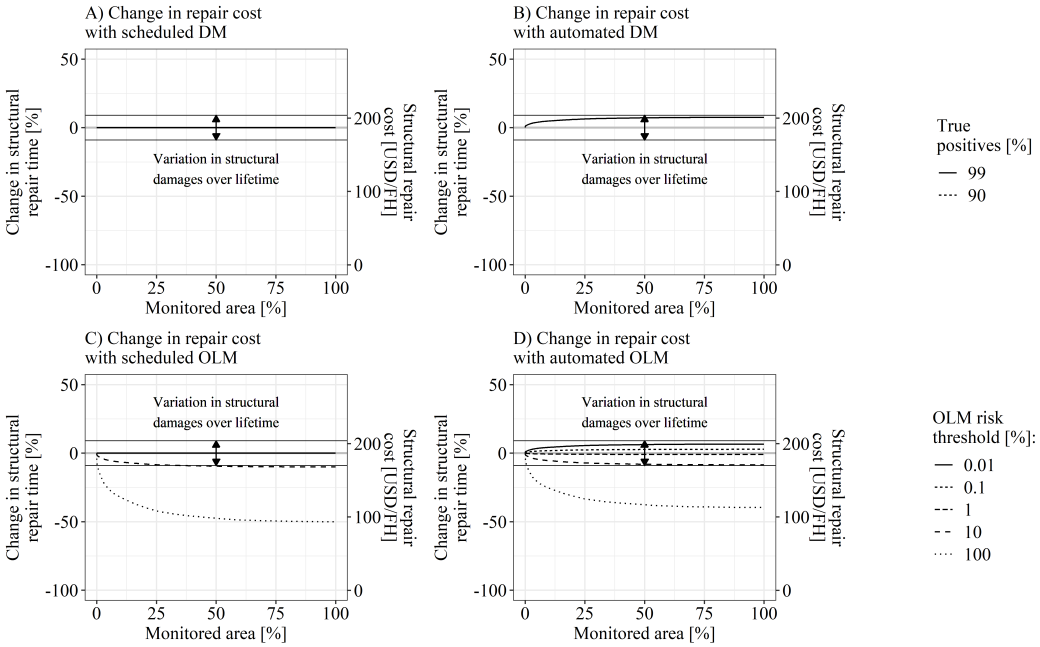

Figure 5.15: Structural repair cost when using A) scheduled DM, B) automated DM, C) scheduled OLM, and automated OLM compared to reference aircraft.

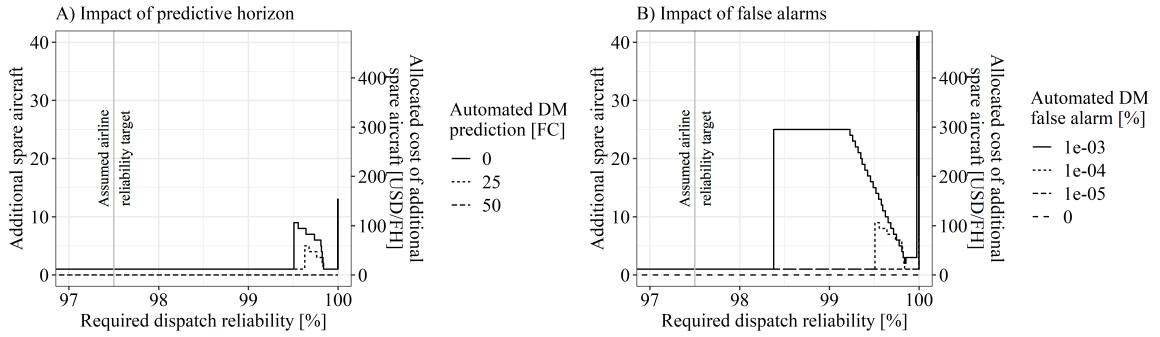

Figure 5.16: Number of spare aircraft required to compensate the decline in aircraft dispatch reliability resulting from an A) insufficient predictive horizon (assuming a false alarm rate of $1{\cdot}10^{-4}$%) and B) high false alarm rate (assuming a prognostic horizon of zero FC) of automated DM.

5.2.6 Spare Aircraft Cost

Based on a given reference aircraft reliability and network topology, a high airline dispatch reliability possibly requires the use of spare aircraft even without SHM, as shown in Section 3.2.3. However, since automated DM adversely impacts the technical dispatch reliability, additional spare aircraft may be needed to compensate additional delay costs summarized in Section 5.2.3. The required number of additional spare aircraft compared to the reference airline without SHM is summarized in Figure 5.16. Hereby, the aircraft dispatch reliability and thus the number of required spare aircraft depend on the targeted airline dispatch reliability, the DM system's predictive horizon, and its false alarm rate. To achieve the targeted dispatch reliability for the reference airline of 97.5%, one spare aircraft is required, resulting in additional CAPEX of USD 11.82 per FH.

5.3 Structural Health Monitoring as Airline Investment

Using the results of the presented cost-benefit analysis, the different SHM approaches can be evaluated as investment opportunities from an airline perspective. First, the investment value of the investigated DM and OLM systems are discussed. The impact of the considered SHM systems on total aircraft operating cost is illustrated as function of the airframe coverage ratio in Figure 5.17. Hereby, all cost factors discussed previously are combined. The airframe coverage is defined as airframe surface area covered by the SHM system divided by the total airframe surface area. Based on the optimum airframe surface coverage ratio for different SHM systems, the NPV of a corresponding investment project over time is shown in Figure 5.18. Finally, the *theoretical cost-savings potential of a perfect DM* system is discussed.

Both *scheduled and automated DM* show significant improvements in aircraft operating cost, depending on the false alarm rate and coverage ratio. Given the introduced weight model, the aircraft operating costs significantly increase when instrumenting more than 75% of the airframe. Regardless of the operating mode, DM systems with very low false alarm rates

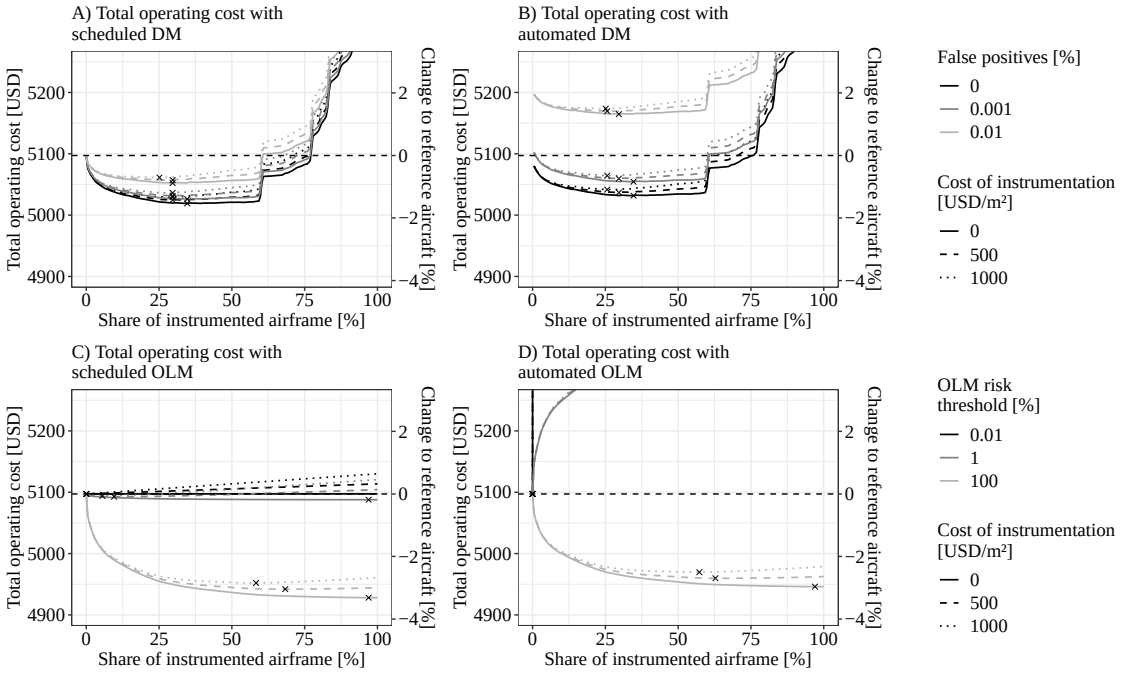

Figure 5.17: Overall impact of A) scheduled DM, B) automated DM, C) scheduled OLM, and D) automated OLM on the operating cost of the reference aircraft. The resulting optimum coverage ratio is marked by "x". Note that automated DM requires lower FP rates compared to scheduled DM to avoid additional cost-intensive ad-hoc inspections.

approaching zero achieve overall cost savings of USD 50–75 per FH, when 25 to 40% of the airframe surface is instrumented. The optimum coverage ratio is dependent on the system performance and cost, where increasing instrumentation cost and FP rate decrease the optimal DM coverage ratio.

For *scheduled and automated OLM*, significant savings in aircraft operating costs are only found when selecting a high risk threshold. While this can lead to an airframe coverage ratio of almost 100%, adverse impacts on the structural integrity of the airframe can be expected, as described in Section 5.1.2. For scheduled OLM, a decreasing risk threshold forfeits the cost benefits of skipping manual inspections, as the OLM also incurs investment cost. For automated OLM, the scheduling of ad-hoc inspections can significantly increase the total operating cost depending on the selected risk threshold.

Assuming the SHM system is sized to its optimum airframe coverage ratio, the NPV for the airline when investing in such a system can be calculated. Figure 5.18 shows the NPV of the investigated SHM systems over their lifetime, which are defined by the aircraft service goals. All presented systems are NPV positive, with a NPV of USD 1.39M for the perfect DM system. Hereby, the assumed installation cost per m^2 of structure includes the entire purchase and installation costs of the system. However, depending on the monitoring performance, their break-even times vary. In practice, airlines require investments to break even after a

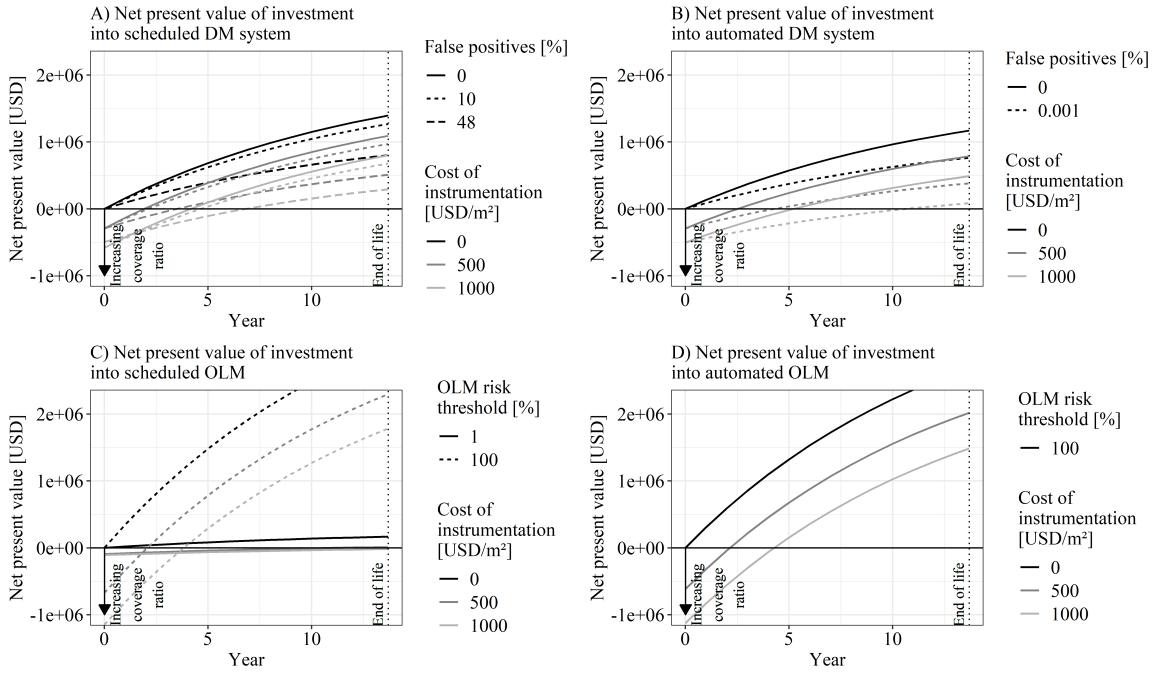

Figure 5.18: NPV of investment into A) scheduled DM, B) automated DM, C) scheduled OLM, and D) automated OLM with an optimal coverage ratio, depending on installation cost and monitoring performance.

certain time. With an assumed break-even time of three years,[2] the feasible design space of the DM systems can be limited further. For a system with an installation cost of over USD 1,000, a break-even requirement of three years, for example, cannot be met.

Finally, the *theoretical cost-savings potential of a perfect DM system* is presented to indicate the maximum cost savings connected to SHM when no false alarms are produced. Furthermore, the simulated weight of the DM equipment, presented in Figure 5.8, is theoretically reduced, where a 100% weight reduction represents a weightless DM system. The impact of a perfect DM system on the operating costs of the reference aircraft and its corresponding NPV are illustrated in Figure 5.19. As shown, less equipment weight and lower instrumentation cost yield a larger share of the instrumented airframe. The maximum achievable NPV of an investment into a perfect, weightless, and costless DM system is USD 1.70M.

5.4 Practical Implications for Design Space of Structural Health Monitoring Concepts Based on Damage Monitoring

Based on the simulated impact of SHM systems on the operational and financial performances of the aircraft and airline presented in previous sections, implications on the design of SHM systems are presented in the following. Using strain measurements from a DM demonstrator

[2] Operational planning horizons and amortization periods of commercial airlines typically do not exceed five years [244, p. 149].

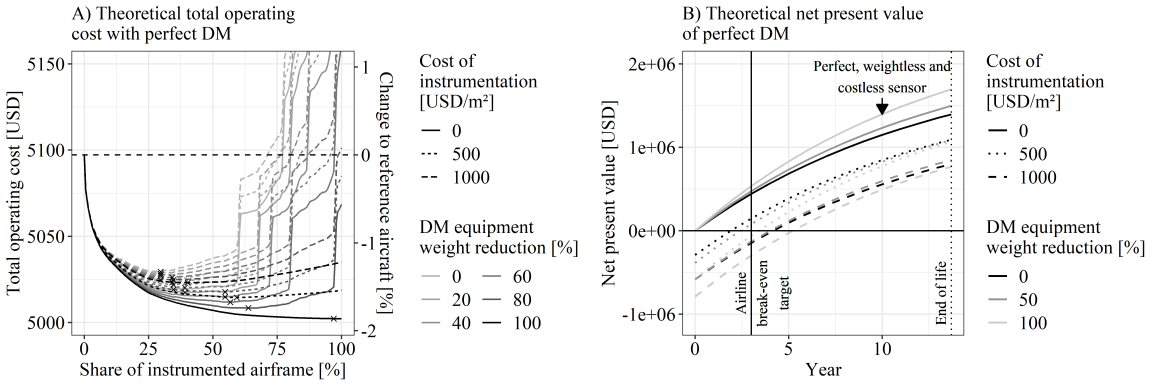

Figure 5.19: Impact of a perfect DM system on A) aircraft operating costs as a function of coverage ratio and instrumentation cost and B) corresponding NPV. The equipment weight variation is based on the simulated DM equipment weight. The resulting optimum coverage ratio is marked by "x".

test performed by IABG, trade-off dimensions in the *calibration of sensor performance and prognostic horizon* are discussed.

With the installation of SHM systems, various performance calibrations are required, which impact the operational efficiency of the aircraft. Without compromising safety margins and allowing cost to be decreased, a high damage detectability, low false alarm rate, and far-reaching prognostic horizon are targeted. The connection between these three targets is illustrated in Figure 5.20 A), based on strain measurements of a sensor used in a SHM demonstrator test conducted at IABG. The change in maximum measured strain indicates the occurrence of current or future structural fatigue damages. Hereby, a high damage detectability requires a low damage-indicator threshold. A low threshold promotes safety by enabling the detection of signs of minor fatigue and ensures the feasibility of a far-reaching prognostic horizon.

However, because the measured signal oscillates over time, a low damage indication threshold may be surpassed frequently, resulting in poor damage classifier performance, schematically illustrated in Figure 5.20 B). In poor damage classifiers, a high damage detectability requires a lax damage classification threshold, which produces a high number of false alarms. As the utilized damage indicator threshold increases, accompanied by a decreasing predictive horizon, the size of the indicator relative to the oscillation of the measured signal (or signal-to-noise ratio) increases, thus enabling better classifiers. Based on the results presented in Section 5.1, this circumstance in the calibration of damage indicators and classifiers impact scheduled DM and automated DM differently. As the inspection intervals specified in the MPD for most structural components are above 10,000 FCs (compare Table A.13), so is the required prognostic horizon to prevent premature preventive replacements. For automated SHM, on the other hand, the simulation results indicate that a prognostic horizon of around 75 FCs (depending on the airline network) is sufficient to conduct all unscheduled structural replacements during on-base overnight checks of the aircraft. Thus, the damage indicator threshold for automated DM can be set at a much higher level than for scheduled DM,

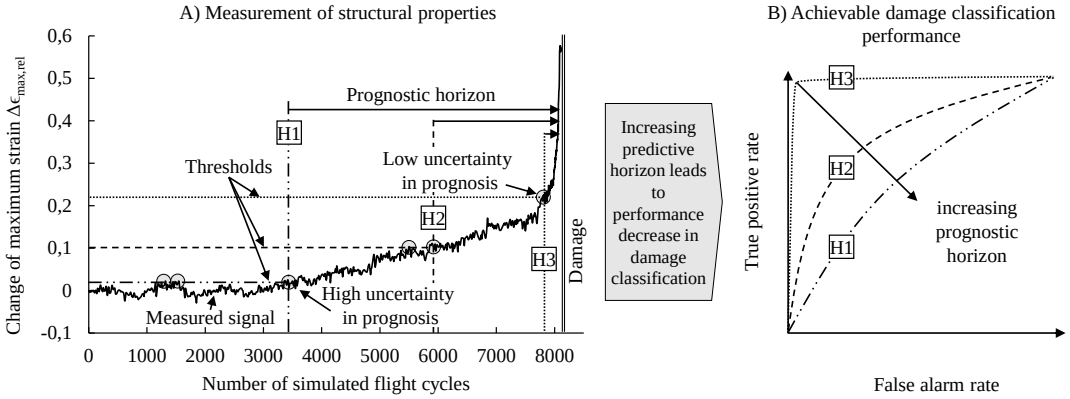

Figure 5.20: A) Connection between damage classification performance and predictive horizon based on results of IABG demonstrator test [245]. B) Schematic impact of prognostic horizon H1 to H3 on achievable damage classification performance.

leading to an almost perfect classifier. Even though the feasibility of this approach has been demonstrated at IABG, a priori knowledge of critical loads and structural properties is required for a correct sensor placement to successfully measure fatigue driving cracks in the structure.

5.5 Performance Enhancement of Hybrid Structural Health Monitoring Systems Using Data Fusion

As indicated in the presented results, the fixed risk threshold used to trigger manual inspections and repairs when using OLM leads to either premature actions or missed damages. However, the aim is to increase the consumable fraction of structural life ideally to 100% of its fatigue life. To this end, a *combination of OLM and DM* in hybrid systems can increase the fraction of consumable life when structural replacements are driven by the risk of fatigue damage. In this work, their interaction is modeled in an HMM, which represents the combination of DM and OLM to calculate the underlying risk of fatigue in the structure. An OLM-driven structural replacement is not based on monitoring individual damages but rather inferring damages according to the initial crack length distribution. Therefore, this approach cannot maximize the consumable life until fatigue damage. To this end, the proposed combination of DM and OLM represented by an HMM can increase the fraction of consumable life until fatigue damage occurs, as illustrated in Figure 5.21. Depending on the classification performance of the DM system, represented by the Lehman parameter, the consumable lifetime increases with DM performance. Additionally, the selected damage classification threshold impacts the performance, where a high TP rate achieved by a small damage classification threshold increases the fraction of consumable lifetime together with the FP rate. A Lehman parameter approaching zero is only of theoretical concern, with the consumable life until fatigue damage approaching 100%.

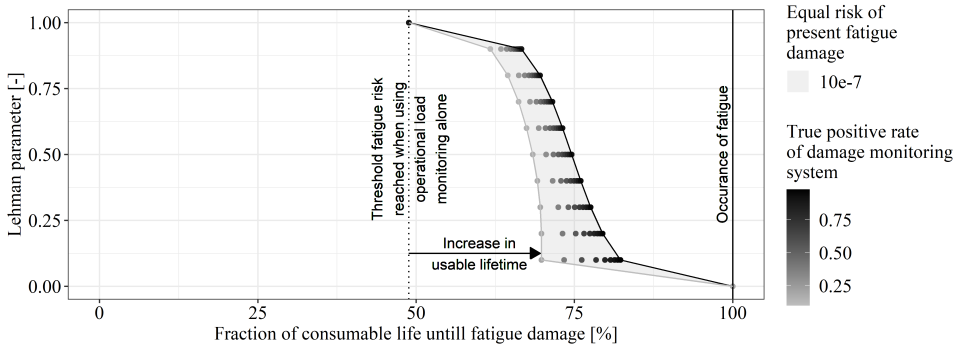

Figure 5.21: Increase in consumable structural lifetime until the predefined risk of fatigue damage is reached, when using a combination of OLM and DM, assuming the DM system does not produce false alarms. The presented results are based on an information fusion process represented by an HMM, previously published in [163].

Chapter 6

Discussion

Work-intensive structural inspections make up 18% of all aircraft maintenance costs or 3–4% of aircraft operating costs [6, p. 275–277, 7, 8, p. 46]. In this context, an automated built-in inspection system, known as SHM, is discussed as a solution to decrease manual labor requirements during airframe inspections without adversely impacting structural safety [11–19]. This thesis expands on current but partially contradicting cost–benefit studies that focus on the individual isolated aspects of SHM. A holistic approach is taken to assess the techno-economic impact of SHM on both aircraft and airline performance [34]. To this end, this chapter discusses the results of this thesis by interpreting key findings, drawing comparisons to similar studies, and discussing methodological limitations.

6.1 Key Findings

The results of the techno-economic evaluation of SHM demonstrate this technology's capability to decrease the reference aircraft's total operating cost. The optimum design of the analyzed SHM system depends on its economic environment and technological properties. The fraction of airframe instrumented with SHM is driven primarily by the cost of labor and capital, the purchase price of the SHM system, and the targeted aircraft dispatch reliability. For DM-based SHM systems, partial airframe instrumentation is preferable to full coverage as the weight of sensors, cables, and data processing units affect aircraft fuel consumption.

For the Airbus A320–based reference aircraft, the operating cost can be reduced by up to 1.9% with ideal DM without impacting the structural integrity of the airframe. With OLM, the operating cost can be reduced by up to 3.4%. Even though OLM exceeds DM in total operating cost savings, OLM can negatively impact the structural integrity of the airframe, as this ensemble-based monitoring approach does not directly observe a damage-dependent physical phenomenon. Therefore, the results indicate that high cost savings from OLM come at the expense of longer times between fatigue damage and repair.

Given the capital cost of the airline, the NPV of an investment into a costless DM system with a perfect classifier is up to USD 1.39M. If the weight of such a system approaches zero, the NPV increases to USD 1.7M. On the contrary, increasing FP rates and instrumentation cost

together with decreasing damage risk thresholds reduce the NPV of an investment into SHM. To improve the monitoring performance, hybrid SHM is evaluated, where the ensemble-based information of OLM is fused with the individual-based information of DM, thus increasing the NPV of SHM.

Furthermore, the results indicate that aircraft retirement based on the actual fatigue condition of the airframe instead of a uniform fleet limit defined in FC and FH allows additional lifetime for aircraft, where experienced loads fall short of design assumptions. Finally, based on the investigated Airbus A320–type reference aircraft, information gathered by SHM is more valuable for airlines when applying it to airframe lifetime extensions rather than to the ex-post weight reduction of fatigue-prone structures to reduce fuel consumption.

6.2 Interpretation of Results

The presented results have significant implications on the development of monitoring systems, the integration of SHM into conceptual aircraft design, and airlines using SHM.

Regarding the design of automated DM, the results indicate that a forecast horizon of 50 FC is sufficient to allow for upcoming structural fatigue damages to be repaired during a scheduled maintenance event. However, for automated DM to be NPV positive, the FP rate must be low enough so that unscheduled structural repairs are avoided during aircraft turnarounds. In the IABG SHM demonstrator test, damage classification was almost perfect for short forecast horizons of approximately 250 FC or less, underscoring the benefits of automated DM.

Additionally, the results show that an overall airframe coverage ratio with SHM between 25 % and 70 % maximizes operating cost savings. The size and performance of an SHM system depend on the location within the airframe and rely on a cost–benefit analysis. Since the information gathered by SHM is considered more beneficial when used to increase fatigue life instead of reducing weight, SHM should not be considered for structural-weight savings when designing the aircraft. During the aircraft design process, SHM should only be considered when it can substitute structurally complex weight–driving access panels and doors. Detailed cost–benefit studies are needed for every aircraft type to reveal promising hotspots where SHM can be used, characterized by high area-specific inspection requirements.

Additionally, the benefits of SHM are dependent on the network in which the aircraft is operated and the organization of airline maintenance activities. To take advantage of automated SHM, airline maintenance operations must accommodate dynamic, ad-hoc structural maintenance. The ability to perform opportunity cost–free structural maintenance during overnight checks defines the requirements for the forecast horizon of an SHM system. Since airline demand is seasonal, a forecast time horizon that allows structural maintenance to be identified a year in advance may be advantageous so that off-season maintenance can be performed, depending on the airline's business model. In addition, the use of SHM may result in structural maintenance being spread out over the life of the aircraft rather than concentrated in a small time frame. Therefore, the introduction of SHM requires flexibility in maintenance organizations when clustering, packaging, and scheduling maintenance tasks. Furthermore,

the weight of an SHM system may reduce the revenue-generating payload, depending on the average seat load and flight distances, which results in additional opportunity costs. The study shows that these costs can significantly exceed the potential savings of structural inspection and life extension. Therefore, the cost of inadequate coverage of structural parts with SHM tends to be less than the additional expenses of over-coverage.

6.3 Comparison of Findings to Similar Studies

Previous cost–benefit studies of SHM presented diverging results, which are compared with those of this thesis in the following. Hereby, DM- and OLM-based SHM approaches are covered along with their results on the aircraft and airline levels.

The thesis assumes that the technological basis for implementing SHM exists, which is supported by previous studies. The use of mountable eddy current sensors for SHM was demonstrated in [139]. However, besides the suggestion of "substantially reduced inspection costs and life extension," the authors presented no detailed cost benefit. For composite structures, the successful use of FBGs to localize an artificial damage is achieved by [145] and confirmed by [141]. Without addressing cost savings, the feasibility of SHM based on CVM and Lamb waves was demonstrated in practice, where five Embraer aircraft were instrumented with sensors and cables for hotspot monitoring [137]. Additionally, [138] studied the trade-offs between the sensor performance, sensor count, and overall sensor network performance and evaluated methods for optimum sensor placement on a structural coupon. [137, 138] suggested that a DM-based SHM system has to be tailored to a specific application.

In this thesis, operational aircraft usage data are considered in two ways. First, OLM-based SHM systems are utilized to substitute manual inspections. [29, 143] reported on the successful use of OLM-based SHM to model airframe fatigue both for military and civil aviation, which can improve the scheduling of manual inspections. Second, operational data can improve the planning of airframe retirement, as suggested with the proposed FDI. A similar approach was presented by [29] with a flight dynamics model to determine the loading cycles at fatigue-critical locations of general aviation aircraft. The presented approach "provides acceptable estimates of the residual fatigue life of the aircraft, thereby allowing a cost-effective and streamlined structural integrity monitoring solution" [29].

In addition to the technical feasibility at the structural level, the implications of SHM have already been evaluated at the aircraft level. Scheduled SHM was suggested for rear passenger and service doors in the Embraer 190, where it could lead to a reduction of 120 working hours every 12000 FC used for a structural fatigue inspection [135]. The reduction in work could be increased to over 250 hours if the SHM systems were able to detect corrosion [135]. Additionally, a higher aircraft availability was proposed, leading to more revenue-generating flights [135]. Moreover, [22] reported a decrease in aircraft downtime from structural maintenance by up to 79 %. In contrast, [148] claimed that the integration of SHM would not significantly decrease the length of the critical path during aircraft maintenance. While time savings from automating structural inspections with SHM are considered in the thesis, the impact of SHM on the critical path of the overall maintenance event, and thus its total length is neglected.

Furthermore, improved "damage detection [is suggested] to decrease the time between structural failure and repair," which can be leveraged to manufacture the "structure 15% lighter when doing condition-based maintenance" [25]. Similar to [25], thesis results indicate a maximum weight savings potential for fatigue-prone aluminum structures of 14.5%. However, not all components of the airframe design are driven by structural fatigue. Additionally, the presented results indicate that airlines benefit more using SHM to increase the airframe lifetime rather than decrease structural weight. Furthermore, this thesis proposes additional weight savings when manual inspections are replaced by DM-based SHM and structural access becomes obsolete. Replacing access panels and doors with lighter structures without cutouts enables airframe weight savings of 15.81 to 29.74 kg, or 0.09% to 0.17% of the assumed total airframe weight of 17,763.4 kg.

Conversely, the required SHM equipment increases the weight of the airframe. For a 25% instrumented airframe, the DM system weighs approximately 300 kg (1.6% of the airframe weight); for a 50% instrumented airframe, the DM system weighs roughly 900 kg (4.8% of the airframe weight). In comparison, the weight of a DM-based SHM system for the entire Boeing 737[1] airframe is approximately 500 kg, or 3% of the total structural weight [31]. With airframe coverage ratios greater than 35%, the calculated weight of the DM system in the thesis exceeds the weight assumed in [31]. While the cost–benefit study considers lighter SHM systems, the estimated weight of the proposed DM system is highly dependent on the comparatively heavy ultrasonic sensors. In [31, 32], the SHM system weight resulted in high added costs due to increased fuel burn and lost revenue. Thus, aircraft operating cost increases of 39% to 69% are estimated when using scheduled SHM as a substitute for manual inspections during a C-check [31, 32]. While reduced revenue through decreased payload capacity is considered in the presented study, the observed seat load factor of 81% is assumed as the typical transported payload. Therefore, the revenue-generating payload is not expected to be reduced for SHM systems weighing below a certain threshold.

Without impacting the probability of failure, condition-based maintenance enabled by automated SHM was shown to decrease the maintenance cost of composite structures by 33.6% [149]. Based on the maintenance cost structure assumed in this thesis, where airframe materials cost USD 53 per FH, airframe repairs cost USD 134 per FH, and airframe inspections cost USD 95 per FH, a 100% airframe coverage with scheduled DM can decrease the structural maintenance cost by up to 33.7%. The cost of additional airframe weight driven by DM equipment and the optimal airframe coverage ratio were not considered by [149]. Maintenance cost savings estimated in this thesis are reduced to 27% when automated DM is used, as damages can be discovered and repaired in between scheduled maintenance intervals. While automated DM can increase repair cost through improved damage detection, it improves structural integrity.

From another perspective, increasing structural health awareness enabled by SHM can feed into integrated vehicle health monitoring to optimize maintenance for the entire aircraft,

[1] Differences in each MTOW, length, wingspan, and wing area between Boeing 737-800 and Airbus A320-200 are less than or equal 5%.

expanding to additional maintenance functions such as logistics [30]. However, these benefits are not considered in this thesis.

6.4 Limitations

The practical implications of this study are limited because of the lack of availability of technical, operational, and financial data, which also influences the selected research design. The first part of this section details the gaps in the available data. The remainder of the section outlines the limitations of the methodology used and provides a link to data accessibility.

6.4.1 Data Availability

Even though the technical feasibility of SHM was demonstrated in [29, 137–139, 141, 143, 145], its benefits depend on the technological and business environment in which it is operated.

On the technical level, the exact airframe geometry, structural properties, loads applied during operation, FMEA results, and full-scale fatigue test data were not available for this thesis, as they comprise proprietary information of the aircraft manufacturer or operator. Therefore, the components of the reference aircraft that drive the design for structural fatigue are unknown. Further, the occurrence of FOD is only considered on the aircraft level, as spatially resolved data could not be obtained. The inspection requirements of the aircraft are based on the MPD. However, repair procedures and connected process metrics are not publicly available and therefore based on general assumptions. The overall architecture of DM-based SHM systems relies on a remodeled approximation of the airframe.

Additionally, the performance assumptions for DM-based SHM are derived from the IABG demonstrator, which represents a simple wing section with a manhole under one-dimensional loading. In practice, complex geometries, practical load cases, and different damage types are expected but not considered in this work. The SHM performance estimates from the IABG demonstrator are applied to the entire airframe, owing to the lack of more suitable data. Additionally, no component-specific reliability data were available for any system of the aircraft. Failures are therefore simulated using MTBF data derived from aircraft dispatch reliability. However, this approach does not allow the identification of local system failure hotspots that may influence structural maintenance planning.

On the business side, the airline cost structure is reconstructed using publicly available records provided by the DOT for aircraft operators based in the United States of America, which breaks down airline cost into high-level cost factors, such as "labor–airframes" and "materials–airframes". A more detailed cost breakdown that allows the reconstruction of individual maintenance processes was not publicly available. Furthermore, the airline maintenance organization is complex—the scheduling of aircraft maintenance, packaging and clustering of inspection tasks, spare parts inventory management, staffing, logistics, and coordination of additional functions require optimization. With no reference case for the aircraft maintenance

management available as part of this thesis, only the clustering and packaging[2] of inspection tasks are considered to avoid an overestimation of maintenance preparation time. The inspection times provided in the MPD, which serve as a basis for this thesis, are based on aircraft in maintenance-ready condition.

Additionally, the airline maintenance organization is influenced by the overall aircraft procurement strategy. Airlines can decrease asset acquisition costs by relying on used aircraft, which in turn require efficient maintenance to be profitable. Alternatively, new aircraft or aircraft with limited use are acquired to decrease their variable cost. Thus, maintenance process times can vary between airlines. This information is often proprietary, as it reveals the profitability structure of a maintenance organization. As a result, maintenance process data are not available as part of this thesis. However, this information would identify time-consuming inspections and the critical path during airframe maintenance, which would help quantify the overall benefits of SHM.

6.4.2 Research Design

The limited accessibility of data also shaped the research design. Methodological limitations extending to the simulation of structural damages, airframe design modifications, modeling of inspections and repairs, aircraft decommissioning, organization of maintenance, and assumed airline strategy are discussed.

This study only considers structural fatigue when evaluating the influence of SHM on airframe design, neglecting FOD, corrosion, and other failure modes. Structural fatigue is simulated with a Paris-Erdogan crack growth approach, in which an arbitrary distribution for the initial crack length is assumed. Although this approach provides a valid approximation of a growing crack, the material properties and loading of the structure have to be known. Since this information was unavailable, crack growth factors for every structural component are fitted using inspection thresholds and intervals stated in the MPD. This method does not accurately remodel the fatigue of individual structural coupons, but it produces a number of fatigue damages on the aircraft level comparable to practical experience. However, this approach does not account for WFD, which drives airframe lifetime limitation. Additionally, to avoid overestimating the structural fatigue of components with short inspection intervals, such as the landing gear, the magnitudes of calculated crack growth factors are capped to an arbitrary maximum. Since the simulated fatigue behavior can only be compared at the aircraft level, the location of structural fatigue hotspots estimated in this thesis with respect to the reference aircraft cannot be validated.

The introduction of SHM can also impact airframe design. Long inspection intervals can be shortened by using built-in test equipment, keeping the aircraft in service, which allows for weight-improved airframe design. The calculated weight savings are based on plate-like aluminum structures designed to withstand fatigue. Complex geometries, variable load scenarios, and differences in component materials are not considered in this study. Additionally,

[2]Process by which similar inspection tasks that require access to the same zone of the aircraft are combined to decrease the overall preparation effort.

the effect of decreasing the thicknesses/weights of the plate-like structures, which may introduce other design-driving failure cases, such as buckling, is neglected. The actual design driver of the analyzed structures is unknown. In addition to the redesign of fatigue-prone structures, the replacement of access doors and panels is evaluated. Depending on their loading, structural cutouts require additional design features to lead the load path through the component appropriately, which increases weight. Therefore, panels and cutouts that are specific for structural inspections can be rendered obsolete by SHM. However, the impact of these openings on the access to a structure in the case of an alarm by the SHM system is unknown. Supplemental information, such as how often a specific area is affected by structural failures, is needed to evaluate the consequences of inspection cutouts.

Continued airworthiness efforts are simulated for the airframe and other technical systems of the aircraft. During scheduled structural maintenance of the reference aircraft, NDT, DI, and GVI are considered as inspection methods. They are distinguished by the probability with which they can detect structural fatigue. If the risk of fatigue exceeds the threshold defined for a specific inspection method, a preventive replacement of the structural component is triggered. However, as the assumed thresholds are based on arbitrary assumptions rather than test data, the actual lengths of structural cracks are unknown. Additionally, this work does not consider human factors, thus assuming perfect manual inspection and repair processes.

The impact of SHM on aircraft retirement is evaluated using the proposed FDI. In practice, this approach can be realized both by DM- and OLM-based SHM. Although the FDI can be implemented by relying only on readily available flight data without increasing structural weight, it can also be calculated using DM if all lifetime limiting structures are instrumented. Since structural components that limit the lifetime of the airframe are unknown, the benefit of delaying aircraft decommissioning with SHM is evenly attributed to the airframe coverage ratio. Thus, only fully instrumented airframes are assumed to achieve the entire proposed lifetime increase.

Based on the seasonality of air transport demand, the maintenance capacity is assumed to be sized to the required annual maximum. Therefore, no capacity constraints are considered for maintenance stations. However, simultaneous detections of structural damages on multiple aircraft with automated DM may result in an unexpected, sharp increase in maintenance demand, which is not considered in this study. Additionally, no distinction is made between daytime and nighttime maintenance, neglecting any fluctuation in worker availability, shift surcharges, and logistic response time.

The selected reference aircraft and airline are based on an analysis of 16,625,103 flights between September 2017 and November 2019 recorded by FR24 and a scheduled flight database for 2018 provided by OAG. Using a simple reference aircraft and reference airline reduces the computational effort of the study and provides representative results, but the benefits of SHM under atypical aircraft usage are not covered.

Furthermore, the payloads experienced by the aircraft during operation are approximated using seat load factor data provided by Sabre. While this provides a good estimation of the number of passengers on each flight, the impact of SHM is driven by the actual weight of the payload. Payload transported in the cargo bay of the aircraft and differences in passenger

weights are neglected. In addition, only the average seat load factor is used—lost revenue from removing payload on flights with a high seat load factor cannot be compensated by a flight with a low seat load factor. Therefore, the opportunity cost of decreased payloads due to SHM equipment weight is systematically underestimated.

Additionally, no aircraft scheduling is performed on the airline level. The impact of aircraft dispatch reliability on the use of spare aircraft and the overall airline dispatch reliability is estimated using a statistical approach. Since this work does not perform flight scheduling, delay propagation and aircraft repositioning through ferry flights within the network are neglected.

Finally, the quantitative analysis of SHM in this thesis does not consider any cost from regulatory requirements, which includes sensor redundancy, staff training, and certification, among others. Because of insufficient data availability and methodological limitations, the presented results on the overall cost and benefit of SHM in commercial aviation are subject to considerable uncertainty.

Chapter 7

Concluding Summary and Outlook

Concluding Summary

This thesis explores the cost and benefits of Structural Health Monitoring (SHM) in commercial aviation using a holistic approach that takes into account physical and technical constraints of the monitoring system as well as organizational and financial constraints of the airlines.

In *Chapter 1*, the conceived benefits of SHM in commercial aviation are presented. Although technical solutions are available, their broad commercial application is currently lacking. This seemingly paradoxical situation is attributed to the lack of comprehension of the effects SHM has on the economics of aircraft and airlines. To better plan the future deployment of such technologies, this thesis aims to investigate the economic impact of SHM at the aircraft and airline levels and identify and quantify profitable applications.

Chapter 2 summarizes and discusses fundamental technological, organizational, and legal contexts that influence the introduction of SHM in commercial aviation. Based on the requirements for the structural integrity of airframes, available SHM solutions and their general capabilities are discussed. The performances of the available SHM approaches strongly depend on the material, present load cases, damage types of the monitored structure, and targeted damage detection accuracy, rendering a general specification of their performances difficult. Furthermore, technical and regulatory requirements in terms of the probability of detection, true positive (TP) rate, and economics, like system durability, false positive (FP) rate, and weight, are discussed. Finally, current cost–benefit analyses of SHM are summarized to reinforce how their study scopes impact the stated cost and benefits of SHM in commercial aviation.

Chapter 3 introduces methods to evaluate the cost and benefits of SHM. Using the Airbus A320 as a retrofit aircraft, the effects of different SHM systems on operational and financial factors are investigated. Airframe fatigue and damages are simulated using the crack growth model of Paris-Erdogan. The calibration of SHM systems for damage detection is based on a demonstrator test performed at Industrieanlagen-Betriebsgesellschaft (IABG). Even though the transferability of demonstrator data to the aircraft level is limited to selected load scen-

arios and damage cases, indicators of the expected performance are obtained. Subsequently, the interactions of damage detection systems and load monitoring systems to improve SHM performance are explored using a Hidden Markov Model to increase the technical potential of SHM. Additionally, simplified scheduling methods are introduced to simulate aircraft maintenance processes. Furthermore, this work provides a simplified approach to evaluate the effect of predictive structural maintenance enabled by SHM on airline reliability. Finally, a cost model is presented to analyze SHM from an investment-decision point of view.

Chapter 4 details the ramifications of the organizational and technological environment in which SHM is used. Subsequently, a reference aircraft and airline are defined to conduct the cost–benefit studies of SHM, and the introduced methods are validated for the selected reference case. Since SHM is not yet used commercially, thus lacking real-world data, the impact of SHM is estimated based on an extrapolation of the current system.

In *Chapter 5*, the cost and benefits of SHM in commercial aviation are analyzed. First, the impact of SHM on operational aspects of aircraft operations is shown. Based on a subsequent discussion of different SHM concepts and design parameters, the financial influences of SHM are presented. Finally, SHM is evaluated as an investment from an airline perspective. The results show that load monitoring allows for improved aircraft decommissioning decisions, representing the greatest benefit of introducing SHM. In addition, the use of load and damage monitoring as a retrofit system can be financially beneficial for airlines that operate their aircraft similarly to how the specified reference aircraft is operated, depending on their performances and system costs. However, the introduction of non-ideal SHM, which adds mass and produces false alarms, is only advantageous for selected hotspots of the aircraft. In general, SHM is only valuable for systems that do not produce a significant number of false alarms. The net present value (NPV) of an ideal damage monitoring (DM) system is estimated at USD 1.39M over the aircraft's lifetime. Maintenance requirements for the SHM system, increased aircraft system complexity, and employee training are not considered in this thesis.

Chapter 6 discusses the key results and their impact on further research and industry practice. A detailed comparison of existing studies supports the assumptions made for this thesis, validating the presented results with respect to possible lifetime extensions, weight savings, and inspection benefits. However, trade-offs at the airline level exist, specifically with life extension and weight savings, which were only partially addressed in previous studies. Discrepancies between the literature and thesis results are primarily due to different assumptions. Finally, the limitations of the data and methodology are discussed. Since most of the required data extend to proprietary company information, the applied methodology is adapted to compensate for the data gaps.

Outlook

In the work at hand, the connection between the performance of SHM systems and their financial impact is analyzed. Therefore, several assumptions are made that possibly impact the overall proposed benefits of SHM.

On the *monitoring system level*, the use of demonstrator test data limits the transferability of results to the entire airframe. Investigated hotspots presenting a beneficial area for SHM may require the detectability of damage modes not covered by the considered SHM system. Additionally, the limited availability of airframe manufacturing data, aircraft loads, and selection of crack growth model may underestimate the possibilities of load monitoring for damage detection. Therefore, more detailed experiments on a wider variety of parts can improve the knowledge about the expected sensor performance. Additionally, the suggested combination of multiple load and damage monitoring systems by means of sensor and data fusion can be experimentally evaluated. Furthermore, the available data from airlines, including aircraft flight performance, operated routes, weather, and maintenance records, may be evaluated in more detail to better predict widespread fatigue damage, a driver for aircraft decommissioning.

The utilized *aircraft simulation model* can be expanded using higher-quality geometrical, material, load, and failure behavior data provided by an aircraft manufacturer. Additionally, such input aids studies on the feasibility of co-opting information for the damage monitoring of systems already installed in the airframe. Furthermore, the study conducted in this work assumes SHM is a retrofit system, neglecting its influence during conceptual aircraft design.

Finally, the current setup of the *air transport system* leads to an almost exclusive focus on fuel efficiency, as it is the largest cost driver for airlines and dictates the environmental impact of the aircraft. Therefore, the airframe has to be as light as possible while withstanding loads for a prescribed duration. The optimum trade-off between airframe weight, durability, and inspectability is dictated by the price of jet fuel and labor cost. Instead of focusing on marginally improving this trade-off with SHM, the use of regenerative energy sources and means of propulsion to mitigate environmental impacts will perspectively allow for a more robust airframe design to decrease inspection cost, even without SHM.

Bibliography

[1] Harro Ranter. Flight safety foundation: Aviation safety network databases, 2021. URL https://aviation-safety.net/database/events/.

[2] Worldbank. Air transport: Passengers carried, 2021. URL https://data.worldbank.org/indicator/IS.AIR.PSGR.

[3] Kaitano Dube, Godwell Nhamo, and David Chikodzi. Covid-19 pandemic and prospects for recovery of the global aviation industry. *Journal of Air Transport Management*, 92: 102022, 2021. ISSN 09696997. doi:10.1016/j.jairtraman.2021.102022.

[4] Vanolli Arnaud. Iata industry statistics: Fact sheet, 2020. URL https://www.iata.org/en/iata-repository/publications/economic-reports/airline-industry-economic-performance---november-2020---data-tables/.

[5] Boeing Aircraft Company. Commercial market outlook 2020 - 2039, 2020. URL https://www.boeing.com/resources/boeingdotcom/market/assets/downloads/2020_CMO_PDF_Download.pdf.

[6] Clarence C. Rodrigues, Stephen K. Cusick, and Antonio L. Cortés. *Commercial aviation safety*. McGraw-Hill Education, New York, sixth edition, 2017. ISBN 1259641821.

[7] United States Department of Transportation. Air carrier financial: Schedule p-5.2, 2021. URL https://www.transtats.bts.gov.

[8] Aircraft Commerce. A320 maintenance cost analysis. *Aircraft Commerce*, (Issue 5 May/Jun):38–48, 1999.

[9] Remzi Saltoğlu, Nazmia Humaira, and Gökhan İnalhan. Aircraft scheduled airframe maintenance and downtime integrated cost model. *Advances in Operations Research*, 2016(2):1–12, 2016. ISSN 1687-9147. doi:10.1155/2016/2576825.

[10] Michael Chun-Yung Niu. *Airframe structural design: Practical design information and data on aircraft structures*. Conmilit Press, Hong Kong, second edition, 2002. ISBN 962-7128-09-0.

[11] C. Boller. Next generation structural health monitoring and its integration into aircraft design. *International Journal of Systems Science*, 31(11):1333–1349, 2000. ISSN 0020-7721.

[12] Christian Boller, Fu-Kuo Chang, and Yozo Fujino, editors. *Encyclopedia of Structural Health Monitoring*. John Wiley & Sons, Ltd, Chichester, UK, 2009. ISBN 9780470058220.

[13] Christian Boller. Structural health monitoring: An introduction and definitions. In Christian Boller, Fu-Kuo Chang, and Yozo Fujino, editors, *Encyclopedia of Structural Health Monitoring*. John Wiley & Sons, Ltd, Chichester, UK, 2009. ISBN 9780470058220.

[14] Roy H. Christensen. Fatigue monitor, U.S. Patent 3136154 (A) 1964.

[15] Darrell R. Harting. Fatigue life gaging methods, U.S. Patent US3272003 (A) 1966.

[16] E. Gb Thomas. Fatigue sensors, U.S. Patent US3782178 (A) 1974.

[17] Howard Warren Smith. Fatigue damage indicator, U.S. Patent US3979949 (A) 1976.

[18] David C. English, Jerry L. Mccauley, and Godfrey A. Holmstrom. Load cell scale, U.S. Patent US4020911 (A) 1977.

[19] Gary G. Cassatt and Richard J. Miller. Flaw growth correlator, U.S. Patent US4164874 (A) 1979.

[20] M. J. Bos. Review of aeronautical fatigue and structural integrity investigations in the netherlands during the period march 2015 to march 2017. *NLR-TP-2017-137*, 2017.

[21] Jose M. Menendez. Market opportunities on fiber optic sensors for aeronautics and aerospace applications. In *Third European Workshop on Optical Fibre Sensors*. International Society for Optics and Photonics, 2007. doi:10.1117/12.738339.

[22] M. M. Derriso, C. D. McCurry, and C. M. Kabban Schubert. A novel approach for implementing structural health monitoring systems for aerospace structures. In *Structural Health Monitoring (SHM) in Aerospace Structures*, pages 33–56. Elsevier, 2016.

[23] P. A. Lloyd. Structural health monitoring systems–benefits and airworthiness issues. *The Aeronautical Journal*, 112(1131):285–289, 2008. ISSN 0001-9240.

[24] Sriram Pattabhiraman, Nam Ho Kim, and Raphael Haftka. Effects of uncertainty reduction measures by structural health monitoring on safety and lifecycle costs of aircrafts. In *51st AIAA/ASME/ASCE/AHS/ASC Structures, Structural Dynamics, and Materials Conference 18th AIAA/ASME/AHS Adaptive Structures Conference 12th*, page 2677, 2010. doi:10.2514/6.2010-2677.

[25] Sriram Pattabhiraman, Nam Ho Kim, and Raphael Haftka. Effect of inspection strategies on the weight and lifecycle cost of airplanes. In *52nd AIAA/ASME/ASCE/AHS/ASC Structures, Structural Dynamics and Materials Conference 19th AIAA/ASME/AHS Adaptive Structures Conference 13t*, page 1763, 2011.

[26] Sriram Pattabhiraman, Christian Gogu, Nam H. Kim, Raphael T. Haftka, and Christian Bes. Skipping unnecessary structural airframe maintenance using an on-board structural health monitoring system. *Proceedings of the Institution of Mechanical Engineers, Part O: Journal of Risk and Reliability*, 226(5):549–560, 2012. ISSN 1748-006X.

[27] Yiwei Wang, Christian Gogu, Nicolas Binaud, B. E.S. Christian, and Raphael T. Haftka. A cost driven predictive maintenance policy for structural airframe maintenance. *Chinese Journal of Aeronautics*, 30(3):1242–1257, 2017. ISSN 10009361.

[28] Yiwei Wang, Christian Gogu, Nicolas Binaud, Christian Bes, Raphael T. Haftka, and Nam-Ho Kim. Predictive airframe maintenance strategies using model-based prognostics. *Proceedings of the Institution of Mechanical Engineers, Part O: Journal of Risk and Reliability*, 232(6):690–709, 2018. ISSN 1748-006X.

[29] Christopher Keryk, Roberto Sabatini, Kyriakos Kourousis, Alessandro Gardi, and Jose M. Silva. An innovative structural fatigue monitoring solution for general aviation aircraft. *Journal of Aerospace Technology and Management*, 10, 2018. ISSN 2175-9146.

[30] Andrew Gyekenyesi. Integrating nondestructive inspections with autonomic logistics and structural health monitoring strategies for aeronautic systems. *Journal of intelligent material systems and structures*, 24(5):574–583, 2013. ISSN 1045-389X.

[31] Ting Dong and Nam Ho Kim. Reviews of structural health monitoring technologies in airplane fuselage maintenance perspective. In *AIAA/AHS Adaptive Structures Conference*, 2018.

[32] Ting Dong and Nam H. Kim. Cost-effectiveness of structural health monitoring in fuselage maintenance of the civil aviation industry. *Aerospace*, 5(3):87, 2018. doi:10.3390/aerospace5030087.

[33] Leroy Fitzwater, Christopher Davis, Tony Torng, and James Poblete. Cost/benefit analysis for intergration of non-deterministic analysis and in-situ monitoring for structural integrity. In *52nd AIAA/ASME/ASCE/AHS/ASC Structures, Structural Dynamics and Materials Conference 19th AIAA/ASME/AHS Adaptive Structures Conference 13t*, page 1700, 2011.

[34] Dominik M. Steinweg and Mirko Hornung. Evaluating the influence of shm on damage tolerant aircraft structures considering fatigue. In *International Committee on Aeronautical Fatigue*, pages 976–993. Springer, 2019.

[35] Lily Koops, editor. *ROC-based Business Case Analysis for Predictive Maintenance–Applications in Aircraft Engine Monitoring*, volume 4, 2018. ISBN 2325-016X.

[36] James A. Hanley and Barbara J. McNeil. The meaning and use of the area under a receiver operating characteristic (roc) curve. *Radiology*, 143(1):29–36, 1982. ISSN 0033-8419.

[37] European Union Aviation Safety Agency. Cs-25: Certification specifications for large aeroplanes - amendment 25, 24.06.2020.

[38] Michael Chung-Yung Niu. *Composite airframe structures: Practical design information and data*. Conmilit Press, Hong Kong, 3rd publ edition, 2000. ISBN 978-9627128069.

[39] Trevor J. Pinch and Wiebe E. Bijker. The social construction of facts and artefacts: or how the sociology of science and the sociology of technology might benefit each other. *Social Studies of Science*, 14(3):399–441, 1984. ISSN 0306-3127. doi:10.1177/030631284014003004.

[40] Society of Automotive Engineers. *Guidelines for implementation of structural health monitoring on fixed wing aircraft: ARP6461*. SAE International, 2013.

[41] Daniel P. Raymer. *Aircraft design: A conceptual approach*. AIAA education series. American Institute of Aeronautics and Astronautics Inc, Reston, VA, sixth edition, 2018. ISBN 1624104908.

[42] Mark S. Saglimbene. Reliability analysis techniques: How they relate to aircraft certification. In *2009 Annual Reliability and Maintainability Symposium*, pages 218–222. IEEE. ISBN 1424425085.

[43] Michael Mohaghegh. Evolution of structures design philosophy and criteria. *Journal of Aircraft*, 42(4):814–831, 2005. ISSN 0021-8669. doi:10.2514/1.11717.

[44] Sérgio M. O. Tavares and Paulo M. S. T. de Castro. *Damage Tolerance of Metallic Aircraft Structures*. Springer International Publishing, Cham, 2019. ISBN 978-3-319-70189-9.

[45] Eaton Aerospace Group. Airbus a318, a319, a320 & a321 overview: Eaton's aerospace product capabilities. 2014.

[46] United States. Division of the Federal Register. *Supplement to the Code of Federal Regulations of the United States of America*. Division of the Federal Register, the National Archives, 1947.

[47] R. G. Eastin and W. Sippel. The "wfd rule"− have we come full circle? In *USAF Aircraft Structural Integrity Program Conference 2011*. San Antonio, Texas, November 29 – December 1, 2011.

[48] United States. Office of the Federal Register. *Code of Federal Regulations: 1949-1984*. U.S. General Services Administration, National Archives and Records Service, Office of the Federal Register, 1970. URL `https://books.google.de/books?id=pRhKzj96B2UC`.

[49] Federal Aviation Administration. Advisory circular 25.571-1: Damage-tolerance and fatigue evaluation of structure, 1978.

[50] Federal Aviation Administration. Part 25-airworthiness standards: Transport category airplanes, 27.10.2020.

[51] R. Eastin. 'wfd' – what is it and what's 'lov' got to do with it? *International Journal of Fatigue*, 31(6):1012–1016, 2009. ISSN 01421123.

[52] Ulf Paul Breuer. *Commercial aircraft composite technology*. Springer International Publishing, Cham, 2016. ISBN 978-3-319-31917-9.

[53] Alan A. Baker, Stuart Dutton, and Donald W. Kelly, editors. *Composite materials for aircraft structures*. AIAA education series. American Institute of Aeronautics and Astronautics, Reston, Va., second edition, 2004. ISBN 9781563475405.

[54] Adrian P. Mouritz. *Introduction to aerospace materials*. Woodhead Publishing in materials. Woodhead Pub, Cambridge, UK, 2012. ISBN 978-1-85573-946-8.

[55] A. S. Warren. Developments and challenges for aluminum–a boeing perspective. In *Materials Forum*, pages 24–31, 2004. ISBN 0883-2900.

[56] Maria Mrazova. Advanced composite materials of the future in aerospace industry. *INCAS BULLETIN*, 5(3):139–150, 2013. ISSN 20668201.

[57] Karl-Heinz Rendigs. Airbus and current aircraft metal technologies, 29.09.2005.

[58] Flight Global. Airbus a320 aircraft profile, 2008. URL `https://www.flightglobal.com/airbus-a320-aircraft-profile/78475.article`.

[59] Harry A. Kinnison and Tariq Siddiqui. *Aviation maintenance management*. McGraw-Hill, New York, NY, 2. ed. edition, 2013. ISBN 978-0071805025.

[60] Martin Hinsch. *Industrial aviation management: A primer in European design, production and maintenance organisations*. Springer, Berlin, Germany, 2019. ISBN 978-3-662-54740-3.

[61] Gregory W. Good, B. van Nakagawara, and Mike Monroney Aeronautical Center. Vision standards and testing requirements for nondestructive inspection (ndi) and testing (ndt) personnel and visual inspectors. 2003.

[62] B. Purna Chandra Rao. Non-destructive testing and damage detection. In N. Eswara Prasad and R.J.H Wanhill, editors, *Aerospace Materials and Material Technologies*, volume 57 of *Indian Institute of Metals Series*, pages 209–228. Springer Singapore, Singapore, 2017. ISBN 978-981-10-2142-8.

[63] Hossein Towsyfyan, Ander Biguri, Richard Boardman, and Thomas Blumensath. Successes and challenges in non-destructive testing of aircraft composite structures. *Chinese Journal of Aeronautics*, 33(3):771–791, 2020. ISSN 10009361.

[64] Federal Aviation Administration. Acceptable methods, techniques, and practices - aircraft inspection and repair: Ac 43.13-1b, 1998.

[65] Guy Gratton. *Initial Airworthiness*. Springer International Publishing, Cham, 2018. ISBN 978-3-319-75616-5. doi:10.1007/978-3-319-75617-2.

[66] Federal Aviation Administration. Part 39 - airworthiness directives, 28.10.2020.

[67] Society of Automotive Engineers. *Guidelines for implementation of structural health monitoring on fixed wing aircraft: ARP6461A*. SAE International, 2021.

[68] International Maintenance Review Board Policy Board. Further advanced definition of structural health monitoring (shm)/addition to msg-3. ip 105. URL `https://www.easa.europa.eu/download/imrbpb/IP%20105.pdf`.

[69] Society of Automotive Engineers. Aerospace industry steering committee on structural health: Standards. URL `http://profiles.sae.org/teaaiscshm/`.

[70] Stuart A. McCrary. *Mastering financial accounting essentials: The critical nuts and bolts*. Wiley finance. John Wiley & Sons, Hoboken, N.J, 2010. ISBN 978-0-470-39332-1.

[71] Decker, William, Brunner, Paul. Summary of accounting principle differences around the world. In Frederick D. S. Choi, editor, *International finance and accounting handbook*. J. Wiley, Hoboken, N.J, 2003. ISBN 0-471-22921-0.

[72] Rigas Doganis. *Flying off Course: Airline Economics and Marketing*. Routledge, Milton, 5th ed. edition, 2019. ISBN 9781138224230. URL `https://ebookcentral.proquest.com/lib/gbv/detail.action?docID=5630611`.

[73] Colin Drury. *Management and cost accounting*. Cengage Learning, Andover, 8. edition, 2012. ISBN 9781408041802.

[74] Alexander Kählert. *Specification and Evaluation of Prediction Concepts in Aircraft Maintenance*. Dissertation, Technische Universität Darmstadt, Darmstadt, 2017.

[75] Hans-Jürgen Warnecke and Carl-Otto Bauer, editors. *Handbuch Instandhaltung*. Verl. TÜV Rheinland, Köln, 1992.

[76] G. Hilfer, N. Rößler, C. Peters, and C. Herrmann. A320 esg full scale fatigue test-lessons learned. In *ICAF 2011 Structural Integrity: Influence of Efficiency and Green Imperatives*, pages 529–537. Springer, 2011.

[77] Airbus SE. Extended service goal (esg), 2021. URL `https://services.airbus.com/en/flight-operations/system-upgrades/operations-extension/extended-service-goal-esg.html`.

[78] John C. Aldrin, Enrique A. Medina, Daniel A. Allwine, Mohammed QadeerAhmed, Joseph Fisher, Jeremy S. Knopp, and Eric A. Lindgren. Probabilistic risk assessment: impact of human factors on nondestructive evaluation and sensor degradation on structural health monitoring. In *AIP Conference Proceedings*, pages 1461–1468. American Institute of Physics. ISBN 0735403996.

[79] Steven Henderson and Steven Feiner. Exploring the benefits of augmented reality documentation for maintenance and repair. *IEEE transactions on visualization and computer graphics*, 17(10):1355–1368, 2011. doi:10.1109/TVCG.2010.245.

[80] Massoud Bazargan. *Airline Operations and Scheduling*. Taylor and Francis, Florence, 2nd edition, 2016. ISBN 9780754679004.

[81] Xiaowen Fu, Tae Hoon Oum, and Anming Zhang. Air transport liberalization and its impacts on airline competition and air passenger traffic. *Transportation Journal*, pages 24–41, 2010. ISSN 0041-1612.

[82] Maximilian M. Etschmaier and Dennis F. X. Mathaisel. Airline scheduling: An overview. *Transportation Science*, 19(2):127–138, 1985. ISSN 0041-1655.

[83] Marco Alderighi, Alessandro Cento, Peter Nijkamp, and Piet Rietveld. Network competition—the coexistence of hub-and-spoke and point-to-point systems. *Journal of Air Transport Management*, 11(5):328–334, 2005. ISSN 09696997. doi:10.1016/j.jairtraman.2005.07.006.

[84] Abdelrahman E.E. Eltoukhy, Felix T.S. Chan, and S. H. Chung. Airline schedule planning: a review and future directions. *Industrial Management & Data Systems*, 117 (6):1201–1243, 2017. ISSN 0263-5577.

[85] P. M. Peeters, J. Middel, and A. Hoolhorst. Fuel efficiency of commercial aircraft: An overview of historical and future trends. *National Aerospace Laboratory NLR*, (NLR-CR-2005-669), 2005.

[86] Federal Aviation Administration. *Economic Values for FAA Investment and Regulatory Decisions: A Guide - 2020 Update: Economic Values Related to Aircraft Performance Factors*. Office of Aviation Policy and Plans, 2020.

[87] Hans-Jürgen Schmidt and Bianka Schmidt-Brandecker. Design benefits in aeronautics resulting from shm. In Christian Boller, Fu-Kuo Chang, and Yozo Fujino, editors, *Encyclopedia of Structural Health Monitoring*. John Wiley & Sons, Ltd, Chichester, UK, 2009. ISBN 9780470058220.

[88] Christophe Le Garrec and François Kubica. In-flight structural modes identification for comfort improvement by flight control laws. *Journal of Aircraft*, 42(1):90–92, 2005. ISSN 0021-8669. doi:10.2514/1.3733.

[89] Mark Voskuijl, Michel J.L. van Tooren, and Daniel J. Walker. Condition-based flight control for helicopters: An extension to condition-based maintenance. *Aerospace Science and Technology*, 42:322–333, 2015. ISSN 12709638. doi:10.1016/j.ast.2015.01.026.

[90] PMGJ Lancelot and Roeland de Breuker. Effect of improved flight and control loads modelling on wing-box preliminary sizing. In *6th Aircraft Structural Design Conference*. Bristol, 2018.

[91] O. Sensburg, J. Becker, H. Lusebrink, and F. Weiss. Gust load alleviation on airbus a300. In *13th Congress of the International Council of the Aeronautical Sciences*. Seattle, 1982.

[92] IATA. Fuel costs of airlines worldwide from 2011 to 2020, as percentage of expenditure, 2020. URL `https://www-statista-com.eaccess.ub.tum.de/statistics/591285/aviation-industry-fuel-cost/`.

[93] Fu-Kuo Chang, editor. *Structural Health Monitoring 2011: Condition-based Maintenance and Intelligent Structures*, 2011. ISBN 978-1-60595-053-2.

[94] Fu-Kuo Chang, editor. *Structural Health Monitoring 2013: A Roadmap to Intelligent Structures*, 2013. ISBN 978-1-60595-115-7.

[95] Fu-Kuo Chang and Fotis Fotis Kopsaftopoulos, editors. *Structural Health Monitoring 2015: System Reliability for Verification and Implementation*, 2015. ISBN 978-1605952758.

[96] Fu-Kuo Chang and Fotis Fotis Kopsaftopoulos, editors. *Structural Health Monitoring 2017: Real-Time Material State Awareness and Data-Driven Safety Assurance*, 2017. ISBN 978-1605953304.

[97] Fu-Kuo Chang, Alfredo Guemes, and Fotis Fotis Kopsaftopoulos, editors. *Structural Health Monitoring 2019: Enabling Intelligent Life-cycle Health Management for Industry internet of Things (IIOT)*, 2019. ISBN 978-1605956015.

[98] Alfredo Güemes, Claus-Peter Fritzen, and Daniel Balageas. *Structural health monitoring*. ISTE, London and Newport Beach, CA, 2006. ISBN 978-1-905209-01-9.

[99] Rih-Teng Wu and Mohammad Reza Jahanshahi. Data fusion approaches for structural health monitoring and system identification: Past, present, and future. *Structural Health Monitoring*, 19(2):552–586, 2020. ISSN 1475-9217.

[100] Theodorus Hendricus Ooijevaar. *Vibration based structural health monitoring of composite skin-stiffener structures*. 2014. ISBN 9789036536240.

[101] W. J. Staszewski, S. Mahzan, and R. Traynor. Health monitoring of aerospace composite structures – active and passive approach. *Composites Science and Technology*, 69(11-12):1678–1685, 2009. ISSN 02663538. doi:10.1016/j.compscitech.2008.09.034.

[102] Amir Nasrollahi, Wen Deng, Zhaoyun Ma, and Piervincenzo Rizzo. Multimodal structural health monitoring based on active and passive sensing. *Structural Health Monitoring*, 17(2):395–409, 2018. ISSN 1475-9217. doi:10.1177/1475921717699375.

[103] Holger Speckmann and R. Henrich. Structural health monitoring (shm) – overview on technologies under development. In *16th World Conference on Nondestructive Testing, Montreal, Canada, August 30–September 3, 2004*. 2003.

[104] Roy Ikegami and Christian Boller. History of shm for commercial transport aircraft. In Christian Boller, Fu-Kuo Chang, and Yozo Fujino, editors, *Encyclopedia of Structural Health Monitoring*. John Wiley & Sons, Ltd, Chichester, UK, 2009. ISBN 9780470058220.

[105] Holger Speckmann. International maintenance review board policy board meeting - structural health monitoring, April 22, 2007.

[106] Christophe Paget, Holger Speckmann, Thomas Krichel, and Frank Eichelbaum. Validation of shm sensors in airbus a 380 full–scale fatigue test. *Encyclopedia of Structural Health Monitoring*, 2009.

[107] Jens Telgkamp. Design principles for aerospace structures. *Encyclopedia of Structural Health Monitoring*, 2009. doi:10.1002/9780470061626.shm106.

[108] Airbus SE. Flight airworthiness support technology. *Airbus Technical Magazine*, (54), 2014.

[109] Branko Glišić and Daniele Inaudi. *Fibre optic methods for structural health monitoring*. John Wiley & Sons, Chichester, West Sussex, England and Hoboken, NJ, 2007. ISBN 9780470517802.

[110] Rolf H. Neunaber. Usage management of military aircraft structures. *Encyclopedia of Structural Health Monitoring*, 2009. doi:10.1002/9780470061626.shm110.

[111] Daniel Betz, Michael N. Trutzel, Lother Staudigel, Meinhard Schmuecker, Eric Huelsmann, U. Czernay, H. C. Muehlmann, and T. Muellert. Fibre optic smart sensing of aviation structures. *Structural Health Monitoring*, 2002. ISSN 1475-9217.

[112] Holger Speckmann. Validation, verification and impletion of shm at airbus. In *9th International Workshop on Structural Health Monitoring*. Stanford, USA, 2013.

[113] Barton. Comparative vacuum monitoring (cvm). In Christian Boller, Fu-Kuo Chang, and Yozo Fujino, editors, *Encyclopedia of Structural Health Monitoring*. John Wiley & Sons, Ltd, Chichester, UK, 2009. ISBN 9780470058220.

[114] Dennis Roach, Jeff Kollgaard, Steve Emergy, Jeff Register, Kyle Colvatio, and Dave Galella. Application and certification of comparative vacuum monitoring sensors for in-situ crack detection, 2006.

[115] Iain G. Hebden, Anthony M. Crowly, and Wayne Black. Overview of the f-35 structural prognostics and health management system. In *9th European Workshop on Structural Health Monitoring: EWSHM 2018*. Manchester, United Kingdom, 2018.

[116] Charles R. Farrar and K. Worden. *Structural health monitoring: A machine learning perspective*. Wiley, Chichester, West Sussex, U.K and Hoboken, N.J, 2013. ISBN 9781118443217. URL `http://site.ebrary.com/lib/alltitles/docDetail.action?docID=10657780`.

[117] S. M. Häusler, P. M. Baiz, S. M.O. Tavares, A. Brot, P. Horst, M. H. Aliabadi, P. de Castro, and Y. Peleg-Wolfin. Crack growth simulation in integrally stiffened structures including residual stress effects from manufacturing. part i: Model overview. *Structural Durability & Health Monitoring*, 7(3):163, 2011. ISSN 1930-2983.

[118] S. M.O. Tavares, S. M. Häusler, P. M. Baiz, PMST de Castro, P. Horst, and M. H. Aliabadi. Crack growth simulation in integrally stiffened structures including residual stress effects from manufacturing. part ii: Modelling and experiments comparison. *Structural Durability & Health Monitoring*, 7(3):191, 2011. ISSN 1930-2983.

[119] Matthias Buderath. Fatigue monitoring in military fixed-wing aircraft. In Christian Boller, Fu-Kuo Chang, and Yozo Fujino, editors, *Encyclopedia of Structural Health Monitoring*. John Wiley & Sons, Ltd, Chichester, UK, 2009. ISBN 9780470058220.

[120] M. Neumair. Requirements on future structural health monitoring systems. In *Proceedings of the 7th RTO Meetings*, pages 11–18, 1998.

[121] M.B Zgela and W. B. Madley. *Durability and Damage Tolerance Testing and Fatigue Life Management: ACF-18 Experience*. 1991.

[122] S. R. Hunt and I. G. Hebden. Validation of the eurofighter typhoon structural health and usage monitoring system. *Smart Materials and Structures*, 10(3):497–503, 2001. doi:10.1088/0964-1726/10/3/311. URL `https://doi.org/10.1088%2F0964-1726%2F10%2F3%2F311`.

[123] Timothy Fallon, Devinder Mahal, and Iain Hebden. F-35 joint strike fighter structural prognosis and health management an overview. In *31st Conference and the 25th Symposium of the International Committee on Aeronautical Fatigue*. Rotterdam, 2009.

[124] J. Sierra-Pérez and J. Alvarez-Montoya. Damage detection in composite aerostructures from strain and telemetry data fusion by means of pattern recognition techniques. In *9th European Workshop on Structural Health Monitoring: EWSHM 2018*. Manchester, United Kingdom, 2018.

[125] D. C. Betz, W. J. Staszewski, G. Thursby, and B. Culshaw. Multi-functional fibre bragg grating sensors for fatigue crack detection in metallic structures. *Proceedings of the Institution of Mechanical Engineers, Part G: Journal of Aerospace Engineering*, 220 (5):453–461, 2006. ISSN 0954-4100.

[126] Ralf Meyer, Tania Kirmse, and Fritz Boden. Optical in-flight wing deformation measurements with the image pattern correlation technique. In Andreas Dillmann, Gerd Heller, Ewald Krämer, Hans-Peter Kreplin, Wolfgang Nitsche, and Ulrich Rist, editors, *New Results in Numerical and Experimental Fluid Mechanics IX*, volume 124 of *Notes on Numerical Fluid Mechanics and Multidisciplinary Design*, pages 545–553. Springer International Publishing, Cham, 2014. ISBN 978-3-319-03157-6. doi:10.1007/978-3-319-03158-3{\textunderscore }55.

[127] *Taxi-aid and Landscape Camera Systems: Airbus A350*. Rosemount Aerospace Inc., 2017.

[128] Carlos Sebastia-Saez. *Exploring Synergetic Aircraft Health Monitoring Systems Utilizing a Systems Engineering Approach*. Master's thesis, Technical University of Munich, Munich, 2020.

[129] Malcolm J. Abzug. Fuel slosh in skewed tanks. *Journal of guidance, control, and dynamics*, 19(5):1172–1177, 1996. ISSN 0731-5090.

[130] J. Hall, T. C.S. Rendall, C. B. Allen, and H. Peel. A multi-physics computational model of fuel sloshing effects on aeroelastic behaviour. *Journal of Fluids and Structures*, 56: 11–32, 2015. ISSN 0889-9746.

[131] Shashank Srivastava, Murali Damodaran, and Boo Cheong Khoo. A computational framework for assessment of fuel sloshing effects on transonic wing flutter characteristics. In *AIAA Scitech 2019 Forum*, page 1527.

[132] S. Egusa, Z. Wang, N. Chocat, Z. M. Ruff, A. M. Stolyarov, D. Shemuly, F. Sorin, P. T. Rakich, J. D. Joannopoulos, and Y. Fink. Multimaterial piezoelectric fibres. *Nature materials*, 9(8):643–648, 2010. ISSN 1476-1122. doi:10.1038/nmat2792.

[133] *IHM Series Proximity Sensors for Aerospace Applications: An Application Note*. Honeywell International Inc., 2017.

[134] David Piotrowski, Dennis Roach, Alex Melton, John Bohler, T. Rice, Stephen Neidigk, and John Linn, editors. *Implementation of structural health monitoring (SHM) into an Airline Maintenance Program*, 2015.

[135] Luís G. dos Santos. Embraer perspective on shm introduction into commercial aviation programs. In *Proceedings of the 8th International Workshop on Structural Health Monitoring*. Stanford, USA, 2011.

[136] Luís Gustavo dos Santos. Embraer perspective on the challenges for the introduction of scheduled shm (s-shm) applications into commercial aviation maintenance programs. In *Key Engineering Materials*, pages 323–330. Trans Tech Publ, 2013. ISBN 3037857153.

[137] F. Dotta, R. P. Rulli, P. A. da Silva, L. C. Vieira, A. K.F. Tamba, G. O.C. Prado, D. Roach, and T. Rice. Shm qualification process and the future of aircraft maintenance. *31st Congr. Int. Counc. Aeronaut. Sci. ICAS 2018*, pages 1–7, 2018.

[138] Huidong Gao and Joseph L. Rose. Sensor placement optimization in structural health monitoring using genetic and evolutionary algorithms. In *Smart Structures and Materials 2006: Sensors and Smart Structures Technologies for Civil, Mechanical, and Aerospace Systems*, page 617410. International Society for Optics and Photonics, 2006.

[139] Neil J. Goldfine, Vladimir A. Zilberstein, Darrell E. Schlicker, Yanko Sheiretov, Karen Walrath, Andrew P. Washabaugh, and Douglas van Otterloo. Surface-mounted periodic

field eddy current sensors for structural health monitoring. In *Advanced Nondestructive Evaluation for Structural and Biological Health Monitoring*, pages 20–34. International Society for Optics and Photonics, 2001.

[140] Hever Moncayo, Johannio Marulanda, and Peter Thomson. Identification and monitoring of modal parameters in aircraft structures using the natural excitation technique (next) combined with the eigensystem realization algorithm (era). *Journal of Aerospace Engineering*, 23(2):99–104, 2010. ISSN 0893-1321.

[141] Nezih Mrad. Potential of bragg grating sensors for aircraft health monitoring. *Transactions of the Canadian Society for Mechanical Engineering*, 31(1):1–17, 2007.

[142] G. O.C. Prado, P. A. Silva, F. M. Simomura, and K. L.O. Pereira. Shm with augumented reality for aircraft maintenance. In *31st Congress of the International Council of the Aeronautical Sciences*, 2018.

[143] Stephen Crane Reed. Indirect aircraft structural monitoring using artificial neural networks. *The Aeronautical Journal*, 112(1131):251–265, 2008. ISSN 0001-9240.

[144] Holger Speckmann and Jean-Pierre Daniel. Structural health monitoring for airliner, from research to user requirements, a european view. In *CANEUS - Conference on Micro-Nano-Technologies*, page 6742, 2004.

[145] H. Takeya, K. Sekine, M. Kume, T. Ozaki, N. Takeda, and N. Tajima. Highly reliable advanced grid structures (i-irags) for aircraft structures using multi-point fbg sensor. In Kazuro Kageyama, editor, *Book of abstracts of the papers presented at the Sixteenth International Conference on Composite Materials*, Tokyo, 2007. Japan Society of Composite Materials. ISBN 9784931136052.

[146] A. K.F. Tamba, L. C. Vieira, G. O.C. Prado, F. Dotta, R. P. Rulli, P. A. da Silva, R. R. Cunha, and J. P. Costa. Corrosion detection in aeronautical structures using lamb waves system for shm. In *31st Congress of the International Council of the Aeronautical Sciences*, 2018.

[147] Fuh-Gwo Yuan. *Structural health monitoring (SHM) in aerospace structures*. Woodhead Publishing, 2016. ISBN 0081001584.

[148] C. Boller, H. Kapoor, and W. T. Goh. Structural health monitoring potential determination based on maintenance process analysis. In *Industrial and Commercial Applications of Smart Structures Technologies*, page 65270C. International Society for Optics and Photonics, 2007.

[149] Xi Chen, He Ren, Cees Bil, and Hongwei Jiang. Synchronizing structural health monitoring with scheduled maintenance of aircraft composite structures. *16149944*, 2014. ISSN 16149944.

[150] Xi Chen, Cees Bil, and He Ren. Influence of shm techniques on scheduled maintenance for aircraft composite structures. In *14th AIAA Aviation Technology, Integration, and Operations Conference*, page 3264, 2014.

[151] Jianzhong Sun, Dan Chen, Chaoyi Li, and Hongsheng Yan. Integration of scheduled structural health monitoring with airline maintenance program based on risk analysis. *Proceedings of the Institution of Mechanical Engineers, Part O: Journal of Risk and Reliability*, 232(1):92–104, 2018. ISSN 1748-006X.

[152] H. A. Richard. Grundlagen und anwendungen der bruchmechanik. *Technische Mechanik. Scientific Journal for Fundamentals and Applications of Engineering Mechanics*, 11(2):69–80, 1990. ISSN 2199-9244.

[153] Erwin Haibach. *Betriebsfestigkeit*. Springer, 2006. ISBN 3540293639.

[154] Hiroshi Tada, Paul C. Paris, and George R. Irwin. The stress analysis of cracks. *Handbook, Del Research Corporation*, 34, 1973.

[155] H. A. Richard, N. H. Schirmeisen, and A. Eberlein. Experimental investigations on mixed-mode-loaded cracks. In *Proceedings of the 4th International Conference on Crack Paths*. Gaeta, Italy, 2012.

[156] Darrell Socie and Julie Bannantine. Bulk deformation fatigue damage models. *Materials Science and Engineering: A*, 103(1):3–13, 1988. ISSN 0921-5093.

[157] S. Schwaigerer and E. Weber. Wanddickenberechnung von stahlrohren gegen innendruck. *Erläuterungen zu DIN*, 2413, 1972.

[158] M. Benachour, A. Hadjoui, M. Benguediab, and N. Benachour. Effect of the amplitude loading on fatigue crack growth. *Procedia Engineering*, 2(1):121–127, 2010. ISSN 18777058.

[159] A. Carpinteri. *Handbook of Fatigue Crack Propagation in Metallic Structures*. Elsevier Science, Oxford, 1994. ISBN 9780444600325. URL `http://gbv.eblib.com/patron/FullRecord.aspx?p=1129951`.

[160] Jack Pink. Structural integrity of landing gears. In *SAE Technical Paper Series*, SAE Technical Paper Series. SAE International400 Commonwealth Drive, Warrendale, PA, United States, 1995. doi:10.4271/952021.

[161] Chap T. Le. A solution for the most basic optimization problem associated with an roc curve. *Statistical methods in medical research*, 15(6):571–584, 2006. ISSN 0962-2802.

[162] Heinz Holling, Walailuck Böhning, and Dankmar Böhning. Likelihood-based clustering of meta-analytic sroc curves. *Psychometrika*, 77(1):106–126, 2012. ISSN 0033-3123.

[163] Dominik Steinweg and Mirko Hornung. Integrated aircraft risk analysis framework for health monitoring systems–a case study for structural health monitoring. In *AIAA Scitech Forum*, 2020.

[164] Lawrence R. Rabiner. A tutorial on hidden markov models and selected applications in speech recognition. *Proceedings of the IEEE*, 77(2):257–286, 1989. ISSN 0018-9219.

[165] Mariette Awad and Rahul Khanna, editors. *Efficient Learning Machines.* Apress, Berkeley, CA, 2015. ISBN 978-1-4302-5989-3. doi:10.1007/978-1-4302-5990-9.

[166] Stuart J. Russell and Peter Norvig. *Artificial intelligence: a modern approach.* Pearson Education Limited, third edition, 2016. ISBN 978-0-13-604259-4.

[167] Peter Cawley. Structural health monitoring: Closing the gap between research and industrial deployment. *Structural Health Monitoring*, 17(5):1225–1244, 2018. ISSN 1475-9217.

[168] Dennis P. Roach. *FAA Research Program Webinar Series on Structural Health Monitoring -: Module 1: Introduction to SHM and Implementation.* Sandia National Lab, Albuquerque, NM, 2016.

[169] Kai-Daniel Büchter, Carlos Saez Sebastia, and Dominik M. Steinweg. Modeling of an aircraft structural health monitoring (shm) sensor network for operational impact assessments. *Structural Health Monitoring*, 2021. ISSN 1475-9217.

[170] V. Janapati, K. Lonkar, and F. K. Chang. Design of optimal layout of active sensing diagnostic network for achieving highest damage detection capability in structures. In *Proceedings of the 6th European Workshop on Structural Health Monitoring, Dresden, Germany*, pages 3–6.

[171] B. H. Nya, J. Brombach, and D. Schulz. Benefits of higher voltage levels in aircraft electrical power systems. In *2012 Electrical Systems for Aircraft, Railway and Ship Propulsion*, pages 1–5. IEEE. ISBN 1467313726.

[172] Dieter Scholz, Ravinka Seresinhe, Ingo Staack, and Craig Lawson, editors. *Fuel consumption due to shaft power off-takes from the engine*, 2013. Aachen: Shaker.

[173] Luftfahrttechnisches Handbuch. Handbuch struktur berechnung (hsb). *Industrie-Ausschuss Struktur Berechnungsunterlagen, Ausgabe C; IASB: Ottobrunn, Germany*, 1978.

[174] D. M. Steinweg and M. Hornung. Cost and benefit of structural health monitoring for commercial aircraft. In *International Council of the Aeronautical Sciences*, 2021.

[175] Airbus SE. *Airbus A320 Maintenance Planning Document.* Blagnac Cedex, France, 34 edition, 2010.

[176] Kay Poggensee. *Investitionsrechnung.* Springer Fachmedien Wiesbaden, Wiesbaden, 2015. ISBN 978-3-658-03090-2.

[177] Maintenance Cost Technical Group. Airline maintenance cost executive commentary: An exclusive benchmark analysis (fy2018 data). *IATA*, 2019.

[178] IATA. *Airline Disclosure Guide: Aircraft acquisition cost and depreciation.* 2016.

[179] Cs300 first flight wednesday, direct challenge to 737-7 and a319neo. *Leeham News and Analysis*, 2015, Feb. 25, 2015. URL `https://leehamnews.com/2015/02/25/cs300-first-flight-wednesday-direct-challenge-to-737-7-and-a319neo/`.

[180] Antonov Company. *AN-148/AN-158 Family Overview*. Antonov Company, 2017.

[181] Scott McCartney. A prius with wings vs. a guzzler in the clouds. *Wall Street Journal*, 12 August 2010.

[182] Boeing. *737 Performance Summary*. Boeing Aircraft Company, 2007.

[183] Boeing Aircraft Company. *757 Performance Summary*. Boeing Aircraft Company, 2007.

[184] Bombardier. *CS100: Environmental Product Declaration*. 2016.

[185] Bombardier. *CS300: Environmental Product Declaration*. Bombardier, 2017.

[186] Aircraft Commerce. Analysing the options for 757 replacement. *Aircraft Commerce*, 2005(Issue No. 42 - August / September).

[187] Leeham News. Boeing 737 max: performance if engine has sfc shortfall. *Leeham News*, 15 April 2015.

[188] Quest Aircraft. *Kodiak Brochure*. Quest Aircraft, 2014.

[189] Anja Kollmuss and Jessica Lane. Carbon offsetting and air travel. 2009.

[190] Bjorn Fehrm. Redefining the 757 replacement: Requirement for the 225/5000 sector. *Leeham News*, 25 February 2015.

[191] Aspire aviation. Boeing: 777 way much better than a330. *Aspire aviation*, December 2010.

[192] Vinay Bhaskara. Updated analysis: Delta order for a350; a330neo hinged on pricing, availability. *Airways News*, 25 November 2014.

[193] Boeing Aircraft Company. *747-8 performance summary*. 2010.

[194] Boeing Aircraft Company. *767 performance summary*. Boeing Aircraft Company, 2006.

[195] Boeing Aircraft Company. *777 performance summary*. Boeing Aircraft Company, 2009.

[196] David Kaminski-Morrow. Aeroflot outlines performance expectations for mc-21s. *Flight Global*, 4 June 2018.

[197] Ulrike Stopka and Thomas Urban. *Investition und Finanzierung*. Springer Berlin Heidelberg, Berlin, Heidelberg, 2017. ISBN 978-3-642-01691-2. doi:10.1007/978-3-642-01692-9.

[198] Federal Aviation Administration. 14 cfr 129.119 - limit of validty, 1994.

[199] Aero.de Luftfahrtnachrichten. Air india bucht airbus esg für alte a320. 13.07.2015. URL https://www.aero.de/news-22067/Air-India-bucht-Airbus-ESG-fuer-alte-A320.html.

[200] Simon Pfingstl, Dominik M. Steinweg, Markus Zimmermann, and Mirko Hornung. On the potential of extending aircraft service time using a fatigue damage index. *Journal of Aircraft*, 2021, 2021. ISSN 0021-8669.

[201] Roland Rennert. *Rechnerischer Festigkeitsnachweis für Maschinenbauteile aus Stahl, Eisenguss-und Aluminiumwerkstoffen*. VDMA-Verlag, 2012. ISBN 3816306055.

[202] M. A. Miner. Cumulative damage in fatigue journal of applied mechanics 12 (1945) no. 3, pp. *A159-A164*, 1945.

[203] Luftfahrttechnisches Handbuch. Massenanalyse. *Industrie-Ausschuss Struktur Berechnungsunterlagen, Ausgabe C; IASB: Ottobrunn, Germany*, 1978.

[204] D. Schütz, H. Lowak, J. B. de Jonge, and J. Schijve. Standardisierter einzelflugbelastungsablauf für schwingfestigkeitsversuche an tragflächenbauteilen von transportflugzeugen. *LBF-Bericht FB-106, Fraunhofer-Institut für Betriebsfestigkeit, Darmstadt*, 1973.

[205] Airbus SE. *A320 Aircraft Characteristics Airport and Maintenance Planning*. Airbus SE, 31707 Blagnac Cedex, 2019.

[206] Eurocontroll. Aircraft performance database: Airbus a320, 2020. URL https://contentzone.eurocontrol.int/aircraftperformance/details.aspx?ICAO=A320.

[207] Tseko Mofokeng, Paul T. Mativenga, and Annlizé Marnewick. Analysis of aircraft maintenance processes and cost. *Procedia CIRP*, 90(4):467–472, 2020. ISSN 22128271. doi:10.1016/j.procir.2020.01.115.

[208] Mansour Bineid. *Aircraft systems design methodology and dispatch reliability prediction*. Cranfield University, 2005.

[209] Leonard MacLean, Alex Richman, and Mark Hudak. Failure rates for aging aircraft. *Safety*, 4(1):7, 2018.

[210] Željko Marušić, Borivoj Galović, and Omer Pita. Optimizing maintenance reliability program for small fleets. *Transport*, 22(3):174–177, 2007. ISSN 1648-4142.

[211] International Transport Association. Air passenger market analysis: Passenger growth slows as covid-19 impacts the industry. URL https://www.iata.org/en/iata-repository/publications/economic-reports/air-passenger-market-analysis---jan-2020/.

[212] Shannon P. Ackert. Basics of aircraft maintenance programs for financiers. *Evaluation & insights of commercial aircraft maintenance programs*, pages 1–23, 2010.

[213] International Civil Aviation Authority. Manual on the regulation of international air transport: Doc 9626. URL https://www.icao.int/Meetings/atconf6/Documents/Doc%209626_en.pdf.

[214] Michael Barot and Juraj Hromkovič. *Stochastik*. Springer International Publishing, Cham, 2017. ISBN 978-3-319-57594-0.

[215] Aura Reggiani, Peter Nijkamp, and Alessandro Cento. Connectivity and concentration in airline networks: a complexity analysis of lufthansa's network. *European Journal of Information Systems*, 19(4):449–461, 2010. ISSN 0960-085X.

[216] Alessandro Cento. *The Airline Industry*. Physica-Verlag HD, Heidelberg, 2009. ISBN 978-3-7908-2087-4.

[217] Linton C. Freeman. Centrality in social networks conceptual clarification. *Social Networks*, 1(3):215–239, 1978. ISSN 03788733.

[218] Airbus SE. *Airbus Aircraft 2018 Average List Prices in USD*. Airbus Media Relations, 2019. URL www.airbus.com/content/dam/corporate-topics/publications/backgrounders/Airbus-Commercial-Aircraft-list-prices-2018.pdf.

[219] Andrew J. Cook and Graham Tanner. European airline delay cost reference values: Updated and extended values. 2015.

[220] R. Golaszewski, W. Spitz, and B. Litvinas. An economic analysis of maximum take-off weight (mtow) reductions under an icao co2 standard. URL https://theicct.org/sites/default/files/publications/Economic_Analysis_of_MTOW_Reductions_07May13_FINAL.pdf.

[221] Shannon P. Ackert. *Aircraft Payload-Range Analysis for Financiers*. Aircraft Monitor, 2013.

[222] Klaus Renger. *Finanzmathematik mit Excel*. Springer Fachmedien Wiesbaden, Wiesbaden, 2016. ISBN 978-3-658-14099-1.

[223] Fran Sérgio Lobato and Valder Steffen. *Multi-Objective Optimization Problems*. Springer International Publishing, Cham, 2017. ISBN 978-3-319-58564-2.

[224] Aircraft performance database: Airbus a320. URL https://contentzone.eurocontrol.int/aircraftperformance/details.aspx?ICAO=A320.

[225] Modernairliners. Airbus a320 specs: What is behind one of the most popular short-haul airliners?, 2021. URL https://modernairliners.com/airbus-a320-introduction/airbus-a320-specs/.

[226] É. Roux. *Turbofan and turbojet engines: database handbook*. Ed. Elodie Roux, 2007. ISBN 9782952938013.

[227] National Aeronautics and Space Administration. Aviation safety reporting system, 2021. URL https://asrs.arc.nasa.gov/.

[228] Arbeitskreis Masseanalyse. Luftfahrttechnisches handbuch, band masseanalyse, 2008.

[229] Dieter Scholz. Maintenance costs: Lecture supplementals, 2021. URL https://www.fzt.haw-hamburg.de/pers/Scholz/materialAFS/MaintenanceCosts.pdf.

[230] Ian Lerche and Brett S. Mudford. How many monte carlo simulations does one need to do? *Energy exploration & exploitation*, 23(6):405–427, 2005. ISSN 0144-5987.

[231] Shuanglei Chu, Fei Liu, and Zhiqiang Wei. The study on dispatch reliability prediction model of civil aircraft. *The Open Mechanical Engineering Journal*, 8(1), 2014.

[232] Iain McCreary. The economic cost of fod to airlines. *www.FODNews.com*, March 2008, 2008.

[233] A. D. Balk. *Safety of ground handling*. NLR-CR-2007-961. National Aerospace Laboratory NLR, 2007.

[234] Nico Hölzel, Christopher Schröder, Thomas Schilling, and Volker Gollnick. A maintenance packaging and scheduling optimization method for future aircraft. In *International Air Transport and Operations Symposium*, 2012.

[235] Aircraft Commerce. *A320 family full maintenance analysis: Issue 44 Feb/Mar*. Aircraft Commerce, 2006.

[236] Luftfahrt Bundesamt. Merkblatt zur abgrenzung von line maintenance und base maintenance in instandhaltungsbetrieben nach teil-145, 2015.

[237] Average annual hours actually worked per worker, 2021. URL https://stats.oecd.org/Index.aspx?DataSetCode=ANHRS.

[238] MIT Global Airline Industry Program. Employees compensation, 2021. URL http://web.mit.edu/airlinedata/www/Employees&Compensation.html.

[239] IATA. Airline maintenance cost executive commentary: An exclusive benchmark analysis (fy2009 data) by iata's maintenance cost task force. 2011.

[240] IATA. Iata economic chart of the week: Why it matters that the airline industry stays value creating for investors. 2019.

[241] Michael Ball, Cynthia Barnhart, Martin Dresner, Mark Hansen, Kevin Neels, Amedeo Odini, Everett Peterson, Lance Sherry, Antonio Trani, and Bo Zou. Total delay impact study: A comprehensive assessment of the costs and impacts of flight delay in the united states. 2010.

[242] European Parliament and Council of the European Union. Regulation establishing common rules on compensation and assistance to passengers in the event of denied boarding and of cancellation or long delay of flights: Flight compensation regulation, 2004.

[243] Christoph P. Dienel, Hendrik Meyer, Malte Werwer, and Christian Willberg. Estimation of airframe weight reduction by integration of piezoelectric and guided wave–based structural health monitoring. *Structural Health Monitoring*, 18(5-6):1778–1788, 2019. ISSN 1475-9217. doi:10.1177/1475921718813279.

[244] Andreas Wald, Christoph Fay, and Ronald Gleich, editors. *Introduction to aviation management*, volume 3 of *Aviation Management*. LIT, Berlin, 2. ed. edition, 2014. ISBN 9783643106261.

[245] Simon Pfingstl, Martin Steiner, Olaf Tusch, and Markus Zimmermann. Crack detection zones: Computation and validation. *Sensors (Basel, Switzerland)*, 20(9), 2020. doi:10.3390/s20092568.

[246] Marcus Vinicius Viana. Sensor calibration for calculation of loads on a flexible aircraft. In *International Forum on Aeroelasticity and Structural Dynamics*. 2015.

[247] Acellent Technologies. *Acellent ScanGenie On-board SMART Layer*. 2021. URL `https://www.acellent.com/products/smart-layer-sensors`.

[248] LUNA Innovations Incorporated. *ODiSI 6000 Series Data Sheet*. 2021. URL `https://lunainc.com/product/odisi-6000-series`.

[249] Wikipedia. Fuel economy in aircraft, 2020. URL `https://en.wikipedia.org/wiki/Fuel_economy_in_aircraft`.

[250] Boeing Aircraft Company. Airport noise and emissions regulations: Airports with noise and emissions restrictions, 2021. URL `https://www.boeing.com/commercial/noise/list.page`.

Appendix A

Appendix

A.1 Task and Skill Codes in Airbus A320 Maintenance Planning Document

Table A.1: Definition and scope of work associated with skill codes used in the Airbus A320 MPD [175].

Skill code	Definition	Scope of work
AF	Airframe	Hydro-mechanical, environmental, fuel, oxygen, and cargo systems. Associated servicing requiring a certain qualification such as flaps/slats, landing gear, THS actuator, structure visual inspection
AV	Instrument	Autopilot, instruments, digital equipment, fire protection
CA	Cabin/utility	Furnishing, galleys
EL	Electrical	Electrical generation, distribution and associated services and components.
EN	Power Plant	Engines, APU accessories, and associated services
NDT	Non-destructive test	All NDT and borescope inspection inspections

Table A.2: Breakdown of skill codes in Airbus A320 MPD by ATA chapter.

Skill code	Aircraft systems		Power plant		Structure	
	[N]	[%]	[N]	[%]	[N]	[%]
Airframe (AF)	588	16.0	25	0.7	2017	54.9
Instrument (AV)	34	0.9	-	-	-	-
Cabin / Utility (CA)	49	1.3	-	-	-	-
Electrical (EL)	175	4.8	-	-	2	0.1
Power Plant (EN)	74	2.0	149	4.1	28	0.8
Non Destructive Testing (NDT)	9	0.2	6	0.2	472	12.9
Radio (RA)	35	1.0	-	-	-	-
Utility (UT)	8	0.2	-	-	-	-
Total	972	26.5	180	4.9	2519	68.6

Table A.3: Definition of task codes in Airbus A320 MPD [175].

Task code	Definition
BSI	Borescope inspection
CHK	Check for condition, leaks, circuit continuity, check fluid reserve on item, check tension and pointer, check fluid level, check detector, check charge pressure, leak check/test.
DI	Detailed inspection
DS	Discard
FC	Functional check/test
GVI	General visual inspection
LU	Lubrication
OP	Operational check/test
RS	Remove for restoration
SDI	Special detailed inspection
SV	Drain, servicing, replenishment (fluid change)
TPS	Temporary protection system
VC	Visual check

Table A.4: Breakdown of task codes in Airbus A320 MPD by ATA chapter.

Task code	Aircraft systems		Power plant		Structure	
	[N]	[%]	[N]	[%]	[N]	[%]
Borescope inspection (BSI)	-	-	5	0.1	-	-
Check[a] (CHK)	25	0.7	3	0.1	1	0.0
Detailed inspection (DI)	189	5.1	67	1.8	1441	39.3
Discard (DS)	64	1.7	24	0.7	-	-
Functional check/test (FC)	144	3.9	3	0.1	23	0.6
General visual inspection (GVI)	80	2.2	32	0.9	518	14.1
Lubrication (LU)	21	0.6	2	0.1	12	0.3
Operational check/test (OP)	232	6.3	13	0.4	56	1.5
Remove for restoration (RS)	95	2.6	1	0.0	-	-
Special detailed inspection (SDI)	21	0.6	19	0.5	467	12.7
Drain, Servicing, Replenishment (SV)	25	0.7	4	0.1	-	-
Temporary protection system (TPS)	19	0.5	-	-	-	-
Visual check (VC)	57	1.6	7	0.2	1	0.0
Total	972	26.5	180	4.9	2519	68.6

[a] Condition, leaks, circuit, fluid level, tension, detector and charge pressure [175, p. 18].

A.2 Summary of Common Airframe Inspection Technologies

Table A.5: Summary of common technological approaches for airframe inspection, adapted from [62, p. 226].

NDT methods	Advantages	Disadvantages
Visual	Inexpensive, highly portable, immediate results, minimum training, minimum part preparation	Surface discontinuities only, generally only large discontinuities, misinterpretation of scratches
Dye penetrant	Portable, inexpensive, sensitive to very small discontinuities, minimum skill required	Locates surface defects only, rough or porous surfaces interfere, test part preparation required, cleanliness required, direct visual detection of results required
Magnetic particle	Can be portable, inexpensive, sensitive to small discontinuities, immediate results, moderate skill required, detects surface and subsurface, relatively fast	Surface accessibility required, test interference with rough surface, part preparation required, ferromagnetic materials only, part demagnetizing required after test
Eddy current	Portable, detects surface and subsurface, discontinuities, moderate speed, immediate results, sensitive to small discontinuities, thickness sensitive, can detect many variables	Surface accessibilty to probe, test interference with rough surface, electrically conductive materials, skill and training required, time consuming for large areas
Ultrasonic	Portable, inexpensive, sensitive to very small discontinuities, immediate results, little part preparation, wide range of materials and thickness can be inspected	Surface accessibility to probe, test interference with rough surfaces, highly sensitive to sound beam, high degree of skill required to set up and interpret, couplant usually required
X-ray radiography	Detects surface and internal flaws, can inspect hidden areas, permanent test record obtained, minimum part preparation	Safety hazard, expensive slow process, highly directional, sensitive to flaw orientation, high degree of skill and experience required, depth of discontinuity not indicated
Isotope radiography	Portable, less expensive than X-ray, detects surface and internal flaws, inspect hidden areas, permanent test record obtained, minimum part preparation	Safety hazard, highly directional, sensitive to flaw orientation, high degree of skill and experience, depth of discontinuity not indicated

A.3 Considered Results of Current Cost-Benefit Studies on Structural Health Monitoring

Table A.6: Overview of considered studies covering the cost and benefit of SHM deployed in aircraft.

Abbreviation	Type	Application	Cost Change	Reference
Bol 07	Quantitative	Inspect. and maint.	0%	[148]
Che 14	Quantitative	Inspect. and maint.	−15%	[149]
Che 14	Quantitative	Inspect. and maint.	−34%	[150]
Che 14	Quantitative	Inspect. and maint.	−52%	[150]
Der 16	Quantitative	Inspect. and maint.	−79%	[22]
Don 18	Quantitative	Inspect. and maint.	39%	[31]
Don 18	Quantitative	Airframe weight	3%	[31]
Don 18	Quantitative	Inspect. and maint.	69%	[32]
Fit 11	Quantitative	Inspect. and maint.	52%	[33]
Llo 08	Quantitative	Inspect. and maint.	−30%	[23]
Pat 10	Quantitative	Inspect. and maint.	−50%	[24]
Pat 11	Quantitative	Inspect. and maint.	−35%	[25]
Pat 11	Quantitative	Airframe weight	−15%	[25]
Pat 12	Quantitative	Inspect. and maint.	−5%	[26]
Sun 18	Quantitative	Inspect. and maint.	−30%	[151]
Wan 17	Quantitative	Inspect. and maint.	−67%	[27]
Wan 18	Quantitative	Inspect. and maint.	−83%	[28]
	qualitative	Airframe weight	decrease	[145]
	qualitative	Decomissioning	decrease	[29]
	qualitative	Structural Modelling	non	[246]
	qualitative	Inspect. and maint.	decrease	[135]
	qualitative	Inspect. and maint.	decrease	[140]
	qualitative	Inspect. and maint.	decrease	[139]
	qualitative	Inspect. and maint.	decrease	[141]
	qualitative	Inspect. and maint.	decrease	[137]
	qualitative	Inspect. and maint.	decrease	[142]
	qualitative	Inspect. and maint.	decrease	[147]
	qualitative	Inspect. and maint.	decrease	[136]
	qualitative	Inspect. and maint.	decrease	[144]
	qualitative	Inspect. and maint.	decrease	[138]
	qualitative	Inspect. and maint.	decrease	[146]
	qualitative	Inspect. and maint.	decrease	[143]
	qualitative	Inspect. and maint.	non	[30]

A.4 Experimental Setup of IABG Damage Monitoring Demonstrator

As part of the STRUBATEX project, an experiment was conducted at IABG to demonstrate the applicability of residual life estimation methods for metallic structures. For this purpose, several strain gauges were strategically placed on a structural specimen that resembled the lower surface of an aircraft wing to determine strain gauge reliability for identifying and detecting cracks in the structure. The corresponding test setup is shown in Figure A.1. Based on the collected data, methods for predicting crack growth were also evaluated.

The corresponding damage classification performance for selected methods is shown in Figure A.2. The performance of the method to correctly detect cracks depends on the sensor position and the data evaluation method. Although the conditions during the structural test were not equivalent to the environmental conditions during the operation of the aircraft, the presented classification results can be used as a first performance indication of a damage monitoring system. However, in commercial applications, the performance will be influenced by other parameters, such as component geometry.

A detailed description of the demonstrator setup, including the sensor placement strategy, is given in [245].

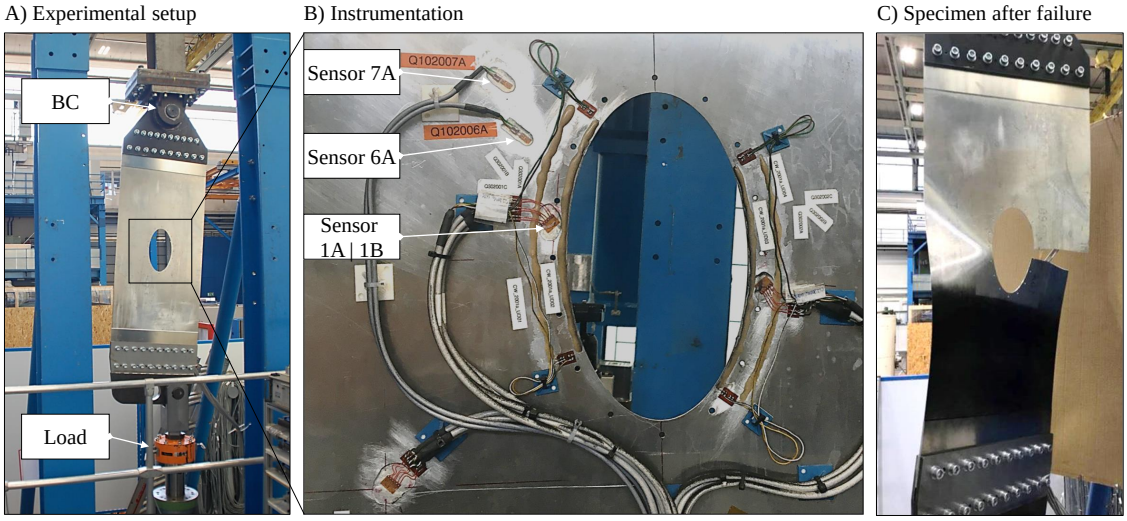

Figure A.1: SHM demonstrator test conducted at IABG. A) General experimental setup. B) Instrumentation for test specimen with strain gauges. C) State of specimen after experiencing a failure. Adapted from [245, p.9–10].

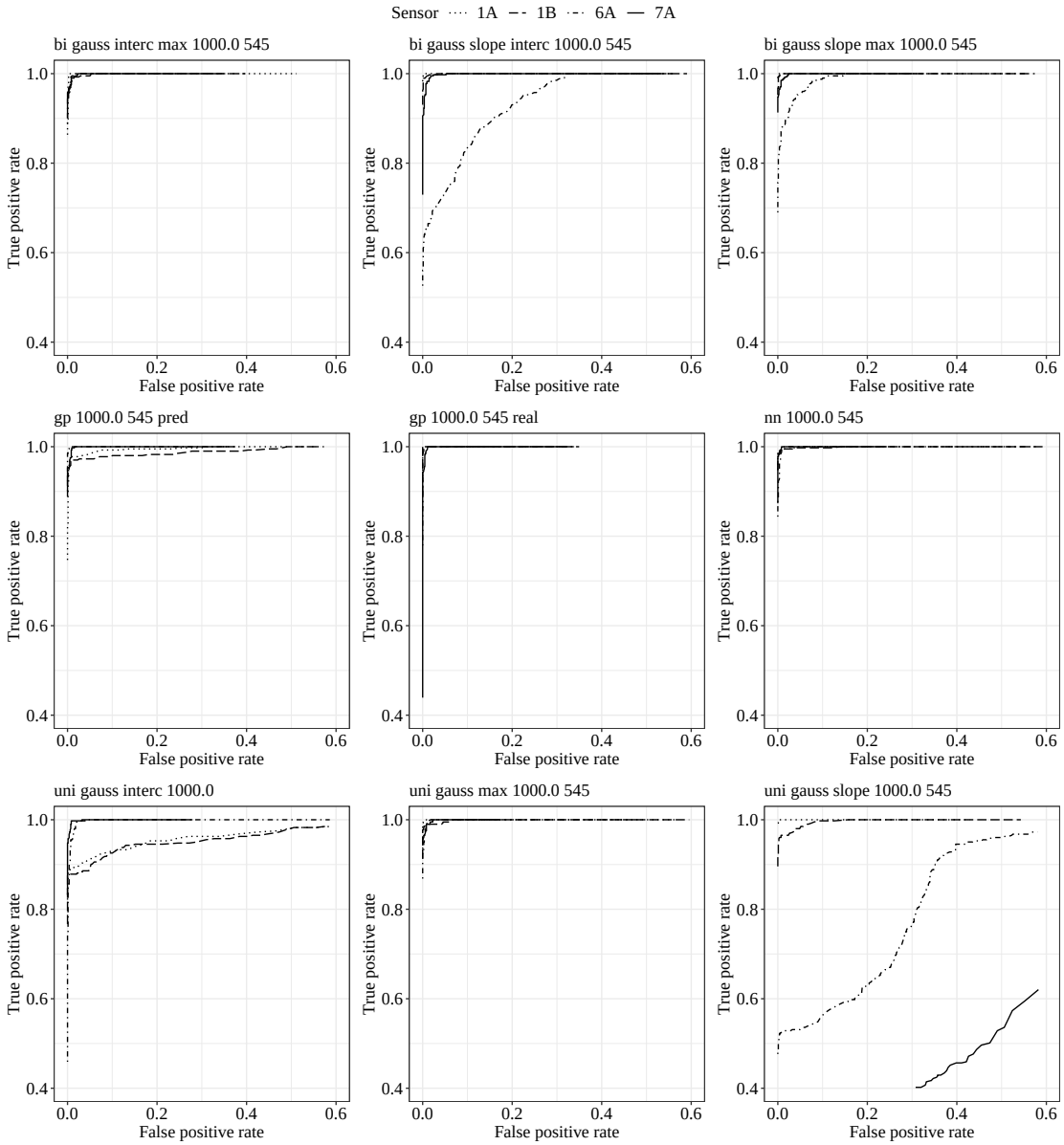

Figure A.2: Damage classification performance of the considered sensors in IABG SHM demonstrator test using different damage classification approaches.

A.5 Mass and Power Assumptions for Structural Health Monitoring Sensor Network

Table A.8: Assumed SHM sensor properties, based on [169].

System	Parameter	Mass figure		Power figure	
		Value	Unit	Value	Unit
Ultrasonic sensors	Overall area density (Acellent ScanGenie) [247]	1673	g/m	4.8	W/m
	Single sensor (overall)	75	g/m	0.3	W
	Minimum per component (sensors + interrogator)	494	g/m	2.5	W
Data network	Linear density of data cables (ARINC 664 cable)	32	g/m	-	
	Connector mass (two per cable)	10	g	-	
	Data collector	500	g	5	W
Power network	*Mass and dissipation loss calculated for each cable in the network*	-		-	
	Connector mass (two per cable)	20	g	-	
Fiber-optic and sensors network	Linear density of optical cable (fiber + jacket) (Sensor/distribution network)	4	g/m	-	
	Connector mass (two per fiber) (Sensor/distribution network)	5	g	-	
	FOS interrogator (LUNA ODiSI 6000, 4 ch.) [248]	39	g/m	0.8	W/m
	Minimum per group	1950	g	40	W

A.6 Historical Development of Aircraft Fuel Efficiency

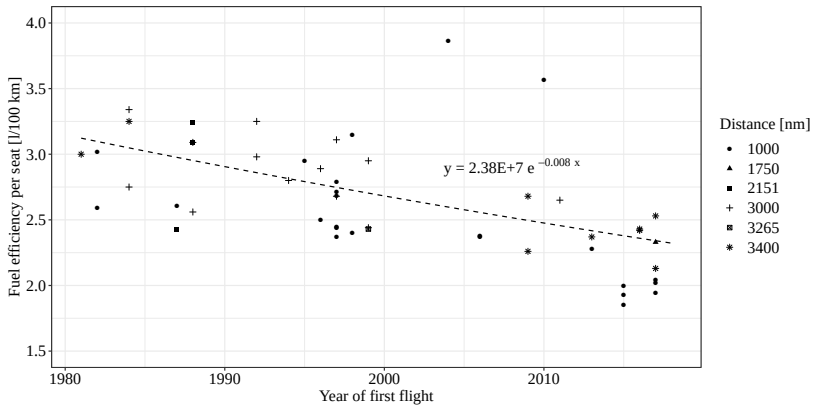

Figure A.3: Development of aircraft specific fuel consumption at entry into service for varying flight distances [179–187, 187–196], reproduced from [249]. The illustrated data is summarized in Table A.9.

Table A.9: Data for fuel consumption development of reproduced from [249].

Model	First flight [Year]	Seats	Distance [nm]	Fuel efficiency [l/(Pax·100 km)]	Ref.
Airbus A220-100	2013	125	1000	2.28	[184]
Airbus A220-300	2015	160	1000	2.00	[185]
Airbus A220-300	2015	135	1000	1.85	[179]
Airbus A319	1995	124	1000	2.95	[186]
Airbus A319Neo	2015	136	1000	1.93	[179]
Airbus A320	1987	150	1000	2.61	[186]
Airbus A320	1987	150	2151	2.43	[189]
Airbus A321-200	1996	180	1000	2.50	[186]
Airbus A321NeoLR	2016	154	3400	2.43	[190]
Airbus A330-200	1997	293	1000	2.37	[186]
Airbus A330-200	1997	241	3000	3.11	[191]
Airbus A330-300	1992	262	3000	2.98	[191]
Airbus A330neo-900	2016	310	3400	2.42	[192]
Airbus A340-300	1992	262	3000	3.25	[191]
Antonov An-148	2004	89	1000	3.86	[180]
Antonov An-158	2010	99	1000	3.57	[180]
Boeing 737 MAX-7	2017	140	1000	1.94	[179]
Boeing 737 MAX-8	2017	162	1000	2.04	[187]
Boeing 737 MAX-8	2017	168	3400	2.13	[187]

(continued on next page)

(continued)

Model [-]	**First flight** [Year]	**Seats** [-]	**Distance** [nm]	**Fuel efficiency** [l/(Pax·100 km)]	**Ref.** [-]
Boeing 737 MAX-9	2017	180	1000	2.02	[187]
Boeing 737 MAX-9	2017	144	3400	2.53	[190]
Boeing 737-600	1998	110	1000	3.15	[182]
Boeing 737-700	1997	126	1000	2.79	[182]
Boeing 737-700	1997	128	1000	2.71	[186]
Boeing 737-800	1997	162	1000	2.44	[182]
Boeing 737-800	1997	160	1000	2.68	[186]
Boeing 737-800W	1997	162	1000	2.45	[187]
Boeing 737-900ER	2006	180	1000	2.38	[182]
Boeing 737-900ERW	2006	180	1000	2.37	[187]
Boeing 747-400	1988	416	2151	3.24	[189]
Boeing 747-8	2011	467	3000	2.65	[193]
Boeing 757-200	1982	190	1000	3.02	[186]
Boeing 757-200	1982	200	1000	2.59	[183]
Boeing 757-200W	1981	158	3400	3.00	[190]
Boeing 757-300	1998	243	1000	2.40	[183]
Boeing 767-200ER	1984	181	3000	3.34	[194]
Boeing 767-200ER	1984	224	3000	2.75	[194]
Boeing 767-200ER	1984	193	3400	3.25	[190]
Boeing 767-300ER	1988	218	2151	3.09	[189]
Boeing 767-300ER	1988	218	3000	3.09	[194]
Boeing 767-300ER	1988	269	3000	2.56	[194]
Boeing 767-400ER	1999	245	3000	2.95	[194]
Boeing 767-400ER	1999	304	3000	2.44	[194]
Boeing 767-400ER	1999	304	3265	2.43	[181]
Boeing 777-200	1994	305	3000	2.80	[195]
Boeing 777-200ER	1996	301	3000	2.89	[191]
Boeing 777-300	1997	368	3000	2.68	[195]
Boeing 787-8	2009	291	3400	2.26	[187]
Boeing 787-8	2009	238	3400	2.68	[190]
Boeing 787-9	2013	304	3400	2.37	[192]
Irkut MC-21	2017	163	1750	2.33	[196]

A.7 Aircraft Depreciation Methods

The methods used to depreciate the book value of aircraft can differ between airlines [178], and depending on the depreciation method, book values over time can differ. The book value of a reference aircraft with a purchase price of USD 50M is illustrated in Figure A.4, when depreciated over 30 years using two different methods. The straight-line method is typically used in the airline industry [176]. In comparison, the sum-of-years' digit method leads to a higher depreciation at the beginning of the aircraft's lifetime. This thesis aims to use a depreciation method that ideally represents the market value of an aircraft. Since aircraft typically require additional refurbishing and inspections over their lifetimes, the second half of the lifetime is typically not as valuable as their first. To represent this behavior, the sum-of-years' digits method is used in this work to depreciate the book value of the aircraft.

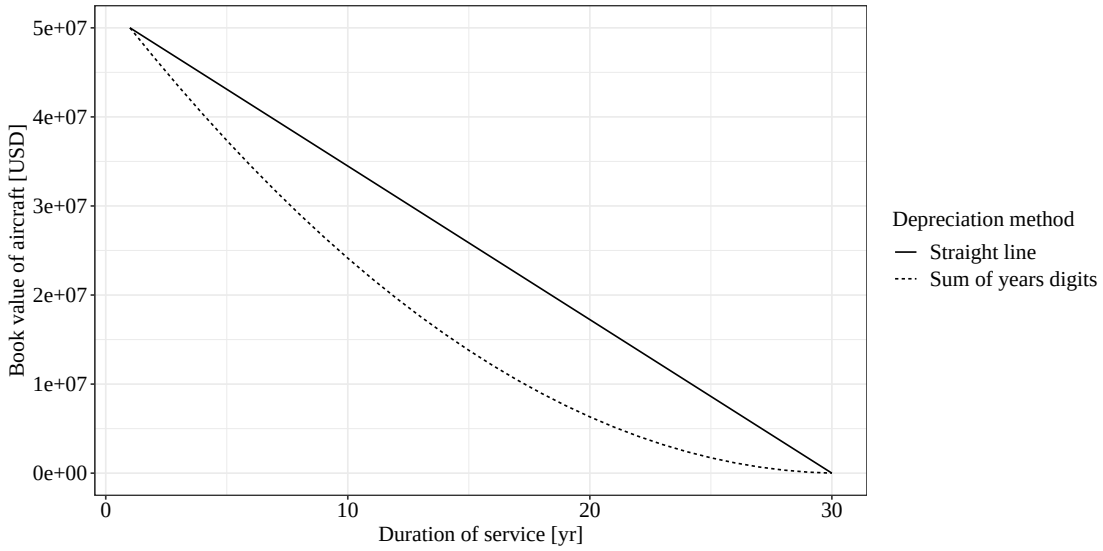

Figure A.4: Difference in book value over time when using different depreciation methods.

A.8 Approximation of Aircraft Usage Data for Fatigue Damage Index

The approximation of aircraft usage data for the calculation of the fatigue damage index (FDI) is based on [200]. The considered Airbus A320 fleet operations are based on ADS-B data provided by Flightradar24. A total of 7,951[1] aircraft are covered over 797 days between September 23$^{\text{rd}}$, 2017 and November 29$^{\text{th}}$, 2019, amounting to 16,625,103 flights. The dataset contains an average of 2.62 flights per aircraft per day, thus covering only a fraction of all flights. The usage behavior of the fleet is thus extrapolated, assuming that the available data is representative of all aircraft. The payload on each flight is approximated by the average seat load factor on a specific origin-destination pair for a single airline, based on leg data provided by Sabre®. The average taxi time is considered by continent based on data made available by Eurocontrol. Available usage data is replicated until the aircraft is retired, assuming unchanged usage behavior over the entire aircraft lifetime. Differences between aircraft variants and versions are neglected. Within the scope of this work, the actual takeoff weight and top of descent on each flight are not available and thus approximated as follows:

A.8.1 Takeoff Weight

Fuel weight and consequently takeoff weight on each flight are calculated by

$$W_{TaxiFuel,dest} = T_{Taxi,dest} \cdot F_{Taxi}, \tag{A.1}$$

where $T_{Taxi,dest}$ is the required taxi time at the destination in minutes and $W_{TaxiFuel,dest}$ is the weight of fuel required at the destination for taxiing in kilograms. The resulting aircraft takeoff weight without fuel for propulsion can be calculated by

$$\begin{aligned} W_{TOWw/oFuel} =& W_{OEW} + W_{misc} \\ &+ LF \cdot N_{Seats} \cdot W_{Pax} \\ &+ W_{TaxiFuel,dest} \end{aligned} \tag{A.2}$$

The weight of required fuel for the cruise flight is derived using the Breguet range equation. To approximate the total fuel weight, a reserve fuel weight $W_{Fuel,res}$ is considered to account

[1] On July 25, 2019, a total of 8,316 Airbus A320s were operational.

for the planning of an alternate airport. Furthermore, the total weight of fuel is increased by a factor $F_{Fuel,res}$ to consider the required fuel for takeoff and holding patterns.

$$W_{Fuel,prop} = \left(W_{TOWw/oFuel} + W_{Fuel,res}\right) \cdot \exp\left(\frac{\frac{d_{flight}}{a \cdot M_c} \cdot g \cdot SFC_{cruise}}{\frac{L}{D}} - 1\right) \cdot F_{Fuel,res} \tag{A.3}$$

Additionally, airline procedures require a predefined minimum of fuel $W_{Fuel,prop,min}$ on takeoff, considered by

$$W_{Fuel,prop} = max\left(W_{Fuel,prop}, W_{Fuel,prop,min}\right). \tag{A.4}$$

In the work at hand, $W_{Fuel,prop,min}$ is considered equal for all airlines. Furthermore, the weight of the aircraft upon takeoff is limited by the MTOW set by the manufacturer:

$$W_{TOW,Total} = min\left(W_{TOWw/oFuel} + W_{Fuel,prop}, W_{MTOW}\right). \tag{A.5}$$

The aim of this approach is to provide a fair proxy of the fuel weight in practice rather than calculate the exact fuel consumption during flight. The consequent takeoff weight over the flight distance for varying seat load factors is illustrated in Figure A.5.

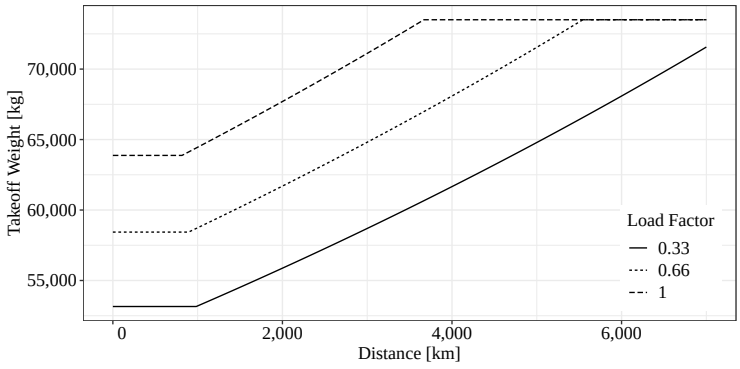

Figure A.5: Assumed aircraft takeoff weight for a given flight distance and load factor, based on [200].

A.8.2 Maximum Flight Altitude

The maximum altitude of every flight is based on the aircraft performance considered by Eurocontrol, summarized in Table A.10. Depending on the distance between origin and destination, the aircraft climbs to the highest attainable flight level, neglecting the semicircular separation rule. The resulting maximum altitude over distance is given in Figure A.6.

Table A.10: Considered aircraft climb performance, based on [224].

Flight phase	**Rate of climb [ft/min]**	**Speed**
Initial climb	2,500	175 kt
Climb to FL 150	2,000	290 kt
Climb to FL 240	1,400	290 kt
MACH climb to FL 390	1,000	MACH 0.78
Cruise	0	MACH 0.79
Initial descent to FL 240	1,000	MACH 0.78
Descent to FL 100	3,500	290 kt
Approach	1,500	250 kt

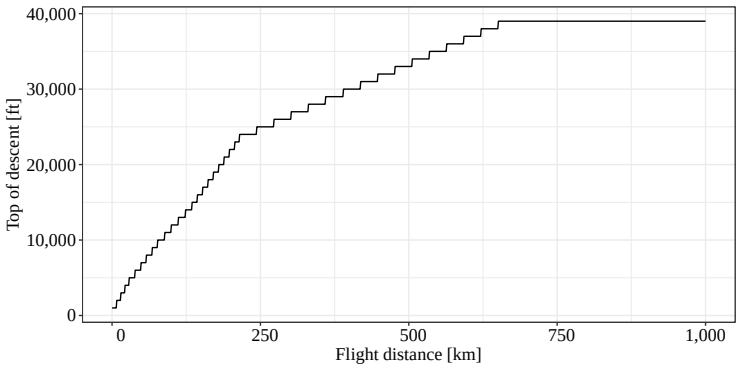

Figure A.6: Assumed takeoff weight and top of descent as function of aircraft flight distance, adapted from [200].

A.9 Sensitivity of Fatigue Damage Index Towards Variable Aircraft Usage

"The influence of the flight distance on the FDI is visualized in Figure A.7, assuming that a single aircraft has been operated on a single flight distance for its entire life until the extended service goal (ESG). As a result of limiting flight cycles and flight hours at predefined values, it can be seen that a longer flight distance than the considered average in the ESG leads to fewer flight cycles until decommissioning r to smaller FDIs. Likewise, a shorter flight distance results in decreased weight of fuel and flight hours. Accumulating these shorter flights over the aircraft lifetime until the service goal is reached reduces the fatigue indices of both the wing through less weight and the fuselage through lower flight altitudes" [200].

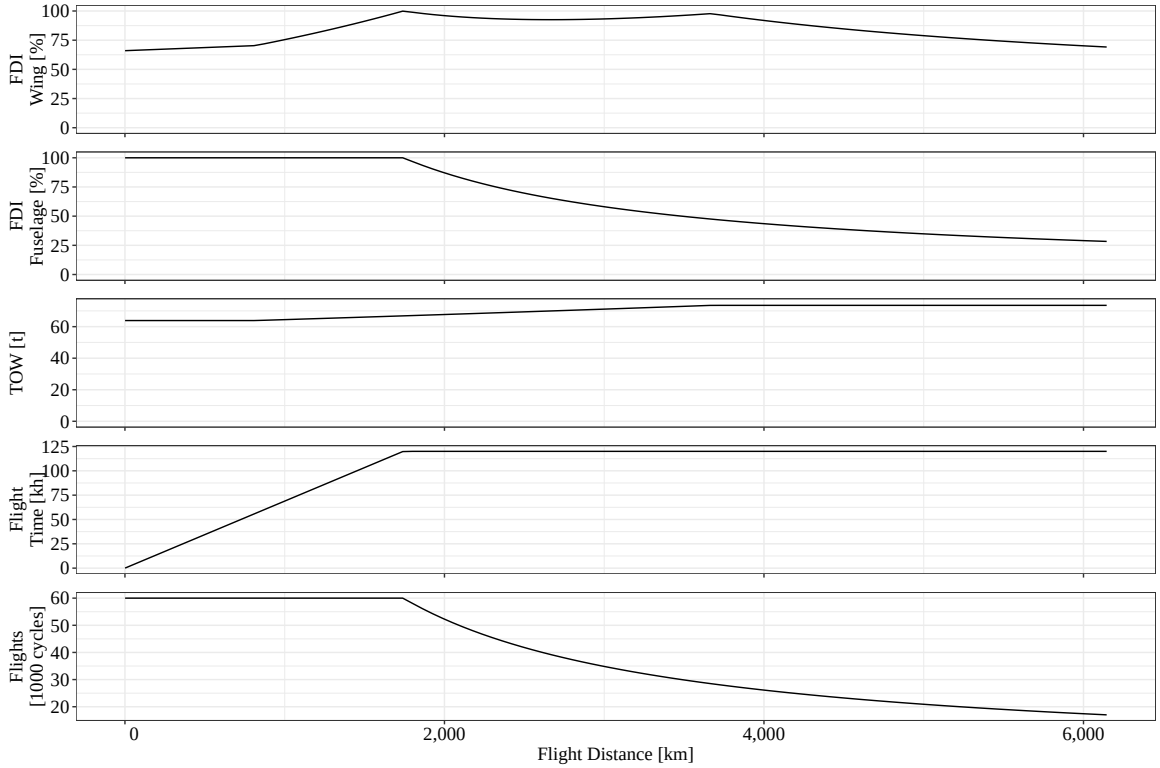

Figure A.7: Influence of average flight distance over aircraft lifetime on flight cycles, flight hours, takeoff weight, and the FDIs of the wing and fuselage.

A.10 Cost Model Input Data

The considered cost components are based on United States department of transportation (DOT) *form 41* data. To simplify the cost model, the individual cost factors used by the DOT are partially summarized using an allocation systematic described in Table A.11. A total of 1,409 combinations of fiscal quarter, aircraft, and airlines are considered. The cost of fuel, crew, leasing, and combined maintenance efforts constitute the overall share of cost of ownership (COO). The comparatively large deviation in fuel cost per flight hour (FH) results from varying fuel prices over time and different load factors, A320 family aircraft-engine combinations, and stage lengths.

Crew costs provided in the *Form 41* data do not include the costs for flight attendants. To factor in their costs in the overall direct operating cost (DOC), flight attendant costs are considered equal to crew costs.

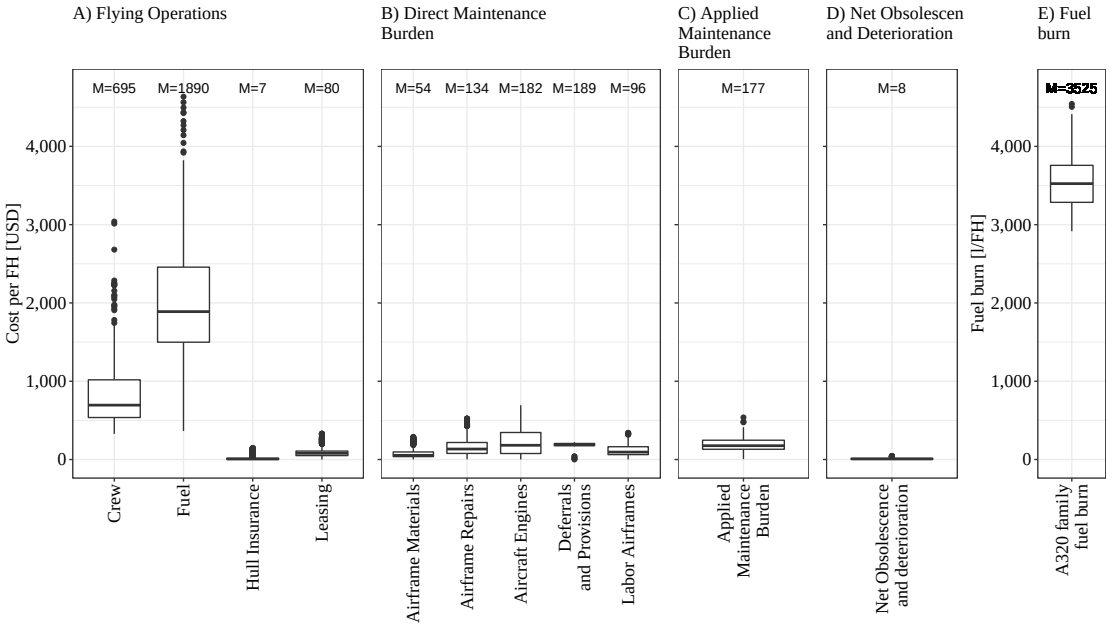

Figure A.8: Airbus A320 family COO based on quarterly reports for major US airlines from 1990 to 2020, adjusted to 2020 USD.

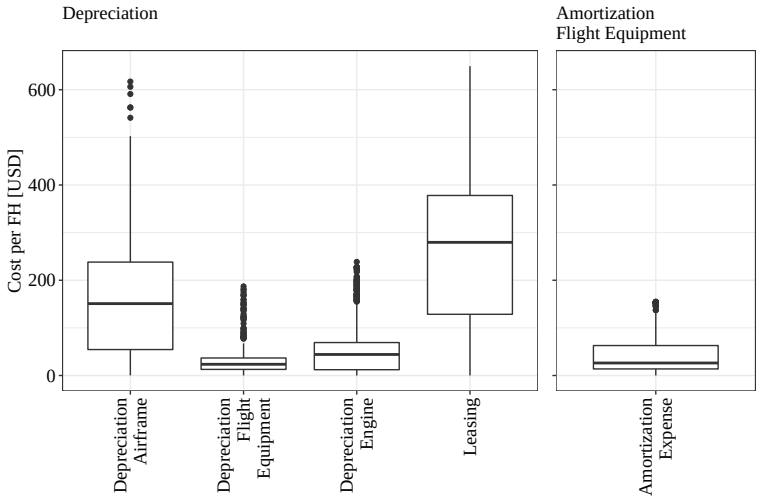

Figure A.9: Leasing and depreciation costs are distinguished depending on the ownership situation of the aircraft. The sum of both multiplied by the aircraft lifetime is assumed to reflect the purchase price of the aircraft.

Table A.11: Allocation systematic from US DOT cost factors to thesis cost factors.

Category	DOT cost factor	Thesis cost factor
Flying operations	Pilots & copilots	Crew
	Other flight personnel	Crew
	Trainees & instructors	Crew
	Personnel expenses	Crew
	Professional & technical fees	Misc. flying operations
	Aircraft interchange charges	Misc. flying operations
	Aircraft fuel	Fuel
	Aircraft oil	Misc. flying operations
	Rentals	Allocated to depreciation cost
	Other supplies	Misc. flying operations
	General	Hull insurance
	Employee benefits & pensions	Crew
	Injuries, loss, & damage	Misc. flying operations
	Payroll	Crew
	Other than payroll	Misc. flying operations
	Other expenses	Misc. flying operations
Direct maintenance	Labor–airframes	Labor airframes
	Labor–aircraft engines	Direct maintenance aircraft engines
	Airframe repairs	Airframe repairs
	Aircraft engine repairs	Direct maintenance aircraft engines
	Aircraft interchange charges	Misc. direct maintenance flight eqpt.
	Materials–airframes	Airframe materials
	Materials–aircraft engines	Direct maintenance aircraft engines
	Allowance–airframes	Misc. direct maintenance flight eqpt.
	Allowance–aircraft engines	Direct maintenance provisions
Applied maintenance	Flight eqpt.	Applied maintenance
Net obsolescence & deterioration	Expendable parts	Net obsolescence & deterioration
Depreciation	Airframes	Depreciation airframes
	Aircraft engines	Depreciation engines
	Airframe parts	Depreciation airframes
	Aircraft engine parts	Depreciation engines
	Other flight eqpt.	Depreciation other flight eqpt.
Amortization	Flight eqpt.	Amortization expense
Expense of interchange	Flying operations	Expense of interchange
Other depr. & amort.	Developmental expense	Other depr. & amort.
	Other intangibles	Other depr. & amort.
	Maintenance eqpt.	Other depr. & amort.
	General ground property	Other depr. & amort.
	Capital leases	Other depr. & amort.

A.11 Global Airport Night Flying Restrictions

Table A.12: Airports with night flight restrictions, based on [250].

Airport IATA code						
ABZ	BVA	FKB	LAX	MXP	RTM	TRK
ACC	CBG	FMM	LBA	NAP	SAN	TRN
ADL	CCR	FMO	LBG	NCE	SBA	TSA
AEP	CDG	FNC	LCY	NRK	SCK	TTN
AGF	CDW	FOK	LEJ	NRN	SCN	TVL
AHO	CEF	FRA	LGB	NRT	SDL	TXL
AIT	CEQ	FUE	LGW	NTE	SDV	UME
AMS	CGF	GIB	LHR	NUE	SEA	VIE
APF	CGI	GIG	LIS	NWI	SEL	VNY
ASE	CGN	GLA	LMP	NYL	SIO	WAW
AUS	CIA	GOT	LNZ	OAJ	SJC	WLG
AZO	CLW	GRZ	LPL	ODE	SJF	YKF
BAH	CMI	GSE	LTN	ONT	SMO	YOW
BBU	CPH	GVA	LUG	OPO	SNA	YQT
BCT	CPT	GYD	LUX	ORL	SOF	YUL
BDA	CRL	HAJ	LYS	ORY	SOU	YVR
BDR	CUF	HAM	MAD	OSL	SPK	YXD
BED	CVT	HHN	MAN	OST	STL	YYZ
BFI	DAL	HNL	MBJ	PAD	STN	ZRH
BHD	DBV	HPN	MEB	PAE	STP	
BHX	DCA	HVN	MFE	PBI	STR	
BIO	DEC	HWD	MGL	PDK	SUA	
BIQ	DEN	HYA	MIR	PED	SUN	
BLQ	DIJ	INN	MLI	PIE	SVQ	
BMA	DOM	ISP	MOB	PNE	SXB	
BOD	DRS	ITM	MOD	PRG	SXF	
BOH	DSA	ITO	MPL	PSM	SXM	
BOS	DTM	JAC	MRS	PSP	SYD	
BQH	DUS	JAD	MRU	PUS	SZG	
BRE	EDI	JER	MRY	PVD	TBU	
BRN	EMA	JNB	MSE	QEF	TEB	
BRS	ERF	KEL	MSP	QLD	TEX	
BRU	EXT	KHH	MST	RAR	TLS	
BSL	FAB	KIR	MTH	REK	TLV	
BUD	FAO	KRN	MTN	RGU	TMP	
BUR	FCO	KWI	MUC	RIC	TOA	
BVA	FDH	LAS	MVY	RST	TRF	

A.12 Freeman Network Centrality Index for Selected Topologies

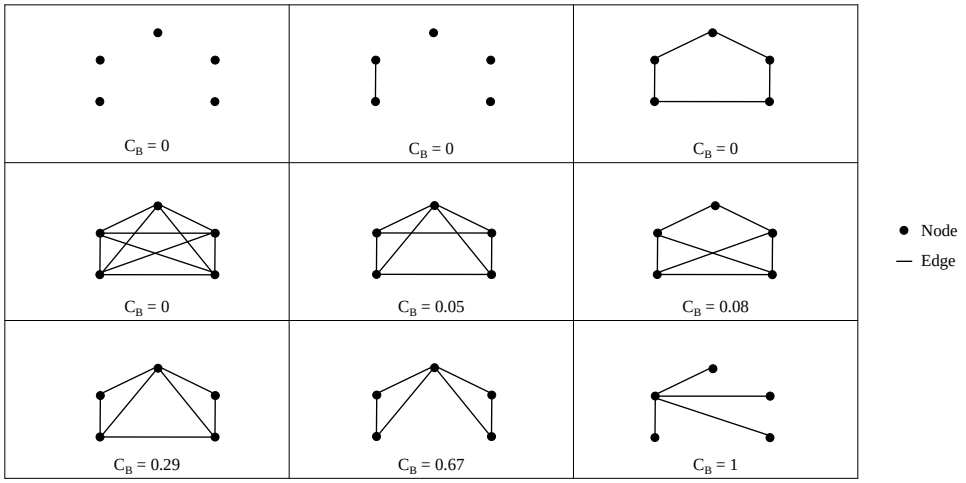

Figure A.10: Selected network topologies and corresponding Freeman network centrality index adapted from [217, pp. 232–236].

A.13 Summary of Reference Aircraft Maintenance Tasks

Table A.13: Summary of considered inspection requirements based on the Airbus A320 MPD.

ATA Chapter	Positions		Tasks		Avg. Task interval			Avg. Task Work[a]	
	[N]	[%]	[N]	[%]	[FC]	[FH]	[yr]	Inspect. [h]	Prep. [h]
Systems - 20 - Standard Practices	36	3.4	98	2.7	-	-	7.8	0.24	2.03
Systems - 21 - Air Conditioning	20	1.9	74	2.0	18000.0	10829.5	5.8	0.40	0.05
Systems - 22 - Auto Flight	3	0.3	7	0.2	-	10125.0	5.5	0.25	0.00
Systems - 23 - Communication	8	0.8	19	0.5	-	12000.0	5.7	0.28	0.02
Systems - 24 - Electrical Power	9	0.9	63	1.7	-	2946.2	3.3	0.36	0.06
Systems - 25 - Equipment /Furnishings	25	2.4	66	1.8	5678.9	10236.0	4.6	0.45	0.02
Systems - 26 - Fire Protection	17	1.6	88	2.4	750.0	11117.2	5.4	0.59	0.04
Systems - 27 - Flight Controls	25	2.4	114	3.1	7177.8	12307.3	5.1	0.59	0.16
Systems - 28 - Fuel	20	1.9	91	2.5	12878.6	9533.0	7.2	0.78	0.52
Systems - 29 - Hydraulic Power	9	0.9	43	1.2	-	7281.1	4.3	0.33	0.04
Systems - 30 - Ice And Rain Protection	6	0.6	13	0.4	-	10750.0	3.7	0.28	0.11
Systems - 31 - Indicating / Recording	7	0.7	15	0.4	-	6112.5	3.7	0.18	0.00
Systems - 32 - Landing Gear	40	3.8	101	2.8	7793.6	7917.6	4.2	0.66	0.70
Systems - 33 - Lights	2	0.2	7	0.2	-	9375.0	1.7	0.20	0.00
Systems - 34 - Navigation	13	1.2	28	0.8	-	8652.3	4.5	0.32	0.02
Systems - 35 - Oxygen	11	1.0	28	0.8	-	19000.0	5.4	1.21	0.00
Systems - 36 - Pneumatic	8	0.8	32	0.9	1800.0	15754.5	6.7	0.65	0.10
Systems - 38 - Water / Waste	7	0.7	24	0.7	-	12119.4	3.8	0.91	0.04
Systems - 44 - Cabin Systems	2	0.2	2	0.1	-	12000.0	6.6	0.20	0.00
Systems - 47 - Inert Gas System	1	0.1	7	0.2	-	19142.9	-	-	0.10
Systems - 49 - Auxiliary Power Unit	19	1.8	52	1.4	-	2466.1	2.5	0.41	0.02
Structure - 52 - Doors	85	8.1	222	6.0	13400.7	13428.4	6.6	0.31	0.10
Structure - 53 - Fuselage	288	27.5	673	18.3	18820.9	33660.8	8.5	0.44	0.76
Structure - 54 - Nacelles/Pylons	37	3.5	133	3.6	15899.3	24124.8	6.6	0.37	0.34
Structure - 55 - Stabilizers	38	3.6	60	1.6	24075.0	6000.0	7.4	0.59	0.31
Structure - 56 - Windows	3	0.3	5	0.1	-	-	2.6	0.23	0.00
Structure - 57 - Wings	237	22.6	1426	38.8	21862.4	35967.4	10.7	0.51	0.28
Power plant - 71 - Power Plant	9	0.9	31	0.8	5589.5	11146.7	7.2	0.20	0.14
Power plant - 72 - Engine	23	2.2	51	1.4	4192.5	3890.9	6.0	1.43	0.13
Power plant - 73 - Engine Fuel / Control	9	0.9	15	0.4	-	5564.3	2.7	0.28	0.03
Power plant - 75 - Bleed Air	7	0.7	11	0.3	4500.0	5700.0	3.4	0.26	0.23
Power plant - 77 - Engine Indicating	1	0.1	2	0.1	-	6000.0	-	0.13	0.00
Power plant - 78 - Exhaust	16	1.5	44	1.2	9721.1	8773.7	6.2	0.28	0.12
Power plant - 79 - Oil	4	0.4	18	0.5	4500.0	2837.5	1.7	0.41	0.02
Power plant - 80 - Starting	3	0.3	8	0.2	1500.0	685.7	1.0	0.25	0.04

[a] Time specified as given in the MPD.

A.14 Reference Aircraft Inspection Effort

Table A.14: Breakdown of reference aircraft inspection requirements by program.

Program	Category	Required work [h]
Structures	Inspection	9,978.2
System and powerplant	Inspection	28,946.2
Zonal program	Inspection	1,464.4
Structures	Preparation	2,507.2
System and powerplant	Preparation	1,507.4
Zonal program	Preparation	1,220.3
Structures	Access	2,559.9
System and powerplant	Access	2,921.5
Zonal program	Access	699.6
Structures	Repair	28,366.2
System and powerplant	Repair	78,565.0
Zonal program	Repair	14,289.6